Titre: Title:	The Short and Long Term Effects of in Vivo Cyclic Axial Compression Applied During Puberty on Bone Growth, Morphometry and Biomechanics
Auteur: Author:	Tanvir Mustafy
Date:	2019
Type:	Mémoire ou thèse / Dissertation or Thesis
Référence: Citation:	Mustafy, T. (2019). The Short and Long Term Effects of in Vivo Cyclic Axial Compression Applied During Puberty on Bone Growth, Morphometry and Biomechanics [Thèse de doctorat, Polytechnique Montréal]. PolyPublie. https://publications.polymtl.ca/3949/

URL de PolyPublie: PolyPublie URL:	https://publications.polymtl.ca/3949/
Directeurs de recherche: Advisors:	Isabelle Villemure, & Florina Moldovan
Programme: Program:	Génie mécanique

POLYTECHNIQUE MONTRÉAL

affiliée à l'Université de Montréal

The Short and Long Term Effects of in *Vivo* Cyclic Axial Compression Applied During Puberty on Bone Growth, Morphometry and Biomechanics

TANVIR MUSTAFY

Département de génie mécanique

Thèse présentée en vue de l'obtention du diplôme de *Philosophiae Doctor*

Génie mécanique

Juillet 2019

POLYTECHNIQUE MONTRÉAL

affiliée à l'Université de Montréal

Cette thèse intitulée :

The Short and Long Term Effects of in Vivo Cyclic Axial Compression Applied During Puberty on Bone Growth, Morphometry and Biomechanics

présentée par **Tanvir MUSTAFY**

en vue de l'obtention du diplôme de Philosophiæ Doctor

a été dûment acceptée par le jury d'examen constitué de :

Maxime RAISON, président
Isabelle VILLEMURE, membre et directrice de recherche
Florina MOLDOVAN, membre et codirectrice de recherche
Nicola HAGEMEISTER, membre
Bettina WILLIE, membre externe

DEDICATION

To my inspiring parents and sister, for being the
pillows, role models, catapults, cheerleading squad
and sounding boards I have needed.

ACKNOWLEDGEMENTS

I thank my friends in Montreal, especially Asif Iqbal, Auria Meher, Sanjida Khuki and Kamrul Islam (Rifat) for their support during my stay here in this beautiful town.

I express my special gratitude to my mother, Tamiza Akter, and my father, Mukter Hussain, for their prayers, unconditional love, support, and encouragement throughout my entire life. I owe my existence to them. Without their love and support, I would have never come this far in my life. I also thank my elder sister Doctor Tania Jebin and my brother in law Doctor Sifullah Bashar, who have inspired me through the tantrum of brainstorming, in those caffeine empowered nights of simulation run and through all the falls and rises I've gone through in Canada reminding me what the science fiction writer Jim Butcher once said "When everything goes to hell, the people who stand by you without flinching - they are your family". Last but not the least I also like to thank my niece, Rushmila, and my nephew, Rayan, who are sent from God to be the bundle of joy in our lives.

I would like to convey my gratitude to Professor Maxime Raison, Professor Nicola Hagemeister, and Professor Bettina Willie for accepting to participate in my Ph.D. Jury.

RÉSUMÉ

Pendant la croissance rapide pubertaire, les os sont sensibles aux stimuli mécaniques environnants. Les sollicitations mécaniques telles que les activités physiques fréquentes peuvent contribuer positivement au développement du squelette. Ces activités peuvent entrainer de faibles impacts (comme la marche, la natation, etc.) ou des impacts élevés (comme la course, le saut, etc.) selon la nature de l'activité physique. En plus de la charge mécanique, les facteurs nutritionnels contribuent également de manière significative au développement osseux pendant les périodes de croissance. Les effets des charges d'impact sur la croissance et le développement osseux au cours de l'adolescence ont été investigués par plusieurs chercheurs dans des études animales et cliniques, mais les résultats sont variables. Les recherches antérieures n'ont pas clairement abordé les effets isolés du chargement d'impact par rapport aux facteurs nutritionnels lors de l'évaluation de la croissance et du développement osseux. De plus, on ne sait toujours pas si les effets induits par les charges mécaniques pendant l'adolescence persistent à l'âge adulte et influencent les propriétés structurelles osseuses à long terme.

L'objectif de cette thèse était d'évaluer *in vivo* les effets des charges cycliques en compression faibles, moyennes et élevées appliquées pendant la puberté sur la croissance osseuse (à maturité squelettique) ainsi que sur la qualité osseuse et la résistance mécanique (à l'âge adulte) en utilisant un modèle animal (tibia de rat). Cet objectif a été atteint en complétant quatre études complémentaires. Tout d'abord, une dose d'exposition aux rayons X à haute résolution mais sécuritaire a été déterminée pour l'imagerie *in vivo* répétée par micro-CT des tibias de rat en croissance qui n'affecterait pas la croissance ou la microstructure osseuses. Deuxièmement, relation contraintes-déplacements a été établie pour les tibias pendant la période de croissance pubertaire du rat. Un outil de modélisation informatique a également été mis au point et validé pour évaluer les contraintes de l'os sous compression. Troisièmement, les effets de trois niveaux de charges cycliques en compression à la puberté sur la croissance osseuse, la morphométrie et la biomécanique ont été évalués à maturité du squelette. Enfin, les effets de ces trois niveaux de charges cycliques en compression appliquées à la puberté sur la microstructure osseuse ont été évalués à la maturité du squelette et après près d'un an d'entraînement à l'âge adulte.

Dans la première étude, trois doses de rayonnement micro-CT de 0,83, 1,65 et 2,47 Gy ont été testées. Les tibias droits de rats Sprague-Dawley mâles ont été scannés à l'aide d'un protocole de

micro-CT *in vivo* de leur 4e à leur 12e semaine d'âge avec ces doses de rayonnement. Les tibias gauches ont servi de témoins. Les tibias gauches n'ont été scannés que le dernier jour, avant le sacrifice. Les cellules de la moelle osseuse ont été étudiées, les taux de croissance osseuse et des analyses histomorphométriques de la plaque de croissance ont été évalués et des paramètres mprphométriques osseux ont été déterminés pour les tibias gauches et droits. Les doses de rayonnement de 1,65 et 2,47 Gy se sont avérées néfastes pour les cellules de la moelle osseuse, pour les hauteurs des zones prolifératives et hypertrophiques et pour les taux de croissance osseuse dans les tibias irradiés. De plus, les doses de rayonnement de 1,65 et de 2,47 Gy ont réduit de façon significative la densité minérale osseuse, l'épaisseur trabéculaire, le nombre de trabécules et l'espacement trabéculaire des tibias irradiés. Les doses de rayonnement de 2,47 Gy ont aussi considérablement réduit l'épaisseur corticale. Cependant, le développement osseux et la morphométrie trabéculaire et corticale n'ont pas été affectés pour le groupe de 0,83 Gy. Les doses de rayonnement de 0,83 Gy ont ensuite été utilisées dans le cadre du projet requérant l'imagerie par micro-CT *in vivo* répétés des rats à l'adolescence, ce qui permet cette dose permettant d'obtenir des images à haute résolution pour des études morphométriques sans nuire à la croissance osseuse.

Dans la deuxième étude, trois groupes de rats (âgés de 4, 8 et 12 semaines) ont été utilisés pour établir la relation entre les déplacements tibiaux des rats et les contraintes. Des valeurs cibles de déformation ont été fixées à 450, 850 et 1250 µε, ce qui correspondait aux valeurs maximales de déformation du tibia humain dans des conditions de marche sans restriction (450 µε), de course en zig-zag en montée (850 µε) et de saut vertical (1250 µε). Des jauges de déformation ont été installées à la surface médio-proximale des tibias de rats et des déplacements en compression variant de 0,5 mm à 3,5 mm ont été appliqués de façon cyclique à 2 Hz. Les déplacements et les déformations enregistrés ont été approximées analytiquement par des relations linéaires. Une approche de modélisation par éléments finis, basée sur les données du micro-CT pour établir la géométrie et les propriétés mécaniques, a également été développée, pour les tibias de rats âgés de 4, 8 et 12 semaines, et utilisée pour évaluer les contraintes osseuses dans des conditions expérimentales de charge sous les conditions de chargement expérimentales. Les résultats de simulations ont montré une bonne concordance avec les contraintes expérimentales, ce qui a permis de valider l'approche de modélisation proposée.

Dans la troisième étude, cinq groupes de rats ont été utilisés pour étudier les effets du chargement cyclique en compression à court terme. Les rats, initialement âgés de 4 semaines, étaient divisés en

groupes : témoin, sham, faible impact (LI), impact moyen (MI) et impact élevé (HI). Les tibias droits des groupes LI, MI et HI ont reçu une charge cyclique en compression correspondant à 450, 850 et 1250 µɛ, respectivement, pendant 5 jours/semaine pour 8 semaines en utilisant un dispositif de compression axiale adapté sur mesure. Les rats ont été sacrifiés à l'âge de 11 semaines. Les paramètres trabéculaires et corticaux de la structure osseuse ont été déterminés par micro-CT, le taux de croissance osseuse par marquage à la calcéine et l'histomorphométrie des plaques de croissance par coloration au bleu de toluidine. Les propriétés mécaniques des os ont été évaluées à partir d'essais de flexion. La charge HI a réduit le poids corporel des rats (12,8 %) et la consommation alimentaire (17 %) par rapport aux shams. Le taux de croissance osseuse a diminué de 6,5 % et de 10,5 %, respectivement, dans les groupes MI et HI. Après 8 semaines de chargement, le groupe HI a montré une augmentation significative de la densité minérale osseuse, de l'épaisseur trabéculaire, de la surface corticale et la surface totale de la diaphyse. La charge ultime et la rigidité ont également augmenté dans les groupes MI et HI comparativement aux shams. Dans l'ensemble, la charge d'impact durant l'adolescence a modérément réduit la croissance osseuse, mais a simultanément amélioré la qualité des os et la biomécanique osseuse à la fin de la période de croissance.

Dans la quatrième étude, cinq groupes de rats (âgés de 4 semaines) ont été utilisés pour étudier les effets à long terme de la charge cyclique en compression à l'adolescence. Les rats ont été divisés en groupes : témoin, sham, faible impact (LI), impact moyen (MI) et impact élevé (HI). Le protocole de mise en charge était similaire à celui de l'expérience à court terme, avec 8 semaines de charge de compression axiale *in vivo* de 4 à 11 semaines d'âge. Après le chargement, les rats ont été gardés dans leur cage pendant une période d'entraînement de 41 semaines. Ils ont été sacrifiés à l'âge de 52 semaines. Les paramètres trabéculaires et corticaux ont été déterminés par des analyses micro-CT et les propriétés mécaniques osseuses ont été évaluées à partir d'essais de flexion trois points. Des muscles tibiaux ont également été extraits et mesurés après le sacrifice. Des modèles par éléments finis des tibias de rats âgés de 52 semaines ont été générés pour évaluer la distribution des contraintes osseuses trabéculaires et corticales sous compression. Les charges HI et MI ont réduit le poids corporel et l'apport alimentaire à la fin de l'adolescence et au début de la période post-pubertaire. Toutefois, le poids corporel et l'apport alimentaire sont finalement revenus à un niveau semblable à celui des shams à 52 semaines. Les charges HI et MI ont augmenté la surface corticale, l'épaisseur et la surface totale de la diaphyse tibiale, ainsi que la densité minérale osseuse,

l'épaisseur trabéculaire et la fraction du volume osseux au niveau des tibias proximaux. Les bienfaits de la charge sur la zone corticale, l'épaisseur et la densité minérale osseuse ont été perdus après 41 semaines d'entraînement à l'âge adulte. Cependant, les avantages induits par la charge sur la résistance mécanique des os ont persisté jusqu'à 52 semaines. Dans l'ensemble, la charge cyclique en compression de niveau élevé effectué pendant l'adolescence a entrainé des bienfaits à long terme pour la structure et la force des os.

Les limites de ce projet de recherche comprennent l'utilisation de tibias de rat mâle seulement pour l'ensemble du projet. L'utilisation de sujets masculins et féminins aurait pu fournir des informations supplémentaires sur les changements osseux associés à la charge, en fonction du sexe. Une autre limitation possible est l'utilisation des résultats mesurés par micro-CT comme indicateur de la qualité de l'os trabéculaire. La charge cyclique en compression de niveau élevé a augmenté les paramètres morphométriques trabéculaires dans notre étude. Aucun essai mécanique en relation à la géométrie trabéculaire possiblement modifiée, qui se traduirait par un tissu trabéculaire plus fort ou non, n'a été vérifiée. L'utilisation d'un modèle de rat est également associée à une limitation de la capacité de résorption de l'os cortical au cours d'une période d'entraînement. Ceci est dû à l'absence de remodelage secondaire des canaux de Haversian dans ce modèle animal; par conséquent, les rats continuent à se développer jusqu'à relativement tard dans la vie. Cependant, des études antérieures ont observé un remodelage osseux dans la structure osseuse corticale du rat adulte en réponse au chargement mécanique. De plus, l'étude des propriétés morphométriques trabéculaires uniquement à partir de la métaphyse proximale des tibias peut être considérée comme une limitation de cette étude. L'inclusion de résultats supplémentaires provenant de la partie distale aurait pu fournir des informations plus détaillées sur les changements induits par la charge dans l'ensemble de la structure tibiale.

Ce projet présente d'importantes contributions méthodologiques et scientifiques. Une nouvelle méthodologie basée sur la micro-CT a été développée pour segmenter la microstructure osseuse trabéculaire et corticale et évaluer la morphologie osseuse sans interférer avec la croissance osseuse et la santé osseuse globale. Un outil d'éléments finis basé sur le micro-CT a également été développé pour l'évaluation non destructive de la mécanique osseuse. À l'aide d'un protocole de chargement finement contrôlé et calibré en fonction de la déformation, cette recherche a permis de surmonter les limites actuelles des études cliniques ou expérimentales visant à établir les effets de la charge cyclique en compression sur la croissance osseuse et a donc fourni des résultats pertinents

: une charge cyclique en compression de niveau élevé pendant la puberté nuit modérément à la croissance osseuse, mais elle favorise la solidité et la mécanique globale des os à maturité et ces avantages persistent à l'âge adulte. D'un point de vue clinique, les résultats de ce projet pourraient mener à des recommandations pour des programmes d'entraînement prescrits aux jeunes athlètes adolescents pratiquant des sports à impact élevé.

ABSTRACT

During the adolescent period, rapidly growing bones react sensitively to induced mechanical stimuli. Mechanical loadings such as daily physical activities can positively contribute to skeletal development. They can range from low impact activities (such as walking, swimming, etc.) to high impact activities (such as running, jumping, etc.) depending on the nature of the physical activity. Along with mechanical loading, nutritional factors also significantly contribute to bone development during growth periods. The effects of impact loadings on bone growth and development during the adolescent period have been investigated by several researchers in animal and clinical studies, but results are inconsistent. Previous research has not clearly addressed the isolated effects of impact loading from nutritional factors while evaluating bone growth and development. Moreover, it is still unclear whether the effects induced by mechanical loading during adolescence remains in adulthood and influence bone structural properties in the long term.

The objective of this thesis was to evaluate the effects of *in vivo* low, medium, and high cyclic axial compression applied during puberty on bone growth (at skeletal maturity) as well as on bone quality and mechanical strength (at adulthood) using an animal (rat tibia) model. This objective was achieved by conducting four interconnected studies. First, a safe yet high-resolution effective radiation dose was determined for repeated *in vivo* micro-CT scanning of the growing rat tibiae, which would not affect bone growth or microstructure. Secondly, rat tibial displacements vs strains relationships were established for the adolescent growing period via a strain calibration study. A computational modeling tool was also developed and validated for assessing bone strains under compressive loading. Thirdly, the effects of three different cyclic axial compression during puberty on bone growth, morphometry and biomechanics were assessed at skeletal maturity. Finally, the effects of three different cyclic axial compression during puberty on bone microstructure were assessed both at skeletal maturity and after almost a year of detraining period at adulthood.

In the first study, three micro-CT radiation doses of 0.83, 1.65 and 2.47 Gy were tested. The right tibiae of male Sprague-Dawley rats were scanned using an *in vivo* micro-CT scanning protocol from their 4th to 12th week of age with these radiation doses. The left tibiae were used as control. The left tibiae were only scanned on the last day, before sacrifice. Bone marrow cells were investigated, bone growth rates and histomorphometric analyses were performed, and bone structural parameters were determined for both left and right tibiae. Radiation doses of 1.65 and

2.47 Gy were found to negatively affect bone marrow cells, proliferative and hypertrophic zone heights, and bone growth rates in the irradiated tibiae. Also, both 1.65 and 2.47 Gy radiation doses significantly reduced bone mineral density, trabecular thickness, trabecular number and significantly increased trabecular spacing in the irradiated tibiae. Moreover, 2.47 Gy radiation doses significantly reduced cortical thickness during the scanning period. However, bone development and morphometry remained unaffected for the 0.83 Gy group. The 0.83 Gy radiation doses was then considered for further use in the project for repeated *in vivo* scanning of rats in the adolescent period, which would provide high-resolution images for morphometric investigation without interfering with bone growth.

In the second study, three groups of rats (4, 8 and 12 week old) were used for establishing rat tibial displacements vs. strains relationship. Target strain magnitudes were 450, 850, and 1250 $\mu\varepsilon$, which corresponded to peak strain values in the human tibia during unrestricted walking (450 $\mu\varepsilon$), zig-zag uphill running (850 $\mu\varepsilon$), and vertical jumping (1250 $\mu\varepsilon$) conditions. Strain gauges were installed at the medio-proximal surface of the rat tibiae and compressive displacements ranging from 0.5 mm to 3.5 mm were applied in a Haversine form at 2Hz frequency. The recorded displacements and strains were plotted in linear fit graphs to establish the required relationships. A micro-CT based finite element modeling approach was also developed, using 4, 8 and 12 week old rat tibiae, and applied to assess bone strains under experimental loading conditions. Computational results showed good agreement with experimental strains in the correlation analyses and Bland Altman analyses, which allowed validating the proposed modeling approach.

In the third study, five groups of rats were used to investigate the effects of cyclic axial compression in the short term period. The rats, initially aged 4 week old, were divided in control, sham, low impact (LI), medium impact (MI), and high impact (HI) groups. The right tibiae of LI, MI, and HI groups received cyclic axial compression corresponding to 450, 850, and 1250 $\mu\varepsilon$, respectively, for 5 days/week and for 8 weeks using a custom made axial compression loading device. Rats were sacrificed at 11 week of age. Trabecular and cortical bone structural parameters were determined by micro-CT, bone growth rate by calcein labeling and histomorphometry of growth plates by toluidine blue staining. Bone mechanical properties were evaluated from bending tests. HI loading reduced rat body weight (12.8%) and food consumption (17%) compared to shams. Bone growth rate was decreased in MI and HI groups by 6.5% and 10.5%, respectively. After 8 weeks of loading, HI group showed a significant increase in bone mineral density, trabecular thickness, cortical and

total surface area. Ultimate load and stiffness were also increased in MI and HI groups compared to shams. Overall, impact loading during adolescence moderately reduced bone growth, but simultaneously improved bone quality and biomechanics at the end of the growing period.

In the fourth study, five groups of rats (aged 4 week old) were used for investigating the effects of cyclic axial compression during adolescence in the long term period. Rats were divided into control, sham, low impact (LI), medium impact (MI), and high impact (HI) groups. The loading protocol was similar to the short term experiment, with 8 weeks of *in vivo* axial compressive loading from 4 to 11 week of age. After the loading regime, rats were kept in their cage for a detraining period of 41 weeks. At the age of 52 week old, they were sacrificed. Trabecular and cortical parameters were determined by micro-CT analyses and bone mechanical properties were evaluated from three-point bending tests. Selective muscles were also extracted and measured after the sacrifice. Finite element models of the 52 week old rat tibiae were generated for assessing the distributions of trabecular and cortical bone strains under compressive loading. HI and MI loadings reduced body weight and food intake at the end of the adolescence period and at the beginning of post-pubertal period. However, both body weights and food intakes eventually returned to a level similar to shams at maturity. HI and MI loadings increased cortical area, thickness and total area at the mid-shaft, and bone mineral density, trabecular thickness and bone volume fraction at the proximal tibiae. Cortical area, thickness, and bone mineral density benefits were lost by 41 weeks of detraining period at adulthood. However, loading-induced benefits on bone mechanical strength persisted at adulthood. Overall, high impact exercise performed during adolescence could provide long-term benefits for bone structure and strength.

Limitations of this research project include using only male rat tibiae for the entire project. Using both male and female subjects could have provided additional sex-dependent insights into bone changes associated with loading. Also, another possible limitation is the use of micro-CT measured outcomes as an indicator for trabecular bone quality. High impact loading increased trabecular morphometric parameters in our study. But if the modified trabecular geometry translates to stronger trabecular tissue or not has not been verified by mechanical testing. The use of a rat model is also associated with a limitation for cortical bone ability of resorption in a detraining period. This is caused due to the lack of secondary remodeling of Haversian canals, hence rats continue to grow until relatively late in life. However, previous studies observed bone remodeling in cortical bone structure of adult rat under mechanical loading conditions. Also, investigating the trabecular

morphometric properties only from the proximal metaphysis of the tibiae can be considered a limitation of this study. Including additional results from the distal part would have provided more detailed information about the loading induced changes throughout the entire tibial structure.

This project presents significant methodological and scientific contributions. A novel micro-CT based methodology was developed for segmenting trabecular and cortical bone microstructure and assessing the bone morphology without interfering with the bone growth and overall bone health. A micro-CT based finite element tool was also developed for non-destructively evaluating bone mechanics. Using a finely controlled and strain-calibrated loading protocol, this research has overcome current limitations of clinical or experimental studies trying to establish the effects of impact loading on bone growth and hence provided essential findings: high cyclic axial compression performed during puberty is moderately detrimental to bone growth, but benefits overall bone strength and mechanics at skeletal maturity, with these benefits persisting up to adulthood. On a clinical point of view, results of this project could lead to recommendations for training programs prescribed to young adolescent athletes involved in high impact sports.

TABLE OF CONTENTS

LIST OF TABLES

LIST OF FIGURES

LIST OF SYMBOLS AND ABBREVIATIONS

AL   Antero-lateral

AM   Antero-medial

BMD   Bone mineral density

BV/TV   Bone volume fraction

CaHA   Calcium hydroxyapatite

Conn.D   Connectivity density

CT   Computed tomography

Ct.Ar   Cortical bone area

CTDI   Computed tomography dose index

Ct.Th   Cortical thickness

Ec.Pm   Endocortical perimeter

HU   Hounsfield Unit

Ma.Ar   Medullary area

PL   Postero-lateral

Ps.Pm   Periosteum perimeter

Tb.N   Trabecular number

Tb.Sp   Trabecular Spacing

Tb.Th   Trabecular thickness

TMD   Tissue mineral density

Tt.Ar   Total area

VOI   Volume of interest

LIST OF APPENDICES

CHAPTER 1   INTRODUCTION

A fundamental precept for bone biomechanics is the adaptation of its microstructure in response to mechanical stimuli regularly imposed on it (Ahn & Grodzinsky, 2009; Duncan & Turner, 1995; M. K. Karlsson, 2004; S. J. Warden, Fuchs, Castillo, & Turner, 2005; Wolff, 1892). Mechanical loadings in the form of physical activity are considered beneficial for bone tissues and for the skeletal system, with enhanced bone quality as well as increased bone mass and mineral content (Chamay & Tschantz, 1972; S. J. Warden, Fuchs, Castillo, Nelson, & Turner, 2007; S. J. Warden et al., 2014; Wolff, 1892). Adolescence or pubertal period is a prime period for bone development, and bones respond more sensitively to the mechanical loadings at this particular growth period (Sievänen, 2012; Spengler, Morey, Carter, Turner, & Baylink, 1983; Weaver, 2002). Considering the many skeletal changes that could occur during adolescence, maintaining these loading effects at adulthood would greatly benefit the skeletal system, improving the overall bone health condition (Health & Services, 2004; Rizzoli, Bianchi, Garabédian, McKay, & Moreno, 2010).

Previous clinical and experimental studies on the effects of loading on bone microstructure hold contradictory results. Few clinical studies reported that normal physiologic activities during childhood could negatively affect bone growth (Bernink, Erich, Peltenburg, Zonderland, & Huisveld, 1983; Caine, Lewis, O'Connor, Howe, & Bass, 2001; Haywood, Clark, & Mayhew, 1986; Lindholm, And, & Ringertz, 1994; Tanghe et al., 1996; Theintz, Howald, Weiss, & Sizonenko, 1993). However, the studies were not well controlled and failed to separate the effects of nutritional factors from mechanical factors. Several experimental studies reported contradictory findings (positive and negative) on the effects of mechanical loading during adolescence (Bourrin, Palle, Pupier, Vico, & Alexandre, 1995; Forwood & Parker, 1987; Niehoff, Kersting, Zaucke, Morlock, & Brüggemann, 2004; Snyder, Zierath, Hawley, Sleeper, & Craig, 1992). Hence, changes in bone microstructure and longitudinal bone growth due to the application of impact loading during adolescence remain to be determined. Moreover, both clinical and experimental studies have been conducted for assessing the possible remaining effects of pubertal exercise on bone structure at adulthood (Bass et al., 1998; Duckham et al., 2014; Gunter et al., 2008; Honda, Sogo, Nagasawa, Kato, & Umemura, 2008; Iwamoto, Yeh, & Aloia, 2000; M. Karlsson et al., 2000; Kontulainen et al., 2001; Kontulainen, Sievänen, Kannus, Pasanen, & Vuori, 2003; Nordström, Olsson, & Nordström, 2005; Pajamäki et al., 2003; S. J. Warden et al., 2007; S. J. Warden et al., 2014).

However, results are again inconsistent on the effects prevailing at adulthood period. Few studies reported the positive effects of pubertal exercise in the long term period (Bass et al., 1998; Duckham et al., 2014; Honda et al., 2008; M. Karlsson et al., 2000; Kontulainen et al., 2001; Kontulainen et al., 2003; S. J. Warden et al., 2007; S. J. Warden et al., 2014), whereas others reported the absence of any skeletal benefits at adulthood (Gunter et al., 2008; Iwamoto et al., 2000; Nordström et al., 2005; Pajamäki et al., 2003). Hence, it is not clearly determined whether impact loading applied during adolescence would affect bone development, quality, and mechanical strength at maturity or how long these effects would remain.

The main purpose of this thesis was to investigate the effects of *in vivo* dynamic impact loadings applied during the adolescence on bone growth, quality and mechanical strength at the end of the growing period as well as effects of loadings on bone quality and mechanical strength after a detraining period at adulthood. To do so, several complementary studies, including investigating a safe radiation doses limit for growing bone, establishing a displacement-strain relationship in the growing bone, developing a non-invasive micro-CT based finite element tool, and completing a symmetry analysis of contralateral limb, etc. were performed.

This thesis includes ten chapters and is submitted as an article-based thesis. Following the Introduction, Chapter 2 presents a literature review on the context of the research, the state of knowledge on mechanobiology of the longitudinal bone growth, bone biomechanics, and bone adaptability to mechanical loading in the form of physical exercise. Chapter 3 introduces the rationale, research questions and objectives of the project. The body of this thesis is composed of four principal articles presented in Chapters 4 to 7. Chapter 4 presents the first article entitled: "*Can repeated in vivo micro-CT irradiation during adolescence alter bone microstructure, histomorphometry and longitudinal growth in a rodent model?*", which was published in PloS one Journal. This article investigates the radiation effects on bone morphometry, bone marrow cells, bone growth rate and growth plate histomorphometry in growing tibiae for three radiation doses from repeated *in vivo* micro-CT scanning in adolescent rats to determine a safe dose level for repeated use in the adolescent period. Chapter 5 introduces the second article entitled: "*Experimental and finite element analyses of bone strains in the growing rat tibia induced by in vivo axial compression*". This article was published in Journal of the Mechanical Behavior of Biomedical Materials and develops the displacement-strain relationship in the growing rats and introduces a finite element modeling tool for validating the experimental bone strains. Chapter 6

presents the third article entitled: "*High Impact Exercise Improves Bone Microstructure and Strength in Growing Rats*", submitted to the Scientific Reports. In this chapter, the effects of *in vivo* impact loadings applied during puberty on bone growth, quality, and mechanics of the bone microstructure at the end of the growing period are discussed. Chapter 7 presents the last article of this thesis entitled: "*Impact Exercise during Adolescence Improves Bone Microstructure and Strength at Adulthood*", submitted to the Journal of Bone and Mineral Research. In this chapter the effects of *in vivo* impact loadings applied during puberty on longitudinal bone development, morphometry and biomechanics are evaluated at the end of puberty as well as at the adulthood. Chapter 8 discusses the overall results of the project and establishes connections between the four articles and the reviewed literature. Chapter 9 summarizes the key contributions of this thesis to the advancement of knowledge in mechanical engineering. Finally, Chapter 10 presents the overall contributions of this thesis and recommendations that future studies.

CHAPTER 2   LITERATURE REVIEW

2.1 Skeletal system

The skeletal system, which is composed of bones, cartilages, ligaments, and other tissues, undertake fundamental functions for the human body. Bones are considered rigid tissues, which contain embedded cells with abundant hard intercellular material, blood, nerves, and other connective tissues (Currey, 2014; Hinwood, 1997). At birth, the human body consists of 300 soft bones. During the growing period and throughout the adolescence, the fusion of some soft bones takes place, and eventually, a total of 206 bones compose the human skeleton at adulthood (Markings, 1995). Bone continues to grow in length and width throughout the adolescent period or childhood. Our skeleton continues to repair itself at the microstructural level as a part of the bone remodeling process (Bourne, 2014). The major functions of bone include: (1) structural support for our body, (2) protection of vital organs and tissues, (3) storage for minerals, and (4) protective environment for marrow (the location for producing white blood cells) (D. B. Burr & Allen, 2019).
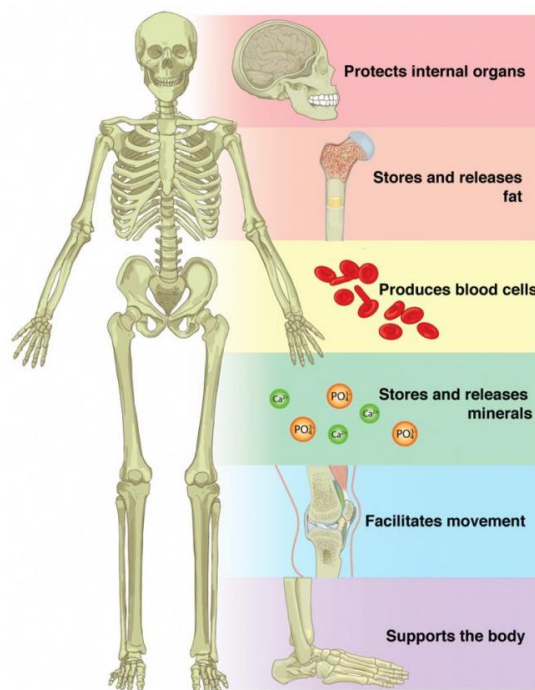
Figure 2.1 Functions of the skeletal system (Adapted from Anatomy and Physiology, Oregon State University, 2019)

2.2   Bone Structure and Composition

2.2.1   Bone Structure

A typical long bone is shown in Figure 2.2. A long bone generally comprises two main parts: the diaphysis and the epiphyses. The epiphysis consists in the main or midsection (tubular shaft) of the bone. It is located between the proximal and distal side of the bone and is mainly composed of dense compact bone. This compact bone surrounds a central marrow cavity structure, which contains red or yellow marrow (Figure 2.2). The epiphyses are the rounded ends of the long bone. Proximal and distal epiphyses are filled with red bone marrow. The narrow area between the epiphysis and diaphysis is called the metaphysis, which contains the epiphyseal plate (or growth plate) (Figure 2.2). The epiphysis is covered with articular cartilage and the zone situated below this region known as the subchondral bone.
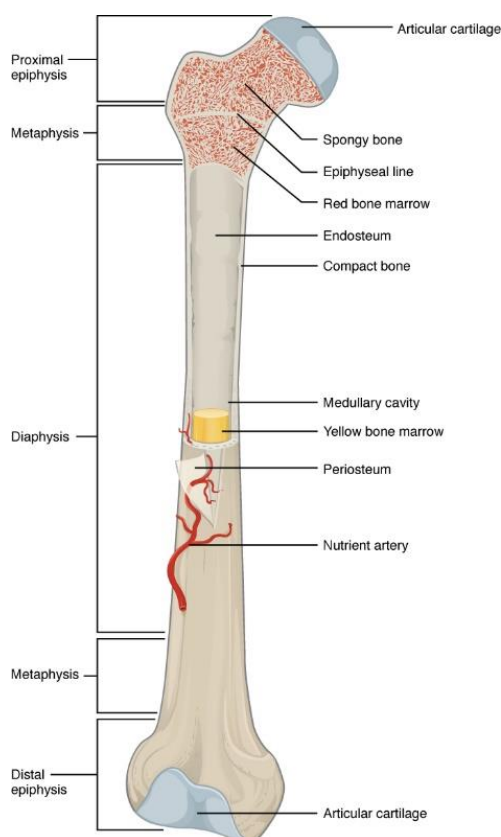
Figure 2.2 Anatomy of a typical long bone (Adapted from Anatomy and Physiology, Rice University, 2013)

2.2.2 Bone Composition

Bone structural pattern is nonhomogeneous. At the macroscopic level, bone is composed of two types of osseous tissue that are identified as trabecular (or cancellous or spongy) and cortical (or compact) bones. Bone is mainly composed of cells embedded in an organic extracellular matrix of fibers. A ground substance also consists of a large portion in the tissue structure. Constitutive cells for bone formation are three types: Osteoblasts, Osteocytes and Osteoclasts. Osteoblasts are bone-forming cells. They are connective tissue cells and found at the bone surface. Osteoblasts generate osteoid, a protein mixture, which eventually mineralizes to become bone. Osteoblasts can be differentiated as osteocytes under stimulation. Osteocytes are mature bone cells. They are trapped and surrounded by the bone matrix. Bone formation, maintenance of matrix and homeostasis of Calcium are the primary functions of osteocytes. Osteoclasts are responsible for bone resorption and remodeling. They are large, multinucleate cells located on bone surfaces in resorption pits.

Cortical bone has a dense structure and forms the outer shell or cortex of the bone. At the cortical bone microscopic level, the structural unit responsible for bone composition is called the osteon, or haversian system (Figure 2.3a). A small canal, the Haversian canal, is situated at the center of each osteon. This canal accommodates blood vessels and nervous fibers. The structural components of the osteon comprise of a concentric series of layers (lamellae) of the mineralized matrix, which surrounds the central canal. Small cavities known as lacunae can be found near the boundaries of each layer, or lamella. The lacunae contain an osteocyte, which is a bone cell and has entombed itself within the bony matrix (Figure 2.3). Also, there exists a number of small channels, called canaliculi. These canals radiate from each lacuna, then connect the lacunae of adjacent lamellae and finally reach the haversian canal (Figure 2.3a). Bone's resistance behavior to mechanical stress is largely contributed from the effective cross-liking of the collagen fibers within the osteon. This feature also accounts for the vulnerability of the cement line, which is considered the weakest portion of the bone microstructure. The cement line is also responsible for the fatigue behavior of the cortical bone, which takes place by dissipating energy through crack propagation. Cracks and micro damages are thus confined to more densely mineralized interstitial bone located between osteons (Hernandez & Keaveny, 2006).

Trabecular bone is composed of trabeculae, which are thin rods or plate shape structure. Red marrow is located between the trabeculae (Figure 2.3b). Trabecular bone does not contain

Haversian canals. Its tissue structure is arranged in a concentric lacunae pattern containing lamellae. Osteocytes receive nutrients through blood vessels, which are located in the red marrow zones. Trabecular bone is surrounded by cortical bone, but its relative thickness varies significantly among bones in accordance with varying functional tasks. Bone marrow is made of blood vessels, nerves, and various cells. This marrow is of importance because of its contribution to blood cells generation during bone load application. It is highly osteogenic in nature and is capable of stimulating bone formation in any parts of the body.

The periosteum is a fibrous layer covering the bones, everywhere except at the joint surfaces, where bones are covered with articular cartilage. Periosteum is permeated by blood vessels and nerve fibers, which lead to the bone via Volkman's canals.
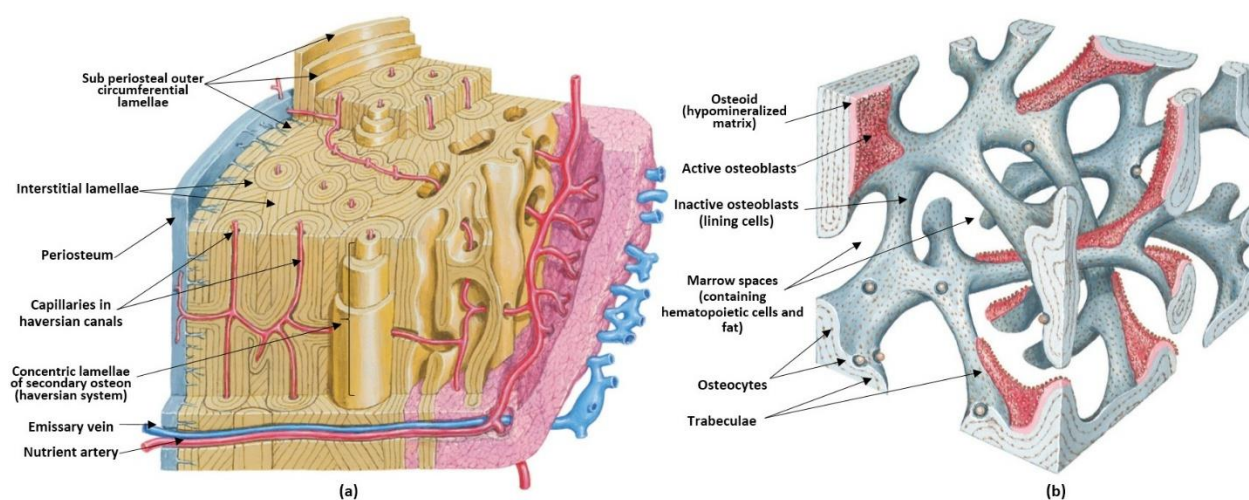
Figure 2.3 (a) Structure of cortical (compact) bone; (b) Structure of trabecular bone. (Iannotti & Parker, 2013)

2.3 Bone Growth and Remodeling

2.3.1 Bone Growth

Bones are important part of the skeletal system, and they begin to form before we are born. After birth, bones grow very fast, then the growth slows down rapidly and again increases the growth later in infancy. Bones continue growing throughout childhood and adolescence.

2.3.1.1   Transverse growth

The width of growing bones increases through appositional growth at the endosteal and periosteal surfaces. This process is called intramembranous bone formation.

<u>Intramembranous bone formation</u>

Intramembranous ossification involves the bone formation process from the mesenchymal connective tissue. This process starts in utero and prevails throughout fetal development. Intramembranous ossification continues till the end of adolescence (Karaplis, 2008). It takes place mostly in flat bones of the skull, the mandible, and the clavicles (collarbones). During the process of intramembranous ossification, the bones are built up from connective tissues. Intramembranous ossification is also an essential process for the rebuilding of broken or damaged bones and natural healing of bone fractures (Brighton & Hunt, 1991).

<u>Stages of intramembranous bone formation</u>

The process of intramembranous ossification of bones is presented in Figure 2.4. It begins with the clustering of mesenchymal cells in the embryonic skeleton and forming specialized cells through the differentiation process (Figure 2.4a). Some of the cells differentiate into capillaries, others transform into osteogenic cells and osteoblasts. Early osteoblasts usually appear in a cluster known as an ossification center (Tortora & Derrickson, 2017).

The osteoid is secreted from osteoblasts and hardens shortly (in a few days) (Figure 2.4b). Then mineralization of osteoid takes place and the osteoblasts transformed into osteocytes in an entrapped condition (Takahashi & Takahashi, 1999; Wojnar, 2010). New osteoblasts are generated through the differentiation process of surrounding cells.

Trabecular matrix is generated through the secretion of osteoid near the capillaries. Osteoblasts located on the trabecular surface become the periosteum (Figure 2.4c). Periosteum then surrounds the surface of the trabecular bone and form a layer of compact bone. Blood vessels get clustered near the trabecular structure, which eventually condensed and forms red marrow (Figure 2.4d) (Dennis, Berkland, Bonewald, & Detamore, 2014; Karaplis, 2008).
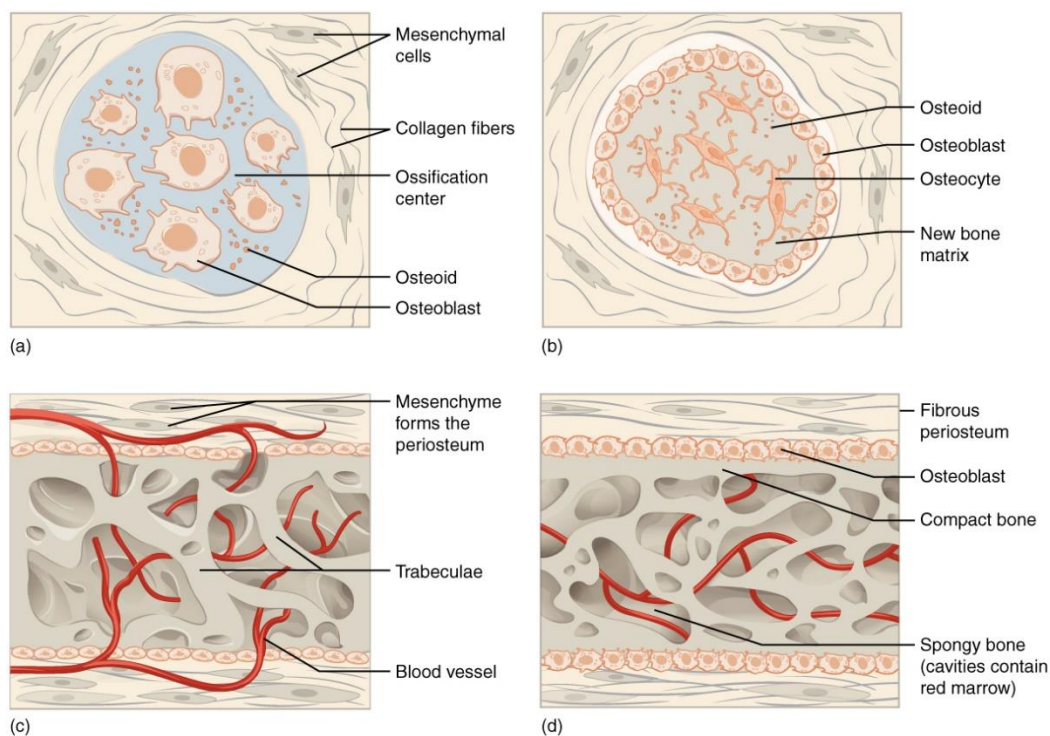
Figure 2.4 Intramembranous ossification comprises four steps: (a) mesenchymal cells group into clusters and ossification centers form; (b) secreted osteoid traps osteoblasts, which then become osteocytes; (c) trabecular matrix and periosteum form; (d) compact bone develops superficial to the trabecular bone, and crowded blood vessels condense into red marrow *(Adapted from Anatomy and Physiology, Rice University, 2013)*

2.3.1.2   Longitudinal growth

Longitudinal growth of long bones and vertebrae develops through the process of endochondral ossification. This process occurs at the epiphyseal growth plates. Longitudinal growth continues until the end of adolescence when growth plates close (Villemure & Stokes, 2009).

The longitudinal section of a growth plate is shown in (Figure 2.5). This cartilaginous tissue is histologically divided into three zones. From the epiphysis to the metaphysis, these zones are identified as: (1) the reserve, (2) the proliferative, and (3) the hypertrophic zones (Dennis et al., 2014; Karaplis, 2008).

The reserve zone (Figure 2.5) lies directly adjacent to the bone epiphysis. Chondrocytes of small size are scattered irregularly throughout its extracellular matrix. This zone does not directly take

part in the longitudinal growth process (Tortora & Derrickson, 2017), but it provides a poll of chondrocytes within the matrix. It also serves to affix the plate to the bone of the epiphysis, and to accommodate the capillaries in the spaces between it. Surrounding bone is the source of the nutrients that, by diffusion, nourish chondrocytes in the other zones of the growth plate (D. B. Burr & Allen, 2019).

The proliferative zone (Figure 2.5) is composed of young proliferating chondrocytes. These cells, which are commonly flattened and partly wedge-shaped, are piled on top of one another like stacks of coins so that they form columns parallel to the longitudinal growth direction. It seems likely that the columnar arrangement is maintained because collagenic fibrils in the partitions of intercellular substance between the columns run longitudinally. Enough cells must be produced at this site in order to replace the dead cells at the diaphyseal surface of the disk (Clarke, 2008; Marks Jr & Odgren, 2002).

The hypertrophic zone (Figure 2.5) contains chondrocytes in various stages of maturation. The cells of this zone, which were priorly in the proliferative zone, gradually mature, become larger and accumulate glycogen in their cytoplasm. They take up more space and, therefore, expand the epiphyseal growth plate longitudinally. They eventually undergo apoptosis. The epiphyseal plate is expanded along the bone axis both by the proliferation of chondrocytes in the second zone and by their maturation in the third zone. At the bottom of the hypertrophic zone, the area around the chondrocytes becomes increasingly calcified. This calcified zone abuts directly on the diaphysis where it is invaded by both capillaries and osteogenic cells from the diaphysis (Ross, Kaye, & Pawlina, 2003; Su et al., 2018).
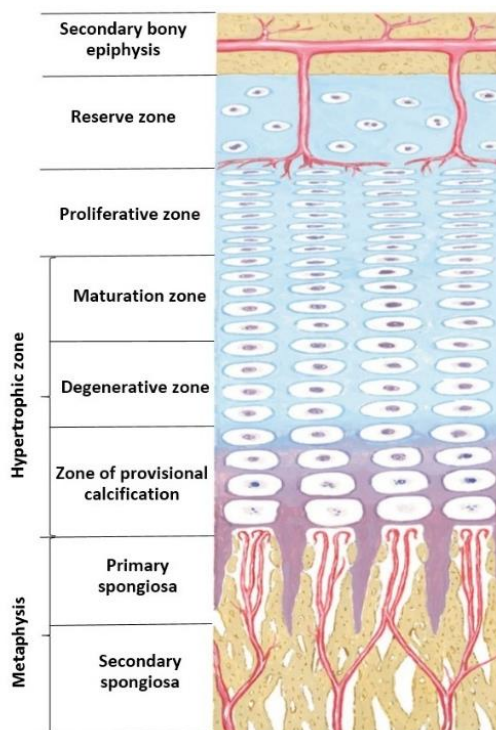
Figure 2.5 Typical section of a growth plate showing its reserve, proliferative and hypertrophic zones (Iannotti & Parker, 2013)

Factors controlling longitudinal growth

Many factors can alter longitudinal bone growth. Some of them are physiological (i.e. systemic dietary, nutrition, hormonal etc.) and some of them arise from pathological conditions (i.e. genetics and mechanical environment) (Mackie, Ahmed, Tatarczuch, Chen, & Mirams, 2008; Myllyharju, 2014; Trueta & Morgan, 1960; Van der Eerden, Karperien, & Wit, 2003).

A. Dietary and nutritional factors

Normal bone development needs regular and optimal dietary intake. Any irregularity in the dietary condition may lead to deficiency pattern and negatively influence endochondral bone formation affecting bone growth (Cashman, 2007). In the occurrence of irregular food intake and dietary disturbances, body weight can also be decreased in parallel to the reduction in skeletal bone growth (Owens, Dubeski, & Hanson, 1993).

Nutrition is another parameter that can affect endochondral bone growth. For example, in vitamin D deficiency, irregular thickening of growth plate occurs due to the failure of vascularization in the uncalcified cartilage of the plate (Holick, 1996). In vitamin C deficiency, the metaphysis is affected so that the bone formation process is reduced. However, the proliferation and calcification of cartilage remain unaffected under such condition (Aghajanian, Hall, Wongworawat, & Mohan, 2015). The normal bone growth process is reported to be affected in both excess and deficiency of vitamin A (Wolbach, 1947), the presence of a sufficient amount of vitamin A being required for a normal bone growth process.

B. Hormonal factors

The rate of skeletal growth can be affected by hormones. These factors can influence the skeletal growth during adolescence and also the maturity process of the bone structure at adulthood (Follis Jr, Park, & Jackson, 1952). The major hormones involved in bone growth and development include the hormones of the pituitary, the adrenals, the thyroid, and the gonads (Sissons & Hadfield, 1955). Pituitary abnormalities can lead to dwarfism and can also be held responsible for acromegaly and giantism. The absence of thyroid hormone can result in histological changes of the epiphysial plates. Hypothyroidism can delay the appearance of ossification centers and cause bone growth retardation. It has been found that cortisone can influence skeletal growth in chick embryo as well as in intact animal researchers (Karnofsky, Ridgway, & Patterson, 1951; Sissons & Hadfield, 1955).

C. Genetic factors

Genetic factors are well known for determining the general body size, however, they also play a vital role in bone growth and development. Several conditions associated with mutant genes result in skeleton abnormalities, such as brachydactyly, syndactyly, osteogenesis imperfecta, osteochondrodystrophies, multiple exostoses etc. (Marini & Brandi, 2010). One of such conditions is the achondroplasia genetic disorder, which can negatively affect endochondral bone growth of the skeleton (Cockayne, 1933). Several other bone diseases have been debated to be originated from a genetic disorder, but a detailed genetic study of such abnormalities was never executed. Moreover, it is rather difficult to analyze the exact effect of genetic factors on bone growth in humans, whereas, the animals are considered to be best suited for such studies. A study by Griineberg (Green, 1948) reported retardation of bone growth in the rat and the mouse sample due

to the negatively affected cartilage by genetic conditions. However, bone growth suppression is not always considered as a primary contribution from the genetic condition, rather they sometimes persist due to the secondary effects from the hormonal imbalance in the developing skeletal system.

D. Mechanical modulation of bone growth

The mechanical environment can also influence bone growth in certain circumstances. Mechanical modulation of bone growth specifically applies to growing bones according to the Hueter-Volkmann principle (Aronsson, Stokes, Rosovsky, & Spence, 1999; Mente, Aronsson, Stokes, & Iatridis, 1999). Indeed, this principle stipulates that increased compression on growth plates reduces growth according to Hueter's law (1862). Conversely, decreased compression stimulates growth according to Volkmann's law (1869) (Villemure, 2002). Numerous *in vivo* studies on several animals and bone sites have provided scientific evidence for this principle (Cancel, Grimard, Thuillard-Crisinel, Moldovan, & Villemure, 2009; Mente et al., 1999; Valteau, Grimard, Londono, Moldovan, & Villemure, 2011), particularly the work of Stokes et al. (I. Stokes, 2002; Ian AF Stokes, Aronsson, Dimock, Cortright, & Beck, 2006; Ian A Stokes, Gwadera, Dimock, Farnum, & Aronsson, 2005).

2.3.2 Bone Remodeling

2.3.2.1 Physiologic skeletal development related to bone remodeling

Bone modeling (uncoordinated formation and resorption) starts in fetal life and this process sustains till the end of the growing period (beginning of early adulthood phase) (Raisz, 1999). This process occurs through the removal of bone from one site and formation of bone at different sites. Peak bone mass is achieved through bone modeling. After the adolescent period, this bone modeling process still continues (Crockett, Rogers, Coxon, Hocking, & Helfrich, 2011). But this time, the old bone gets replaced by the newly formed bone at the same location. This maintenance phenomenon is called bone remodeling (Crockett et al., 2011; Raisz, 1999; Siddiqui & Partridge, 2016). The skeletal system undergoes continuous remodeling throughout life due to its metabolically active state condition. In order to preserve the structural integrity of the skeleton and to act as a storehouse of calcium and phosphorus, bone remodeling is imperatively needed (Hadjidakis & Androulakis, 2006). Old bones can get damaged due to aging or daily physical loading. So, bone remodeling is essential for replacing damaged bone tissue. Any hindrance in such

activity could lead to the condition of osteoporosis, which is considered to be a worldwide health concern (Courpron, Meunier, & Vignon, 1975). The entire process of bone remodeling is coordinated through a number of cells in a composed manner. This process mainly comprises two phases, namely bone formation and bone resorption. Moreover, a parity between these two phases is crucial for preserving bone mass and systemic mineral homeostasis (Courpron et al., 1975; Hadjidakis & Androulakis, 2006; Parfitt, 1982; Peltz, Brewer, Bernstein, Hart, & Ross, 1991).

Phases of bone remodeling

To achieve a normal physiological bone remodeling, a balance between bone formation and bone resorption is required. For the proper functioning of these two processes, a direct communication is needed to be established among different bone cells. Bone forming cells (osteoblasts and osteocytes) and bone resorbing cells (osteoclasts), together with their precursor cells, are arranged in specialized units called bone multicellular units (BMU) (Courpron et al., 1975). This BMU unit act primarily to achieve normal physiologic bone remodeling. Bone remodeling cycle comprised of controlled sequential phases (Figure 2.6). The first phase, the activation phase (Siddiqui & Partridge, 2016), is responsible for detecting the remodeling signal, which has usually been described as resorption by osteoclasts (Figure 2.6). The second phase is the resorption, where osteocytes are generated by osteoblasts in response to signals. The duration of the resorption phase usually depends on the differentiation and activity of the responsible stimulus for the osteoclast (Figure 2.6). The third phase is the reversal, where all osteoclasts are disappeared in a composed manner (Figure 2.6). The fourth phase is the formation, where the osteoclastic cells get replaced by the osteoblastic cells. Next, the termination of bone remodeling initiates by the osteoblast differentiation. The next phase is the quiescence, where the newly modified bone surface is maintained till the next cycle of bone remodeling gets initiated (Figure 2.6) (Siddiqui & Partridge, 2016).
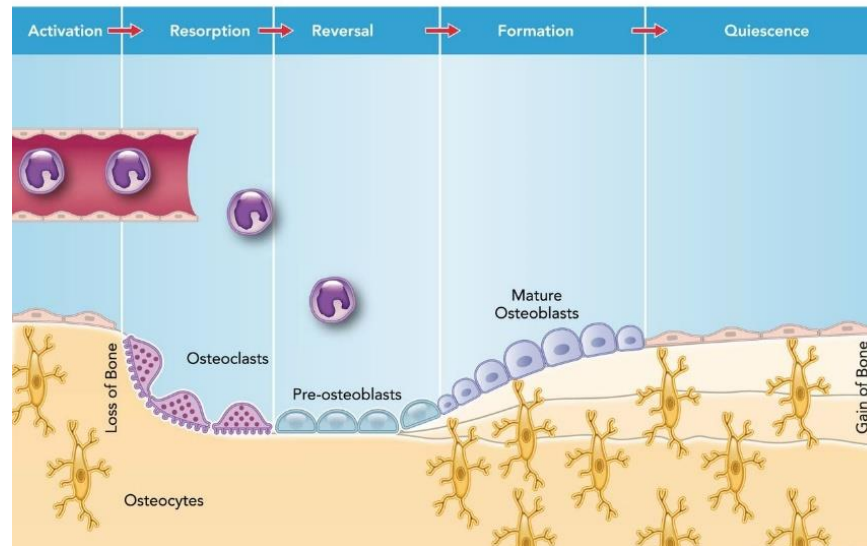
Figure 2.6 Schematic of physiological bone remodeling (Siddiqui & Partridge, 2016)

2.3.2.2 Mechanical loading induced bone modeling and (re)modeling

Our skeletal system is designed to sustain imposed mechanical loading. The adaptation of bone tissue under mechanical stress and the resulting morphological modification was proposed earlier back in 1880s. This idea was first proposed in a qualitative form by Roux in 1881 and in a mathematical form by Wolff in 1892 (Ruff, Holt, & Trinkaus, 2006). Roux stated that bone cells have the property of reacting with functional stimuli and respond by establishing locally appropriate structural changes of bone tissue (Roux, 1881). Wolff's law stated that bone structures are oriented in form and mass to resist better to the extrinsic forces (Wolff, 1892). Wolf's law additionally implies that the under mechanical stress condition, trabecular structure reacts rapidly by rearranging the trabeculae, which is followed by the cortical bone structure modification (Winkelstein, 2012). This bone remodeling theory based on the mechanical stimuli gives an insight into the existence of variation in bone tissue structure depending on their locations in the skeletal system. This phenomenon can be seen in a professional tennis player who has a bigger bone in the serving arm resulting from the adaptation of bone undergoing increased loading (H. H. Jones, Priest, Hayes, Tichenor, & Nagel, 1977). Also, an effect of disuse of bone can be seen from the bone loss suffered by the astronauts experiencing microgravity in space (Vico et al., 2000).

<u>Process of mechanical loading induced bone remodeling</u>

Different animal studies have been performed to assess the response of bone cells under mechanical loading condition. Several *in vitro* studies have confirmed the responding nature of individual bone cells (i.e. osteocytes and osteoblasts) under applied mechanical stimulus (Crockett et al., 2011). The same actors (cells) responsible for maintaining the normal physiologic bone remodeling are also involved in the mechanical bone remodeling process. However, the signals, which are produced at an earlier time point due to loading, include prostaglandins, nitric oxide, and signaling proteins (Bonewald & Johnson, 2008; Jacobs, Temiyasathit, & Castillo, 2010). In osteocytes, activation of the signaling proteins initiates after experiencing fluid shear stress from external loading (Huesa, Helfrich, & Aspden, 2010; Norvell, Alvarez, Bidwell, & Pavalko, 2004; Santos, Bakker, Zandieh-Doulabi, de Blieck-Hogervorst, & Klein-Nulend, 2010). The exact mechanism of the signal initialization and sensing of imposed loading by bone cells *in vivo* are still needed to be determined. However, the basic principle from this mechanically induced bone remodeling has been used for designing mechanical therapies to increase bone mass and to fight against osteoporosis (Cardoso et al., 2009).

2.4   Bone biomechanics

The prime and foremost role of the skeleton is to withstand load bearing. The skeletal system is designed in such a way that it protects internal organs. Also, the system provides rigid supports and attachment sites for muscles to generate body movement or to provide stability. Bone has state of the art inherited properties, which allow it to carry out these vital roles. Bone is a living tissue and a complex structure, and as such, it is vulnerable to disease, injury, and effects of aging. This vascularized hardened tissue is composed of an organic phase (mainly collagen) and inorganic phase (mineral hydroxyapatite) in order to meet its mechanical characteristics (Smith, 1983). Bone stands out as one of the body's hardest materials, with dentin and enamel in the teeth being harder than bone.

2.4.1   Mechanical testing and mechanical properties

Constitutive relations

The biomechanical behavior of bone under different loading conditions is mainly assessed by its rigidity, strength and hardness response. Rigidity refers to the stiffness of bone and its resistance to change of shape, strength refers to its resistance to fracture while hardness is characterized by

bone's resistance to penetration and a permanent indentation. Bone mechanical response depends on its mechanical and geometric properties as well as on its loading mode, direction, rate, and frequency.

2.4.1.1 Elasticity

Bone strength can be assessed from the developed relationship between the imposed loading (external force/stress) and the corresponding bone geometrical change (displacement/strain) under specific test configurations. This curve is also known as the load-deformation (or stress/strain) curve (Holtrop, 1975). An example of the load-deformation curve is presented in (Figure 2.7). Under mechanical loading, bone can deform with volumetric and/or angular changes. Bone deformation refers to any changes in the size or shape of the bone due to an imposed force. When this deformation takes place, a limit up to 3% in deformation is considered to be an elastic limit in the load-deformation curve (Holtrop, 1975). This is called an elastic limit because if the loading is removed at this point, bone recovers and returns to its original undeformed state. This curve is used to assess the strength and rigidity of a material (Hay, 2013; Holtrop, 1975). The curve presents the elastic region, yield point, plastic region, and ultimate failure point. The elastic region represents the phase of the material when it is perfectly elastic. The material will return to its original position if it is unloaded before crossing of this elastic region (Figure 2.7). The yield point is defined as the stress (load) after which the material deformation occurs more quickly with no or little increase in load (Figure 2.7).
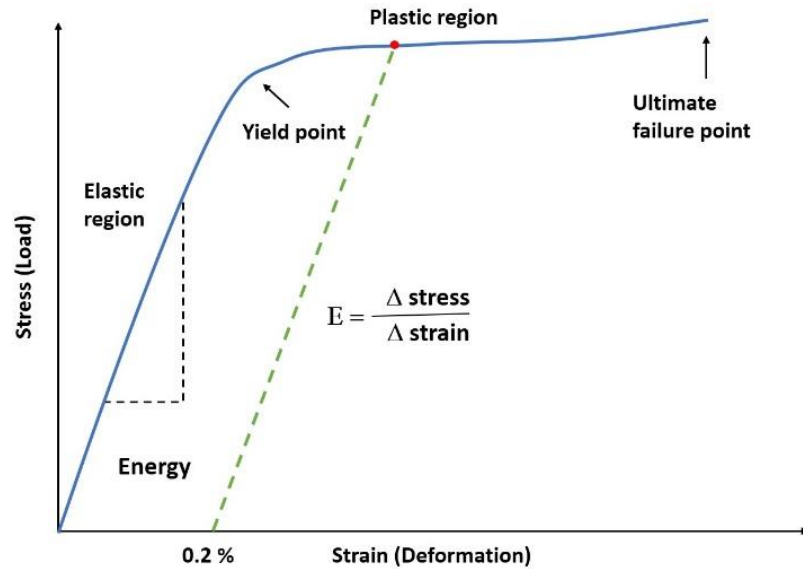
Figure 2.7 The load-deformation curve illustrates the performance strength characteristic of a material when subjected to the load. During the load application, an (A) initial elastic response prevails and leads to a (B) yield point. With further loading, it goes into the (C) plastic response when the material is deformed permanently or is broken. The strength of the material is determined by the (D) energy or area under the curve. The elasticity module (or rigidity) is determined by the (E) slope of the curve during the elastic response phase (Bankoff, 2012)

2.4.1.2 Plasticity

As the loading application continues in the non-elastic zone, bone tissue will start to yield. Bone micro-cracks will start to form at this point. This yield point marks the end of the elastic limit. If loading continues beyond this point, then the bone will reach to the plastic region of the load-deformation curve (Hay, 2013; Holtrop, 1975) (Figure 2.7). Bone tissue starts to deform permanently in this phase and even if the load is completely removed at this phase, there will remain a permanent deformation in the bone (Bankoff, 2007; Hay, 2013; Holtrop, 1975). If loading continues beyond this phase, then this will lead to ultimate failure (Figure 2.7). The ultimate failure point is the maximum load that a material can sustain before completely breaking. After this point, the material has very limited (zero) strength to bear additional loading.

2.4.1.3 Viscoelasticity

Bone also exhibits viscoelastic behavior, although not as much as soft tissues such as articular cartilage, intervertebral disc, ligaments and tendons, etc.. This implies that its mechanical behavior depends on the rate of loading along with the duration. Bone becomes stiffer and can sustain higher loading until failure with an increasing loading rate. Bone stores more energy while loaded at higher rates (Figure 2.8). The loading rate has clinical significance as it controls fracture patterns and tissue damage at failure. When the bone is fractured, the stored energy is released. At a lower loading rate, the energy dissipation is less and can cause minor cracks with less damage to bone and soft tissues. With a higher loading rate, the energy dissipation is greater, and can cause more severe bone and soft tissue damages.
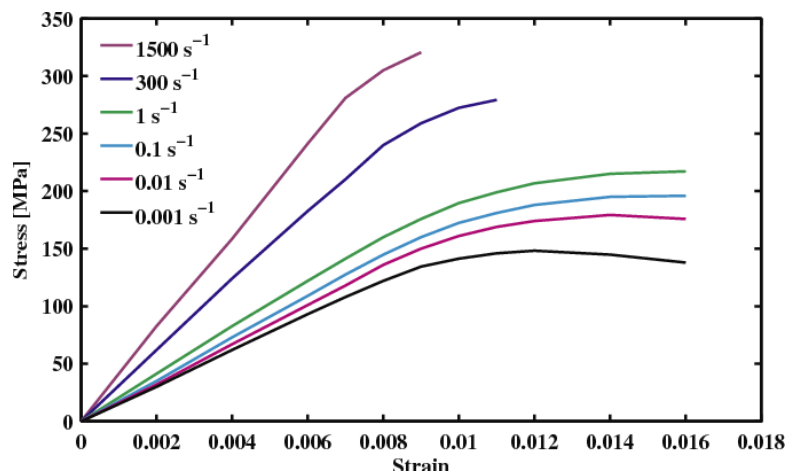
Figure 2.8 Viscoelasticity of bone tissue as a function of strain rate (cortical bone) (Johnson, Socrate, & Boyce, 2010)

Mechanical testing

Bone mechanical testing is conducted to assess the mechanical properties of whole bones or bone tissues under various loading conditions. Generally, bone mechanical testing is similar to the process applied in other structural materials and composites. Testing methods are based on fundamental principles of mechanics (Evans & Lebow, 1952; Gerard, 1961; Roark, 1954). They include monotonic loading procedures (tension, compression, torsion, bending, and fracture toughness test) and dynamic loading procedures (progressive loading, fatigue loading, and dynamic mechanical analysis). The most widely used techniques are detailed in the next sections.

2.4.1.4   Compression and Tension

Both tension and compression tests are considered as standard uniaxial tests. In both cases, the specimens are loaded in a mechanical testing machine, and axial load or displacement is applied.

Compressive Test Specimen Preparation and Setup

Specimens for compressive tests are usually prepared as cylindrical or square samples. To avoid the unwanted buckling during the test, the height to width ratio (aspect ratio) is generally kept lower than 2.0 (Norma, 2005). Before placing the specimen under the loading platens, the specimens are polished sufficiently to ensure the parallelism of its two ends. An extensometer is attached often for shortening measurement. With an additional extensometer attached for lateral deformation measurement, the Poisson's ratio in compression can be measured by combining the measurement from attached strain gage. For testing trabecular bones, both ends can be embedded in plastic resins to ensure uniform load application on the specimens.
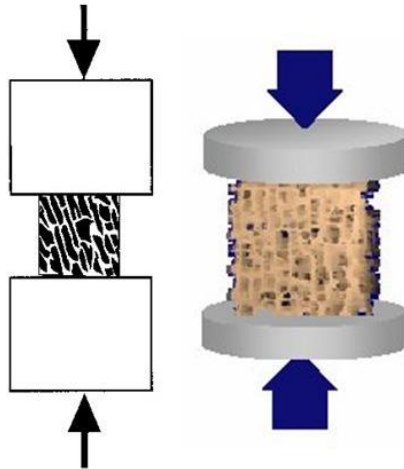
Figure 2.9 Compression test setup for trabecular bone samples (Adapted from Mechanics of Bone by Bethany Jacobs, 2017)

Tensile Specimen Preparation and Setup

Specimens have gripping regions at both ends and are usually attached to strain gauges for displacement measurement. The gripping regions are clamped tightly to avoid any sliding during experimentation. An extensometer can be attached in the gage region for elongation measurement. With an additional extensometer, it is possible to measure the width change and the Poisson's ratio

in tension. To avoid the accidental crushing of trabecular bone under large gripping forces, both ends of the specimen can be embedded in plastic resins to ensure secure clamping without failure.
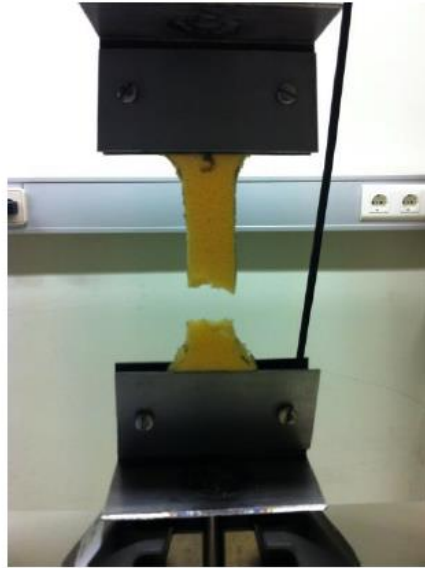
Figure 2.10 Tensile strength test setup (Adapted from the European Space Agency)

Experimental Procedure

Specimen are generally loaded until failure under tension or compression loading at a constant loading rate. The test can either be force controlled or displacement controlled. The required load (P) and elongation (or shortening) in the gage region (δL) can be estimated with the extensometer. The uniaxial stress can be calculated as: $\sigma = \dfrac{P}{A}$, with A being the cross-sectional area of the specimen in the gage region. Moreover, the axial strain (ε) can be calculated as: $\varepsilon = \dfrac{\delta L}{L_o}$, with δL being the elongation of the specimen and L_o is the original gage length. If the deformation in width (δW) is measured, the lateral strain (ε_L) can be determined as: $\varepsilon_L = \dfrac{\delta W}{W_o}$ and Poisson's ratio in tension can be calculated as: $\nu = -\dfrac{\varepsilon_L}{\varepsilon}$.

Determination of Mechanical Properties

Experimental stress-strain curves can be obtained by plotting the stress with respect to the strain as in (Figure 2.7). The following mechanical properties can then be obtained from the graph: elastic modulus (rigidity), yield stress/strain, ultimate stress, strain at failure, and toughness. The elastic modulus is measured as: $E = \dfrac{\Delta\sigma}{\Delta\varepsilon}$ in the elastic part of the curve. The yield stress is determined using the 0.2% strain offset method (Figure 2.7). At yield point, the values of stress and strain are considered as the yield stress, σ_{ys} and the yield strain, ε_{ys}, respectively.

2.4.1.5 Three- and four-point bending

Bending test of bone tissue is generally carried out in two different configurations: three-point bending and four-point bending. Specimens are prepared in the shape of prismatic beams or kept as a whole bone sample. To reduce shear effects, the length of the beam is taken longer than the cross-sectional dimensions of the specimen. For 3-point bending tests, the specimen is placed on two supports and loaded at the center portion. The maximum bending moment is then applied at the center of the specimen. For 4-point bending tests, the specimen is placed on two supports, and it is loaded with two equal forces placed symmetrically on the top of the specimen. The maximum bending moment is then applied uniformly between the two applied forces.

For 3-point bending, the modulus of elasticity is calculated as: $E = \dfrac{48L^3}{I}\dfrac{\Delta P}{\Delta\delta}$, with $\Delta P/\Delta\delta$ being the slope of the initial linear region of the load-displacement curve, I being the moment of inertia of the cross-section and L being the length of support span of the specimen.

For 4-point bending, the modulus of elasticity is expressed as: $E = \dfrac{a^2}{6I}\left(3l - 4a\right)\dfrac{\Delta P}{\Delta\delta}$, with a being the distance from the support to the nearest load.

Also, the flexural strength of the material is calculated using the following equations,

$\sigma_c = \dfrac{P_c L c}{4I}$, for 3-point bending, and $\sigma_c = \dfrac{P_c a c}{I}$, for 4-point bending.

In these equations, P_c is the load at failure, I is the moment of inertia, c is the distance between the bottom surface and the neutral plane of the beam. The above equations are valid only for specimens

with uniform cross-sections. If the specimens have irregular cross-sections, then the equations will need modifications according to the respective cross-sections.
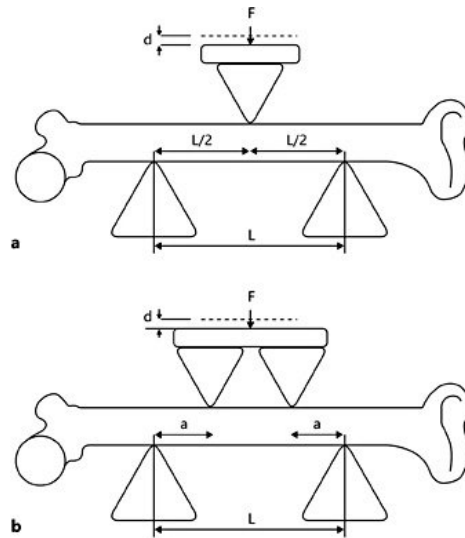
Figure 2.11 (a) Three-point bending test configuration, (b) 4-point bending test, F = applied forces; d = resulting displacement; a and L = lengths (Oksztulska-Kolanek, Znorko, Michałowska, & Pawlak, 2016)

2.4.1.6 Torsion (Shear)

Torsion tests are used to measure shear properties of bone tissue material. Specimens are generally prepared as a solid circular or annular cross-section with a reduced gage region. Both ends are clamped properly and subjected to torsion in the testing machine. The testing procedure can be torsional load controlled or angular displacement controlled. Specimens are generally loaded at a constant rate up to failure.

The maximum shear stress (τ) and strain (γ) can be calculated as: $\tau = \dfrac{Tr}{I_P}$; and $\gamma = \dfrac{\phi r}{L}$, where T is the applied torque, r is the radius of the gage region of the specimen, φ is the twist angle, I_P is the polar moment of inertia of the cross-section, and L is the gage length.

The shear stress-strain curve can also be obtained to calculate the shear modulus (G) as: $G = \dfrac{\Delta\tau}{\Delta\gamma}$

Also, shear yield strength (τ_{ys}), ultimate shear strength (τ_{ut}), and shear strain at failure (γ_f) can be measured in a similar approach as in tension/compression tests.
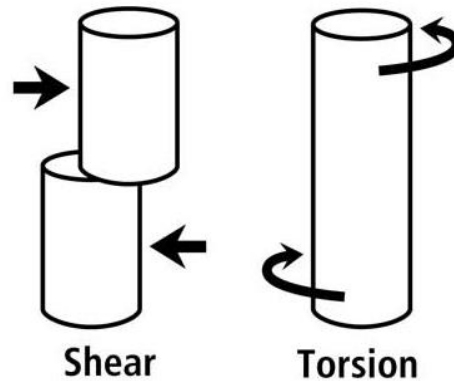
Figure 2.12 Schematic diagram of shear and torsion loading conditions that can be imparted to a bone or bone region (Adapted from Shear Resistance-Priority Hypothesis)

2.4.1.7   Fatigue

Tensile, compressive, bending and torsional loading can be used to assess the fatigue properties of bone. Preparations of the specimen are similar to the process described for the previous methods. An additional requirement is a testing machine which can apply cyclic repetitive loading. The mean stress (σ_m), applied stress amplitude (σ_a), and cycle number are the three controlling factors of a fatigue test. Dehydration also needs to be monitored during the whole testing procedure as it could have a significant impact on the test result. So, a water bath system is essential to keep the specimen hydrated during the test period. The results of the fatigue test can be assessed through an S-N diagram, which represents a plot of Constant Amplitude Stress Level (S) versus Number of Cycles to Failure (N).

2.5 Mechanical loading of bone during adolescence

2.5.1 Clinical Studies

Bone growth is a dynamic process that is influenced by several factors during the adolescence. Growing bones go through a continuous process of bone adaptation with respect to their mass, size, and micro-architecture in response to undergoing mechanical stimuli. Mechanical forces can come from both internal and external sources. Internal loading includes muscle forces and gravitational forces associated with body weight while external loading spans from forced exercise to controlled mechanical stimuli applied on the skeleton on a regular basis. During normal physiologic voluntary activities, muscle forces produce the greatest loads on bone structure (Hart et al., 2017). Physical/sport activities during growth are considered a key source of mechanical loading to influence bone mass and micro-architecture. For the past couple of decades, researches have investigated the effects of exercise during growth on bone mass and density. For this reason, gymnasts and athletes were studied in their pubertal period or during their active training period and their body height, weight and bone strengths were thereafter assessed both in the short term and in long term periods. A summary is provided here for clinical studies in the short term and the long term periods (Table 2.1, 2.2).

2.5.1.1 Short Term

Table 2.1 Clinical studies investigating the effect of loading on growing bones (short term period)

Study	Subjects	Activity	Measurements	Important Findings	Limitations of the studies
Haywood et al. (Haywood et al., 1986)	Female gymnasts and swimmers	Effects of training between female gymnasts and swimmers	Height, weight, skinfolds	Swimmers were significantly taller, heavier than gymnasts	1. Nutritional factors were not monitored
Theintz et al. (Theintz et al., 1993)	Female gymnasts	Effects of physical training during puberty for 2.35 years	Height, sitting height, leg length, weight, body fat	Heavy training during adolescence can reduce growth rate	2. Body weights were not monitored regularly, rather taken at the end of the study
Lindholm et al. (Lindholm et al., 1994)	Female gymnasts	Effects of gymnastic training during pubertal period	Height, weight, estimated final height	Gymnasts grow more slowly than controls and ended up 3.5–7.5 cm shorter than expected	
Tanghe et al. (Tanghe et al., 1996)	Female high performance and recreational gymnasts	Effects of performance vs recreational training intensity on bone growth	Height, weight, sitting height, leg length	High performance group is shorter than the recreational group	3. Repetitions, peak load, frequency of the exercise were not mentioned in the study
Caine et al. (Caine et al., 2001)	Female gymnasts	Effects of intensive gymnastics training during puberty	Body height, body weight	Heavily involved female gymnasts may experience reduced growth during training	4. Mainly focused on voluntary exercise, so no fixed hours/day

Table 2.1 (continued) Clinical studies investigating the effect of loading on growing bones (short term period)

Damsgaard, R., et al. (Damsgaard, R., et al., 2001)	Children participating in competitive sports	Effects of participating in swimming, tennis, handball, and gymnastics	Anthropometric variables, body composition and pubertal development	No effect of training on body composition or pubertal development was found	exercise routine has been applied
Amigó, Alfredo Irurtia, et al. (Amigó, Alfredo Irurtia, et al., 2009)	Male gymnasts	Effects of short routines on 6 different apparatus: floor, pommel horse, still rings, vault, parallel bars and bar	Height, weight, somatotype and body composition	Gymnasts showed a growth pattern considered as normal in the variables analyzed in the study	

2.5.1.2   Long Term

Table 2.2 Clinical studies investigating the effect of loading on growing bones (long term period)

Study	Subject	Activity	Measures	Important Findings	Limitations of the studies
Bass et al. (Bass et al., 1998)	Prepubertal female gymnasts	Effects of exercise before puberty at adulthood	Bone mineral density (BMD) and bone strength	Bone benefits are maintained and improve fracture risk at adulthood and	1. Nutritional factors were not monitored
Karlsson et al. (M. Karlsson et al., 2000)	Male soccer players	Effects of soccer played at young age	Bone mineral density (BMD) and bone strength	Bone benefits are observed after 10–20 years of playing	2. Body weights were not monitored regularly
Kontulainen et al. (Kontulainen et al., 2001)	Female racquet sports players	Effects of exercise on the exercised arm bone mineral content	Bone mineral content (BMC)	Maintenance of the bone gain is independent of the starting age of activity	3. Repetitions, peak load, frequency of the exercise not mentioned in the study
Kontulainen et al. (Kontulainen et al., 2003)	Female tennis and squash players	Effects of impact-loading on mass, size, and strength of humerus and radius of Players	Bone morphology and compressional bone strength	Exercise during growing years increase bone strength	
Nordström et al. (Nordström et al., 2005)	Ice hockey players	Effects of physical activity during growing at adulthood	Bone mineral density (BMD) and cross-sectional properties	Benefits of BMD is lost within 3 years of cessation of sports career	

Table 2.2 (continued) Clinical studies investigating the effect of loading on growing bones (long term period)

Gunter et al. (Gunter et al., 2008)	Prepubertal children	Effects of seven months of jumping exercise	Bone mineral content (BMC)	Effects prevail for a short period but diminish over time	4. Focused on voluntary sports activities, so no fixed hours/day exercise routine has been applied
Warden et al. (S. J. Warden et al., 2014)	Professional baseball players	Dominant-to-nondominant arm differences at adulthood	Bone morphometry and mechanical properties	Half of the bone size and one-third of the bone strength benefits of physical activity during youth maintained lifelong	
Duckham et al. (Duckham et al., 2014)	Female patient	Adolescent physical activity	Bone morphometry and mechanical properties	Benefits to tibia bone size, content, and strength seemed to persist into young adulthood	5. Contradictory results on the existence of bone benefits at adulthood

2.5.2 Experimental *in vivo* animal studies

Several studies have been performed to assess the effects of loading on animal bone microstructure using controlled exercise and/or forced loading regime (Bourrin et al., 1995; Caine et al., 2001; Theintz et al., 1993; Welch, Weaver, & Turner, 2004; X. Yang et al., 2013). The first technique for artificial loading of bones in an *in vivo* condition was introduced by Jiri Hert in 1960s where he loaded the rabbit tibiae with stainless steel pins using an electromechanical device (Hert, 1971; Liskova, 1971). Assessment of bone strains during the physiologic condition for human tibia was introduced by Lanyon, also in the 1960s (L. Lanyon & Smith, 1969). Lanyon attached strain gauges to the bone surface and recorded electrical impulse for registering bone strains (L. Lanyon & Smith, 1969).

The established ideas provided by these studies later used in a number of species and different skeletal sites exhibited good agreement with respect to the peak strains achieved under similar loading applications (Hert, 1969; Lance E Lanyon & Rubin, 1984; Lee, Maxwell, & Lanyon, 2002; Rubin & Lanyon, 1985). Later, more experiments were performed combining the strain gauge technique with the non-invasive loading conditions using varieties of animal models, including sheep, pigs, roosters, turkeys, rats, and mice, etc. which paved the way to better understand bone adaptive response under controlled loading (Biewener & Bertram, 1993; Bright & Rayfield, 2011; Gardinier, Rostami, Juliano, & Zhang, 2018; L. E. Lanyon, 1973; S. Warden & Turner, 2004). Nowadays, several researchers are adapting this technique with a focus on the rat and mouse models due to the convenience of loading application in these models. A summary is provided here for experimental studies in growing rodent models in the short term and the long term periods (Table 2.3, 2.4).

2.5.2.1 Short Term

Table 2.3 Experimental animal studies investigating the effect of loading on growing bones (short term period)

Study	Animal model	Activity	Measurements	Important Findings	Limitations of the studies
Forwood & Parker (Forwood & Parker, 1987)	Pubescent rat tibia & femur (22 days old)	Intensive exercise program for 1 month (1 h/day for 5 day/week for 4 weeks)	Bone length and weight, width of the epiphyseal plate	Significant reductions in bone length, weight, and width of proximal epiphyseal plate	1. Food intakes were not monitored
Snyder et al. (Snyder et al., 1992)	Growing rat hindlimb and forelimb	Run-trained (2 h/day for 5 day/week for 10 weeks)	Bone growth, muscles, bone mineral content	Minimal effect on bone growth (other parameter no effect)	2. Body weights were not monitored regularly, rather taken at the end of the study
Bourrin et al. (Bourrin et al., 1995)	Young rat tibia (9 week old)	Intensive treadmill running (1.5 h/day for 7 day/week for 5 weeks)	Dynamic and static bone cell activities, bone growth	Significant reductions in longitudinal bone growth and number of osteoclast profiles	3. Contradictory results on the effects of exercise on bone growth were reported
Niehoff et al. (Niehoff et al., 2004)	Growing rat femur (3 week old)	Dose-dependent voluntary exercise-running for 8 week	Bone length, histomorphometric parameters and mechanical properties	No differences in mechanical properties or bone length. But increased level of mineralization for exercise group	4. Bone morphometric data were not assessed during the study period

2.5.2.2 Long Term

Table 2.4 Summary of previous experimental studies on the effect of loading on growing bones (long term period)

Study	Subject	Activity	Measures	Important Findings	Inadequacies of the studies
Pajamäki et al. (Pajamäki et al., 2003)	Rats femoral neck and midshaft (5 week old)	Effects of pubertal treadmill exercise after 42 weeks of detraining (3 min/day for 3 day/week for 14 weeks)	Bone morphology and bone strength	Exercise-induced bone benefits are eventually lost after detraining period	1. Food intakes were not monitored
Iwamoto et al. (Iwamoto et al., 2000)	Rats femur and tibia (4 week old)	Effects of pubertal treadmill running after 4 weeks of detraining (18 min/day for 5 day/week for 8 and 12 weeks)	Bone morphometric properties	Lost the benefits gained through exercise	2. Body weights were not monitored regularly, rather taken at the end of the study
Warden et al. (S. J. Warden et al., 2007)	Rats forearm (5 week old)	Effects of pubertal forearm axial compression loading after 92 weeks of detraining (360 cycles/day for 3 day/week for 7 weeks)	Bone morphometry, Bone mineral content, and mechanical properties	Induced loading tend to last long into the adulthood	3. Bone morphometric data were assessed at the end, not in intermittent detraining time points
Honda et al. (Honda et al., 2008)	Rats (12 week old)	Effects of pubertal jump training after 24 weeks of detraining (10 jumps/day for 5 day/week for 8 weeks)	Bone morphometric properties	Benefits from jump training are preserved after 24 weeks of detraining period at adulthood	4. Contradictory results on the existence of bone benefits at adulthood

In most of the published clinical studies, researchers have not provided a clear, distinct separation between the nutritional and mechanical factors. The studies have not considered the intensity, repetitions, peak load, and frequency of the loadings/exercise applied. Rather they expressed the physical exercise regime hours per week. Hence, it becomes challenging to isolate the loading effects on the growing bones based on these studies. Moreover, in the conducted short term and long term animal studies, reported results are contradictory. Some reported absence of exercise-induced effects, whereas some reported positive and negative effects on the bone microstructure due to an impact exercise regime. However, most of these studies only measured the BMC and aBMD of the bone, which is an alternative measure for bone strength. Hence, these studies failed to provide a detailed analysis on the effects of loadings on the cross-sectional property of bone, as well as on the internal bone architecture. Hence, still, there is a paucity of data for the longitudinal investigation of bone microstructure and strength under pubertal loading for a short term period at the end of adolescence as well as for a long term disuse period at skeletal maturity.

2.6   Imaging techniques of bone geometry and microarchitecture

To date, a number of imaging techniques have been developed and used to assess bone microstructure ranging from macroscale to the nanoscale. These imaging techniques have opened a window of possibilities for investigating bone growth or development process through longitudinal studies.

2.6.1 Quantitative CT

Quantitative computed tomography (QCT) is an imaging technique, which can be used for the three-dimensional assessment of skeletal geometry within an *in vivo* setup condition (Genant, Engelke, & Prevrhal, 2008). The original 2D QCT was developed to scan through isolated thick slices of the bone sample. The scans were acquired through tilting the CT scanner gantry and correcting the alignment with respect to the same as the sample (Munoz, Boutroy, Delmas, & Bouxsein, 2005). The latest advanced 3D QCT has overcome those limitations and can be used for rapid multiple acquisitions of the desired scanning image sets. Primarily, macroscopic scanning can be performed by the QCT scanning system. The mechanism of the QCT involves producing X-rays, which are attenuated by the testing sample and detecting the signal on the opposite side. Both the source and signal detectors rotate during the scanning process. QCT can produce a spatial

resolution for trabecular thickness ranging from 60 to 150 μm and trabecular separation between trabeculae from 300 to 1000 μm (Schnitzler, Biddulph, Mesquita, & Gear, 1996). With a single scan, QCT can be used to acquire images with slice width 10 mm along with a 20 s image acquisition time. QCT can give 3D trabecular and cortical bone geometry with the measurement of volumetric bone mineral density (BMD). QCT can be used with low radiation doses, and this system can measure the peripheral and central sites (hip and spine). However, the system is comparatively costlier and can also give a false high reading in the case of dense structure.

Figure 2.13 QCT of the forearm using a dedicated peripheral scanner (Adams, 2009)

2.6.2 High-resolution Peripheral QCT (Preclinical microCT)

High-resolution peripheral quantitative computed tomography (HR-pQCT) has been developed for assessing the morphometric parameters via 3D analysis primarily in the peripheral sites such as the distal radius and tibia (Kazakia & Majumdar, 2006; Munoz et al., 2005). The functioning principle for the HR-pQCT is similar to the QCT technique. HR-pQCT can be used to obtain images of higher spatial resolution ranging between 40 and 150 μm (Ralph Müller, 2002). In a clinical setup, a single 2.5 mm axial CT slice can be acquired through the scanned distal radius

[64]. The pQCT acquires one slice, whereas the standard clinical imaging protocol for HR-pQCT, XCT II can acquire several images. The standard settings used for XtremeCT II are as follows: energy- 68.0kVp, current- 1470nA, field of view- 14.0cm, integration time- 43ma, isotropic voxel size- 60.7m, scan time- 2.0min, stack length- 10.197mm. It has a similar advantage as the QCT imaging technique and can assess the bone mineral density (BMD) in isolated trabecular and cortical bone segments. Moreover, due to its improved resolution , it can be used to measure microarchitectural bone morphologic parameters such as bone volume fraction (BV/TV), trabecular thickness (Tb.Th), trabecular separation (Tb.Sp), and trabecular number (Tb.N) precisely (Burghardt, Kazakia, & Majumdar, 2007; MacNeil & Boyd, 2007). Also, the trabecular morphometric measurements using HR-pQCT can be correlated with the ones measured with micro-CT, the currently most acceptable and standardized imaging system for trabecular morphology assessment (MacNeil & Boyd, 2007). HR-pQCT can be used for assessing the microstructural and biomechanical properties of the radius and tibia segments. HR-pQCT holds several advantages over the QCT counterparts, in the case of low doses resolution and costs. Also, trabecular bone loss can be identified at an earlier stage using the HR-pQCT imaging technique compared to the QCT.
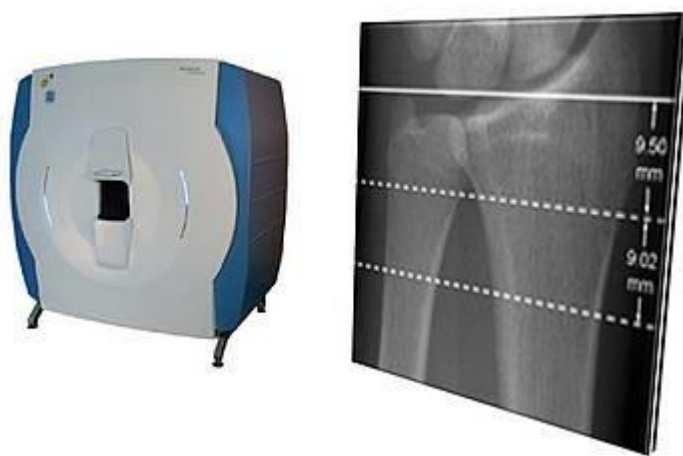
Figure 2.14 SCANCO Medical's XtremeCT (HR-pQCT scanner) with a Scout View of a region to be scanned (Adapted from SCANCO Medical)

2.6.3 Micro-CT

Micro-computed tomography (micro-CT) is similar to the previously presented image acquisition techniques; it processes the scanned images taken from multiple angles via x-rays and compiles them into a 3D image set. The basic principle of micro-CT lies within the use of X-rays contrast to differentiate among various tissue structure. Due to the calcification of the tissue structure in the skeletal system, which can be segmented based on different X-ray contrast, micro-CT imaging of bone is widely used and probably the most preferred mode of bone investigation approach worldwide for small animals. Moreover, micro-CT can provide an isotropic resolution for ex vivo measurements as precise as 1 to 6 μm, and, the resolution for *in vivo* scanning process for living animals can be as precise as 9 μm.

In micro-CT scanners, the object is illuminated via an X-ray source, and the resulted magnified projection images are saved through another planar X-ray detector. During scanning, the hundreds of images are collected at different angular views, which are later synthesized by a computer program to produce a virtual 3D stack of cross-sections of the object. Using the stack of image sets, 3D morphometric analyses can be performed to obtain micro-architectural properties.

Micro-CT *in vivo* imaging technique has enabled the pathway for analyzing the geometry and microstructure of bone tissue of living animals to detect any longitudinal change, bone adaptation or bone loss within the same living creature at a higher resolution. However, it has some limitations, including the restriction of specimen size of 100-mm diameter and 140-mm length in the scanner and the danger of affecting bone health with high or repeated doses of X-ray radiation.

2.6.3.1 Primary micro-CT parameters for scanning regime

The primary micro-CT imaging parameters for generating reliable bone morphometry data using micro-CT scanning system includes the following: (Adapted from Bouxsein, Boyd et al. 2010)

I. Voxel size (μm^3): The dimensions of the three directional coordinate systems for the scanned micro-CT image.

II. X-ray energy Energy (keV): Energy is proportional to the frequency (or $1/\lambda$) of X-ray photons.

III. X-ray tube potential (peak) (kVp): The applied peak electric potential of X-ray tube for generating X-ray photons to accelerate electrons.

IV.   X-ray intensity (mA.s, µA): The registered tube current (µA) of X-ray system or the product of applied current and time (mA . s)

V.   Integration time (ms): The required duration for taking isolated tomographic projection.

VI.   Frame averaging (n): For completing isolated tomographic projection, the required number of measurements taken repeatedly.

VII.   Projection (n): The required number of viewpoints from image reconstruction

2.6.3.2   Trabecular bone parameters

Trabecular bone micro-architectural measurements mostly include the followings parameters (Bouxsein et al., 2010):

I.   Bone mineral density (BMD) (g.cm^{-3}): It is defined as the volumetric density of calcium hydroxyapatite (CaHA) in biological tissue. Phantoms with known density of CaHA are used for the calibration of BMD. For trabecular structure, the BMD is measured as the combined density of a predefined volume of interest (VOI) containing both bone and soft tissue (i.e. medullary trabecular volume of interest for tibia).

II.   Bone volume fraction (BV/TV) (%): It is the ratio of the segmented bone volume to the total volume of the selected ROI (region of interest).

III.   Trabecular thickness (Tb.Th) (mm): It is the direct three-dimensional measurement of average trabecular thickness which is usually determined with a 3D sphere-fitting method.

IV.   Trabecular number (Tb.N) (1/mm): It is the direct three-dimensional measurement of average trabecular number calculated per unit length within a predefined ROI and measured using a 3D sphere-fitting method.

V.   Trabecular separation (Tb.Sp) (mm): It is the direct three-dimensional measurement of the average surface to surface separation distance of the trabeculae within a predefined ROI and measured using a 3D sphere-fitting method.

VI.   Connectivity density (Conn.D) (1/mm^3): It is an assessment of the degree of connectivity of trabeculae, volumetric number of bifurcations.

2.6.3.3 Cortical bone parameters

Cortical bone micro-architectural measurements mostly include the followings parameters (Bouxsein et al., 2010):

I. Tissue mineral density (TMD) (g.cm^{-3}): It is defined as the volumetric density measurement of the calcified bone tissue (i.e. cortical bone structure). This measurement excludes the surrounding soft tissue and provides the material density of only the bone itself.

II. Cortical bone area (Ct.Ar) (mm^2): It is the area measured for each transverse section and is calculated as the cortical volume divided by the thickness of each slice multiplied by the total number of slices.

III. Total area (Tt.Ar) (mm^2): It is the area that includes all bone, marrow, and porosity. This area is usually enclosed by the periosteal perimeter.

IV. Medullary area (Ma.Ar) (mm^2): It is the area enclosed by endocortical perimeter on any given transverse section.

V. Cortical thickness (Ct.Th) (mm): It is a direct measurement of the average thickness on any given transverse section.

VI. Endocortical perimeter (Ec.Pm) (mm): It is the perimeter of the endosteum. Calculated indirectly considering marrow area to be a circular section.

VII. Periosteum perimeter (Ps.Pm) (mm): It is the perimeter of the periosteum. Calculated by dividing the periosteal surface area of a short span by the diaphyseal span length.
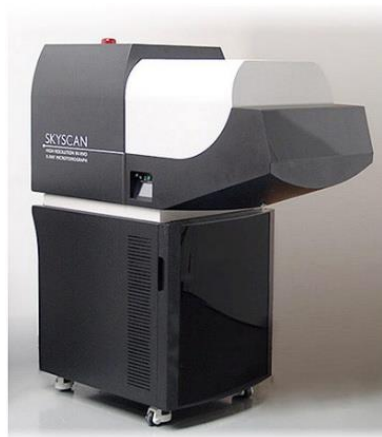
Figure 2.15 SKYSCAN 1176 (*in vivo* micro-CT scanner) (Adapted from www.bruker.com)

2.7 Finite element (FE) modeling of bone

Computational modeling is considered an effective technique for the investigation of bone mechanical behavior or properties. The relationship between bone and its mechanical environment, as well as between bone and its biological environment can be assessed through this technique. FE technique can provide knowledge on stress and strain distributions in hard and soft tissues, which cannot be measured *in vivo*.

Finite Element (FE) method is being used very frequently for estimation of strength and stiffness of whole bones and trabecular bone tissue. It is also used to measure the stress-strain distributions within bone tissues. FE analysis has been used as a non-invasive tool for internal loading estimation and for assessing the bone tissue fracture (Bessho et al., 2009; Bessho et al., 2007). In addition to predicting bone strength, FE analysis also used as a tool for validating theories of mechanobiological regulation of bone mass structure (Beaupré, Orr, & Carter, 1990) and to investigate the pathophysiology of skeletal fragility as well as skeletal diseases (Kim et al., 2003).

2.7.1 Hierarchical levels of bone for FE modeling

Depending on the hierarchical levels of bone structure, FE modeling can range from the macroscale to the nanoscale.

2.7.1.1 Macroscale

Bones vary in shapes and sizes at the macroscopic or organ level of FE modeling (Figure 2.16a), depending on the skeletal site and at nature of loading conditions. In these models, loading scenarios can be applied in a complex manner involving muscles and tendons forces. Loads are usually applied through the joint surface of the bone. Comprehensive and physiological boundary conditions are required at this modeling level for accuracy and efficiency. Failure prediction, as well as fracture propagation, can be modeled at this macroscale level (Ruffoni & Van Lenthe, 2017).

2.7.1.2 Mesoscale

In order to distinguish trabecular bone from compact cortical bone, an accuracy of hundreds of micrometers is essential. At the mesoscale, trabecular bone is modeled with this accuracy (Figure 2.16a). Trabecular bone is porous in nature and contains plate-like struts. The mesoscale modeling

approach is important as it sheds light on the relationship between architectural and mechanical properties of the trabecular structure, which can be investigated to understand mechanical improvement and bone loss under loading/unloading conditions (Ruffoni & Van Lenthe, 2017).

2.7.1.3 Microscale

The level of densification for the cortical bone goes around hundreds of micrometers. Several distinguishable ultrastructural features (i.e. osteocyte lacunae and the canal network) can be modeled if a higher magnification (3-5 μm) is considered at microscale level (Figure 2.16a) (Ruffoni & Van Lenthe, 2017).

2.7.1.4 Nanoscale

At the nanoscale level of FE modeling, building blocks of bone can be simulated with proper boundary conditions (Figure 2.16a). The propagation of cracks in the composite material can be investigated through the assessment of the geometrical setup of the protein matrix and mineral crystals in bone tissue structure (Ruffoni & Van Lenthe, 2017).
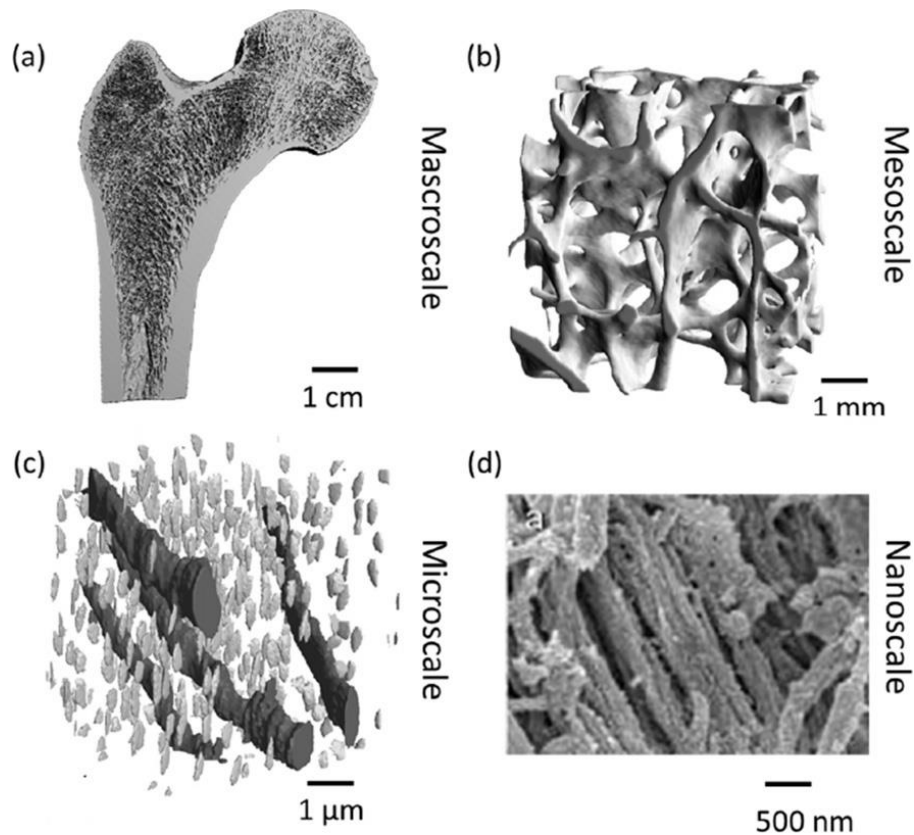
Figure 2.16 Schematic overview of the hierarchical levels of bone (Ruffoni & Van Lenthe, 2017). (a) At the macroscale, a micro-CT image femur section (image courtesy of Thomas Mueller, ETH Zurich, Switzerland). (b) At the mesoscale, micro-CT image of a femoral head trabecular bone section. (c) At the microscale, canal network and osteocyte lacunae are visible with synchrotron radiation nano-computed tomography (Adapted from Schneider, P.; Stauber, M.; Voide, R.; et al. Journal of Bone and Mineral Research 2007) (d) At the nanoscale, scanning electron micrographs of mineralized collagen fibrils in a human bone specimen (image courtesy of Paul Hansma, UCSB, Santa Barbara, USA)

2.7.2 Macroscale: Whole bone FE modeling

In vivo measurements of stress and strain cannot be accomplished non-invasively. Hence, researchers use "subject-specific" FE modeling to investigate mechanical loading response on bone microstructure. These FE models use two computational approaches for estimating the mechanical behavior of bone: continuum-level FE and microstructural-level FE.

2.7.2.1   Continuum-Level FE modeling

<u>Geometry</u>

In continuum-level FE modeling, the trabecular structure is considered as a continuum. Quantitative computed tomography (QCT) scanned images are used to convert each voxel from the 3D scan to geometry based finite element (Faulkner, Cann, & Hasegawa, 1991; Ruffoni & Van Lenthe, 2017) model. In this approach, much higher resolution (slice thickness depending on the scanning system) is used, and the models do not resolve individual trabeculae (Figure 2.17). With the use of high-resolution MRI or peripheral QCT (pQCT), it is possible to have a high resolution in order to take account the trabecular structure in the developed FE model (Walter Pistoia, Van Rietbergen, Laib, & Ruegsegger, 2001). In continuum level FE modeling, computational time can be saved even using a complex material model structure involving inhomogeneity, anisotropy, and nonlinearity due to the simplification of the geometric structure.

<u>Mechanical properties</u>

In continuum-level FE modeling, mechanical properties for trabecular bone are generally assigned with regression techniques established between the given mechanical property and QCT density (Crawford, Cann, & Keaveny, 2003). Empirical conversion approaches are used to derive elastic modulus values from the bone mineral density (BMD) based on QCT images (Helgason et al., 2008). Elastic modulus is usually considered isotropic but non-isotropic values are often considered for the FE simulation. Material properties are usually taken from mechanical tests using the same bone samples conducted prior to the FE modeling (Ruffoni & Van Lenthe, 2017). In previous studies, it has been found that for continuum level FE, strength predictions of the bone in an *in vivo* condition can give higher accuracy compared to the prediction based on BMD (Crawford et al., 2003; Jasper Homminga, Huiskes, Van Rietbergen, Rüegsegger, & Weinans, 2001).

<u>Applications</u>

The continuum level-FE modeling is widely applicable for predicting bone strength *in vivo* for the skeletal sites where only QCT imaging is clinically feasible (Ruffoni & Van Lenthe, 2017). This method can be a valuable tool for comparing bones from healthy and osteoporotic individuals, where computation time is of main priority. The modeling approach for the entire bone has a significant drawback in the calculation of stress and strain values on the irregular bony surface.

However, it is still an ongoing research field to assess the impact of bone surface irregularity on the strength and stiffness of the whole bone FE modeling (Crawford et al., 2003; Jasper Homminga et al., 2001). Also, this modeling approach might not be able to track precisely the changes in bone stiffness and strength in follow up studies due to the limitations of details on bone microstructure (van Lenthe & Müller, 2006). Moreover, this method has the limitations of including internal microarchitecture of bones, hence individual trabecular features or thin cortical/trabecular shell structure covering the core trabecular individuals might not be available with this method of modeling.
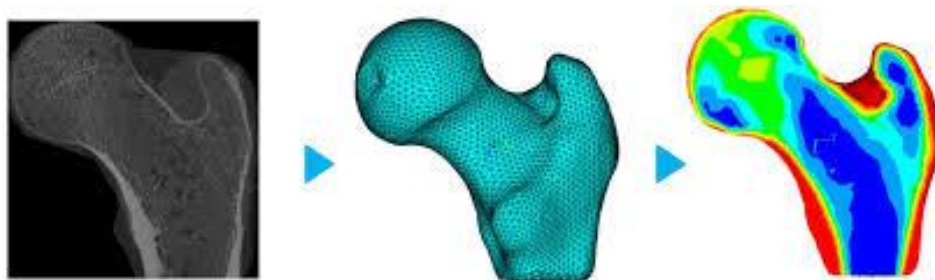
Figure 2.17 Continuum-level FE model of a human proximal femur obtained from CT images (Marangalou, J. H., 2013)

2.7.2.2 Micro-FE modeling

Geometry

The availability of high-resolution digital imaging, including micro-computed tomography (μCT) and high-resolution magnetic resonance imaging (HR-MRI), have paved the way to create FE models of the bone microstructure at the micro level. The developed method is called microstructural FE (micro-FE) analysis or voxel FEA, where high-resolution digital imaging is combined with the FE modeling (Ruffoni & Van Lenthe, 2017). These models are developed by acquiring high resolution images through scanning process and then converting each image voxel occupied by bone tissue directly into a brick shape finite element (Christen, Webster, & Müller, 2010; Scott J Hollister, Brennan, & Kikuchi, 1994; R. Müller & Rüegsegger, 1995; B. van Rietbergen, Weinans, Huiskes, & Odgaard, 1995). Moreover, models with tetrahedral elements

can also be generated by adapting image based mesh generation softwares (Scott J. Hollister & Riemer, 1993; Young, Raymont, Xuan, & Cotton, 2010). Due to the fineness in the mesh and high accuracy of the models, the voxel-to-element conversion approach can however result in a large number of elements. For instance, a generated voxel FE model of a human vertebra can be made up of around 60 million elements coupled with 200 million degrees of freedom (Eswaran, Gupta, & Keaveny, 2007). To reduce the computational time and resources for handling such a large number of elements, custom codes are often used. These codes can perform calculations with varying solving techniques and deploy multiple processing units to speed up the calculation time (Christen et al., 2010; B. van Rietbergen et al., 1995).

Mechanical properties

Bone tissue properties adopted in micro-FE modeling can follow several options. A homogeneous modulus of elasticity can be considered for the whole model (Torcasio, Zhang, Duyck, & van Lenthe, 2012). However, the modulus of elasticity can also be assigned to each converted voxel based on its respective bone density (Helgason et al., 2008; Jasper Homminga et al., 2001). Due to the availability of the high-resolution scanning system, it is now possible to exactly determine the distribution of bone density based on the grayscale images (Jasper Homminga et al., 2001; Mustafy, Londono, & Villemure, 2019; B. van Rietbergen et al., 1995). So, with the use of known bone density from the scanning system provided phantoms and the calculated bone density from the grayscale images, a correlation can be achieved between the elastic modulus and the scanned image density (Helgason et al., 2008; R. Müller & Rüegsegger, 1995). As a result, the resulting FE model can have non-homogeneous material properties, which can be personalized for each voxel element (Mustafy et al., 2019; Ruffoni & Van Lenthe, 2017). Isotropic and linear elastic material models for micro FE modeling methods are reported to provide accurate predictions of bone stiffness and small deformations for the whole bone structure (Christen et al., 2010; Kabel, van Rietbergen, Dalstra, Odgaard, & Huiskes, 1999; W. Pistoia et al., 2002; van Lenthe & Müller, 2006).

Applications

Micro FE modeling for whole bone can be implemented in various fields of studies. It can be used to assess the relationship among the apparent mechanical properties of trabecular/cortical bone,

tissue structure, and mechanical properties of the bone tissue. Also, it can be used to measure the stress-strain distributions within individual trabeculae under an applied load (J. Homminga et al., 2004; Ruffoni & Van Lenthe, 2017; B Van Rietbergen, Huiskes, Eckstein, & Rüegsegger, 2003). Using nonlinear micro FE modeling, the simulation of failure and assessment of post-yield behavior can also be possible (Christen et al., 2013; Christen et al., 2010; van Lenthe & Müller, 2006).
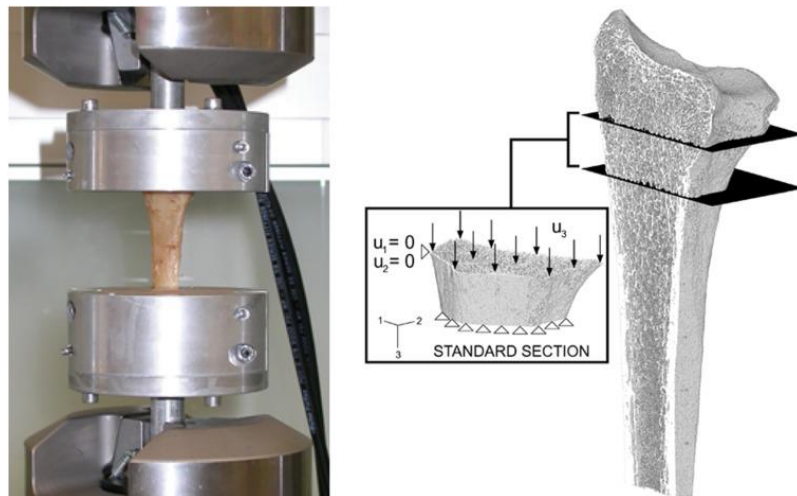
Figure 2.18 Micro FE model of a distal radius section (9 mm long) scanned with HR-pQCT. The nodes at the proximal side were fixed, while axial compression was applied on the distal end (Zysset, Dall'ara, Varga, & Pahr, 2013)

CHAPTER 3 PROJECT RATIONALE, RESEARCH QUESTIONS AND OBJECTIVES

3.1 Rationale

Based on the review of the literature, the rationale of the project can be explained as follows:

- Bone growth occurs at the cartilaginous growth plates, which enable chondrocyte proliferation, hypertrophy and cartilage matrix secretion leading to endochondral ossification mechanism and longitudinal bone growth.

- Bones continue to grow in length until early adulthood, with peak growth rates during infancy and puberty.

- During puberty, rapidly growing bones become more sensitive to their surrounding mechanical environment.

- The pubertal growth period offers a favorable condition for effectively applying impact loading in the form of physical activity on the skeletal system.

- In clinical studies on athletes, researchers have not provided a distinct separation between nutritional and mechanical factors. In experimental studies, results on the effects of impact loading are inconsistent and most of these studies used adult/post pubertal animal models.

- The effects of well-controlled impact loading applied during the puberty on longitudinal bone growth, quality and mechanics remain to be investigated at the end of the growing period.

- Whether the effects of impact loading applied during the puberty persist in the long term into adulthood and influence bone structural properties or not remain to be determined.

- Micro-CT scanning can provide high resolution 3D images of trabecular and cortical bone microarchitecture, but it is not clear what dose of scanning radiation preserve normal bone development during adolescence.

- Micro-CT based finite elements model can be used to non-destructively and longitudinally evaluate bone mechanical properties *in vivo*.

3.2 Research Questions

Q1. What micro-CT radiation dose level can be safely used in a growing rat model without affecting its bone development?

Q2. What are the effects of cyclic axial compression applied during puberty on longitudinal bone growth, quality, and mechanics at the end of the growing period?

Q3. Do the induced changes in bone quality and mechanics from cyclic axial compression applied during the pubertal period persist into adulthood?

3.3 Objectives

The overall objective of this project was to evaluate the effects of *in vivo* low, medium, and high impact loadings applied during puberty on bone growth (at skeletal maturity) as well as on bone quality and mechanical strength (at skeletal maturity and at adulthood) using a rat model. In the following sections, the four specific objectives, which helped to respond to the research questions, are presented.

Objective 1: To investigate the effects of radiation doses from repeated *in vivo* micro-CT scanning on bone morphometry, bone marrow cells, bone growth rate, and growth plate histomorphometry in adolescent rat tibiae.

This objective had four main steps:

1. To configure three radiation dose levels, which would enable a reasonable high-quality image for the trabecular and cortical bone tissue investigation.

2. To scan the right tibiae of three radiation rat groups during their adolescent period on a weekly basis.

3. To investigate, at sacrifice, bone growth rate, growth plate histomorphometry and bone marrow cells in the scanned vs contralateral tibiae.

4. To investigate trabecular and cortical bone morphometric properties in the scanned vs contralateral tibiae.

An overview of the timeline for Objective 1 is given in figure 3.1.
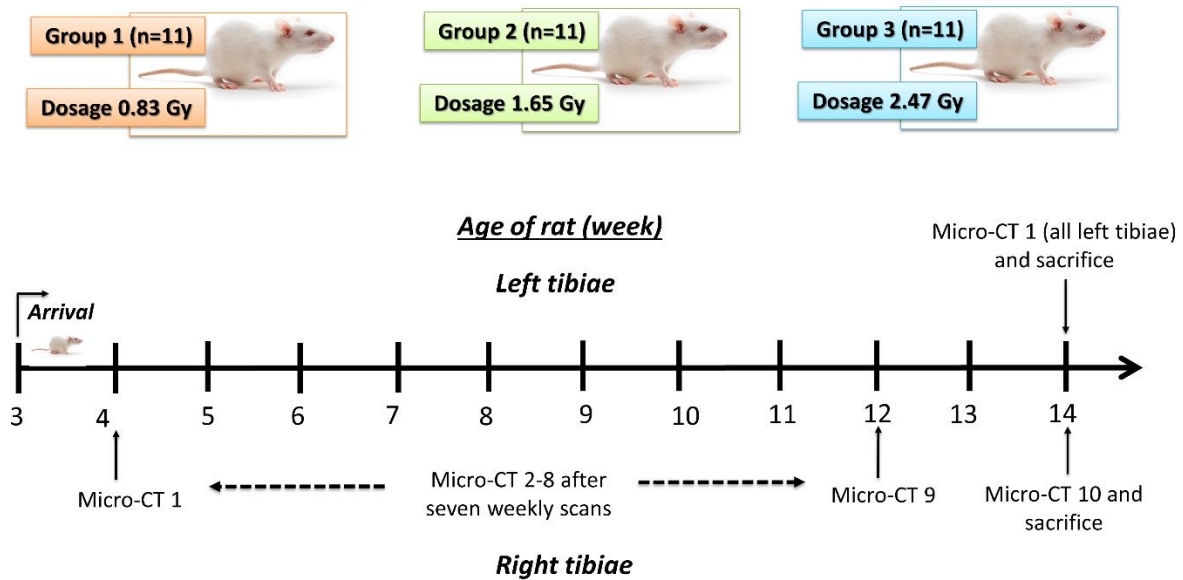
Figure 3.1 An overview of the project timeline for Objective 1

Objective 2: To investigate the relationship between applied displacement and bone tissue deformation for the rat tibia in the adolescent period and to develop a non-invasive micro-CT based finite element modeling tool for the non-destructive and longitudinal evaluation of bone mechanics.

This objective consisted of four steps:

1) To implement three age groups of rats of 4, 8 and 12 week old.

2) To develop a protocol for the installation of strain gauge near the medio-proximal surface of the tibia, the application of dynamic compressive displacements and simultaneous registration of displacements and tibial strains.

3) To establish the linear axial displacement-strain relationship curves for the three age groups of rats (range: displacement from 0.5 to 3.5 mm; strain from 150 $\mu\varepsilon$ to 1950 $\mu\varepsilon$).

4) To develop and experimentally validate a micro-CT based finite element modeling tool for non-destructively and longitudinally assessing bone strains.

Objective 3: To investigate the effects of cyclic axial compression applied during puberty on longitudinal bone growth, quality and mechanics at the end of the growing period.

This objective consisted of seven steps:

1) To implement five groups of rats: (a) control, (b) sham, (c) low impact (LI), (d) medium impact (MI), and (e) high impact (HI).

2) To apply the axial displacements during the pubertal period (from 4th to 11th week of age) to reach the target tensile strains of 450, 850, and 1250 µε, respectively for the LI, MI, and HI groups of rat tibiae.

3) To weekly scan the right tibiae with a micro-CT scanner from 4 to 11 week of age.

4) To longitudinally investigate trabecular and cortical bone morphometric parameters in the right tibiae and compare among rat groups.

5) To longitudinally investigate body weight and food intake during the loading period for assessing the effects of cyclic axial compression on the rats' overall health.

6) To investigate, at sacrifice (age = 11 week old), bone growth rate and growth plate histomorphometry in the right tibiae and compare among rat groups

7) To extract, at sacrifice, tibial bone mechanical properties using three-point bending tests and compare among rat groups.

An overview of the timeline for Objective 3 is given in figure 3.2.

Experimental design
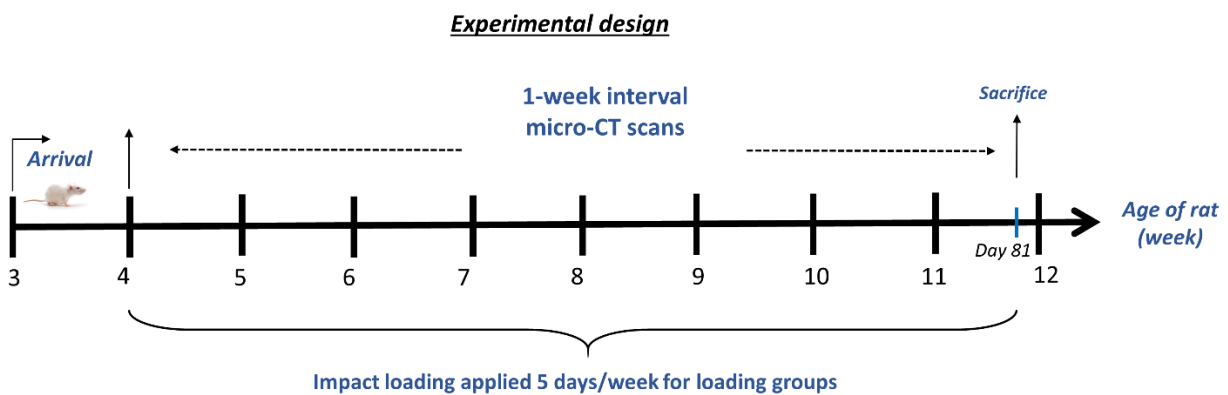
Figure 3.2 An overview of the project timeline for Objective 3

Objective 4: To investigate the effects of cyclic axial compression applied during puberty on longitudinal bone development, quality and mechanics of the bone microstructure at the end of the growing period and verify whether effects persist into adulthood.

This objective consisted of eight steps:

1) To implement five groups of rats: (a) control, (b) sham, (c) low impact (LI), (d) medium impact (MI), and (e) high impact (HI).

2) To apply the axial displacements during the pubertal period (from 4th to 11th week of age) to reach the target tensile strains of 450, 850, and 1250 $\mu\varepsilon$, respectively for the LI, MI, and HI groups of rat tibiae

3) To scan the right tibiae with a micro-CT scanner, weekly in the adolescent period, monthly in the post-pubertal period and bi-monthly at adulthood.

4) To investigate trabecular and cortical bone morphometric parameters in the right tibiae and compare among rat groups at different time points.

5) To investigate body weight and food intake during the loading and detraining period for assessing the effect of cyclic axial compression on the rat's overall health.

6) To extract, at sacrifice (age = 52 week old), tibial bone mechanical properties using three-point bending tests and compare among rat groups.

7) To extract selective tibial muscles and compare muscle weights among rat groups for evaluating the cyclic axial compression effects.

8) To use the micro-CT based finite element modeling tool (2nd objective) for assessing bone strains in trabecular and cortical sections of the 52 week old tibiae under compressive loading conditions.

An overview of the timeline for Objective 4 is given in figure 3.3.
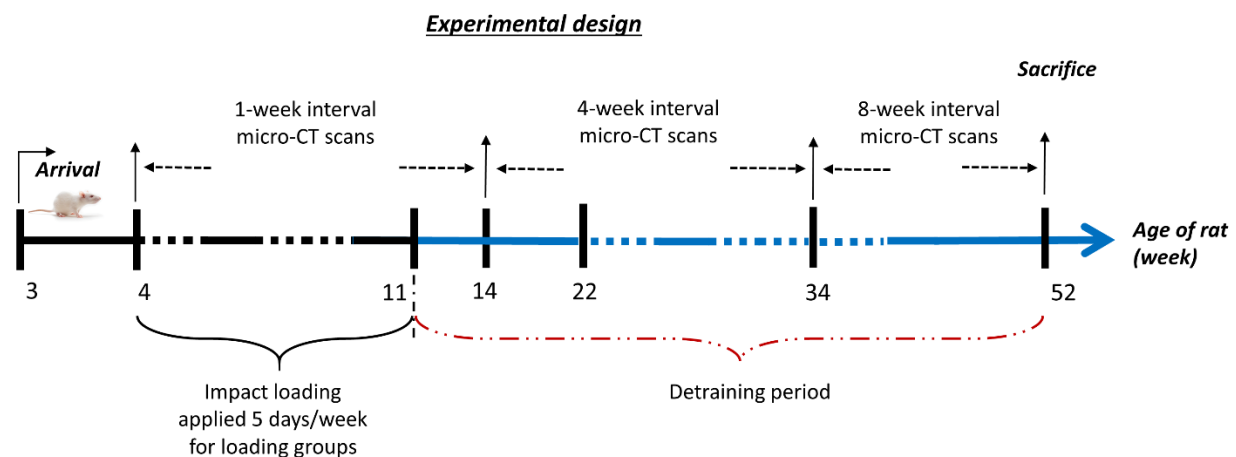
Figure 3.3 An overview of the project timeline for Objective 4

The four articles, which represent the body of this thesis, address the four objectives as shown in the following diagram:

Article 1 (Chapter 4)	Article 2 (Chapter 5)	Article 3 (Chapter 6)	Article 4 (Chapter 7)
Objective 1	Objective 2	Objective 3	Objective 4
R.Question 1	R.Questions 2, 3	R.Question 2	R.Question 3

CHAPTER 4   ARTICLE #1: CAN REPEATED *IN VIVO* MICRO-CT IRRADIATION DURING ADOLESCENCE ALTER BONE MICROSTRUCTURE, HISTOMORPHOMETRY AND LONGITUDINAL GROWTH IN A RODENT MODEL?

This chapter introduces the first article written in the context of this thesis and responds to the first objective of this thesis as detailed in Chapter 3.

This article was published in PLOS ONE © in November 15th, 2018.

The contribution of the first author in the preparation, obtaining the results, writing and literature review of this paper is estimated at 85%.

Contribution of all authors:

Tanvir Mustafy: Conceptualization, Data curation, Formal analysis, Investigation, Methodology, Project administration, Software, Visualization, Writing - original draft.

Aurélie Benoit: Resources.

Irene Londono: Data curation, Resources.

Florina Moldovan: Methodology, Supervision.

Isabelle Villemure: Conceptualization, Funding acquisition, Methodology, Project administration, Resources, Supervision, Writing - review & editing.

4.1 Abstract

In vivo micro-computed tomography (micro-CT) can monitor longitudinal changes in bone mass and microstructure in small rodents but imposing high doses of radiation can damage the bone tissue. However, the effect of weekly micro-CT scanning during the adolescence on bone growth and architecture is still unknown. The right proximal tibia of male Sprague-Dawley rats randomized into three dose groups of 0.83, 1.65 and 2.47 Gy (n = 11/group) were CT scanned at weekly intervals from 4th to 12th week of age. The left tibia was used as a control and scanned only at the last time point. Bone marrow cells were investigated, bone growth rates and histomorphometric analyses were performed, and bone structural parameters were determined for both left and right tibiae. Radiation doses of 1.65 and 2.47 Gy affected bone marrow cells, heights of the proliferative and hypertrophic zones, and bone growth rates in the irradiated tibiae. For the 1.65 Gy group, irradiated tibiae resulted in lower BMD, Tb.Th, Tb.N and a higher Tb.Sp compared with the control tibiae. A decrease in BMD, BV/TV, Tb.Th, Tb.N and an increase in Tb.Sp were observed between the irradiated and control tibiae for the 2.47 Gy group. For cortical bone parameters, no effects were noticed for 1.65 and 0.83 Gy groups, but a lower Ct.Th was observed for 2.47 Gy group. Tibial bone development was adversely impacted and trabecular bone, together with bone marrow cells, were negatively affected by the 1.65 and 2.47 Gy radiation doses. Cortical bone microstructure was affected for 2.47 Gy group. However, bone development and morphometry were not affected for 0.83 Gy group. These findings can be used as a proof of concept for using the reasonable high-quality image acquisition under 0.83 Gy radiation doses during the adolescent period of rats without interfering with the bone development process.

4.2 Keywords

4.3 Introduction

In vivo micro-computed tomography (micro-CT) is an efficient tool for the non-destructive evaluation of laboratory animals and the *in vivo* tracking of longitudinal changes in bone mass and bone microstructure due to disease and/or bone adaptation processes (Y. Jiang, Zhao, White, &

Genant, 2000; Waarsing et al., 2004). Micro-CT has emerged as an advancement from the simple X-ray imaging into an essential technique, which is now used for laboratory research, tissue engineering, and numerical modeling (Mustafy, Arnoux, et al., 2018; Mustafy, El-Rich, Mesfar, & Moglo, 2014; Mustafy, Moglo, Adeeb, & El-Rich, 2014, 2016). Micro-CT can be used to longitudinally monitor bone micro-architecture in growing animals at different developmental stages. It can provide animal specific high-resolution data of time-related changes in desired bone locations. Changes can result from pathological or therapeutic stimuli, assuming minimal or no effects of the micro-CT scanning radiations on the radiated bone structural system (Laperre et al., 2011; Mitchell & Logan, 1998; Williams & Davies, 2006). However, as the micro-CT system might impose relatively high ionizing radiation doses (Cowan et al., 2007; Rüegsegger, Koller, & Müller, 1996), frequent or recurrent exposures to such doses of the scanned bony parts could induce some side effects, including growth hindrance, deformities of the skeleton, bone loss or other hematological abnormalities (Dudziak et al., 2000; Gal, Munoz-Antonia, Muro-Cacho, & Klotch, 2000; Matsumura, Jikko, Hiranuma, Deguchi, & Fuchihata, 1996; Mitchell & Logan, 1998; Williams & Davies, 2006).

High-radiation doses scans provide better image sets, which further facilitate the assessment of trabecular and cortical bone structures with higher accuracy (Ford, Thornton, & Holdsworth, 2003; Hasan et al., 2018; Laperre et al., 2011). However, this dose increment might pose a risk to the normal bone development process. Bone tissue damage can occur with doses as low as 250 mGy (Bushberg, Seibert, Leidholdt, Boone, & Goldschmidt, 2003; Waarsing et al., 2004). Cell death might occur due to the irreparable DNA damage resulting from excessive doses (Laperre et al., 2011; Olive, Banáth, & Durand, 1990). Low radiation doses can also trigger the DNA damage checkpoint activation, which results in a decreased cell proliferation (Iliakis, Wang, Guan, & Wang, 2003). Hence, an effective approach must be established to acquire high-quality images while using minimal radiation exposure. This can be achieved by efficaciously optimizing the scanning parameters to produce a low radiation dose which will provide an acceptable image quality without affecting the bone tissue.

Different studies use different approaches to investigate bone structure. Some studies need a single micro-CT scan whereas some need repeated CT scans. The impact of single radiation dose on longitudinal bone growth has been extensively investigated. Human long bones can exhibit swelling and fragmentation symptoms for doses ranging from 3–5 Gy (Mitchell & Logan, 1998).

Also, it has been reported that a radiation dose in the order of 5 Gy can affect the bone regeneration process while a dose limit of 2.5 Gy showed no such impacts (Jacobsson, Jönsson, Albrektsson, & Turesson, 1985). A rabbit femur exposed to 3.5 Gy radiation dose showed a significant reduction in the growth of long bones (Bisgard & Hunt, 1936), whereas no adverse effects were noticed for 400 mGy and lower radiation doses on the proliferation and differentiation of osteoblasts in adult Sprague-Dawley rats (Dare et al., 1997).

Repeated micro-CT measurements deemed to be necessary especially when tracking changes in bone development. Repeated measurements can provide valuable information on bone quality in post-surgical scenarios or in response to physical exercise or pharmaceutical treatment. However, repeated CT-scans can also cause a threat to the bone if it crosses a safe limit. Numerous animal studies have been performed to assess the impact of repeated micro-CT radiation doses on the whole body or the exposed limb. In a recent study (Judex et al., 2005), repeated (4 scans) doses effects of 1255 mGy and 453 mGy were investigated in adult mice (17 weeks old) femurs and no effects were found. In another study (Brouwers, Van Rietbergen, & Huiskes, 2007), adult Wister rats (30 weeks old) underwent 8 weeks *in vivo* scanning on their right tibia using doses as high as 939 mGy per scan. Bone structural measurements remained unaffected under the applied scanning regime. Another study (Klinck, Campbell, & Boyd, 2008) used adult mice aged 12 week old (exposed to 845.9 mGy) and adult rats aged 8 months old (exposed to 596.6 mGy) and found a decrease in the trabecular bone volume fraction in the radiated tibiae compared to the control ones.

Both single and repeated radiation studies demonstrate that various animal protocols showed divergent adaptability for the level of radiation doses applied. In addition to the difference in experimental protocols, variances in animal size, shape and anatomy, which put the skeleton under thicker or thinner skin, could be partly responsible for such differences in response to radiations. Hence, radiation results from one animal model and protocol could not be directly extrapolated to another. Moreover, most of the radiation doses related studies were performed on adult animal models, where the bone tissue has already peaked to its skeletal maturity. However, no such studies have been performed to define limit values below which radiation doses can be used safely for a growing animal model, in which bones have not reached their skeletal maturity.

Thus, the objective of this study was to evaluate radiation effects on bone morphometry, bone marrow cells, bone growth rate and growth plate histomorphometry in growing tibiae for three

radiation doses from repeated *in vivo* micro-CT scanning in adolescent rats. Results of this study will provide knowledge on weekly radiation doses protocol which can provide high-quality image sets to adequately investigate trabecular and cortical compartments, without causing damage to bone development during the rat adolescent growing period. The present study covered the rat adolescent period, which spans from the beginning of the 4th week of age to the end of 12th week period (Sengupta, 2013), resulting in a 9-week scanning period to investigate the radiation doses effects by comparing the irradiated and non-radiated limbs. The radiation dose of the first group was set at 0.83 Gy/scan, evaluated as the baseline to produce reasonable image quality for bone development investigation purpose. Two-fold (1.65 Gy/scan) and three-fold (2.47 Gy/scan) dose values were tested along with the same protocols for the second and third radiation groups.

4.4 Materials and methods

4.4.1 Animals

21 days old male Sprague-Dawley rats (n = 33) were obtained from Charles River Laboratories, Montreal, Canada. Rats were randomly divided into three doses groups: 0.83 Gy, 1.65 Gy and 2.47 Gy (n =11 per group). They were given 1-week of acclimatization before starting the experiment. Rats were housed two and three per cage (dimension 53 × 35.5 cm) at 25°C with a 12:12-hour light-dark cycle and provided with a standard laboratory diet and water ad libitum. Body weight was monitored weekly. The experimental protocol and all animal procedures were carried out in accordance with the guidelines of the Canadian Council on Animal Care (CCAC) and were approved by the Institutional Animal Care Committee at the Research Center of Sainte-Justine University Hospital, Montreal, Canada.

4.4.2 Repeated micro-CT scanning

A micro-CT scanner was used to perform nine weekly basis repeated CT scans of the proximal right tibia of the rats from their 4th to 12th weeks of age. A final scan was performed at the 14th week. The two-week interval for the last scan was chosen to assess the maximal radiation exposure effect after the end of the exposure protocol (Hélène Engström, 1986; H Engström, Jansson, & Engström, 1983). The imaging system was a Skyscan 1176 *in-vivo* micro-CT (Skyscan, N.V., Belgium) scanner with rotatable X-ray source and detector. Each rat was anesthetized (2%

isoflurane, 1.0 L/min O₂) and maintained on anesthetic gasses for the duration of the scanning. The rat was secured in the carbon fiber half-tube bed of the Skyscan 1176, and the right tibia was positioned into a Styrofoam holder of cylindrical shape. This procedure was performed to place the rat tibia in the scanning midline of the scanner and to eliminate any unwanted movement of the tibia during the radiation period. (Figure 4.1) (Perilli et al., 2010). The left tibia together with the tail were folded towards the animal's head and placed alongside the animal on the carbon fiber half-tube bed using masking tape. An ophthalmic gel was applied to the eyes of the rat during the entire scanning period to prevent dryness. The radiated tibia was subjected to X-rays solely, without irradiating the contralateral limb (left tibia).
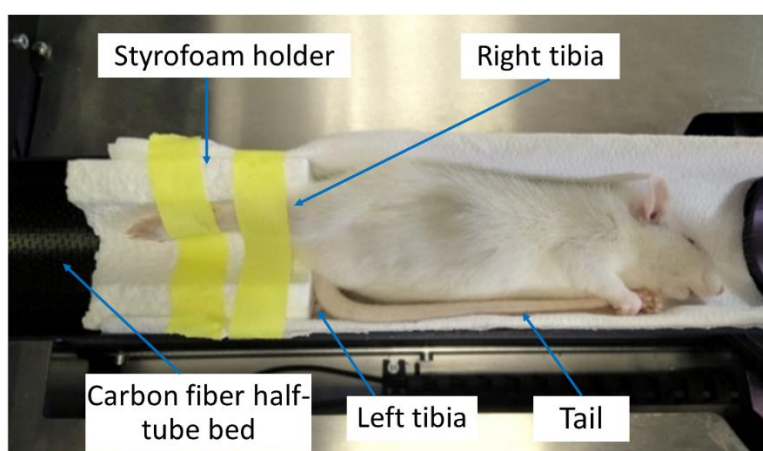
Figure 4.1 Rat positioning on the Skyscan 1176 scanner for *in vivo* scanning. The rat was placed sideways on the scanning bed while kept anesthetized (anesthesia mask not shown). This configuration was adapted to facilitate the positioning of the irradiated leg (right) into the iso-center of the scanning chamber. The right tibia was secured into a Styrofoam holder (1 cm thick) of cylindrical shape and firmly held with a medical adhesive tape. The non-radiated leg (left) was folded towards the animal's head and placed alongside the animal with its tail

For the first radiation group (0.83 Gy), all scans were performed on the anesthetized rats with an isotropic voxel size of 18µm. The choice of 18µm was made based on the previous findings (Isaksson et al., 2011; Longo, Sacco, Salmon, & Ward, 2016), which enables a reasonable high-quality image for the trabecular and cortical bone tissue investigation. An overview of image acquisition and reconstruction parameters for three radiation groups have been given in a tabular format (Table 4.1). For 0.83 Gy group, the isotropic voxel size generated 1,336×1,680 CCD

detector array. Total irradiation time was 5 min 34 sec and the scanning consisted of a stack of 304 images. For the second radiation group (1.65 Gy), image acquisition parameters were similar to the first group except for an improvement in the additional frame averaging (2 frame averaging versus 1 frame averaging) (Table 4.1). This improvement resulted in a finer detector array compared to the previous one (1,336×2,000 CCD detector array versus 1,336×1,680 CCD detector array). Total irradiation time was 11 min 9 sec and the scanning consisted of a stack of 395 images. For the third radiation group (2.47 Gy), an isotropic voxel size of 9µm was chosen for acquiring high-quality image sets for assessing trabecular and cortical bone microarchitecture. Image acquisition parameters were similar to the first group (Table 4.1). However, due to the improvement in isotropic voxel size (9µm versus 18µm), a finer detector array was generated compared to the first group (2,672×3,560 CCD detector array versus 1,336×1,680 CCD detector array). Total irradiation time was 16 min 39 sec and the scanning consisted of a stack of 304 images.

For all groups, the left tibia was used as a control and scanned only on the last (14th week) scanning time point. Euthanasia of the rats was performed after the last scan (14th weeks of age) using a CO_2 chamber. For all rats, weight monitoring was conducted on a weekly basis to assess the impact of anesthesia and irradiation on rat development. The acquisition covered the proximal tibial section of the rat tibia. The delivered doses of 0.83 Gy, 1.65 Gy and 2.47 Gy computed tomography dose index (CTDI) were calculated based on the manufacturer specifications (Bruker micro-CT). The provided specifications (Bruker micro-CT) followed the dose measurements using a UNFORS PS-2 patient skin dosimeter. Shielding was provided with acrylic plastic (PMA) tubes of various wall thicknesses to simulate soft biological tissue. Local absorbed radiation dose rate (mGy/min) for tibia, femur, etc. have been provided by the manufacturer for different scan settings scenarios (Micro-CT). The data that accurately matched with our scanning parameters (65 kV, 385 µA, full x-ray, and 1-mm Al filter) have been extracted and local absorbed dose rate have been multiplied by the scanning time to get the resulted doses for our study (Johnson, 2017) (Appendix A). For an approximation, the tissue at all depths was assumed to be a cylinder and the dose rate of all tissue cylinder diameters averaged between the dose in the air (zero depth) and the dose at the cylinder center (half diameter) (Micro-CT).

Table 4.1 Image acquisition and reconstruction parameters of the rat proximal tibiae for the three doses groups

	0.83 Gy	1.65 Gy	2.47 Gy
Scanning parameters			
Voxel size (µm)	18	18	9
Voltage (kV)	65	65	65
Current (µA)	385	385	385
Rotation step (over 180º)	0.65º	0.50º	0.65º
Exposure time (ms)	350	350	1140
Frames averaged per projection	1	2	1
Filter	AL 1mm	AL 1mm	AL 1mm
Approximate scan time (min)	6	11	17
Reconstruction Parameters			
Filter	Gaussian	Gaussian	Gaussian
Smoothing kernel	1	1	1
Ring artifact reduction	4	4	4
Beam hardening correction (%)	10	10	10
Attenuation coefficient	0.000-0.049	0.000-0.049	0.000-0.049
Analysis Parameters			
Thresholding	Global, 65	Global, 65	Global, 65

All micro-CT scans were obtained using the SkyScan 1176 model, Bruker-microCT.

Scanned image sets were reconstructed by applying filtered back-projection algorithm (software NRecon, v.1.6.10, Skyscan, Kontich, Belgium) (Perilli et al., 2010). A total height of 10 mm cross-sectional images was reconstructed for every scanned set. The reconstruction started from the beginning of the knee joint and extended distally into the tibial diaphysis. The resolution of the processed images for first and second radiation groups was 1500 × 1500 pixels each, 17.48 µm isotropic voxel size, and the images were 8-bit in size (256 gray levels). The third radiation group produced images with 2700 × 2700 pixels each, 8.74 µm isotropic voxel size, and the images were 8-bit in size (256 gray levels).

4.4.3 Calcein injections

For measurement of longitudinal bone growth rate, calcein was used to label the bone line on the surface of the tibia. Injections of calcein (Sigma-Aldrich, St. Louis, MO, USA), a fluorescent marker, were made intraperitoneally at a dosage of 15 mg/Kg (Valteau, Grimard, Londono, Moldovan, & Villemure, 2011). Injections were done 5 and 2 days prior to euthanasia.

4.4.4 Bone marrow cell assessment

After CO_2 asphyxiation, followed by decapitation, both tibiae were collected. Left (control) and right (irradiated) tibiae were sawed off to keep 10 mm on both proximal and distal sides using an ISOMET 1000 Precision Saw (Buehler, An ITW Company, Illinois, USA). To determine cell radiation damage, bone marrow cells were collected from both control and radiated tibiae. Bone marrow cells were flushed by applying pressure with a needle filled with HBSS (Hank's balanced saline solution) in the sawed part of the tibiae. A cell count was performed on the collected cell suspensions on HBSS with trypan blue (0.4% solution, Sigma-Aldrich, Oakville, ON, Canada). Using the trypan blue test, the number of living and dead cells and their corresponding percentages were determined for both control and radiated tibiae. From these values, percentage of unaffected bone marrow cells was calculated by dividing the total number of live cells by the number of total cells (live + dead).

4.4.5 Tissue processing

Formalin solution (Anachemia, Montreal, QC, Canada) was used to fix the proximal sections (~10 mm) from each tibia for a duration of 48h. Thereafter, graded alcohol solutions were used for dehydration, xylene was used for clarification and methylmethacrylate (MMA) (Fisher Scientific Canada, Nepean, ON, Canada) was used for embedding process (Ménard et al., 2014). When the polymerization was completed, a microtome (Leica SM2500) setup was used to cut the blocks of the tibiae into 6 µm sections. Only the proximal sections were used in this study. To cover the 40-50% of the growth plate depth, the tibiae were cut along the longitudinal bone axis for 36 slides, six series of six slides, which contain two sections per slide. To facilitate the growth rate measurements, the first slide of each series (6 slides, 12 sections total) per proximal tibia were set aside from light. A microscope (Leica DMR with Retina Qimaging Camera) was used for slice observation while using 5x magnification for growth rate measurements.

4.4.6 Bone growth rate

The distance between two calcein labels was divided by the time interval (3 days) between the two applied injections to calculate the bone growth rate (Hunziker & Schenk, 1989). An in-house built Matlab program was used for this purpose. The distance was automatically calculated as the mean

value of 100 segments parallel to the longitudinal growth direction with both calcein lines modeled as splines (Ménard et al., 2014; Valteau et al., 2011) (Figure 4.2A).

4.4.7 Growth plate histomorphometry

Heights of the proliferative and hypertrophic zones, the hypertrophic cell height as well as the number of proliferative cells per column were measured for the histomorphometric analysis, similarly to previous work (Ménard et al., 2014; Valteau et al., 2011) (Figure 4.3A and 4.3B). Hypertrophic cell height and the number of proliferative chondrocytes per column were measured as they are considered to be the indirect markers of bone growth (Ménard et al., 2014; Valteau et al., 2011). To measure heights, a similar approach to the bone growth rate measurements was implemented with 10x magnified image sets. Values from 100 segmental measurements were averaged for the assessment of zonal heights (Figure 4.3A). A 20x magnified image set was used to measure the hypertrophic cell height along the longitudinal growth direction (Figure 4.3B). The number of proliferative chondrocytes per column was measured from 20x magnified image sets for six random columns per growth plate (Figure 4.3B). For a single proximal tibial segment, histomorphometric parameters were measured by averaging 72 values, 6 values per section, 12 values per microscope slide with a six series repetition.
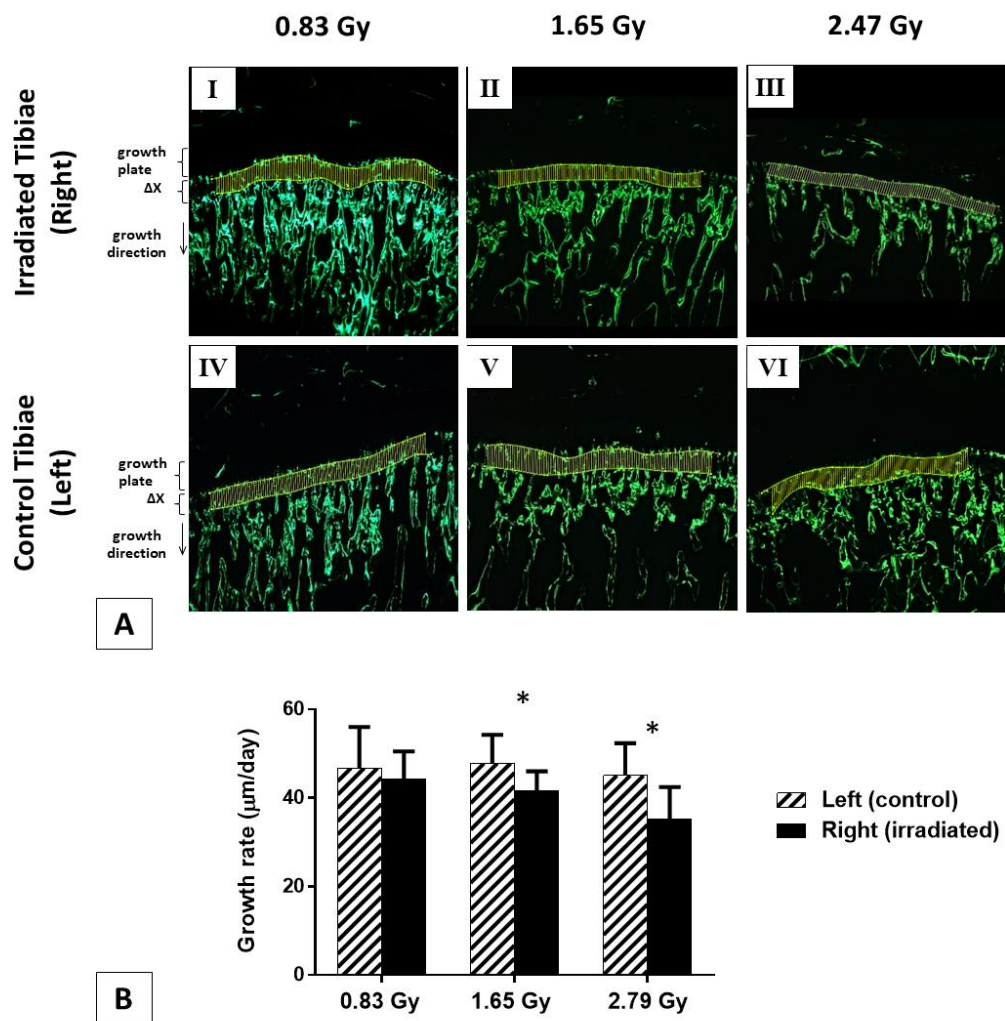
Figure 4.2 Bone growth rates (μm/day) measurements. (A) 5x magnified microscopic images of the tibial metaphysis labeled twice with calcein for representative irradiated and control tibiae from three doses groups (I-VI). Bone growth (ΔX, μm) measured as the mean distance between the two calcein lines, which were modeled as splines and divided by the time interval (3 days) between the two applied injections. (B) Growth rates (μm/day) of rat proximal tibiae for 0.83, 1.65 and 2.47 Gy radiation groups (mean value ± SD). *: a significant difference ($p < 0.05$) between the control (left) and irradiated (right) tibiae for each radiation dose
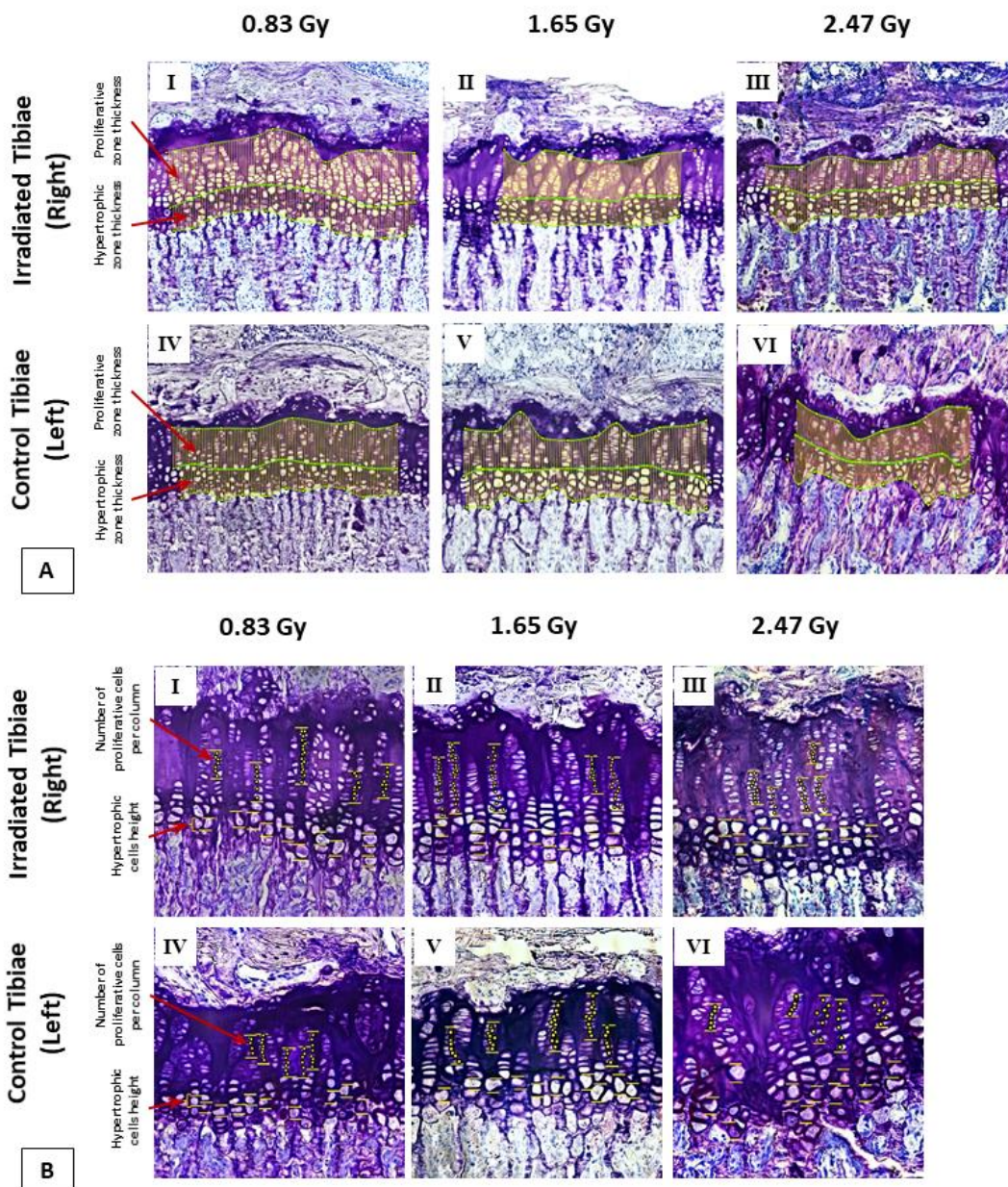
Figure 4.3 Histomorphometry measurement. (A) Growth plate section embedded in MMA and stained with toluidine blue (10x). Evaluation of the hypertrophic and proliferative zonal thicknesses for three doses groups. (B) Growth plate section embedded in MMA and stained with toluidine blue (20x). Evaluation of the hypertrophic cell height and number of proliferative cells per column for three doses groups

4.4.8 Trabecular and cortical bone morphometry

A volume of interest (VOI) was defined for morphometric analysis from the reconstructed image sets. The VOI included the proximal metaphysis, covering both trabecular and cortical bony segments (software CT Analyzer v.1.13, Skyscan, Kontich, Belgium). The proximal metaphysis of the tibia contains the growth plate and is responsible for blood supply and vascular stasis in growing bone. This part is also very sensitive to radiation exposure compared to the other regions of the bone (Eifel, Sampson, & Tucker, 1990). So, absence of radiation effects on this bony region could presumably be considered as to have no effects on the epiphysis and the metaphysis parts as well (Brouwers et al., 2007). The VOI was selected as a percentage of the entire tibial length (L) to keep consistency with the growing tibial length from 4th to 14th week of age. To exclude the primary spongiosa, the VOI started at ~1mm distal to the growth plate and extended for 10% of the total tibial length (L) (Lynch et al., 2010) (Figure 4.4).
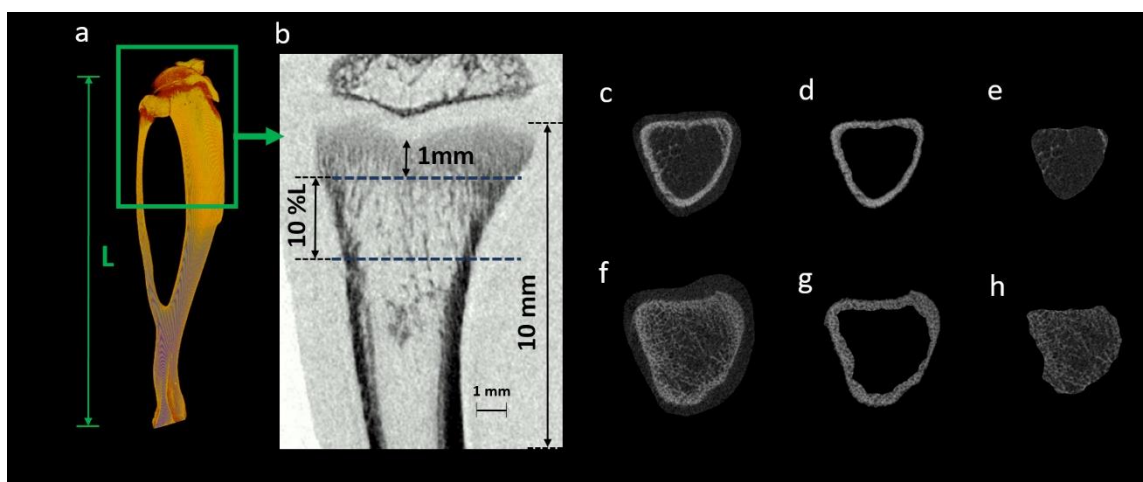
Figure 4.4 *In vivo* scanning of proximal tibia and bone segmentation process. (a) A representative 3D reconstructed tibia showing the total tibial length (L). (b) Scanned proximal tibial cross-section (10 mm in height) of the rat tibia. This representative image was acquired from a 17.48-μm pixel size scanning at 0.83 Gy radiation dose. VOI consisting trabecular and cortical bone, for morphometric parameters evaluation, beginning at ~1mm distal to the growth plate and extending for 10% of the total tibial length (L). Proximal (f) and distal (c) tibial sections are illustrated. The cortical (d, g) and trabecular (e, h) bone regions were segmented using a semi-automatic bone segmentation algorithm

An in-house algorithm was developed for semi-automatically segmenting the trabecular and cortical bone. The segmentation was done by delineating the periosteum and endosteum surface in a semi-automatic algorithm based approach (Boyd, Davison, Müller, & Gasser, 2006; Buie, Campbell, Klinck, MacNeil, & Boyd, 2007). A global gray threshold value of 65 corresponding to an equivalent density of 0.413 g/cm3 of calcium hydroxyapatite (CaHA), was set for all the analysis (Boyd et al., 2006; Lynch et al., 2010). Morphometric analysis was performed using CTAn software v.1.13 for the selected VOI of trabecular bone to evaluate the following bone structural parameters: bone mineral density (BMD), bone volume fraction (BV/TV), connectivity density (Conn.Dn), trabecular number (Tb.N), trabecular thickness (Tb.Th), and trabecular spacing (Tb.Sp) (Bouxsein et al., 2010). Excluding the VOI of trabecular bone from the selected dataset, cortical bone VOI was also extracted. Cortical microarchitectural measurements, including tissue mineral density (TMD), cross-sectional area inside the periosteal envelope (Tt.Ar), cortical bone area (Ct.Ar), cortical thickness (Ct.Th), periosteum perimeter (Ps.Pm), endocortical perimeter (Ec.Pm), medullary area (Ma.Ar), and mean eccentricity (Ecc) were evaluated using the cortical bone VOI (Bouxsein et al., 2010).

The morphometric measurement process was appraised for reproducibility test. To do so, five scans of the right tibia were acquired from a dead rat in different orientations. After the completion of each scan, the rat was completely removed from the scanner bed and repositioned again in a different orientation. The same micro-CT scanning, image reconstruction, VOI selection and morphometric analysis protocols as the ones used for the radiation effects experiment were used in this reproducibility evaluation. The coefficient of variation (CV) was then determined by the five scans. The resulting reproducibility was high, with CV found to be less than 2% for BV/TV, Ct. Th., Ec. Pm., and Ma. Ar., less than 3% for BMD, TMD, Tb.Th, Tb.N, Tt. Ar., Ps. Pm., and Ecc., and less than 4% for Ct. Ar., Tb.Sp, and Conn.Dn.

4.4.9 Statistical analysis

Statistical analyses were performed using SPSS Statistics (v. 23, IBM). Comparisons were made at the 14th week between the irradiated and non-radiated tibiae for impacts on bone marrow cells, bone growth rate, growth plate histomorphometry, and bone morphometry for each dose group (Mustafy, Londono, & Villemure, 2018). ANOVA test (general linear model) was performed to determine time effects, radiation dose, and their interaction on body weight. A paired Student's t-

test was performed for determining any significant differences in absolute and percentage numbers of viable cells, in average bone growth rates and in histomorphometric and bone structural parameters measured at the 14th week for both irradiated and control tibiae. Moreover, structural properties of trabecular and cortical bone microstructure of the irradiated tibiae from three doses groups were statistically analyzed on 14th week scanning data. A one-way ANOVA with Tukey's multiple comparisons was performed to assess the significant group difference and pairwise comparisons. For each group, the series mean value was used to replace any values which were missing due to the movement of rats during a scanning procedure or due to the reconstruction error. For all the groups, this missing value incident occurred a total of five times (once in the 0.83 Gy group at 8th week of age, twice in the 1.65 Gy group at 6th and 9th week of age, and twice in the 2.47 Gy group at 7th and 11th week of age). Results were considered statistically significant for p < 0.05.

4.5 Results

4.5.1 Bone growth rate

The average bone growth rate measured at the 14th week in irradiated tibiae for 1.65 and 2.47 Gy group resulted in growth rate reductions of 13.1% and 21.8% respectively with respect to the control tibiae. These reductions were statistically significant ($p < 0.05$) (Figure 2.2B). No significant difference was observed for the bone growth rate in the 0.83 Gy group (Figure 2.2B).

4.5.2 Growth plate histomorphometry

Significant differences were found in the zone thickness for both HZ and PZ in 1.65 and 2.47 Gy groups, whereas no significant difference was found for the 0.83 Gy group between the irradiated and control tibiae (Figure 4.5a and 4.5b). Hypertrophic cell heights and numbers of proliferative chondrocytes per column were found to be similar for irradiated and non-radiated tibiae for all three groups (Figure 4.5c and 4.5d).
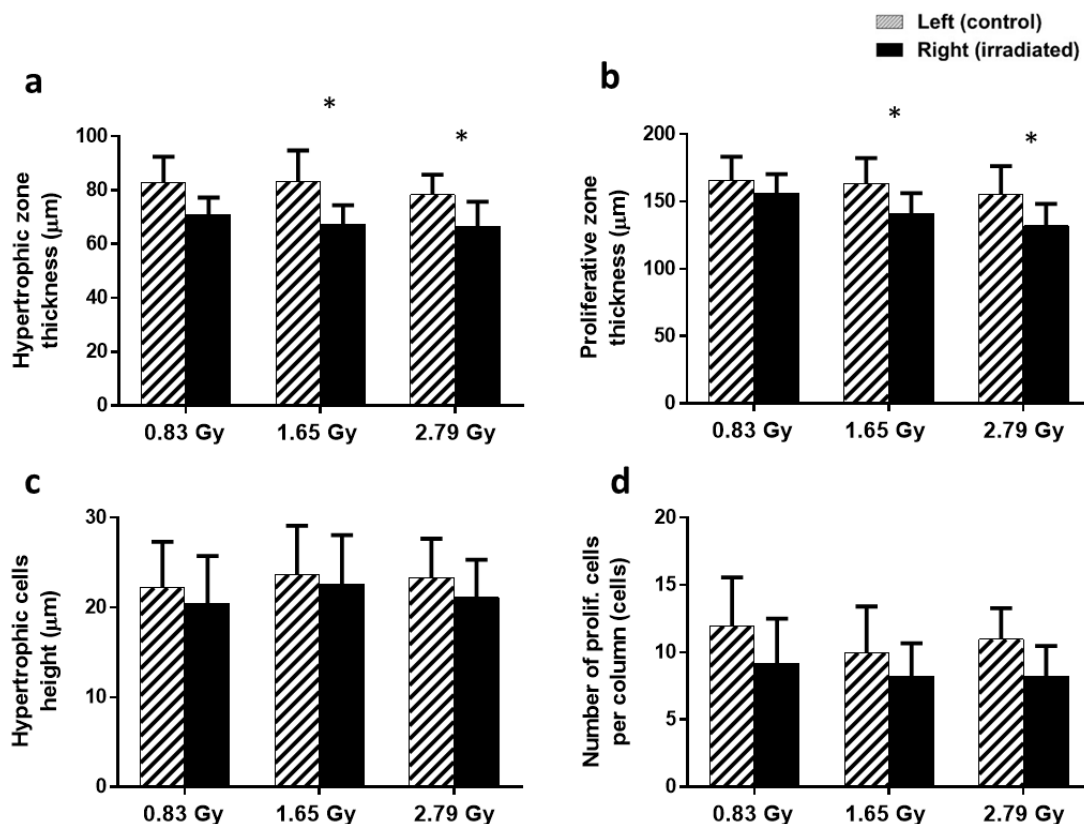
Figure 4.5 Histomorphometry measurements comparison for control and irradiated tibiae. (a-d) Growth plate histomorphometry measurements of rat proximal tibiae for 0.83, 1.65 and 2.47 Gy radiation groups (mean value ± SD). *: a significant difference ($p < 0.05$) between the control (left) and irradiated (right) tibiae for each radiation dose

4.5.3 Trabecular and cortical bone morphometry: comparative analysis at the 14th week

The effect of repeated *in vivo* irradiation was assessed by comparing the repeatedly irradiated right tibiae to the singly irradiated left tibiae at the 14th week of age. Morphometric parameters of both trabecular and cortical bones were compared within each group to assess the radiation effect. For the trabecular bone morphometry, 0.83 Gy group showed no significant difference between the irradiated tibiae and their contralateral controls (Figure 4.6). For both the 1.65 and 2.47 Gy group, a significant decrease in BMD, Tb.Th, Tb.N, and a significant increase for Tb.Sp was observed

between the irradiated and control tibiae (Figure 4.6). Moreover, a significant decrease in BV/TV was also observed for the 2.47 Gy group (Figure 4.6).
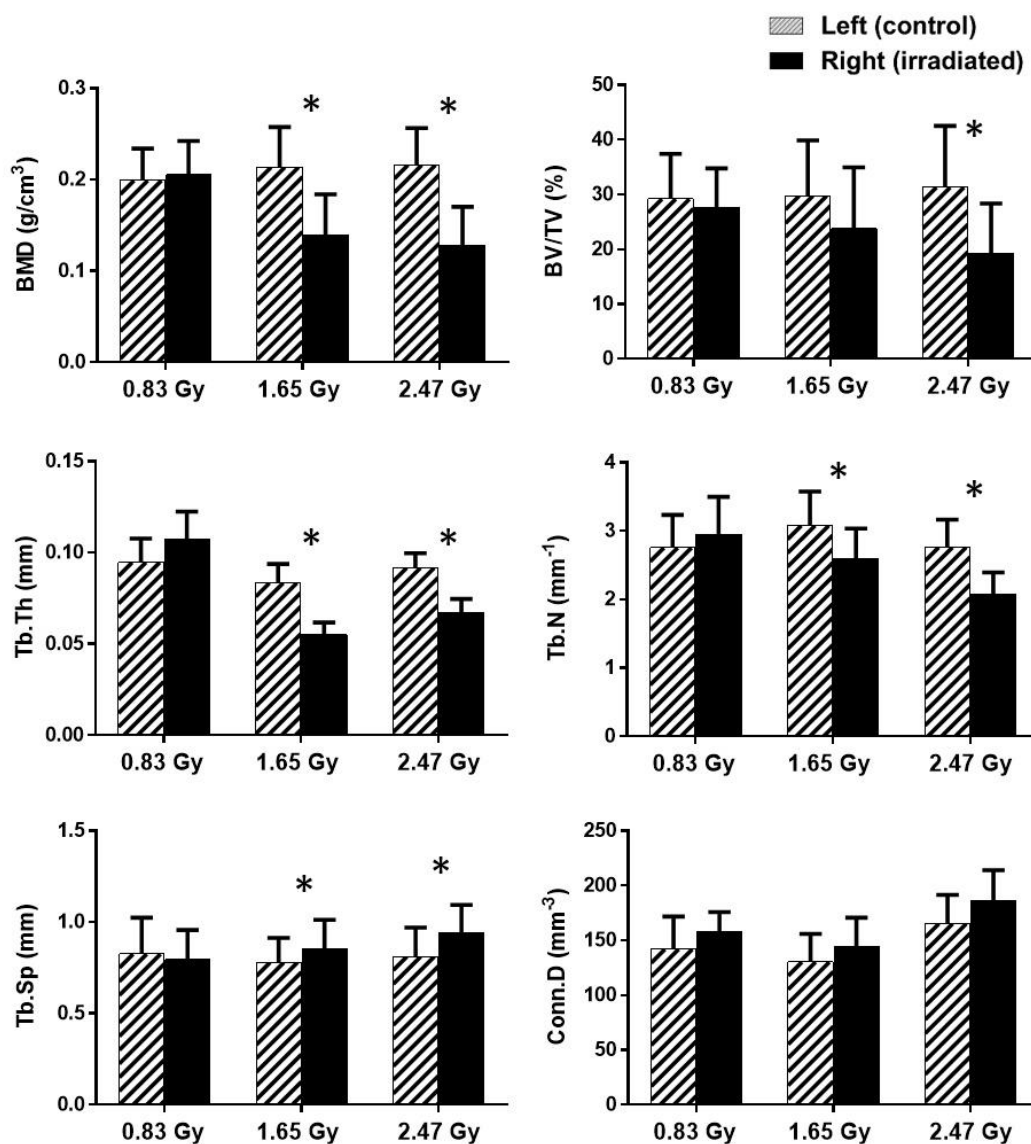
Figure 4.6 Mean values and standard deviations of the trabecular bone parameters for the left (hatched columns), and right tibia (black columns) at 14th week of age (n = 11/group).

*: a significant difference ($p < 0.05$) between the control (left) and irradiated (right) tibiae for each radiation dose

For the cortical bone morphometry, no differences were found between the irradiated and control tibiae at the 14th week of age for both 0.83 and 1.65 Gy group (Figure 4.7). However, irradiated tibiae resulted in lower Ct.Th compared to the controlled ones for the 2.47 Gy group (Figure 4.7).
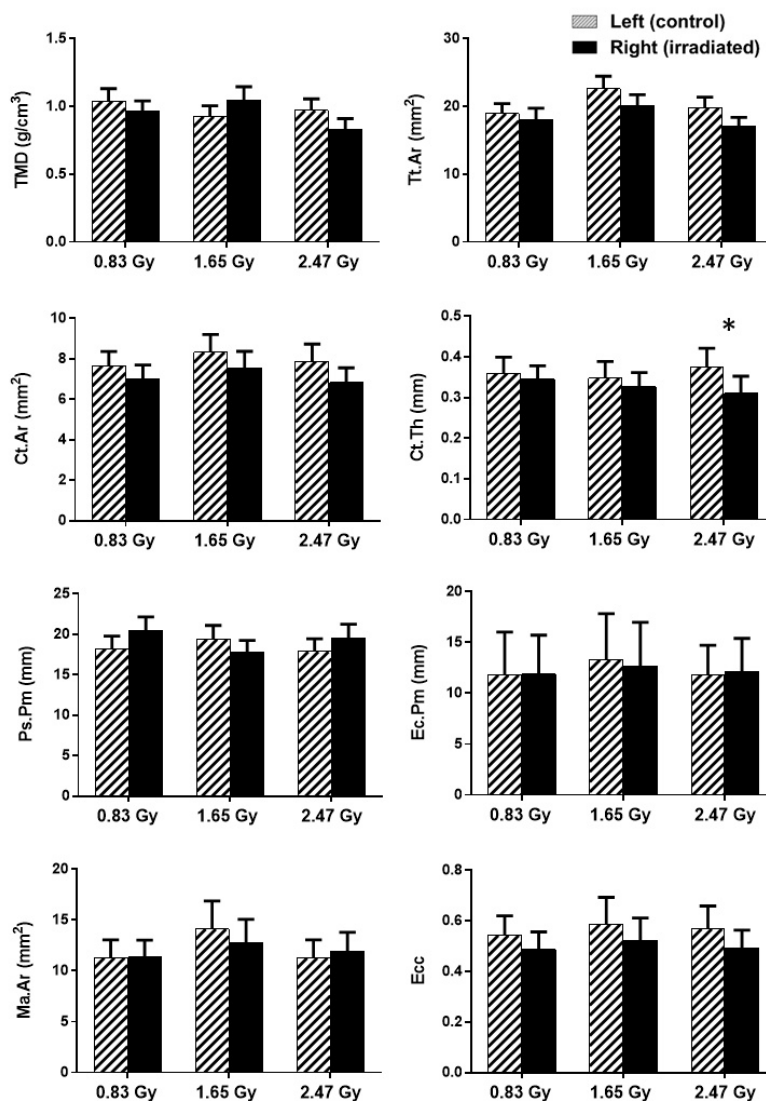
Figure 4.7 Mean values and standard deviations of the cortical bone parameters for the left (hatched columns), and right tibiae (black columns) at 14th week of age (n = 11/group)

*: a significant difference ($p < 0.05$) between the control (left) and irradiated (right) tibiae for each radiation dose

4.5.4 Trabecular and cortical bone morphometry: 9-week longitudinal comparative analysis

Bone morphometric changes were assessed in the right proximal tibia during the entire adolescent period (from 4th to 14th week of age) for each rat. Trabecular bone parameters showed changes with rat development in the different groups. For the 0.83 Gy group, a significant increase ($p < 0.05$) was observed for BMD, BV/TV, Tb.Th, and Tb.N from the 4th to the 14th week old period (Table 4.2). However, a decrease was observed for Conn.Dn values within the same study period (Table 4.2). A significant increase for Tb.Sp and a decrease for Tb.Th were observed for both 1.65 Gy and 2.47 Gy group (Table 4.2). However, an increase in Tb.N for 1.65 Gy and a decrease in Conn.Dn and BMD were observed for 1.65 Gy and 2.47 Gy group respectively (Table 4.2). A significant increase ($p < 0.05$) was observed for Tt.Ar, Ct.Ar, Ps.Pm, Ec.Pm, Ma.Ar, and Ecc for all three groups (Table 4.3). However, for TMD and Ct.Th values, a significant increase was only observed for 0.83 Gy and 1.65 Gy groups (Table 4.3).

Tukey's post hoc multiple comparison tests revealed differences among different groups for the 14th week scanning data (Table 4.4). 0.83 Gy group showed significant difference with the 1.65 Gy group for BMD, Tb.Th, Conn.Dn, and Tt.Ar parameters (Table 4.4). Comparing 0.83 Gy and 2.47 Gy groups, significant differences were found for BMD, Tb.Th, Tb.N, Tb.Sp, Conn.Dn, Ct.Th, and Ps.Pm parameters (Table 4.4). The 1.65 Gy group showed significant differences with the 2.47 Gy group for Tt.Ar parameter only (Table 4.4).

4.5.5 Body weight

Body weights were similar for rats of all groups at the beginning of the experiment (4th week of age) (Figure 4.8). A time effect (weight gain) was observed in rats as they were in their growing phase. However, no effects of dose or dose/time interaction were found and no loss of hair was observed during the study period (Figure 4.8). At the end of the experiment, average body weights of 0.83, 1.65 and 2.47 Gy groups were 572.2 ± 40.8, 534.1 ± 25.5, and 519.2 ± 23.1 g, respectively.
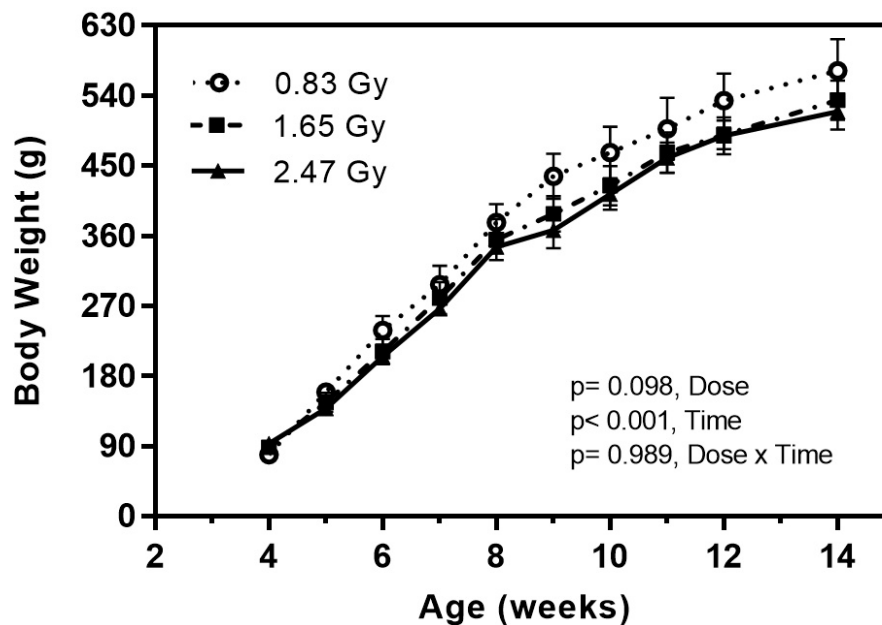
Figure 4.8 Body weight of male Sprague Dawley rats for three doses groups over the adolescent period. ANOVA test (general linear model) was performed to determine time effects, radiation dose, and their interaction on body weight. N = 11 rats per group (mean value ± SD)

Table 4.2 Longitudinal assessment of trabecular microarchitecture of the right proximal tibial metaphysis in three doses groups of rats.

Trabecular structural properties	Dose (Gy)	Age (week)									
		4	5	6	7	8	9	10	11	12	14
BMD (g.cm^{-3})											
	0.83	0.156 ± 0.035	0.163 ± 0.027	0.150 ± 0.024	0.171 ± 0.029	0.183 ± 0.04	0.172 ± 0.051	0.179 ± 0.044	0.185 ± 0.026	0.200 ± 0.031	0.205 ± 0.037 α
	1.65	0.162 ± 0.028	0.173 ± 0.046	0.163 ± 0.038	0.179 ± 0.041	0.121 ± 0.031	0.131 ± 0.016	0.131 ± 0.02	0.111 ± 0.036	0.125 ± 0.035	0.139 ± 0.045
	2.47	0.173 ± 0.015	0.192 ± 0.045	0.184 ± 0.029	0.186 ± 0.035	0.141 ± 0.051	0.14 ± 0.018	0.121 ± 0.051	0.121 ± 0.036	0.132 ± 0.034	0.128 ± 0.042 γ
BV/TV (%)											
	0.83	18.78 ± 5.23	20.05 ± 4.12	21.89 ± 6.42	22.27 ± 7.13	20.72 ± 4.13	21.07 ± 3.12	19.94 ± 6.14	21.51 ± 7.12	22.78 ± 5.12	27.56 ± 7.21 α
	1.65	20.55 ± 8.23	21.52 ± 7.4	22.72 ± 8.24	23.77 ± 5.13	19.74 ± 8.23	19.77 ± 5.13	19.34 ± 8.13	22.3 ± 6.12	21.46 ± 7.24	23.76 ± 11.23
	2.47	22.47 ± 10.12	23.63 ± 8.23	20.12 ± 7.40	21.23 ± 6.40	18.75 ± 8.24	19.34 ± 7.23	18.84 ± 5.34	19.44 ± 6.14	17.76 ± 8.42	19.14 ± 9.23
Tb.Th (mm)											
	0.83	0.078 ± 0.012	0.083 ± 0.012	0.081 ± 0.012	0.086 ± 0.013	0.087 ± 0.012	0.079 ± 0.011	0.084 ± 0.012	0.085 ± 0.015	0.087 ± 0.015	0.107 ± 0.015 α
	1.65	0.093 ± 0.014	0.094 ± 0.011	0.086 ± 0.010	0.078 ± 0.010	0.075 ± 0.010	0.074 ± 0.012	0.076 ± 0.010	0.072 ± 0.012	0.062 ± 0.013	0.055 ± 0.006 β
	2.47	0.103 ± 0.011	0.105 ± 0.011	0.097 ± 0.012	0.089 ± 0.015	0.093 ± 0.011	0.094 ± 0.011	0.088 ± 0.012	0.078 ± 0.011	0.076 ± 0.011	0.067 ± 0.007 γ
Tb.N (mm^{-1})											
	0.83	2.208 ± 0.457	2.104 ± 0.435	2.453 ± 0.508	2.578 ± 0.533	2.473 ± 0.482	2.447 ± 0.477	2.642 ± 0.515	2.577 ± 0.483	2.82 ± 0.529	2.946 ± 0.552 α
	1.65	1.972 ± 0.379	1.863 ± 0.358	2.15 ± 0.414	2.12 ± 0.408	2.234 ± 0.414	2.163 ± 0.401	2.22 ± 0.411	2.41 ± 0.402	2.33 ± 0.388	2.601 ± 0.434 β
	2.47	2.651 ± 0.496	2.55 ± 0.477	2.678 ± 0.501	2.489 ± 0.466	2.102 ± 0.359	1.961 ± 0.335	2.16 ± 0.369	2.1 ± 0.326	1.83 ± 0.284	2.072 ± 0.321 γ
Tb.Sp (mm)											
	0.83	0.839 ± 0.187	0.817 ± 0.182	0.784 ± 0.174	0.763 ± 0.159	0.819 ± 0.17	0.71 ± 0.151	0.766 ± 0.163	0.751 ± 0.153	0.85 ± 0.173	0.794 ± 0.162
	1.65	0.646 ± 0.133	0.612 ± 0.126	0.671 ± 0.138	0.726 ± 0.14	0.752 ± 0.146	0.781 ± 0.154	0.751 ± 0.148	0.795 ± 0.145	0.831 ± 0.152	0.855 ± 0.156 β
	2.47	0.752 ± 0.131	0.723 ± 0.126	0.723 ± 0.126	0.711 ± 0.124	0.777 ± 0.135	0.795 ± 0.134	0.743 ± 0.125	0.773 ± 0.126	0.892 ± 0.145	0.929 ± 0.151 γ
Conn.Dn (mm^{-3})											
	0.83	189.8 ± 32.5	195.5 ± 39.1	234.7 ± 46.9	188.4 ± 32.6	178.5 ± 30.9	189.3 ± 32.8	234.1 ± 34.5	173.2 ± 25.5	164.3 ± 24.2	157.9 ± 29.2 α
	1.65	263.4 ± 40.9	258.2 ± 40.1	273.8 ± 42.5	295 ± 54.2	219.5 ± 40.3	232.6 ± 42.7	266.4 ± 45.2	145.3 ± 24.6	132.1 ± 22.4	144.7 ± 26.1 β
	2.47	208.8 ± 30.3	220.2 ± 31.9	255.2 ± 37	210.2 ± 30.5	233.2 ± 43.2	189.2 ± 35.1	225.8 ± 41.8	205.2 ± 27.7	178.3 ± 24.1	186.6 ± 27.4

Values are expressed as Mean ± SD, n = 11/group. Within each dose (0.83, 1.65 and 2.47 Gy), different symbols (α, β, γ) denote statistical significance ($p < 0.05$) from 4th to 14th week of age.

Abbreviations: BMD, bone mineral density; BV/TV, bone volume fraction; Tb.Th, trabecular thickness; Tb.N, trabecular number; Tb.Sp, trabecular spacing; Conn.Dn, connectivity density.

Table 4.3 Longitudinal assessment of cortical microarchitecture of the right proximal tibial metaphysis in three doses groups of rats.

Cortical structural properties	Dose (Gy)	Age (week)									
		4	5	6	7	8	9	10	11	12	14
TMD (gm.cm⁻³)											
	0.83	0.773 ± 0.063	0.803 ± 0.065	0.828 ± 0.08	0.873 ± 0.085	0.824 ± 0.08	0.858 ± 0.084	0.831 ± 0.082	0.852 ± 0.084	0.884 ± 0.087	0.961 ± 0.078 $^\alpha$
	1.65	0.743 ± 0.08	0.783 ± 0.085	0.782 ± 0.085	0.823 ± 0.078	0.852 ± 0.08	0.802 ± 0.076	0.783 ± 0.074	0.883 ± 0.102	0.902 ± 0.104	1.043 ± 0.101 $^\beta$
	2.47	0.718 ± 0.069	0.744 ± 0.072	0.752 ± 0.069	0.783 ± 0.071	0.802 ± 0.073	0.783 ± 0.09	0.802 ± 0.092	0.773 ± 0.089	0.794 ± 0.092	0.83 ± 0.08
Tt.Ar (mm²)											
	0.83	10.54 ± 1.04	12.05 ± 1.19	15.42 ± 1.52	17.73 ± 1.81	18.6 ± 1.9	19.41 ± 1.99	19.84 ± 2.03	20.07 ± 0.17	20.45 ± 0.18	18.08 ± 1.46 $^\alpha$
	1.65	11.75 ± 1.11	14.23 ± 1.35	18.23 ± 1.73	18.07 ± 1.45	19.69 ± 1.58	20.38 ± 1.63	20.52 ± 2.15	19.19 ± 2.01	18.89 ± 1.98	20.05 ± 1.78 $^\beta$
	2.47	10.1 ± 0.99	11.04 ± 1.09	13.37 ± 1.32	14.88 ± 1.31	16.34 ± 1.44	17.34 ± 1.52	17.58 ± 1.88	16.23 ± 1.73	16.34 ± 1.74	17.03 ± 1.34 $^\gamma$
Ct.Ar (mm²)											
	0.83	3.289 ± 0.356	4.586 ± 0.496	5.53 ± 0.599	5.132 ± 0.556	5.808 ± 0.592	5.884 ± 0.6	6.542 ± 0.667	7.261 ± 0.74	7.469 ± 0.762	7.013 ± 0.685 $^\alpha$
	1.65	2.96 ± 0.302	4.62 ± 0.472	6.002 ± 0.614	5.994 ± 0.711	6.424 ± 0.762	7.32 ± 0.869	6.784 ± 0.867	7.728 ± 0.988	7.685 ± 0.982	7.55 ± 0.817 $^\beta$
	2.47	2.835 ± 0.321	4.05 ± 0.459	4.735 ± 0.536	4.23 ± 0.479	5.323 ± 0.649	6.23 ± 0.759	5.954 ± 0.726	6.34 ± 0.773	6.67 ± 0.952	6.823 ± 0.732 $^\gamma$
Ct.Th (mm)											
	0.83	0.196 ± 0.02	0.251 ± 0.026	0.235 ± 0.024	0.281 ± 0.029	0.288 ± 0.03	0.335 ± 0.035	0.364 ± 0.036	0.383 ± 0.037	0.373 ± 0.036	0.344 ± 0.033 $^\alpha$
	1.65	0.232 ± 0.024	0.244 ± 0.025	0.215 ± 0.022	0.242 ± 0.028	0.263 ± 0.031	0.272 ± 0.032	0.312 ± 0.037	0.353 ± 0.042	0.325 ± 0.039	0.326 ± 0.035 $^\beta$
	2.47	0.22 ± 0.031	0.223 ± 0.031	0.18 ± 0.025	0.212 ± 0.034	0.249 ± 0.04	0.224 ± 0.036	0.258 ± 0.041	0.263 ± 0.051	0.281 ± 0.055	0.309 ± 0.042
Ps.Pm (mm)											
	0.83	13.48 ± 1.29	13.5 ± 1.29	15.45 ± 1.48	18.68 ± 2.24	19.23 ± 2.3	19.19 ± 2.3	17.23 ± 1.86	19.71 ± 2.12	19.78 ± 2.13	20.48 ± 1.64 $^\alpha$
	1.65	11.96 ± 1.22	12.67 ± 1.29	16.18 ± 1.65	15.43 ± 1.76	18.08 ± 2.06	18.8 ± 2.14	18.57 ± 2.56	16.4 ± 2.26	18 ± 2.48	17.72 ± 1.51 $^\beta$
	2.47	12.67 ± 1.52	14.22 ± 1.71	16.34 ± 1.96	16.34 ± 1.77	18.75 ± 2.03	19.34 ± 2.09	18.84 ± 1.73	17.89 ± 1.65	18.63 ± 1.72	19.49 ± 1.73 $^\gamma$
Ec.Pm (mm)											
	0.83	9.51 ± 2.96	9.68 ± 3.01	11.15 ± 3.47	12.58 ± 4.62	12.68 ± 4.66	13.03 ± 4.79	12.92 ± 3.82	12.68 ± 3.75	12.77 ± 3.77	11.88 ± 3.84 $^\alpha$
	1.65	10.45 ± 3.35	10.98 ± 3.52	12.39 ± 3.97	12.32 ± 4.27	12.91 ± 4.48	12.81 ± 4.44	13.13 ± 3.85	12 ± 3.51	11.86 ± 3.47	12.66 ± 4.32 $^\beta$
	2.47	9.54 ± 2.68	9.37 ± 2.64	10.42 ± 2.93	11.57 ± 4	11.76 ± 4.07	11.81 ± 4.08	12.08 ± 3.81	11.14 ± 3.51	11.02 ± 3.47	12.18 ± 3.23 $^\gamma$
Ma.Ar (mm²)											
	0.83	7.25 ± 1.37	7.46 ± 1.41	9.89 ± 1.87	12.59 ± 2.14	12.79 ± 2.17	13.52 ± 2.3	13.3 ± 2.18	12.81 ± 2.1	12.98 ± 2.13	11.34 ± 1.67 $^\alpha$
	1.65	8.79 ± 1.86	9.6 ± 2.03	12.23 ± 2.59	12.08 ± 2.36	13.26 ± 2.59	13.06 ± 2.55	13.73 ± 2.58	11.46 ± 2.15	11.2 ± 2.11	12.81 ± 2.26 $^\beta$
	2.47	7.27 ± 1.39	6.99 ± 1.33	8.64 ± 1.65	10.65 ± 1.86	11.01 ± 1.92	11.11 ± 1.94	11.62 ± 1.93	9.89 ± 1.64	9.67 ± 1.61	11.91 ± 1.88 $^\gamma$
Ecc											
	0.83	0.383 ± 0.07	0.372 ± 0.068	0.437 ± 0.08	0.482 ± 0.082	0.473 ± 0.081	0.525 ± 0.09	0.539 ± 0.081	0.569 ± 0.086	0.582 ± 0.087	0.486 ± 0.069 $^\alpha$
	1.65	0.421 ± 0.098	0.442 ± 0.103	0.483 ± 0.113	0.534 ± 0.109	0.505 ± 0.103	0.539 ± 0.11	0.528 ± 0.09	0.613 ± 0.105	0.627 ± 0.107	0.523 ± 0.087 $^\beta$
	2.47	0.341 ± 0.065	0.362 ± 0.069	0.382 ± 0.073	0.44 ± 0.075	0.442 ± 0.075	0.473 ± 0.081	0.55 ± 0.083	0.512 ± 0.078	0.522 ± 0.079	0.492 ± 0.07 $^\gamma$

Values are expressed as Mean ± SD, n = 11/group. Within each dose (0.83, 1.65 and 2.47 Gy), different symbols (**α, β, γ**) denote statistical significance (**$p < 0.05$**) from 4th to 14th week of age.

Abbreviations: TMD, tissue mineral density; Tt.Ar, cross-sectional area inside the periosteal envelope; Ct.Ar, cortical bone area; Ct.Th, cortical thickness; Ps.Pm, periosteum perimeter; Ec.Pm, endocortical perimeter; Ma.Ar, medullary area; Ecc, mean eccentricity.

Table 4.4 ANOVA test with Tukey's multiple comparisons for the trabecular and cortical bone structural properties of the irradiated rat tibiae for three radiation groups on the 14th week.

| | | Statistical Comparison | | |
| | | Irradiated (right) tibia | | |
	ANOVA *p*-values	0.83 Gy - 1.65 Gy	0.83 Gy - 2.47 Gy	1.65 Gy - 2.47 Gy
Trabecular bone structural properties				
BMD (gm/cm^3)	**< 0.001**	Yes	Yes	No
BV/TV (%)	0.067	-	-	-
Tb.Th (mm)	**< 0.001**	Yes	Yes	No
Tb.N (mm^{-1})	**0.003**	No	Yes	No
Tb.Sp (mm)	**0.039**	No	Yes	No
Conn.Dn (mm^{-3})	**0.025**	Yes	Yes	No
Cortical bone structural properties				
TMD (gm.cm^{-3})	0.056	-	-	-
Tt.Ar (mm^2)	**0.048**	Yes	No	Yes
Ct.Ar (mm^2)	0.704	-	-	-
Ct.Th (mm)	**0.044**	No	Yes	No
Ps.Pm (mm)	**0.017**	No	Yes	No
Ec.Pm (mm)	0.421	-	-	-
Ma.Ar (mm^2)	0.572	-	-	-
Ecc	0.302	-	-	-

The given *p*-values are the results of a one-way ANOVA comparing the bone structural properties of the irradiated tibiae on the 14th week among three doses groups. A bold value indicates a significant difference at ***p* < 0.05**. The "Statistical Comparison" columns indicate whether the radiation groups were significantly different using Tukey's post-hoc pairwise comparisons.

4.5.6 Bone marrow cells

Results showed no significant difference ($p = 0.93$) between percentage of unaffected bone marrow cells for control (93.2%) and irradiated tibiae (91.1%) at the 14th week for 0.83 Gy group (Table 4.5). However, for 1.65 Gy group, a significant difference was observed ($p = 0.04$) between percentage of unaffected bone marrow cells for control (87.3%) and irradiated tibiae (71.6%) (Table 4.5). A significant difference was also observed ($p = 0.02$) between control (88.7%) and irradiated tibiae (70.8%) for the 2.47 Gy group (Table 4.5).

Table 4.5 Percentage of unaffected bone marrow cells for 0.83, 1.65 and 2.47 Gy radiation groups extracted from trypan blue test (mean value ± SD).

Radiation group	Tibiae	Unaffected bone marrow cells (%)	p-values
0.83 Gy	Control	93.20 ± 3.45	0.926
	Irradiated	91.11 ± 4.23	
1.65 Gy	Control	87.34 ± 7.37	**0.037**
	Irradiated	71.56 ± 9.27	
2.47 Gy	Control	88.67 ± 6.62	**0.021**
	Irradiated	70.84 ± 8.51	

Values are expressed as Mean ± SD. Both tibiae (n = 11 rats/group) were used for the analysis. A bold value indicates a significant difference (***p < 0.05***) between the control (left) and irradiated (right) tibiae for each radiation dose.

4.6 Discussion

In this study, we investigated the effects of nine weeks *in vivo* scanning regime on the rat proximal tibiae under three different radiation doses. We used growing rats (n = 33), for which the right proximal tibia was irradiated while the left tibia was used as a non-radiated contralateral control. Bone growth, histomorphometry, morphology, and bone architecture during the growing period were assessed to identify the effects of repeated *in vivo* irradiation in the adolescent period. This study would optimally provide an effective radiation doses protocol, which would be "safe" to use for the growing rats. An effective radiation dose can be marked as "safe" if high-quality image sets can be acquired during the bone growing period without influencing the bone tissue health. We induced radiation doses with a higher frequency than generally used in bone investigation studies (Stadelmann et al., 2015; Yu & Rahim, 2013), but similar to recent radiation effect investigation studies (Brouwers et al., 2007; Klinck et al., 2008). Our adapted highest dose of radiation (2.47 Gy/scan) for 9 weeks is also within the limit of single dose of irradiation (2.5 Gy) for the tibial metaphysis of adult (10 and 14 months old) rabbits (Jacobsson et al., 1985), where no significant alteration in bone formation was found. However, we investigated the growing animals (4th to 14th week of age) and our adapted radiation groups (0.83, 1.65 and 2.47 Gy) demonstrated mixed impacts on the bone microstructure during the study period.

4.6.1 Radiation doses of 1.65 and 2.47 Gy adversely impacted tibial bone development during the adolescent growth period

Indeed, our results showed that these radiation doses reduced the hypertrophic and proliferative zone heights, which eventually inhibited bone growth rate of proximal tibiae. Both hypertrophic and proliferative cellular activities have an important impact on endochondral bone formation (E. B. Hunziker, 1994). The main functions of the proliferative zone consist of matrix production and cellular proliferation (Kember & Walker, 1971). Active cell replication takes place in this zone and chondrocytes are oriented in column formation along longitudinal bone growth (Dodds, 1930). The main functions of the hypertrophic zone include generating hypertrophic chondrocytes by terminal differentiation of the proliferative zone chondrocytes farthest from the epiphysis, preparing the matrix for calcification and to calcify the matrix (Ali, 1976). Proliferative chondrocytes eventually increase in volume to generate the hypertrophic chondrocytes (Sissons, 1955). In the proliferative zone, cells undergo rapid replication (Kember & Walker, 1971). In this region, chondrocyte divides, assume a flattened appearance, and become organized into columns parallel to the long axis of the bone (Dodds, 1930). Eventually, column elongation occurs through spatially coordinated cell division and rotational movements (Dodds, 1930). Hence, it is expected that any significant changes in these two zones will influence bone growth (E. B. Hunziker, 1994). For the 0.83 Gy group, growth plate histomorphometry remained unaffected for the irradiated tibiae (Figure 4.5). However, for 1.65 and 2.47 Gy groups, a significant reduction in zone heights was observed for irradiated tibiae in the hypertrophic and proliferative area (Figure 4.5a and 4.5b). As a result, a significant reduction in overall bone growth rate for the irradiated tibiae was observed for both groups (Figure 4.2B). This decline in bone growth rate can be correlated with the reduction in proliferative and hypertrophic zone heights, which has also been observed in other studies (Kember & Walker, 1971; Walker & Kember, 1972). The average bone growth rates measured for both tibia in 0.83 Gy group are moreover similar to normal longitudinal bone growth rates observed in the rat tibia (Ménard et al., 2014). This indicates that the longitudinal bone growth was not affected by the 0.83 Gy radiation doses, which agree with other studies (Brouwers et al., 2007; E. Hunziker & Schenk, 1989), where also no effects of irradiation on the longitudinal bone growth were reported when using a similar radiation exposure level. The significantly reduced bone growth measured in 1.65 and 2.47 Gy groups also agree with the findings from other studies (Bandstra et

al., 2008; H Engström et al., 1983; Willey, 2008), where inhibition of bone growth was reported due to the effects of *in vivo* irradiation.

4.6.2 Trabecular bone, together with bone marrow cells, were negatively affected when undergoing repeated radiation doses of 1.65 and 2.47 Gy

Our results showed that trabecular bone quantity and microstructure were adversely impacted for 1.65 and 2.47 Gy groups (Figure 4.6 and 4.9).
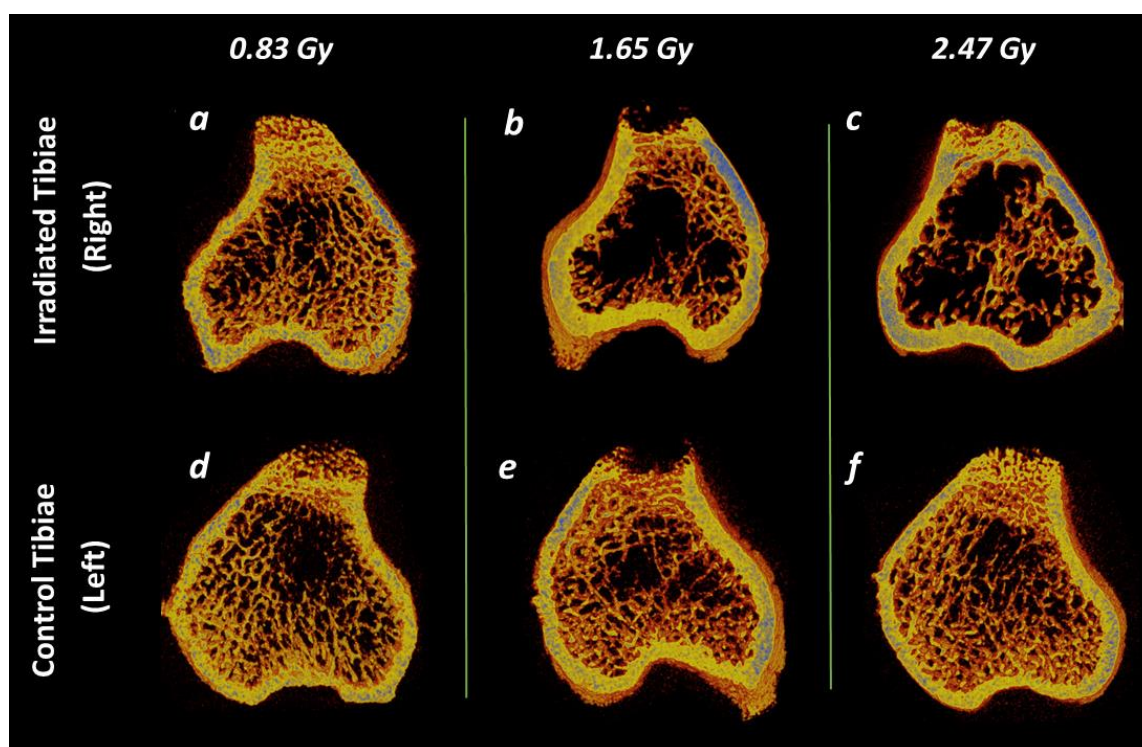
Figure 4.9 Trabecular and cortical bone representation after the 9-weekly *in vivo* micro-CT scans. (a - f) Representative 3D micro-CT images of metaphyseal bone structure of the irradiated (right) and non-irradiated control (left) tibiae at 14th week of age after 0.83, 1.65 and 2.47 Gy radiation doses during the rat adolescent period. 3D micro-CT images within each radiation dose portray tibiae from the same rat, randomly selected to be representative of its respective dose group

However, our findings showed no significant differences between the irradiated and contralateral tibiae for the trabecular bone microarchitectures for 0.83 Gy group of rats (Figure 4.6). Our findings are supportive of a study using adult rats (Longo et al., 2016) (12 weeks old), where no radiation

effects (0.60 Gy) were found on the proximal tibiae after a 3-month study period with monthly scanning regime. In another study (Brouwers et al., 2007), adult Wister rats (30 weeks old) underwent 8 weeks *in vivo* tibial scanning under doses of 939 mGy per scan, but the bone structural measurements remained unaffected. However, our findings showed significant effects on the irradiated tibiae for 1.65 and 2.47 Gy groups.

Our repeated weekly *in vivo* irradiation resulted in a lower BMD in the irradiated tibia only for 1.65 and 2.47 Gy groups (Figure 4.6). From the longitudinal data, it can be observed that the 0.83 and 2.47 Gy group showed respectively a significant increase and decrease for the irradiated tibia in the BMD value from 4th to 14th week period (Table 4.2). In general, bone mineral content tends to increase at the young age for healthy bone (Banu, Wang, & Kalu, 2002). Also, in the adolescent period, soft tissue thickness of the proximal tibia increases due to the bone growth in this period (Ammann, Rizzoli, Slosman, & Bonjour, 1992). It might be possible that for the 1.65 and 2.47 Gy group, the radiation doses affected the proximal tibial thickness by increasing the osteoclastic activity during the irradiation process (Willey et al., 2008). This phenomenon might have triggered the significant decrease in BMD in the irradiated tibiae for these groups (Figure 4.6 and 4.9). This reasoning is supported by another study, where the effect of radiation was assessed in the spine and the hip on 49 radiology and 40 non-exposed workers over ten years period (Kunt & Dayıoğlu, 2011). A significant decrease in BMD was found among the workers who were exposed to the radiation. Also, other studies irradiating mice with 1-2 Gy doses reported a lower BMD after 12 weeks of post-irradiation (Bandstra et al., 2008; Hamilton et al., 2006; Lee et al., 2013).

An increase in BV/TV is often correlated with a rise of BMD for normal bone growth (S.-D. Jiang, Jiang, & Dai, 2007), which indicates a higher bone quality. This normal bone development phenomena can be observed for the 0.83 Gy group as the BV/TV values increased significantly during the adolescent period (Table 4.2). For the 0.83 and 1.65 Gy group, no significant difference was found between the contralateral tibiae on the 14th week (Figure 4.6). However, BV/TV values decreased significantly compared to the control ones for the 2.47 Gy group (Figure 4.6), which could be associated with the diminishing trend observed earlier in the longitudinal BMD values for the same group. Our findings are supported by a study where a weekly radiation dose of 0.846 Gy over 5 weeks resulted in a decreased BV/TV in adult mice (12-week old) (Klinck et al., 2008). Also, another study reported a 30% loss in 10-week old mice BV/TV after performing three 0.776 Gy dose scans separated by 2-week intervals (Laperre et al., 2011).

As for Tb.Th, Tb.N, and Tb.Sp, no difference was found between the irradiated and control tibiae for the 0.83 Gy group (Figure 4.6), while Tb.Th and Tb.N were significantly increased in the growing period for this group (Table 4.2). The increment of Tb.Th during the growing period indicates normal bone growth process (Brouwers et al., 2007; Campbell, Buie, & Boyd, 2008; Lu, Cui, Zuo, Lin, & Wu, 2015). Moreover, the observed increase in Tb.N is associated with the concomitant increase in BV/TV for the young age period (Kirmani et al., 2009). These findings agree with results from other radiation effects investigation studies using 30 weeks old rats (0.60 Gy) (Brouwers et al., 2007), and 17 weeks old ovariectomized mice (1.30 Gy) (Judex et al., 2005). In both of these studies, Tb.N, Tb.Th and Tb.Sp remained unaffected. However, for the 1.65 and 2.47 Gy groups, Tb.Th and Tb.N values were significantly lower and the Tb.Sp values were significantly higher in the irradiated tibiae (Figure 4.6). From the longitudinal data, a significant decrease for Tb.Th and a significant increase in Tb.N and Tb.Sp were observed for 1.65 Gy group (Table 4.2), whereas the 2.47 Gy group showed a significant decrease for Tb.Th and an increase for Tb.Sp only in the scanning period (Table 4.2). These phenomena indicate the occurrence of a radiation-induced bone loss through a decreased connectivity and a gradual thinning of the trabecular structure (Figure 4.9). Our data are supportive of previous findings from a mice study where a 5-6 Gy radiation exposure for 3 days and 14 days resulted in decreased Tb.Th, Tb.N, and an increased Tb.Sp (Sibonga, Iwaniec, & Wu, 2011). Another mice study using 0.846 Gy radiation dose for 5 weekly scans at 2 weeks interval reported a lower Tb.Th, Tb.N, and a higher Tb.Sp (Klinck et al., 2008).

As for Conn.Dn, no significant difference was observed between the irradiated and control tibiae at the 14th week for all three groups (Figure 4.6). However, a significant decrease was observed from the longitudinal data for both 0.83 and 1.65 Gy groups (Table 4.2). Connectivity density is vital in the maintenance of bone strength and trabecular connectivity is a fundamental property of 3D bone networks. As Conn.Dn provides a measure of unconnected trabeculae, this decrement could occur because the bone was still in the growing phase while the trabecular structure was changing with time. This observation also agrees well with the findings from other rat studies (Boyd et al., 2006; Brouwers et al., 2007), where Conn.Dn was also decreased with the age of the rats.

Also from ANOVA test with Tukey's multiple comparisons, it has been observed that for trabecular bone, 0.83 Gy group showed significant differences with the 1.65 and 2.47 Gy groups

for BMD, Tb.Th, Tb.N, Tb.Sp, and Conn.Dn, whereas, no significant differences for the trabecular bone microstructure were found between 1.65 and 2.47 Gy groups (Table 4.4). This indicates higher similarities of trabecular morphometric data between 1.65 and 2.47 Gy group compared with the 0.83 Gy group. This observation agrees with our morphometric findings as both of this group demonstrated similar adverse effects on the bone microarchitecture compared to the 0.83 Gy group (Figure 4.9). It has been reported that a radiation dose, if too high, can cause cell death, and the effects can be apparent within hours, days, or weeks after the exposure period (PROMULGATION). Therefore, a two-week interval for the last scan was implemented in this study considering the possibility that the maximal radiation exposure effect could occur after the end of the exposure protocol (Hélène Engström, 1986; H Engström et al., 1983). Bone marrow cells remained unaffected for 0.83 Gy group, which agrees with the conjecture based on CTDI (Dare et al., 1997; Dudziak et al., 2000), and with a recent study (Brouwers et al., 2007) (30 weeks old rats, 600 mGy), where no cell damage due to radiation was reported. However, for the 1.65 and 2.47 Gy groups, significant differences were observed between control and irradiated tibiae. This phenomena confirm the negative impacts of 1.65 and 2.47 Gy doses on bone tissue health and can also be correlated with the detrimental effects observed by these doses on the trabecular structure found in our study (Jacobsson, Kälebo, Tjellström, & Turesson, 1987).

4.6.3 Cortical bone quantity and microstructure were slightly deteriorated under repeated radiation dose of 2.47 Gy

As opposed to trabecular bone, tested radiation doses had no profound effects on cortical bone microarchitecture. Indeed, for all three groups, there was no significant difference observed between the irradiated and the control tibia for TMD, Tt.Ar, Ct.Ar, Ps.Pm, Ec.Pm, Ma.Ar, and Ecc (Figure 4.7). From the longitudinal data, a significant increase was observed for Tt.Ar, Ct.Ar, Ps.Pm, Ec.Pm, Ma.Ar, and Ecc in all groups, whereas TMD and Ct.Th increased for 0.83 and 1.65 groups indicating the normal bone growing phenomenon (Table 4.3). However, the cortical thickness (Ct.Th) showed a significant difference at the 14th week scanning time point and decreased in the irradiated tibia compared to the control ones for the 2.47 Gy group (Figure 4.6). It could be possible that the radiation dose might have affected more intensively the vascularization of the proximal tibia. Vascularization is essential for bone formation and bone remodeling, transporting nutrients and the oxygen supply and allowing endothelial cells to communicate with

osteoprogenitors and osteoclasts (Villars et al., 2002). Moreover, if this process gets affected, a potential bone tissue destruction can occur (Kaigler, Wang, Horger, Mooney, & Krebsbach, 2006). Another possible reason could be the redistribution of bone mass from the endosteal region to the sub-periosteal region of the tibia. If this redistribution happens, it generally results in reduced cortical thickness of the bone diaphysis (Li, Jee, Ke, Mori, & Akamine, 1991). Our findings can be confirmed from another study (Michel et al., 2015) where a single 80-Gy radiation exposure for the 8-week-old rat hind limbs substantially decreased the cortical thickness and created wide bone gaps in the bone microstructure. Also from ANOVA test with Tukey's multiple comparisons, it has been observed that for cortical bone, 0.83 Gy group showed significant differences with the 1.65 and 2.47 Gy groups for Tt.Ar, Ct.Th, and Ps.Pm, whereas, significant difference for only Tt.Ar was found between 1.65 and 2.47 Gy groups (Table 4.4). This findings indicate the vulnerability of cortical bone microarchitecture under the radiation doses of 1.65 and 2.47 Gy group which is in agreement to our morphometric findings.

4.6.4 Comparisons among protocols used in similar radiation studies and strengths of the current study

Differences found between our results and published studies might result from different factors. The positioning of the animal's limb in the scanner bed can be considered a possible factor for discrepancies among the studies. Since the right proximal tibia (irradiated) was exposed to radiation for 9 weeks (from 4th to 14th week of age), the frequent stretching of the right tibiae might have induced an effect on the bone tissue microstructure. As the radiation chamber rotates around the object for scanning, the right tibia was always pulled away from the body and fixed on the Styrofoam holder with the masking tape during the scanning period. The contralateral tibia was folded along with the tail outside the Styrofoam holder. This stretching could make the rat put a reduced pressure on right tibia for a short period of time right after the scanning period, which could lead to bone loss (Brouwers et al., 2007). However, as we have followed the same approach throughout the whole study, this effect (if any) should be similar for all the animals and hence the relative comparison allows to draw conclusions. Also, it was presumed that the left tibia remained unaffected during the scanning of the right tibia. Nevertheless, it is possible that systemic radiation effects have occurred and affected the left tibia (Brouwers et al., 2007). However, as we only irradiated the proximal tibial portion, which covered a small segment compared to the whole body,

these systemic effects are expected to be non-significant. Also, changes in the body weight were compared with the literature (Benoit et al., 2016; Brower, Grace, Kotz, & Koya, 2015) to check for any sudden weight loss and no anomalies were found. Using various animal models might also be another contributing factor for discrepancies. It has been observed from the literature that, for mice, the scanning time interval might be more critical than the radiation doses (Meganck & Liu, 2017). Also, in some cases, a similar amount of radiation exposure for both mice and rats have produced divergent results. Rat bone structure seems to be more resilient to the same amount of radiation exposure compared to the mice (Bandstra et al., 2008; Brouwers et al., 2007; Hamilton et al., 2006; Judex et al., 2005; Klinck et al., 2008). One possible reason could be the presence of larger and thicker skeletons in rats compared to mice, which might provide an additional absorbing capacity of the induced radiation for rats. Another reason for the discrepancies might be the age of the animals used in different studies. In most studies, an adult animal model has been used compared to our adolescent model (Boyd et al., 2006; Brouwers et al., 2007; Judex et al., 2005). Bone remodeling gets slower with aging (Compston, 2011), and bone turnover rate shifts towards bone resorption (Bagi, Ammann, Rizzoli, & Miller, 1997; Francisco, Yu, Oliver, & Walsh, 2011). As a result, the bone microstructure behavior is expected to be different in these studies compared to ours. Nonetheless, it remains difficult to make a comparison of our findings with other studies as none of them investigated the effects of *in vivo* micro-CT irradiation in a rat model during its growing period (4th to 14th week of age) (Sengupta, 2013). Also, the scanning protocol, radiation doses, types of scanner, and animal positioning during scanning can contribute to differences in results between different animal studies.

Despite some limitations, our current study possesses a number of strengths. First, to authors' best knowledge, this study is the first of its kind to investigate the effects of repeated *in vivo* micro-CT irradiation using an animal model during its entire growing period. Second, three different levels of radiation doses have been investigated using the same image reconstruction parameters to facilitate the comparison among results from different groups. Third, we scanned the non-radiated control legs (left tibiae) only at the end point (14th week of age). This method of using an internal control decreases the use of extra animals for control and reduces the variability in the extracted data sets. Furthermore, results from the current study possess insightful information regarding bone microarchitecture during the bone development period, which would be useful to the bone and orthopedic research community.

4.7 Conclusion

In conclusion, using 1.65 and 2.47 Gy doses might yield better image quality for bone tissue investigation but possess a high risk of altering the bone growing process in the rat adolescent period. Our results showed that, under radiation doses of 1.65 and 2.47 Gy, trabecular bone, together with bone marrow cells, as well as tibial bone development were adversely impacted. Also, cortical bone quantity and microstructure was slightly deteriorated under repeated radiation doses of 2.47 Gy. Hence, it appears from our results that 1.65 and 2.47 Gy doses affected significantly the bone marrow cells, histomorphometric and morphological parameters, and longitudinal bone growth of the immature rats. However, the 0.83 Gy radiation exposure did not affect the bone tissue structure for the growing rats. These findings can be used as a proof of concept for using the reasonable high-quality image acquisition under 0.83 Gy radiation doses during the entire growing period of rats without interfering with the bone development process. Our study also advances the knowledge on the evaluation of the radiation effects during the adolescent period of animal models in order to provide functional information for the design of future *in vivo* studies, in which the repeated radiation exposure is necessary and can induce additional impacts on the outcomes. Considering that the radiation damage also depends on other factors (scanning protocol, systemic effects, site-specificity), which are not micro-CT system specific, careful consideration should be adapted for future studies.

4.8 Acknowledgements

4.9 References

Ali, S. (1976). *Analysis of matrix vesicles and their role in the calcification of epiphyseal cartilage.* Paper presented at the Federation proceedings.

Ammann, P., Rizzoli, R., Slosman, D., & Bonjour, J. P. (1992). Sequential and precise in vivo measurement of bone mineral density in rats using dual-energy x-ray absorptiometry. *Journal of Bone and Mineral Research, 7*(3), 311-316.

Bagi, C., Ammann, P., Rizzoli, R., & Miller, S. C. (1997). Effect of estrogen deficiency on cancellous and cortical bone structure and strength of the femoral neck in rats. *Calcified tissue international, 61*(4), 336-344.

Bandstra, E. R., Pecaut, M. J., Anderson, E. R., Willey, J. S., De Carlo, F., Stock, S. R., . . . Bateman, T. A. (2008). Long-term dose response of trabecular bone in mice to proton radiation. *Radiation research, 169*(6), 607-614.

Banu, J., Wang, L., & Kalu, D. (2002). Age-related changes in bone mineral content and density in intact male F344 rats. *Bone, 30*(1), 125-130.

Benoit, A., Mustafy, T., Londono, I., Grimard, G., Aubin, C.-E., & Villemure, I. (2016). In vivo dynamic compression has less detrimental effect than static compression on newly formed bone of a rat caudal vertebra. *Journal of musculoskeletal & neuronal interactions, 16*(3), 211.

Bisgard, J. D., & Hunt, H. B. (1936). Influence of Roentgen Rays and Radium on Epiphyseal Growth of Long Bones 1. *Radiology, 26*(1), 56-68.

Bouxsein, M. L., Boyd, S. K., Christiansen, B. A., Guldberg, R. E., Jepsen, K. J., & Müller, R. (2010). Guidelines for assessment of bone microstructure in rodents using micro–computed tomography. *Journal of Bone and Mineral Research, 25*(7), 1468-1486.

Boyd, S. K., Davison, P., Müller, R., & Gasser, J. A. (2006). Monitoring individual morphological changes over time in ovariectomized rats by in vivo micro-computed tomography. *Bone, 39*(4), 854-862.

Brouwers, J. E., Van Rietbergen, B., & Huiskes, R. (2007). No effects of in vivo micro-CT radiation on structural parameters and bone marrow cells in proximal tibia of wistar rats detected after eight weekly scans. *Journal of Orthopaedic Research, 25*(10), 1325-1332.

Brower, M., Grace, M., Kotz, C. M., & Koya, V. (2015). Comparative analysis of growth characteristics of Sprague Dawley rats obtained from different sources. *Laboratory animal research, 31*(4), 166-173.

Buie, H. R., Campbell, G. M., Klinck, R. J., MacNeil, J. A., & Boyd, S. K. (2007). Automatic segmentation of cortical and trabecular compartments based on a dual threshold technique for in vivo micro-CT bone analysis. *Bone, 41*(4), 505-515.

Bushberg, J. T., Seibert, J. A., Leidholdt, E. M., Boone, J. M., & Goldschmidt, E. J. (2003). The essential physics of medical imaging. *Medical Physics, 30*(7), 1936-1936.

Campbell, G., Buie, H., & Boyd, S. (2008). Signs of irreversible architectural changes occur early in the development of experimental osteoporosis as assessed by in vivo micro-CT. *Osteoporosis international, 19*(10), 1409-1419.

Compston, J. (2011). Age-related changes in bone remodelling and structure in men: histomorphometric studies. *Journal of osteoporosis, 2011*.

Cowan, C. M., Aghaloo, T., Chou, Y.-F., Walder, B., Zhang, X., Soo, C., . . . Wu, B. (2007). MicroCT evaluation of three-dimensional mineralization in response to BMP-2 doses in vitro and in critical sized rat calvarial defects. *Tissue engineering, 13*(3), 501-512.

Dare, A., Hachisu, R., Yamaguchi, A., Yokose, S., Yoshiki, S., & Okano, T. (1997). Effects of ionizing radiation on proliferation and differentiation of osteoblast-like cells. *Journal of dental research, 76*(2), 658-664.

Dodds, G. (1930). Row formation and other types of arrangement of cartilage cells in endochondral ossification. *The Anatomical Record, 46*(4), 385-399.

Dudziak, M. E., Saadeh, P. B., Mehrara, B. J., Steinbrech, D. S., Greenwald, J. A., Gittes, G. K., & Longaker, M. T. (2000). The effects of ionizing radiation on osteoblast-like cells in vitro. *Plastic and reconstructive surgery, 106*(5), 1049-1061.

Eifel, P. J., Sampson, C. M., & Tucker, S. L. (1990). Radiation fractionation sensitivity of epiphyseal cartilage in a weanling rat model. *International Journal of Radiation Oncology* Biology* Physics, 19*(3), 661-664.

Engström, H. (1986). Effects of irradiation on growing bones. *Swedish dental journal. Supplement, 45*, 1-47.

Engström, H., Jansson, J., & Engström, C. (1983). Effect of Local Irradiation on Longitudinal Bone Growth in the Rat: A tetracycline labelling investigation. *Acta Radiologica: Oncology, 22*(2), 129-133.

Ford, N., Thornton, M., & Holdsworth, D. (2003). Fundamental image quality limits for microcomputed tomography in small animals. *Medical Physics, 30*(11), 2869-2877.

Francisco, J. I., Yu, Y., Oliver, R. A., & Walsh, W. R. (2011). Relationship between age, skeletal site, and time post-ovariectomy on bone mineral and trabecular microarchitecture in rats. *Journal of Orthopaedic Research, 29*(2), 189-196.

Gal, T., Munoz-Antonia, T., Muro-Cacho, C. A., & Klotch, D. W. (2000). Radiation effects on osteoblasts in vitro: a potential role in osteoradionecrosis. *Archives of Otolaryngology–Head & Neck Surgery, 126*(9), 1124-1128.

Hamilton, S. A., Pecaut, M. J., Gridley, D. S., Travis, N. D., Bandstra, E. R., Willey, J. S., . . . Bateman, T. A. (2006). A murine model for bone loss from therapeutic and space-relevant sources of radiation. *Journal of applied physiology, 101*(3), 789-793.

Hasan, A., Byambaa, B., Morshed, M., Cheikh, M. I., Shakoor, R. A., Mustafy, T., & Marei, H. (2018). Advances in osteobiologic materials for bone substitutes. *Journal of Tissue Engineering and Regenerative Medicine*.

Hunziker, E., & Schenk, R. (1989). Physiological mechanisms adopted by chondrocytes in regulating longitudinal bone growth in rats. *The Journal of physiology, 414*(1), 55-71.

Hunziker, E. B. (1994). Mechanism of longitudinal bone growth and its regulation by growth plate chondrocytes. *Microscopy research and technique, 28*(6), 505-519.

Iliakis, G., Wang, Y., Guan, J., & Wang, H. (2003). DNA damage checkpoint control in cells exposed to ionizing radiation. *Oncogene, 22*(37), 5834-5847.

Isaksson, H., Töyräs, J., Hakulinen, M., Aula, A., Tamminen, I., Julkunen, P., . . . Jurvelin, J. (2011). Structural parameters of normal and osteoporotic human trabecular bone are affected differently by microCT image resolution. *Osteoporosis international, 22*(1), 167-177.

Jacobsson, M., Jönsson, A., Albrektsson, T., & Turesson, I. (1985). Alterations in bone regenerative capacity after low level gamma irradiation: a quantitative study. *Scandinavian journal of plastic and reconstructive surgery, 19*(3), 231-236.

Jacobsson, M., Kälebo, P., Tjellström, A., & Turesson, I. (1987). Bone cell viability after irradiation: an enzyme histochemical study. *Acta Oncologica, 26*(6), 463-465.

Jiang, S.-D., Jiang, L.-S., & Dai, L.-Y. (2007). Changes in bone mass, bone structure, bone biomechanical properties, and bone metabolism after spinal cord injury: a 6-month longitudinal study in growing rats. *Calcified tissue international, 80*(3), 167-175.

Jiang, Y., Zhao, J., White, D., & Genant, H. (2000). Micro CT and Micro MR imaging of 3D architecture of animal skeleton. *J Musculoskelet Neuronal Interact, 1*(1), 45-51.

Johnson, T. (2017). *Introduction to health physics*: Mcgraw Hill.

Judex, S., Chung, H., Torab, A., Xie, L., Rubin, C., Donahue, L., & Xu, S. (2005). *Micro-CT induced radiation does not exacerbate disuse related bone loss.* Paper presented at the Proceedings of the 51st annual meeting of the orthopaedic research society.

Kaigler, D., Wang, Z., Horger, K., Mooney, D. J., & Krebsbach, P. H. (2006). VEGF scaffolds enhance angiogenesis and bone regeneration in irradiated osseous defects. *Journal of Bone and Mineral Research, 21*(5), 735-744.

Kember, N., & Walker, K. (1971). Control of bone growth in rats. *Nature, 229*(5284), 428.

Kirmani, S., Christen, D., Van Lenthe, G. H., Fischer, P. R., Bouxsein, M. L., McCready, L. K., . . . Müller, R. (2009). Bone structure at the distal radius during adolescent growth. *Journal of Bone and Mineral Research, 24*(6), 1033-1042.

Klinck, R. J., Campbell, G. M., & Boyd, S. K. (2008). Radiation effects on bone architecture in mice and rats resulting from in vivo micro-computed tomography scanning. *Medical engineering & physics, 30*(7), 888-895.

Kunt, H., & Dayıoğlu, H. (2011). The effects of radiation on bone mineral density of radiology workers depending on the device they use. *Eur J Gen Med, 8*(4), 318-322.

Laperre, K., Depypere, M., van Gastel, N., Torrekens, S., Moermans, K., Bogaerts, R., . . . Carmeliet, G. (2011). Development of micro-CT protocols for in vivo follow-up of mouse bone architecture without major radiation side effects. *Bone, 49*(4), 613-622.

Lee, J.-H., Lee, H.-J., Yang, M., Moon, C., Kim, J.-C., Jo, S.-K., . . . Kim, S.-H. (2013). Establishment of a murine model for radiation-induced bone loss using micro-computed tomography in adult C3H/HeN mice. *Laboratory animal research, 29*(1), 55-62.

Li, X., Jee, W., Ke, H., Mori, S., & Akamine, T. (1991). Age-related changes of cancellous and cortical bone histomorphometry in female Sprague-Dawley rats. *Cells and Materials, 1*, 25-25.

Longo, A. B., Sacco, S. M., Salmon, P. L., & Ward, W. E. (2016). Longitudinal Use of Micro-computed Tomography Does Not Alter Microarchitecture of the Proximal Tibia in Sham or Ovariectomized Sprague–Dawley Rats. *Calcified tissue international, 98*(6), 631-641.

Lu, H., Cui, L., Zuo, C., Lin, S., & Wu, T. (2015). Evaluation of morphological parameters of bone formation in Sprague–Dawley rats of different ages by in vivo fluorochrome labeling. *Italian Journal of Zoology, 82*(1), 33-40.

Lynch, M. E., Main, R. P., Xu, Q., Walsh, D. J., Schaffler, M. B., Wright, T. M., & van der Meulen, M. C. (2010). Cancellous bone adaptation to tibial compression is not sex dependent in growing mice. *Journal of applied physiology, 109*(3), 685-691.

Matsumura, S., Jikko, A., Hiranuma, H., Deguchi, A., & Fuchihata, H. (1996). Effect of X-ray irradiation on proliferation and differentiation of osteoblast. *Calcified tissue international, 59*(4), 307-308.

Meganck, J. A., & Liu, B. (2017). Dosimetry in Micro-computed Tomography: a Review of the Measurement Methods, Impacts, and Characterization of the Quantum GX Imaging System. *Molecular Imaging and Biology, 19*(4), 499-511.

Ménard, A. L., Grimard, G., Valteau, B., Londono, I., Moldovan, F., & Villemure, I. (2014). In vivo dynamic loading reduces bone growth without histomorphometric changes of the growth plate. *Journal of Orthopaedic Research, 32*(9), 1129-1136.

Michel, G., Blery, P., Pilet, P., Guicheux, J., Weiss, P., Malard, O., & Espitalier, F. (2015). Micro-CT analysis of radiation-induced osteopenia and bone hypovascularization in rat. *Calcified tissue international, 97*(1), 62-68.

Micro-CT, B. Skyscan 1176 in vivo scanning: X-ray dosimetry.

Mitchell, M. J., & Logan, P. M. (1998). Radiation-induced changes in bone. *Radiographics, 18*(5), 1125-1136.

Mustafy, T., Arnoux, P.-J., Benoit, A., Bianco, R.-J., Aubin, C.-E., & Villemure, I. (2018). Load-sharing biomechanics at the thoracolumbar junction under dynamic loadings are modified by anatomical features in adolescent and pediatric vs adult functional spinal units. *Journal of the Mechanical Behavior of Biomedical Materials, 88*, 78.

Mustafy, T., El-Rich, M., Mesfar, W., & Moglo, K. (2014). Investigation of impact loading rate effects on the ligamentous cervical spinal load-partitioning using finite element model of functional spinal unit C2–C3. *Journal of biomechanics, 47*(12), 2891-2903.

Mustafy, T., Londono, I., & Villemure, I. (2018). Can the contralateral limb be used as a control during the growing period in a rodent model? *Medical engineering & physics, 58*, 31-40. doi: https://doi.org/10.1016/j.medengphy.2018.04.013

Mustafy, T., Moglo, K., Adeeb, S., & El-Rich, M. (2014). *Investigation of Upper Cervical Spine Injury due to Frontal and Rear Impact Loading Using Finite Element Analysis.* Paper presented at the ASME 2014 International Mechanical Engineering Congress and Exposition.

Mustafy, T., Moglo, K., Adeeb, S., & El-Rich, M. (2016). Injury mechanisms of the ligamentous cervical C2–C3 Functional Spinal Unit to complex loading modes: Finite Element study. *Journal of the Mechanical Behavior of Biomedical Materials, 53*, 384-396.

Olive, P. L., Banáth, J. P., & Durand, R. E. (1990). Heterogeneity in radiation-induced DNA damage and repair in tumor and normal cells measured using the" comet" assay. *Radiation research, 122*(1), 86-94.

Perilli, E., Le, V., Ma, B., Salmon, P., Reynolds, K., & Fazzalari, N. (2010). Detecting early bone changes using in vivo micro-CT in ovariectomized, zoledronic acid-treated, and sham-operated rats. *Osteoporosis international, 21*(8), 1371-1382.

PROMULGATION, N. L. O. NATO Handbook on the Medical Aspects of NBC Defensive Operations AMedP-6 (B).

Rüegsegger, P., Koller, B., & Müller, R. (1996). A microtomographic system for the nondestructive evaluation of bone architecture. *Calcified tissue international, 58*(1), 24-29.

Sengupta, P. (2013). The laboratory rat: relating its age with human's. *International journal of preventive medicine, 4*(6).

Sibonga, J., Iwaniec, U., & Wu, H. (2011). Pilot Study: Unique Response of Bone Tissue During an Investigation of Radio-Adaptive Effects in Mice.

Sissons, H. (1955). Experimental study on the effect of local irradiation on bone growth. *Progress in radiobiology. Edinburgh: Oliver and Boyd*, 436-448.

Stadelmann, V. A., Potapova, I., Camenisch, K., Nehrbass, D., Richards, R. G., & Moriarty, T. F. (2015). In Vivo MicroCT Monitoring of Osteomyelitis in a Rat Model. *BioMed research international, 2015*.

Valteau, B., Grimard, G., Londono, I., Moldovan, F., & Villemure, I. (2011). In vivo dynamic bone growth modulation is less detrimental but as effective as static growth modulation. *Bone, 49*(5), 996-1004.

Villars, F., Guillotin, B., Amedee, T., Dutoya, S., Bordenave, L., Bareille, R., & Amedee, J. (2002). Effect of HUVEC on human osteoprogenitor cell differentiation needs heterotypic gap junction communication. *American Journal of Physiology-Cell Physiology, 282*(4), C775-C785.

Waarsing, J., Day, J., Van der Linden, J., Ederveen, A., Spanjers, C., De Clerck, N., . . . Weinans, H. (2004). Detecting and tracking local changes in the tibiae of individual rats: a novel method to analyse longitudinal in vivo micro-CT data. *Bone, 34*(1), 163-169.

Walker, K., & Kember, N. (1972). Cell kinetics of growth cartilage in the rat tibia ii. Measurements during ageing. *Cell Proliferation, 5*(5), 409-419.

Willey, J. S. (2008). *Radiation-induced osteoporosis: Bone quantity, architecture, and increased resorption following exposure to ionizing radiation.* Clemson University.

Willey, J. S., Lloyd, S. A., Robbins, M. E., Bourland, J. D., Smith-Sielicki, H., Bowman, L. C., . . . Bateman, T. A. (2008). Early increase in osteoclast number in mice after whole-body irradiation with 2 Gy X rays. *Radiation research, 170*(3), 388-392.

Williams, H., & Davies, A. (2006). The effect of X-rays on bone: a pictorial review. *European radiology, 16*(3), 619-633.

Yu, H., & Rahim, N. A. A. (2013). *Imaging in Cellular and Tissue Engineering*: CRC Press.

CHAPTER 5   ARTICLE #2: EXPERIMENTAL AND FINITE ELEMENT ANALYSES OF BONE STRAINS IN THE GROWING RAT TIBIA INDUCED BY *IN VIVO* AXIAL COMPRESSION

This chapter introduces the second article written in the context of this thesis and responds to the second and third objective of this thesis as detailed in Chapter 3.

This article was published in Journal of the Mechanical Behavior of Biomedical Materials © in March 13th, 2019.

The contribution of the first author in the preparation, obtaining the results, writing and literature review of this paper is estimated at 85%.

Contribution of all authors:

Tanvir Mustafy: Design of experiment, obtaining the results, analysis, interpretation of results, article writing and editing, responsible for the integrity of the work.

Irene Londono: Technical help, Resources.

Isabelle Villemure: Conceptualization, Funding acquisition, Methodology, Project administration, Resources, Supervision, Writing - review & editing.

5.1 Abstract

Knowledge of the relationship between applied *in vivo* mechanical loading and induced bone strains is essential to better understand the mechanobiological response of bone. However, most rat tibial load-strain studies are limited to adult vs growing rodent models. The objective of this study was to develop and validate a voxel based FE modeling approach to investigate bone strains from *in vivo* rat tibial compression during the adolescent period. Voxel based finite element (FE) models were derived from micro-CT scans and combined with antero-medial (AM) longitudinal strain gauge measurements to quantify bone strains in the tibiae of 4, 8 and 12 week old (n=6/group) male rats. FE models were used to simulate the *in vivo* tibial compression and resulting longitudinal FE strains in the AM, postero-lateral (PL) and antero-lateral (AL) regions were compared with gauge (AM) strains and with rat growth. The effects of varying gauge location were also investigated. The good agreement between the AM gauge strains and corresponding FE strain allowed validating the modeling approach. Interestingly, greatest FE strains were observed in the postero-lateral (PM) region, compared to the antero-medial (AM) and antero-lateral (AL) regions, indicating possible limitations associated to considering peak strains in the installed gauge region only. Peak strains at the experimental site (AM) and from FE models (AL and PL) were found to be decreasing with age, due to increasing tibial cortical area and thickness with age. Variations in strain gauge placement induced non-negligible changes in strain magnitudes, hence emphasizing the importance of gauge installation reproducibility in experimental studies. This voxel based finite element analysis, combined with strain gauge measurements, provides detailed age-dependent force-strain data in different regions of the adolescent rat tibiae during *in vivo* axial loading, which should be resourceful to the bone and orthopedic research community for designing *in vivo* noninvasive loading protocols for growing rodents.

5.2 Keywords

Rat tibia, Adolescence, *In vivo* compression, Strain gauge measurements, Micro-CT, Voxel based finite element models

5.3 Introduction

Bone is a mechanoresponsive tissue, which remodels its architecture and material properties in response to mechanical loading (Frost, 2004; A. G. Robling, Burr, & Turner, 2001). This mechanoresponsive behavior is investigated using *in vivo* mechanical loading models (Raab-Cullen, Akhter, Kimmel, & Recker, 1994; C. H. Turner, Forwood, Rho, & Yoshikawa, 1994). Changes in mechanical loading during bone development and adulthood can result in anabolic or catabolic stimuli for bone (Klein-Nulend, Burger, Semeins, Raisz, & Pilbeam, 1997; Pitsillides et al., 1995). Researchers have developed controlled loading protocols using several animal models to investigate the intrinsic relationship between mechanical loading and resulting bone remodeling. Some commonly used loading protocols for rats and mice models are the *in vivo* tibial bending models (Akhter, Cullen, Pedersen, Kimmel, & Recker, 1998; C. Turner, Akhter, Raab, Kimmel, & Recker, 1991; C. Turner, Forwood, & Otter, 1994), the dynamic loading using isolated avian ulnar model (Clinton & Lanyon, 1984), mouse caudal vertebrae loading model (Duncan Webster et al., 2010; D Webster, Wirth, van Lenthe, & Müller, 2012), and the forelimb compression models (Hsieh, Robling, Ambrosius, Burr, & Turner, 2001; Lee, Maxwell, & Lanyon, 2002; Torrance, Mosley, Suswillo, & Lanyon, 1994).

Knowledge of the relationship between applied *in vivo* mechanical loading and induced bone strains is essential to better understand bone response under different loading conditions (Mustafy, Arnoux, et al., 2018; Sugiyama et al., 2012). Experimental protocols have been established to investigate *in situ* bone mechanical response by measuring electrical resistance through strain gauges attached on bone surfaces in a variety of living animals, including rats and humans (Lanyon & Smith, 1969; Rubin & Lanyon, 1982; Torrance et al., 1994; C. Turner et al., 1991). In most of these studies, resulting *in vivo* strains have been measured on cortical bone surfaces using strain gauges (Kuruvilla, Fox, Cullen, & Akhter, 2008; LaMothe, Hamilton, & Zernicke, 2005; Torcasio, Zhang, Duyck, & van Lenthe, 2012; Uthgenannt & Silva, 2007; Zhang, Tanaka, Jiang, Su, & Yokota, 2006). In other studies, strains have been calculated through beam theory or surface digital image correlation (Giorgi & Dall'Ara, 2018; Oliviero, Giorgi, & Dall'Ara, 2018; Price, Li, Novotny, & Wang, 2010; Sztefek et al., 2010). To assess bone strains throughout the whole three dimensional bone structure, micro-CT based finite element (FE) analyses have also been used and proven to be efficient tools for generating models both at macro- and microscopic scales (Mustafy,

El-Rich, Mesfar, & Moglo, 2014; Patel, Brodt, & Silva, 2014; Stadelmann et al., 2009; Torcasio et al., 2012; Yang et al., 2014). One method used to generate FE models of the bone structure involves the direct conversion of the 3D voxels of micro-CT images to FE meshes, by implementing a voxel-to-element conversion approach (Müller & Rüegsegger, 1995; van Rietbergen, Weinans, Huiskes, & Odgaard, 1995).

To better understand the mechanoresponsive behavior of bone, rat/mice tibial loading studies have been implemented by several researchers (Fritton, Myers, Wright, & Van der Meulen, 2005; Iwamoto, Yeh, & Aloia, 1999; Lynch et al., 2010). However, most of the existing rat tibial load-strain studies have been limited to adult rats (>76 days old) (post-adolescent period) vs growing or immature rats (from 28 to 76 days old) (Akhter, Raab, Turner, Kimmel, & Recker, 1992; Hsieh et al., 2001; Jeffery, Murphey, Stallone, Bloomfield, & Hogan, 2007; Torcasio et al., 2012). However, it has been reported that the appositional and longitudinal growth of long bones is most effectively influenced by mechanical stimuli during the rat adolescent period (from 34 to 70 days old) (Bergmann et al., 2010; Omi, Nakamura, & Ezawa, 1998; A. Robling, Duijvelaar, Geevers, Ohashi, & Turner, 2001; Sengupta, 2013). Hence, to better understand how bone growth and remodeling are modulated under loading, the relationship between *in vivo* loading and strains during the bone growing period should be established. Due to the small size and shape constraints of immature rat tibiae, a single uniaxial strain gauge is usually used to characterize strains at local sites on the tibial diaphysis (Hsieh et al., 2001; Jeffery et al., 2007). As a result, strain distribution throughout the whole tibia cannot be assessed, but would be of interest to investigate strains in specific tibial regions to have a better understanding of the load response on an irregular tibial surface. Moreover, there is still a paucity of data on the strain distribution within the whole tibia during bone growth, although it would be relevant for the design of mechanobiological studies using young rat models.

The objective of this study was to develop and validate a voxel based FE modeling approach to investigate bone strains from *in vivo* rat tibial compression during the adolescent period. To do so, *in vivo* strain gauge measurements and voxel based FE modeling derived from micro-CT scanning were combined for rat tibiae aged 4, 8 and 12 week old, respectively corresponding to the beginning of pubertal, mid-pubertal and end of the pubertal period (Sengupta, 2013). Bone structural parameters, effects of varying strain gauge locations and strains in different directions of the tibiae were also investigated.

5.4 Materials and methods

5.4.1 Animals

Experiments were performed using 18 male Sprague Dawley rats (Charles River Laboratories, Montreal). Rats were divided into three groups (n = 6/group) (Benoit et al., 2016). These groups of rats were received at the animal facility at the age of 21, 49 and 77 days old, respectively and were allowed to acclimate in the animal facility for one week prior to the experiments. The rats were housed two per cage (dimension 53×35.5 cm) at 25°C with a 12:12-hour light-dark cycle and had access to standard laboratory diet and water ad libitum. The experimental protocol and all animal procedures were carried out in accordance with the guidelines of the Canadian Council on Animal Care (CCAC) and were approved by the Institutional Animal Care Committee at the Research Center of Sainte-Justine University Hospital, Montreal, Canada.

5.4.2 Strain gauge measurements

After CO_2 asphyxiation, followed by decapitation, right tibiae were collected for each rat group. Only the right tibiae were used in this study as it has been reported previously that the contralateral tibia can be considered symmetric for the biomechanical purpose during the growing period (Mustafy, Londono, & Villemure, 2018). The right leg was isolated by sawing off from the middle of the femur to the toes. After the leg collection, an incision was made near the medio proximal surface of the leg. Overlying skin and muscles were then removed to expose the bonding surface, polished with an abrasive paper and cleaned with ethanol solution. A single element strain gauge (C2A-06–015LW-120; dimensions: 0.86mm × 1.32mm, Micro-Measurements Group, Raleigh, NC, USA) was bonded with cyanoacrylate (M-Bond 200; Micro-Measurements Group) at 35% of the tibial length (L) in its antero-medial (AM) surface (Figure 5.1, 5.5-II).

Following gauge installation, the incision remained open with the lead wires bonded to the strain gauge for strain reading. The other end of the wires were connected to quarter-bridge completion and analog input modules (NI9944 and NI9237, National Instruments). The tibia was positioned between two custom-made loading cups, which were attached to a Mach-1 V500C loading device (Biomomentum Technologies, Montreal, Canada) (Figure 5.1). A compressive preload of 0.5 N was applied to keep the tibia in position. Haversine waveform displacements were subseqently applied at 2Hz with a 0.10 sec rest insertion between two displacement cycles. Displacements

ranging from 0.5 mm to 3.5 mm were applied with a 0.25 mm increment. Strain data was recorded simultaneously at 2.5 kHz with a PC via Labview software (Labview 8.6, NI). Resulting reaction forces were simultaneously recorded with the Mach-1 load cell (allowable maximum loads limits ± 150 g to ± 10 kg) with load precision being 1 part in 20,000 of the maximum (7.5 mg minimum). Prior to testing, the strain measurement process was appraised for reproducibility. To do so, five strain gauge readings were acquired for a certain displacement level under different orientations of the leg. After the completion of a single reading, the tibia was completely removed from the loading cups and repositioned again in a different orientation.
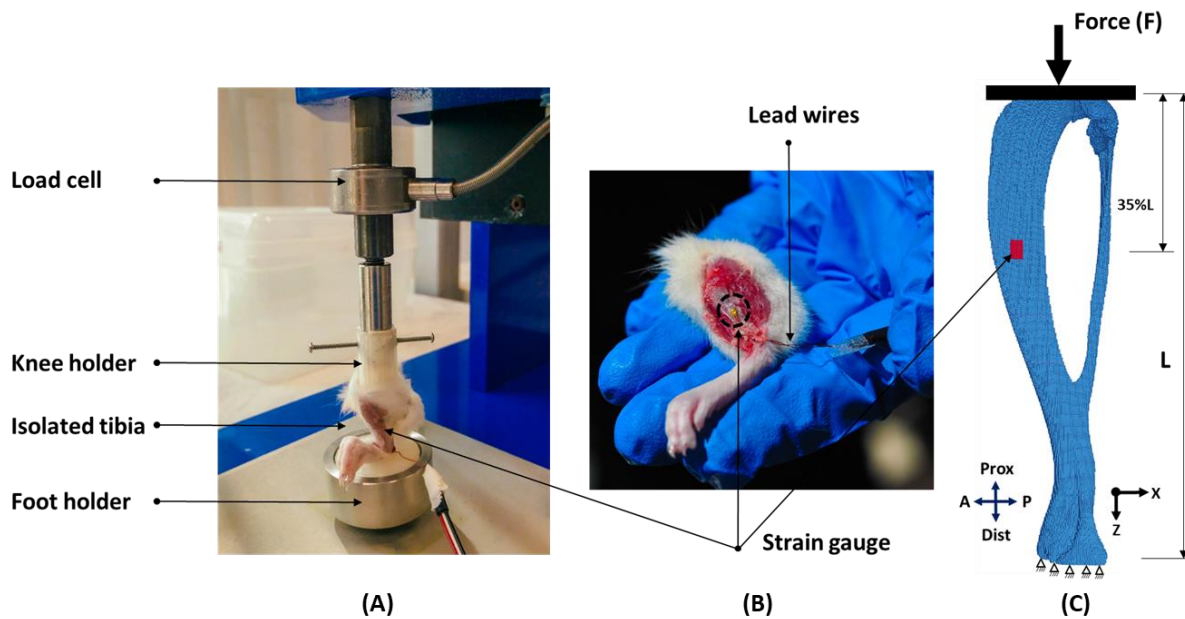
Figure 5.1 (A) Experimental setup for the *in vivo* rat tibial compression with strain gauge attached to the tibia. (B) Overlying skin and muscles of the tibia were retracted to expose the strain gauge with lead wires. (C) Geometric and boundary conditions of a representative rat tibia illustrating the strain gauge site at 35% of the tibial length (highlighted in red). A compressive force (F) was applied at the top. At the distal end, pin conditions were applied to all nodes. A = anterior, P = posterior

5.4.3 Micro-CT imaging

All right tibiae (n=18) were scanned prior to strain gauge installation. They were scanned again after strain gauge installation but before strain measurement. After strain gauge reading, the lead wires attached to the gauge were cut, and the gauge was left intact on the tibial surface. The muscles

and soft tissues were cleaned off from the tibiae and stored in Phosphate-buffered saline (PBS) solution at room temperature for micro-CT scanning. All the tibiae were scanned a third time with the bonded strain gauges remaining on the tibial diaphysis. This allowed to identify the strain gauge site on the tibial surface and to make sure that the tibia was not damaged or fractured during the strain gauge installation or loading procedure. All scans were completed with a Skyscan 1176 *in-vivo* micro-CT (Skyscan, N.V., Belgium) scanner with rotatable X-ray source and detector. Full X-ray power was used with a source voltage 65 KV, current 384 µA and 1-mm thick aluminum filter for beam hardening artifact reduction. Scanning resolution was 18 µm for a 2,000×1,336 CCD detector array. The exposure time was 350 ms, the rotation step 0.65°, with 1 frame averaging, and gantry direction in CC (craniocaudal). During acquisition, the scanning consisted of a stack of 1,354 images (4 week old rat tibia) to 2,344 images (12 week old rat tibia). The acquisition covered the knee joint from just above the proximal tibia and extended up to the tibiofibular joint.

5.4.4 Voxel based finite element analysis

5.4.4.1 Geometry

The cross-section images obtained from micro-CT scans were reconstructed using a filtered back-projection algorithm (software NRecon, v.1.6.10, Skyscan, Kontich, Belgium). The reconstructed images were of 772×772 pixels each, 17.48 µm pixel size, and stored as 8-bit images (256 gray levels). Both the baseline micro-CT scans (before strain gauge installation) and post micro-CT scans (with bonded strain gauge on the tibial surface) were reconstructed for FE geometry creation. The reconstructed micro-CT images of each tibial specimen were processed using an in-house Matlab mesh generation program to generate a 3D voxel-based finite element model, where 8-noded brick elements were used to represent bone voxels (van Rietbergen et al., 1995). A global gray threshold value of 65, corresponding to an equivalent density of 0.413 g/cm^3 of calcium hydroxyapatite (CaHA), was used for extracting bone geometry (Boyd, Davison, Müller, & Gasser, 2006; Hasan et al., 2018; Lynch et al., 2010). This threshold value was extracted as the average gray level value of bone and non-bone peaks of the plotted histogram (Christiansen, 2016; Dufresne, 1998) from micro-CT data of rat tibiae during the 4th to 14th week of age period (Mustafy, Benoit, Londono, Moldovan, & Villemure, 2018).

A mesh convergence analysis was performed on the isolated 4, 8 and 12 week old rat tibia using 18, 36, 54, 72, 90 and 108 μm voxel resolutions (Figure 5.2). Using the 18 μm images as the reference image set, coarser voxel resolution models of 36, 54, 72, 90, and 108 μm were generated. For 18 μm voxel resolution model, 1x1x1 pixels were converted directly to 3D voxel-based model with our in-house Matlab mesh generation program. To generate 36 μm voxel resolution model, sets of 2x2x2 pixels in 18 μm resolution images were condensed with an in-house Matlab mesh generation program to generate the 3D voxel-based finite element model. Similarly, for the 54, 72, 90 and 108 μm voxel resolution models, sets of 3x3x3, 4x4x4, 5x5x5, and 6x6x6 pixels, respectively, were condensed to generate 3D voxels.
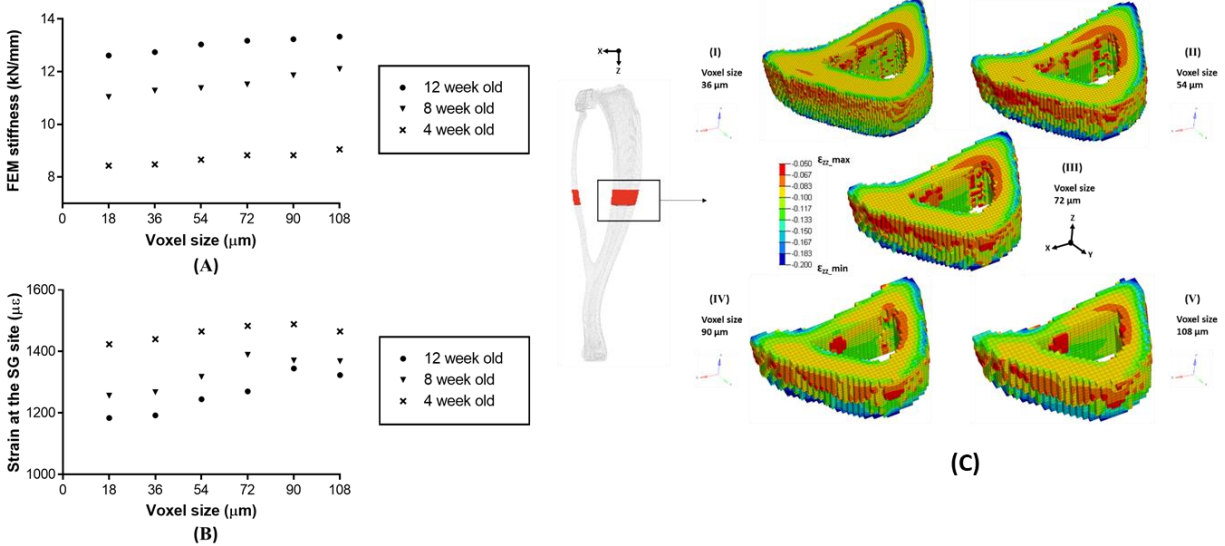
Figure 5.2 (A) Stiffness of the finite element model of the tibia under compression for different voxel sizes. (B) Computational strain at the strain gauge site of the tibia under compression for different voxel sizes. (C) Distribution of longitudinal strains (ε_{ZZ}) in the representative tibial section for different voxel sizes

5.4.4.2 Material properties

Linear elastic, isotropic but non-homogeneous material properties were assigned to the voxels in the generated model. Poisson's ratio was considered as 0.3 (Torcasio et al., 2012). The elastic modulus was assigned to each voxel based on the bone density and Hounsfield Unit (HU) value. In order to relate the Hounsfield Unit (HU) value with the bone density, two steps of calibrations were performed. Firstly, using similar scanning parameters used for the experimented tibiae, a tube

of water (approximately matching the width of the animal's leg) was scanned with the micro-CT scanner. The scanning images were then reconstructed with similar parameters used for the experimented tibiae. Then, using the already established linear equations of Hounsfield unit for water (HU=0) and for air (HU=-1000) (Rho, Hobatho, & Ashman, 1995), the following grayscale-HU relationship was evaluated using the reconstructed image set:

$$HU = 17.952 * grayscale - 1000 \quad (I)$$

Secondly, a phantom calibration was performed using Bruker-MicroCT bone mineral density calibration phantoms with CaHA (Calcium Hydroxyapatite) concentrations of 0.25 and 0.75 g.cm^{-3} representing cortical and trabecular bone tissue samples (Brucker micro-CT, Kontich, Belgium). Calibration phantoms were scanned in a tube of water as the water closely imitates the x-ray absorption of soft biological tissue around the rat tibia (Bruker, 2016). The scanning parameters and reconstruction parameters were similar to the parameters used for the experimented tibiae. Assuming the relationship between Hounsfield units and bone apparent density to be linear (Rho et al., 1995; Yang, Ma, & Guo, 2010), a linear regression with the values for trabecular and cortical phantom samples resulted in the following HU-density relationship:

$$\rho = 3.685 x 10^{-3} * HU - 0.073 \quad (II)$$

The Young's modulus (E) was then related to the bone density (ρ) of each voxel using the following equation,

$$E = E_{max} * \left(\frac{\rho}{\rho_{max}} \right)^2 \quad (III) \ \text{(Chen, Wu, Liu, Yang, \& Cui, 2015)},$$

where, $E_{max} = 9.89 \, GPa$, which represented the maximum value of the Young's modulus for the cortical bone structure of 12 week old rat tibiae (Mustafy, Londono, et al., 2018), and $\rho_{max} = 1.683 \, g.cm^{-3}$, which represented the maximum value of density calculated from all the tibial samples (n=18) used in this study.

5.4.4.3 Loading and boundary conditions

Simplified boundary conditions for the tibia were adapted to represent the experimental set up under loading cups (Figure 5.1C). To do so, the proximal end of each tibia (<0.5 mm in length)

was cropped to get rid of irregular bony structures and for facilitating load application on a flat surface. Out of plane rotations were restricted to avoid the instability in the model. At the distal end, all nodes were constrained in the X and Y directions. An increasing compressive force up to 35.5 N was then applied in the longitudinal (Z) direction at the proximal tibial end. The maximum compression value was chosen to stay under a safe limit of 50 N, which has been reported previously (Li, Jiang, Yan, Jiang, & Dai, 2011) to cause micro damage in adult (6 months old) rat tibia. Simulations were performed using the finite element commercial software ABAQUS 6.14 with its non-linear implicit solver (Abaqus, 2014). All simulations were analyzed with Intel Xeon CPU with 3.50 GHz, equipped with 14 Cores and 28 Logical Processors and with an installed Physical Memory (RAM) of 512 GB.

5.4.5 Strains evaluation

5.4.5.1 Comparison of strains measured from experimental and finite element modeling at antero-medial (AM) location

Exact gauge locations on the tibial surface of the FE models have been identified by registering the baseline micro-CT models (n=18) with the post micro-CT models (n=18). Reconstructed images of a post micro-CT tibial model was imported into DataViewer v.1.5.2. Then, an iterative optimization-based rigid 3D registration algorithm was employed using ImageJ (NIH, Bethesda, USA) to align the post micro-CT model and baseline micro-CT model on top of each other (Mustafy, Londono, et al., 2018). This method allowed us to determine the gauge location in the AM tibial region accurately. Under the applied load, nodal strains spanning the surface area of gauge site (0.86 mm x 1.32 mm) centered at the 35% of total tibial length (L) were calculated along the longitudinal (Z) direction and further averaged (Figure 5.1, 5.5-I). Strain readings were extracted under compression ranging from 5.5N (=5+0.5N preload) to 35.5N (= 35+0.5N preload). Experimental strains and longitudinal strains evaluated from FE modeling of the rat tibiae from three different age groups were compared to assess the correlation coefficient and the relationship between them (Figure 5.3).
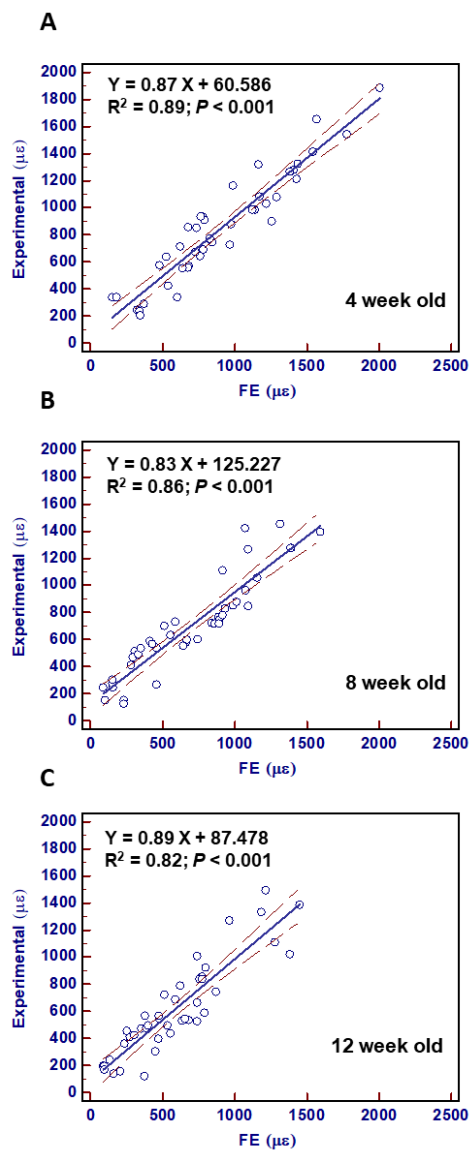
Figure 5.3 Linear regression between experimental strains and longitudinal strains evaluated from finite element models of the rat tibiae for the three different age groups (A-C). Correlation coefficient between the two approaches is calculated based on the 95% confidence interval for the regression line

The Bland-Altman technique (Bland & Altman, 1986) was used to assess the agreement between experimental and FE model derived strains of the rat tibiae for three different age groups (Figure 5.4). The results were comparable with limits of agreement determined as mean difference $\pm$ 1.96 standard deviations (i.e. 95% confidence interval of the difference) (Bland & Altman, 1986). Results summary with statistical comparison are also listed in Table 5.1.
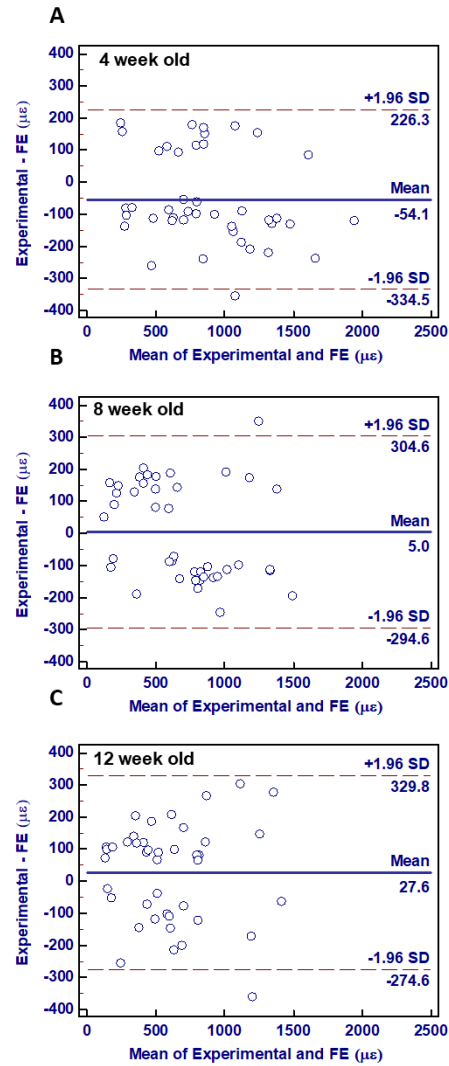
Figure 5.4 Bland-Altman plots comparing experimental and finite element model derived strains of the rat tibiae for the three different age groups. (A, B, C)***** The difference between experimental and FE modeling strains plotted against the mean of experimental and FE modeling strains

* *The central line (mean) indicates the bias and the outer lines (± 1.96 SD) indicate the limits of agreement (LoA)*

Table 5.1 Results from Bland-Altman test between experimental and FE modeling strain results for rat tibiae of three age groups.

Bland-Altman test	4 week old	8 week old	12 week old
Sample size	42	42	42
Arithmetic mean	-54.08	4.99	27.58
95% CI	-98.66 to -9.50	-42.63 to 52.62	-20.46 to 75.63
Standard deviation	143.03	152.84	154.18
Lower limit	-334.48	-294.56	-274.61
Upper limit	226.31	304.56	329.78
t statistic	-1.534	1.868	-0.071
r value	0.24	0.18	0.02
P value	0.133	0.069	0.543

5.4.5.2   Strains at antero-lateral (AL) and postero-lateral (PL) regions

Strains were complementarily evaluated at the antero-lateral (AL) and postero-lateral (PL) tibial regions located at the same level as the installed AM strain gauge (Figure 5.5-I, 5.5-II). Strain gauge surface areas were considered located at the mid-point of the AL and PL regions (Figure 5.5-II). Strains were then evaluated along the longitudinal direction (Z) for each of these areas under the applied loading and boundary conditions previously presented.

5.4.5.3   Strains at varying gauge locations

Moreover, the effects of modifying gauge location on the resulting FE modeling strains (AM) have been investigated in order to assess the sensitivity of the FE modeling results to strain gauge placement. Strains were more precisely evaluated for gauge locations varying by ~±0.5mm along the anterior-posterior (x) or the proximal-distal (z) directions at 35N force (Figure 5.1C), and further compared with experimentally measured strains at gauge location (Figure 5.1C).

5.4.6   Cortical bone structural parameters

In order to evaluate the effects of geometry changes on strain distributions along the tibia, cortical bone area (Ct.Ar; mm^2), cortical thickness (Ct.Th; mm) as well as maximum and minimum moment of inertia (I_{MAX}, I_{MIN}; mm^4) were evaluated from the selected VOI$_{SP}$ (volume of interest for structural parameters) and cross-sections. A stack of images was selected as the VOI$_{SP}$ from each

micro-CT tibial scans at 35%L (i.e. at experimental strain gauge site). The VOI_{SP} was 1.32 mm in height (strain gauge length) and consisted of 74 CT scan slices in total. Also, the tibial length (mm) and tibial curvature in anterior-posterior and medial-lateral directions (C_{AP}, C_{ML}; μm) were measured (Mustafy, Londono, et al., 2018) for the entire tibia. Calculations were performed for all the tibiae (n=18) from three age groups. Results were tabulated as means ± standard deviations.
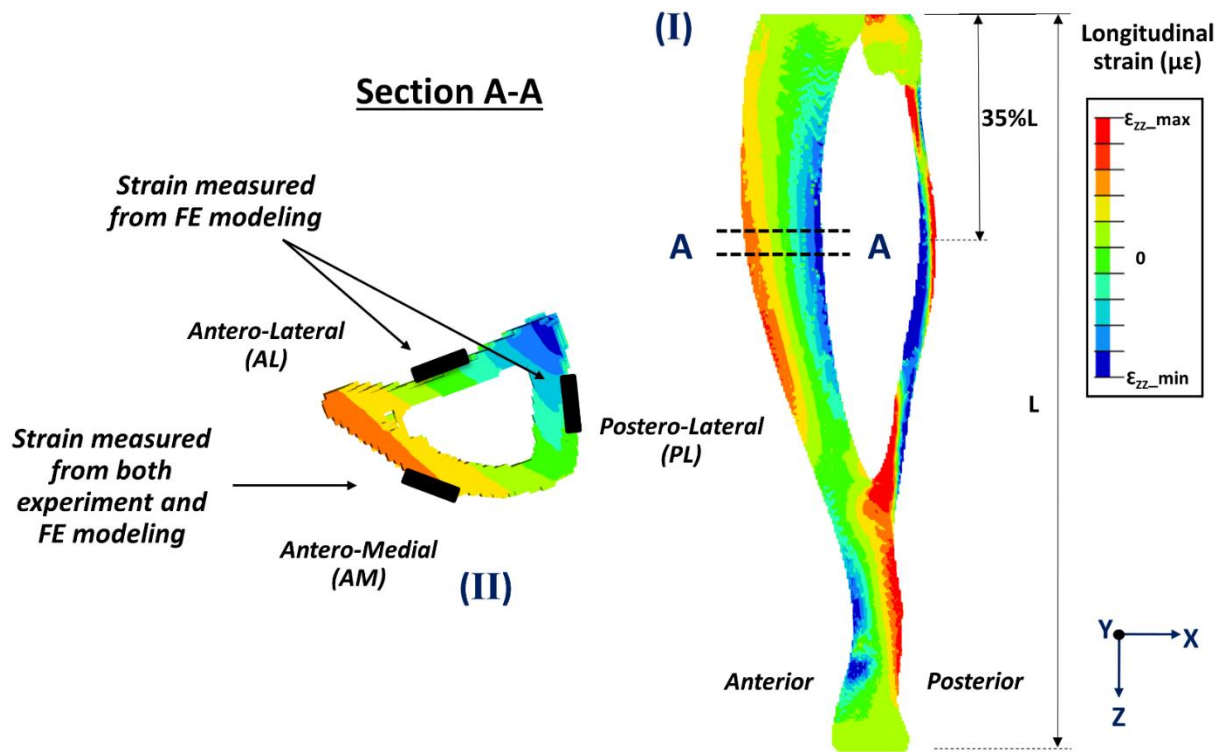
Figure 5.5 (I) Longitudinal strain distribution throughout the whole rat tibia loading model (12 week old). (II) 3D section of the rat tibial geometry showing locations of the experimental (AM) and FE modeling (AL, PL and AM) strains in the transverse cross-section containing the strain gauge

5.4.7 Statistical analyses

Linear regression analyses were performed to validate the FE modeling strains, and to compare the strains at strain gauge location (AM) with the computational strains at AL and PL tibial regions. Strains at varying gauge locations were statistically compared. The Bland-Altman technique was further used to assess the accuracy of the computational strains. Results were considered

statistically significant for $p < 0.05$. All statistical analysis were performed with SPSS Statistics version 23 (SPSS Inc., Chicago, IL, USA) and MedCalc version 12.2.1 (MedCalc Software, Mariakerke, Belgium).

5.5 Results

5.5.1 Mesh convergence results

Overall stiffness and strains at the strain gauge site were calculated for all the models and compared with respect to the 18 μm (scanning resolution) model. The differences (%) in stiffness were found as 1.1, 1.9, 4.7, 4.9 and 7.4%, respectively for the 36, 54, 72, 90 and 108 μm 4 week old models (Figure 5.2A). For 8 week models, these differences were 2.2, 2.7, 4.3, 7.3 and 9.6%, and for 12 week models, these differences were 1.2, 2.1, 4.4, 5.3 and 5.8% with respect to 36, 54, 72, 90 and 108 μm voxel models. A moderate change was observed between 36 and 54 μm models and a steep change was observed between 54 and 72 μm models (Figure 5.2A). However, the differences remained below 3% for 36 μm models across all age groups. Moreover, some trabecular microstructure disappeared with increased voxel mesh size of 54 μm and above (Figure 5.2C). Also, it has been reported in the literature that in order to consider the mechanical properties within each voxel to be homogeneous, a narrow range of mineralization is required and can only be achieved by adapting a voxel mesh size of less than 40 μm for micro-CT based FE modeling analysis (Gross, Pahr, Peyrin, & Zysset, 2012; Ramezanzadehkoldeh & Skallerud, 2017). Hence, the 36 μm model was initially selected as the model resolution for this study. Local strains at the installed strain gauge site of the tibiae were also investigated to further assess the voxel size selection (Figure 5.2B). It was observed that a change in voxel size from 18 to 36 μm resulted in a strain difference of 1.12, 0.93 and 0.73%, whereas, a change from 36 to 54 μm led to a 3.4, 4.7 and 5.3% strain difference for 4, 8 and 12 week old tibiae respectively (Figure 5.2B). Accordingly, it was concluded that the 36 μm (0.036 mm) voxel mesh was sufficiently converged. The number of elements varied from 5.66×10^7 to 4.79×10^8, from 4 to 12 week old rat tibial model.

5.5.2 Strain analyses

5.5.2.1 Comparing experimental and FE modeling strains at antero-medial (AM) gauge location

Strains measured from FE analyses were compared with the corresponding experimental strains. The correlations for the strains were 0.91, 0.87 and 0.85 for 4, 8 and 12 week old rat tibiae respectively ($p<0.001$ for all cases). The mean difference between experimental and FE modeling strains for 4 week old rat tibiae was -54.1 $\mu\varepsilon$ (95% CI on difference: -98.7 to -9.5 $\mu\varepsilon$; LoA: -334.5 to 226.3 $\mu\varepsilon$), for 8 week old rat tibiae was +5.0 $\mu\varepsilon$ (95% CI on difference: -42.6 to 52.6 $\mu\varepsilon$; LoA: -294.6 to 304.6 $\mu\varepsilon$), and for 12 week old rat tibiae was +27.6 $\mu\varepsilon$ (95% CI on difference: -20.5 to 75.6 $\mu\varepsilon$; LoA: -274.6 to 329.8 $\mu\varepsilon$) (Figure 5.4). Accordingly, no significant bias of FE strain measurements ($p>0.05$) compared with the experimental reference for three age groups were found (Table 5.1).

5.5.2.2 Strains at antero-lateral (AL) and postero-lateral (PL) regions

FE modeling strains extracted for the PL and AL regions were plotted for each age group against the experimental strains (Figure 5.6) for increasing compression loading. FE modeling strains for the AM region were also plotted in the same graph for comparison (Figure 5.6). Under 35N compression, peak strains in AM, AL and PL regions all decreased with rat age (Figure 5.6). Correlations between the experimental strains and FE modeling strains at the PL and AL regions showed strong correlations for both PL ($r^2=0.79$; maximum) and AL ($r^2=0.79$; maximum) ($p<0.001$ for all cases) (Figure 5.6).

5.5.2.3 Strains at varying gauge locations

Effects of varying gauge location by ~±0.5mm in the anterior/posterior or the proximal/distal directions under a 35N compression are presented on Figure 5.7. A 0.5 mm proximal translation in gauge location induced a FE modeling strain reduction varying between 4% and 10% compared to the experimental strain (Figure 5.7A), whereas strain gauge placement toward the distal direction induced a FE modeling strain increase varying between 9% and 11% compared to the experimental strain (Figure 5.7A). No statistical significance was observed for the proximal and distal location strains compared with the experimental strains for three age groups (Figure 5.7A). Changes in

gauge location towards the anterior and posterior directions caused respectively a FE modeling strain increase varying between 17% and 31% and decrease varying between 21% and 39% compared to the experimental strain (Figure 5.7B).

(A)　　　　　　　　(B)　　　　　　　　(C)
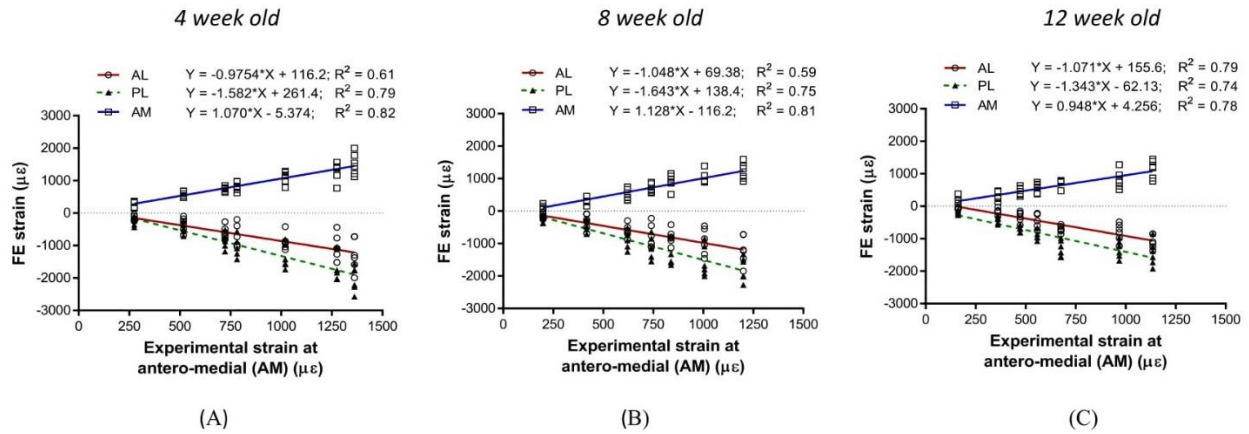
Figure 5.6 Experimental strain at the strain gauge location vs FE modeling strain at the AL, PL and AM regions of the rat tibia for three different age groups (A-C)
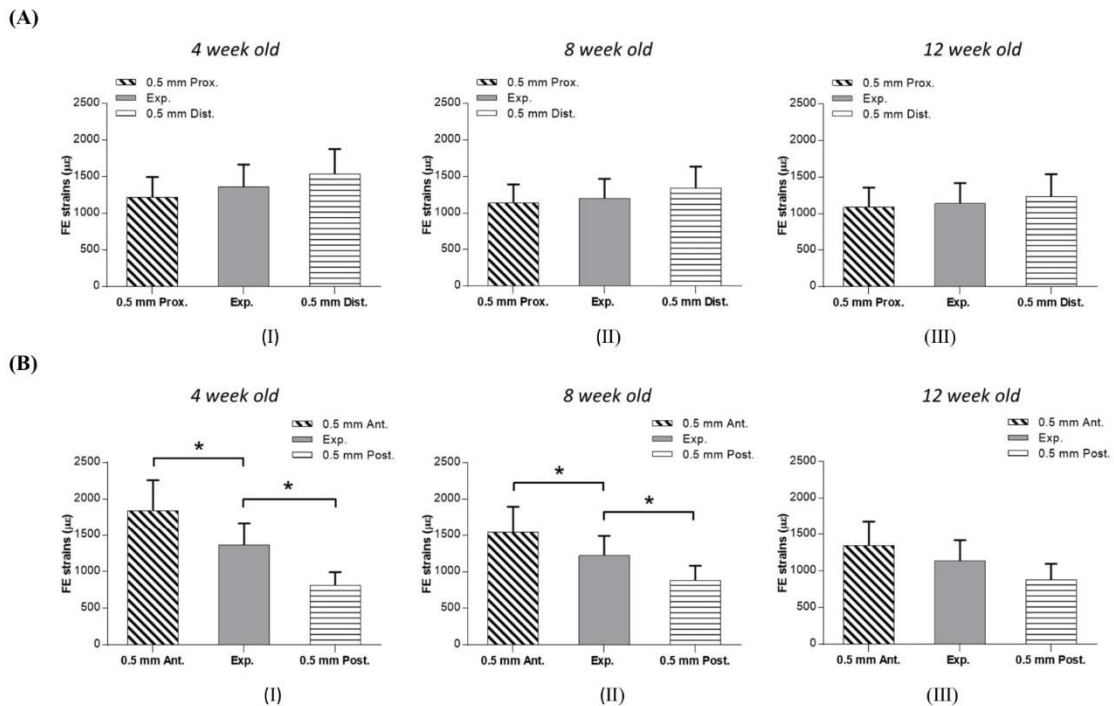
Figure 5.7 (A) FE modeling strains (mean value ± SD) measured at +0.5 mm toward the proximal or distal side of the tibiae with respect to the experimentally measured strains (mean value ± SD)

under 35N load. (B) FE modeling strains (mean value ± SD) measured at +0.5 mm toward the anterior or posterior side of the tibiae with respect to the experimentally measured strains (mean value ± SD) under 35N load. Asterisk represents a significant difference with *p < 0.05

For 4 week old tibiae, significant difference was observed for posterior location strain compared to the experimental data, whereas, anterior location strain remained non-significant (Figure 5.7B). For 8 and 12 week old tibiae, no significance was noticed for anterior/posterior directional strain when compared with the experimental data (Figure 5.7B).

Table 5.2 Cortical bone structural parameters for rat tibiae (mean ± SD).

	4 week old	8 week old	12 week old
Cortical bone parameters at strain gauge location (35%L)			
Cortical bone area, Ct.Ar (mm^2)	2.79 ± 0.3	5.53 ± 0.3	7.67 ± 0.5
Cortical thickness, Ct.Th (mm)	0.062 ± 0.1	0.337 ± 0.1	0.481 ± 0.1
Maximum moment of inertia, I_{MAX} (mm^4)	1.52 ± 0.6	6.21 ± 1.8	9.97 ± 2.4
Minimum moment of inertia, I_{MIN} (mm^4)	1.35 ± 0.3	3.89 ± 1.4	5.82 ± 1.9
Whole tibial measurements			
Antero-posterior tibial curvature, C_{AP} (µm)	625 ± 113	1123 ± 311	1363 ± 319
Medio-lateral tibial curvature, C_{ML} (µm)	366 ± 61	622 ± 111	751 ± 125
Tibial length (mm)	23.87 ± 4.1	34.6 ± 6.9	38.67 ± 5.0

5.5.2.4   Cortical bone structural parameters

At strain gauge levels (35%L), cortical bone area (Ct.Ar) changed from 2.79 to 7.67 mm^2 from 4th to 12th week period, respectively (Table 5.2). Cortical thickness (Ct.Th) progressed from 0.062 to 0.481 mm at gauge levels with rat development. Also, tibial length varied from 23.87 to 38.67 mm from 4th to 12th week period (Table 5.2). Maximum and minimum moment of inertia (I_{MAX}, I_{MIN}) almost quadrupled, whereas, tibial curvatures (C_{AP}, C_{ML}) were found to be doubled during the adolescent period (Table 5.2).

5.6 Discussion

The overall goal of this study was to develop a voxel based FE modeling approach to study bone strain in rat tibia under *in vivo* axial compression during the adolescent period. The model was further validated by comparing FE modeling strains with corresponding experimentally measured strains. The relationships between the experimental and FE modeling strains evaluated at different tibial regions, but in the same level of gauge installation site, were assessed. The sensitivity of FE modeling strains to gauge placement was also investigated.

5.6.1 Predicted FE modeling strains and experimental strains showed strong agreements across the three rat age groups

The strains predicted by the FE models were correlated to the strains measured through the experimental method for three age groups of rats. High correlations (0.91, 0.87 and 0.85) were observed between the experimental and FE strains (Figure 5.3), which are in good agreement with other studies, where a coefficient of determination of 0.95 and 0.66 were reported for the experimental vs. computational strain comparisons for adult rat (Torcasio et al., 2012) and young mice (Yang et al., 2014) tibiae under axial loading respectively. Also, our results can be comparable to the findings by Akter et al. (Akhter et al., 1992), who showed high coefficients of determination when comparing *in vivo* strains induced by four points bending vs. the experimental strains (R^2=0.87) in adult rat tibiae. Moreover, Bland-Altman analysis revealed that (Figure 5.4) the bias throughout the mean of experimental and FE modeling strain value remained constant as indicated by a non-significant ($p = 0.133$, 0.069 and 0.543 for 4, 8 and 12 week old tibiae respectively) correlation (r = 0.24, 0.18 and 0.02 for 4, 8 and 12 week old tibiae respectively) between the average versus the difference (Table 5.1). Also, the data revealed that, 95% of the time, our FE models will predict a strain value compared to the experimental method with a precision from -98.66 to 75.63 µε (Table 5.1) across all three groups. This reported data can also be relatable to previous studies (H. Gray, Zavatsky, Taddei, Cristofolini, & Gill, 2007; H. A. Gray, Taddei, Zavatsky, Cristofolini, & Gill, 2008) for human cadaveric tibia and composite tibia, where mid diaphysis strains were evaluated by axial loading and FE modeling method, and FE models could predict experimental strains with more than 80% and 73% accuracy respectively.

5.6.2 Under compression, the greatest longitudinal strains develop in the PL region, compared to the AM and AL regions

A strong correlation between FE modeling and experimental strains (at gauge location) was found, hence validating the robustness of our finite element models. Under 35N loading, maximum longitudinal strains occurred at the PL region (compressive). These strains were on average 1.37 and 1.22 times greater than longitudinal strains occurring at AL (compressive) and AM (tensile) regions, respectively (Figure 5.6). Our findings are in good agreement with finite element predictions (Moustafa et al., 2012; Stadelmann et al., 2009; Willie et al., 2013) and experimental outcomes (Patel et al., 2014) from several mice studies. Strain gauges are generally installed at easily accessible bone locations, which can provide a flat surface for good bone to gauge bonding (Bilezikian, Raisz, & Martin, 2008). However, peak strains could develop in areas different than the instrumented ones, as shown in this study. Hence, investigations should not be restricted to a single region of the tibia; complementary experimental and modeling approaches should be combined to better track peak strains for a specific loading condition.

5.6.3 Under similar compression, strains decrease with age during the adolescent period

Strains in all three regions (AM, AL and PL) decreased with age for tibiae undergoing the same compressive loading (Figure 5.6). For the AM region, the peak FE modeling strain at 35N loading was shown to decrease from 4 week old group by 20.5% and 27.7%, respectively for 8 and 12 week old rat tibiae (Figure 5.6). Similar phenomena were observed at AL and PL regions. For AL region, the peak FE modeling strain decreased from 4 week old group by 7.2% and 26.3% for 8 and 12 week old groups, respectively (Figure 5.6). For PL region, the peak FE modeling strain decreased from 4 week old group by 11.6% and 25.2% for 8 and 12 week groups, respectively (Figure 5.6). A possible reason for this strain decrement could be the measured increase in geometrical properties (Ct.Ar and Ct.Th) with age (Table 5.2). From the generalized Hooke's law, forces and displacements (or stresses and strains) are linearly related (Necas & Hlavácek, 2017; Rychlewski, 1984) with $\sigma = E\varepsilon, \Rightarrow \varepsilon = \sigma/E$; where $\sigma = $ stress $= F\,(force)/A\,(area)$, $E = $ modulus of elasticity and $\varepsilon = $ strain (Necas & Hlavácek, 2017). Strains hence depend on the applied force, cross-sectional area (in this case, Ct.Ar) and elastic modulus. When the parameter Ct.Ar increases,

then the strain decreases, for a constant elastic modulus. As the same tibial level (35% of the tibial length) was considered for AM, AL and PL strain comparisons, we can assume similar variations in elastic modulus at this level among the tibiae (Mente & Lewis, 1989). Hence, the observed strain decrement could be explained, at least partly, by the measured change in Ct.Ar, which indeed also increased from 4, to 8 and to 12 week old tibiae (Table 5.2). Also, the moment of inertia at 35% of the tibial length was found to be increased during the adolescent period (Table 5.2). As stress is inversely proportional to the moment of inertia at a certain section (Bansal, 2010; Pilkey & Pilkey, 1994), higher stress was expected with lower moment of inertia. Hence, higher strains were observed at 4 week of age compared to the 12 week group in our study. Peak strains measured in our study agree with strain values obtained in another study, where 12 week old rat tibiae underwent 10 N compression at 25%L (Torcasio et al., 2012). Despite gauge placement variations between the two studies, their measured strains (~350 ± SD µε) remained within the limits of our experimental strains for the 12 week old group at 10N compressive loading.

5.6.4 Changes in strain gauge placement along anterior-posterior direction has greater impact on the resulting FE modeling strains compared to changes along the proximal-distal direction

FE modeling strains were computed by varying the location of the strain gauge from its experimental location. Strain gauge location was varied by ~±0.5mm along the anterior-posterior or along the proximal-distal axes under 35N load (Figure 5.7), representing 2.1, 1.4 and 1.3% of the total tibial length for 4, 8 and 12 week old rat tibiae, respectively. Results showed that these slight modifications in gauge location could greatly impact the resulted strains. Indeed, a proximal gauge displacement caused a strain decrease ranging from 21.38% to 11.38% and a distal gauge displacement induced a strain increase ranging from 18.78% to 8.56% (Figure 5.7A) with age. Also, a posterior gauge displacement caused a strain decrease ranging from 58.48% to 40.46% and an anterior gauge displacement caused a strain increase ranging from 51.30% to 36.56% (Figure 5.7B) with age. With increasing tibial length during adolescence (Table 5.2), smaller strain increases/decreases due to gauge displacement were expected in the 12 week old group. The greater changes observed for gauge displacement along the anterior-posterior direction could be explained by considering that the same amount of gauge displacement caused a greater relative shift in anterior-posterior direction compared to the proximal-distal, which then led to a greater strain

variation in the anterior-posterior direction. Also, as the tibiae are curved more in the anterior-posterior direction compared to the medial-lateral direction (Table 5.2), the resulted stress and strain in our study are expected to vary more in this direction under compressive loading scenarios (Brassey et al., 2013; Ghali, Neville, & Brown, 2014; Wineman & Kolberg, 1995). Indeed, gauge variations (~±0.5mm) represented 2.1, 1.4 and 1.3% of the total tibial length (proximal-distal direction), whereas they represented 19.3, 11.5 and 10.1% of the tibial width (anterior-posterior direction) for 4, 8 and 12 week old tibiae, respectively. Hence, care should be taken to ensure reproducible gauge installation *in vivo,* especially along the anterior-posterior direction for compression loading.

5.6.5 Limitations

In this study, a maximum modulus of elasticity value of 9.89 GPa, extracted from three-point bending tests (Mustafy, Londono, et al., 2018), was used to model no-homogeneous bone mechanical properties. Higher values of 10 and 13.8 GPa were also reported by other researchers (Huang et al., 2003; Torcasio et al., 2012) to represent the adult rat tibia. However, a good agreement between experimental and FE modeling strains justified our chosen value for the elastic modulus. Strain gauge location was assumed consistent across three age groups. However, after observing the micro-CT images, a small variation in the strain gauge location toward the anterior-posterior or proximal-distal direction was noticed in some rats from different groups. As average strains were used for comparisons, this gauge location effect was considered not affecting the conclusions of this study. In addition, experimental conditions were modeled without including soft tissues, such as muscles, ligaments and cartilage, although it is known that viscoelastic soft tissues can play a role in dynamic simulation environments (Dodge et al., 2012; Yang et al., 2014). However, experimental compression was applied using a quasi-static approach in this study. Several researchers have reported that the bone alignment with respect to the loading direction can be problematic (Giorgi & Dall'Ara, 2018; Kumar, Dantzig, Jasiuk, Robling, & Turner, 2010; Torcasio et al., 2012). However, we used a simplified approach and considered a uniform loading direction in the finite element models for all the rat tibiae in different groups. In future, additional steps can be taken to match the experimental bone alignment with the computational modeling approach. Lastly, only compressive loading was investigated in this study. Other loading modes

could introduce tibial bending across different axis or torsion, which might cause greater changes in neutral axis position leading to different strains across different tibial sections (Patel et al., 2014).

5.7 Conclusion

A voxel based finite element modeling approach was developed and validated for growing rat tibiae under compressive loading. To authors' best knowledge, no other studies have been performed to assess the tibial strains in the adolescent or immature rats. Strong correlations between FE modeling and experimental strains were found, hence indicating the robustness of our finite element modeling approach. Interestingly, greatest longitudinal strains were observed in the PL region, compared to the AM and AL regions. Thus, an *in vivo* loading study should consider assessing strains at different regions to report the peak strain in a specific section. Also, peak strains at the experimental site (AM) and obtained from FE models (AL and PL) were found to be decreasing with age, probably due to the change in geometrical properties with age. In addition, strain gauge placement was found to induce non-negligible strain magnitude changes, hence emphasizing the importance of gauge installation reproducibility in experimental studies. It is expected that the age-dependent force-strain data reported in this research will be resourceful to the bone and orthopedic research community for designing *in vivo* noninvasive loading protocols for growing rodents.

5.8 Acknowledgements

5.9 References

Abaqus, V. (2014). 6.14 Documentation. *Dassault Systemes Simulia Corporation, 651*.

Akhter, M., Cullen, D., Pedersen, E., Kimmel, D., & Recker, R. (1998). Bone response to in vivo mechanical loading in two breeds of mice. *Calcified tissue international, 63*(5), 442-449.

Akhter, M., Raab, D., Turner, C., Kimmel, D., & Recker, R. (1992). Characterization of in vivo strain in the rat tibia during external application of a four-point bending load. *Journal of biomechanics, 25*(10), 1241-1246.

Bansal, R. (2010). *A textbook of strength of materials*: Laxmi Publications.

Benoit, A., Mustafy, T., Londono, I., Grimard, G., Aubin, C.-E., & Villemure, I. (2016). In vivo dynamic compression has less detrimental effect than static compression on newly formed bone of a rat caudal vertebra. *Journal of musculoskeletal & neuronal interactions, 16*(3), 211.

Bergmann, P., Body, J.-J., Boonen, S., Boutsen, Y., Devogelaer, J.-P., Goemaere, S., . . . Rozenberg, S. (2010). Loading and skeletal development and maintenance. *Journal of osteoporosis, 2011*.

Bilezikian, J. P., Raisz, L. G., & Martin, T. J. (2008). *Principles of bone biology*: Academic Press.

Bland, J. M., & Altman, D. (1986). Statistical methods for assessing agreement between two methods of clinical measurement. *The lancet, 327*(8476), 307-310.

Boyd, S. K., Davison, P., Müller, R., & Gasser, J. A. (2006). Monitoring individual morphological changes over time in ovariectomized rats by in vivo micro-computed tomography. *Bone, 39*(4), 854-862.

Brassey, C. A., Margetts, L., Kitchener, A. C., Withers, P. J., Manning, P. L., & Sellers, W. I. (2013). Finite element modelling versus classic beam theory: comparing methods for stress estimation in a morphologically diverse sample of vertebrate long bones. *Journal of the Royal Society Interface, 10*(79), 20120823.

Bruker. (2016). HU and BMD calibration in Bruker-MicroCT CT-analyser.

Chen, G., Wu, F., Liu, Z., Yang, K., & Cui, F. (2015). Comparisons of node-based and element-based approaches of assigning bone material properties onto subject-specific finite element models. *Medical engineering & physics, 37*(8), 808-812.

Christiansen, B. A. (2016). Effect of micro-computed tomography voxel size and segmentation method on trabecular bone microstructure measures in mice. *Bone reports, 5*, 136-140.

Clinton, T., & Lanyon, L. (1984). Regulation of bone formation by applied dynamic loads. *J Bone Joint Surg Am, 66*, 397-402.

Dodge, T., Wanis, M., Ayoub, R., Zhao, L., Watts, N. B., Bhattacharya, A., . . . Yokota, H. (2012). Mechanical loading, damping, and load-driven bone formation in mouse tibiae. *Bone, 51*(4), 810-818.

Dufresne, T. (1998). Segmentation techniques for analysis of bone by three-dimensional computed tomographic imaging. *Technology and Health Care, 6*(5, 6), 351-359.

Fritton, J., Myers, E., Wright, T., & Van der Meulen, M. (2005). Loading induces site-specific increases in mineral content assessed by microcomputed tomography of the mouse tibia. *Bone, 36*(6), 1030-1038.

Frost, H. M. (2004). A 2003 update of bone physiology and Wolff's Law for clinicians. *The Angle Orthodontist, 74*(1), 3-15.

Ghali, A., Neville, A., & Brown, T. G. (2014). *Structural analysis: a unified classical and matrix approach*: Crc Press.

Giorgi, M., & Dall'Ara, E. (2018). Variability in strain distribution in the mice tibia loading model: A preliminary study using digital volume correlation. *Medical engineering & physics, 62*, 7-16.

Gray, H., Zavatsky, A. B., Taddei, F., Cristofolini, L., & Gill, H. (2007). Experimental validation of a finite element model of a composite tibia. *Proceedings of the Institution of Mechanical Engineers, Part H: Journal of Engineering in Medicine, 221*(3), 315-324.

Gray, H. A., Taddei, F., Zavatsky, A. B., Cristofolini, L., & Gill, H. S. (2008). Experimental validation of a finite element model of a human cadaveric tibia. *Journal of biomechanical engineering, 130*(3), 031016.

Gross, T., Pahr, D. H., Peyrin, F., & Zysset, P. K. (2012). Mineral heterogeneity has a minor influence on the apparent elastic properties of human cancellous bone: a SRμCT-based finite element study. *Computer Methods in Biomechanics and Biomedical Engineering, 15*(11), 1137-1144.

Hasan, A., Byambaa, B., Morshed, M., Cheikh, M. I., Shakoor, R. A., Mustafy, T., & Marei, H. (2018). Advances in osteobiologic materials for bone substitutes. *Journal of Tissue Engineering and Regenerative Medicine*.

Hsieh, Y. F., Robling, A. G., Ambrosius, W. T., Burr, D. B., & Turner, C. H. (2001). Mechanical loading of diaphyseal bone in vivo: the strain threshold for an osteogenic response varies with location. *Journal of Bone and Mineral Research, 16*(12), 2291-2297.

Huang, T., Lin, S., Chang, F., Hsieh, S., Liu, S., & Yang, R. (2003). Effects of different exercise modes on mineralization, structure, and biomechanical properties of growing bone. *Journal of applied physiology, 95*(1), 300-307.

Iwamoto, J., Yeh, J., & Aloia, J. (1999). Differential effect of treadmill exercise on three cancellous bone sites in the young growing rat. *Bone, 24*(3), 163-169.

Jeffery, J., Murphey, M., Stallone, J., Bloomfield, S., & Hogan, H. (2007). *Characterizing Strain in the Tibia of Rats Exposed to Hindlimb Unloading with an Exercise Countermeasure.* Paper presented at the ASME 2007 Summer Bioengineering Conference.

Klein-Nulend, J., Burger, E. H., Semeins, C. M., Raisz, L. G., & Pilbeam, C. C. (1997). Pulsating fluid flow stimulates prostaglandin release and inducible prostaglandin G/H synthase mRNA expression in primary mouse bone cells. *Journal of Bone and Mineral Research, 12*(1), 45-51.

Kumar, N. C., Dantzig, J. A., Jasiuk, I. M., Robling, A. G., & Turner, C. H. (2010). Numerical modeling of long bone adaptation due to mechanical loading: correlation with experiments. *Annals of biomedical engineering, 38*(3), 594-604.

Kuruvilla, S., Fox, S., Cullen, D., & Akhter, M. (2008). Site specific bone adaptation response to mechanical loading. *J Musculoskelet Neuronal Interact, 8*(1), 71-78.

LaMothe, J. M., Hamilton, N. H., & Zernicke, R. F. (2005). Strain rate influences periosteal adaptation in mature bone. *Medical Engineering and Physics, 27*(4), 277-284.

Lanyon, L., & Smith, R. (1969). Measurements of bone strain in the walking animal. *Research in veterinary science, 10*(1), 93-94.

Lee, K., Maxwell, A., & Lanyon, L. (2002). Validation of a technique for studying functional adaptation of the mouse ulna in response to mechanical loading. *Bone, 31*(3), 407-412.

Li, Z.-C., Jiang, S.-D., Yan, J., Jiang, L.-S., & Dai, L.-Y. (2011). Small-animal PET/CT assessment of bone microdamage in ovariectomized rats. *The Journal of Nuclear Medicine, 52*(5), 769.

Lynch, M. E., Main, R. P., Xu, Q., Walsh, D. J., Schaffler, M. B., Wright, T. M., & van der Meulen, M. C. (2010). Cancellous bone adaptation to tibial compression is not sex dependent in growing mice. *Journal of applied physiology, 109*(3), 685-691.

Mente, P., & Lewis, J. (1989). Experimental method for the measurement of the elastic modulus of trabecular bone tissue. *Journal of Orthopaedic Research, 7*(3), 456-461.

Moustafa, A., Sugiyama, T., Prasad, J., Zaman, G., Gross, T., Lanyon, L., & Price, J. (2012). Mechanical loading-related changes in osteocyte sclerostin expression in mice are more closely associated with the subsequent osteogenic response than the peak strains engendered. *Osteoporosis international, 23*(4), 1225-1234.

Müller, R., & Rüegsegger, P. (1995). Three-dimensional finite element modelling of non-invasively assessed trabecular bone structures. *Medical engineering & physics, 17*(2), 126-133.

Mustafy, T., Arnoux, P.-J., Benoit, A., Bianco, R.-J., Aubin, C.-E., & Villemure, I. (2018). Load-sharing biomechanics at the thoracolumbar junction under dynamic loadings are modified by anatomical features in adolescent and pediatric vs adult functional spinal units. *Journal of the Mechanical Behavior of Biomedical Materials, 88*, 78.

Mustafy, T., Benoit, A., Londono, I., Moldovan, F., & Villemure, I. (2018). Can repeated in vivo micro-CT irradiation during adolescence alter bone microstructure, histomorphometry and longitudinal growth in a rodent model? *PLOS ONE, 13*(11), e0207323. doi: 10.1371/journal.pone.0207323

Mustafy, T., El-Rich, M., Mesfar, W., & Moglo, K. (2014). Investigation of impact loading rate effects on the ligamentous cervical spinal load-partitioning using finite element model of functional spinal unit C2–C3. *Journal of biomechanics, 47*(12), 2891-2903.

Mustafy, T., Londono, I., & Villemure, I. (2018). Can the contralateral limb be used as a control during the growing period in a rodent model? *Medical engineering & physics, 58*, 31-40. doi: https://doi.org/10.1016/j.medengphy.2018.04.013

Necas, J., & Hlavácek, I. (2017). *Mathematical theory of elastic and elasto-plastic bodies: an introduction* (Vol. 3): Elsevier.

Oliviero, S., Giorgi, M., & Dall'Ara, E. (2018). Validation of Finite Element models of the Mouse Tibia using Digital Volume Correlation. *Journal of the Mechanical Behavior of Biomedical Materials*.

Omi, N., Nakamura, T., & Ezawa, I. (1998). Modulation of bone mass and turnover in growing rats by voluntary weight-bearing exercise and glucose supplementation. *Journal of nutritional science and vitaminology, 44*(3), 409-421.

Patel, T. K., Brodt, M. D., & Silva, M. J. (2014). Experimental and finite element analysis of strains induced by axial tibial compression in young-adult and old female C57Bl/6 mice. *Journal of biomechanics, 47*(2), 451-457.

Pilkey, W. D., & Pilkey, W. D. (1994). *Formulas for stress, strain, and structural matrices*: Wiley New York.

Pitsillides, A. A., Rawlinson, S., Suswillo, R., Bourrin, S., Zaman, G., & Lanyon, L. (1995). Mechanical strain-induced NO production by bone cells: a possible role in adaptive bone (re) modeling? *The FASEB Journal, 9*(15), 1614-1622.

Price, C., Li, W., Novotny, J. E., & Wang, L. (2010). An in-situ fluorescence-based optical extensometry system for imaging mechanically loaded bone. *Journal of Orthopaedic Research, 28*(6), 805-811.

Raab-Cullen, D., Akhter, M., Kimmel, D., & Recker, R. (1994). Bone response to alternate-day mechanical loading of the rat tibia. *Journal of Bone and Mineral Research, 9*(2), 203-211.

Ramezanzadehkoldeh, M., & Skallerud, B. H. (2017). MicroCT-based finite element models as a tool for virtual testing of cortical bone. *Medical engineering & physics, 46*, 12-20.

Rho, J.-Y., Hobatho, M., & Ashman, R. (1995). Relations of mechanical properties to density and CT numbers in human bone. *Medical engineering & physics, 17*(5), 347-355.

Robling, A., Duijvelaar, K., Geevers, J., Ohashi, N., & Turner, C. (2001). Modulation of appositional and longitudinal bone growth in the rat ulna by applied static and dynamic force. *Bone, 29*(2), 105-113.

Robling, A. G., Burr, D. B., & Turner, C. H. (2001). Skeletal loading in animals.

Rubin, C. T., & Lanyon, L. E. (1982). Limb mechanics as a function of speed and gait: a study of functional strains in the radius and tibia of horse and dog. *Journal of Experimental Biology, 101*(1), 187-211.

Rychlewski, J. (1984). On Hooke's law. *Journal of Applied Mathematics and Mechanics, 48*(3), 303-314.

Sengupta, P. (2013). The laboratory rat: relating its age with human's. *International journal of preventive medicine, 4*(6).

Stadelmann, V. A., Hocké, J., Verhelle, J., Forster, V., Merlini, F., Terrier, A., & Pioletti, D. P. (2009). 3D strain map of axially loaded mouse tibia: a numerical analysis validated by experimental measurements. *Computer Methods in Biomechanics and Biomedical Engineering, 12*(1), 95-100.

Sugiyama, T., Meakin, L. B., Browne, W. J., Galea, G. L., Price, J. S., & Lanyon, L. E. (2012). Bones' adaptive response to mechanical loading is essentially linear between the low strains associated with disuse and the high strains associated with the lamellar/woven bone transition. *Journal of Bone and Mineral Research, 27*(8), 1784-1793.

Sztefek, P., Vanleene, M., Olsson, R., Collinson, R., Pitsillides, A. A., & Shefelbine, S. (2010). Using digital image correlation to determine bone surface strains during loading and after adaptation of the mouse tibia. *Journal of biomechanics, 43*(4), 599-605.

Torcasio, A., Zhang, X., Duyck, J., & van Lenthe, G. H. (2012). 3D characterization of bone strains in the rat tibia loading model. *Biomechanics and modeling in mechanobiology, 11*(3-4), 403-410.

Torrance, A., Mosley, J., Suswillo, R., & Lanyon, L. (1994). Noninvasive loading of the rat ulna in vivo induces a strain-related modeling response uncomplicated by trauma or periostal pressure. *Calcified tissue international, 54*(3), 241-247.

Turner, C., Akhter, M., Raab, D., Kimmel, D., & Recker, R. (1991). A noninvasive, in vivo model for studying strain adaptive bone modeling. *Bone, 12*(2), 73-79.

Turner, C., Forwood, M., & Otter, M. (1994). Mechanotransduction in bone: do bone cells act as sensors of fluid flow? *The FASEB Journal, 8*(11), 875-878.

Turner, C. H., Forwood, M., Rho, J. Y., & Yoshikawa, T. (1994). Mechanical loading thresholds for lamellar and woven bone formation. *Journal of Bone and Mineral Research, 9*(1), 87-97.

Uthgenannt, B. A., & Silva, M. J. (2007). Use of the rat forelimb compression model to create discrete levels of bone damage in vivo. *Journal of biomechanics, 40*(2), 317-324.

van Rietbergen, B., Weinans, H., Huiskes, R., & Odgaard, A. (1995). A new method to determine trabecular bone elastic properties and loading using micromechanical finite-element models. *Journal of biomechanics, 28*(1), 69-81.

Webster, D., Wasserman, E., Ehrbar, M., Weber, F., Bab, I., & Müller, R. (2010). Mechanical loading of mouse caudal vertebrae increases trabecular and cortical bone mass-dependence on dose and genotype. *Biomechanics and modeling in mechanobiology, 9*(6), 737-747.

Webster, D., Wirth, A., van Lenthe, G., & Müller, R. (2012). Experimental and finite element analysis of the mouse caudal vertebrae loading model: prediction of cortical and trabecular bone adaptation. *Biomechanics and modeling in mechanobiology, 11*(1-2), 221-230.

Willie, B. M., Birkhold, A. I., Razi, H., Thiele, T., Aido, M., Kruck, B., . . . Duda, G. N. (2013). Diminished response to in vivo mechanical loading in trabecular and not cortical bone in adulthood of female C57Bl/6 mice coincides with a reduction in deformation to load. *Bone, 55*(2), 335-346.

Wineman, A., & Kolberg, R. (1995). Mechanical response of beams of a nonlinear viscoelastic material. *Polymer Engineering & Science, 35*(4), 345-350.

Yang, H., Butz, K. D., Duffy, D., Niebur, G. L., Nauman, E. A., & Main, R. P. (2014). Characterization of cancellous and cortical bone strain in the in vivo mouse tibial loading model using microCT-based finite element analysis. *Bone, 66*, 131-139.

Yang, H., Ma, X., & Guo, T. (2010). Some factors that affect the comparison between isotropic and orthotropic inhomogeneous finite element material models of femur. *Medical engineering & physics, 32*(6), 553-560.

Zhang, P., Tanaka, S. M., Jiang, H., Su, M., & Yokota, H. (2006). Diaphyseal bone formation in murine tibiae in response to knee loading. *Scandinavian Journal of Medicine & Science in Sports, 16*(4), 294-295.

CHAPTER 6   ARTICLE #3: HIGH IMPACT EXERCISE IMPROVES BONE MICROSTRUCTURE AND STRENGTH IN GROWING RATS

This chapter introduces the third article written in the context of this thesis and responds to the second objective of this thesis as detailed in Chapter 3.

The manuscript of this article was submitted to Scientific Reports © on 10th May 2019.

The sections of this article are structured following the format of the Scientific Reports journal.

The contribution of the first author in the preparation, obtaining the results, writing and literature review of this paper is estimated at 85%.

Contribution of all authors:

Tanvir Mustafy: Conceptualization, Data curation, Formal analysis, Investigation, Methodology, Project administration, Software, Visualization, Writing - original draft.

Irene Londono: Data curation, Resources.

Florina Moldovan: Methodology, Supervision.

Isabelle Villemure: Conceptualization, Funding acquisition, Methodology, Project administration, Resources, Supervision, Writing - review & editing.

6.1 Abstract

Physical activity is beneficial for skeletal development. However, impact sports during adolescence, leading to bone growth retardation and/or bone quality improvement, remains unexplained. This study investigated the effects of *in vivo* low (LI), medium (MI), and high (HI) impact loadings applied during puberty on bone growth, morphometry and biomechanics using a rat model. 4-week old rats (n=30) were divided into control, sham, LI, MI, and HI groups. The impact was applied on the right tibiae, 5 days/week for 8 weeks mimicking walking (450$\mu\varepsilon$), uphill running (850$\mu\varepsilon$) and jumping (1250$\mu\varepsilon$) conditions. Trabecular and cortical parameters were determined by micro-CT, bone growth rate by calcein labeling and toluidine blue staining followed by histomorphometry. Bio-mechanical properties were evaluated from bending tests. HI group reduced rat body weight and food consumption compared to shams. Bone growth rate also decreased in MI and HI groups despite developing thicker hypertrophic and proliferative zone heights. HI group showed significant increment in bone mineral density, trabecular thickness, cortical and total surface area. Ultimate load and stiffness were also increased in MI and HI groups. We conclude that impact loading during adolescence reduces bone growth moderately but improves bone quality and biomechanics at the end of the growing period.

6.2 Keywords

Rat tibia, Adolescence, Mechanical loading, Bone growth, Histomorphometry, Microcomputed tomography

6.3 Introduction

A fundamental tenet of bone biomechanics is the adaptation phenomenon of bone microstructure under regularly applied mechanical loading (Karlsson, 2004; Warden, Fuchs, Castillo, & Turner, 2005). It has been hypothesized by "Wolff's law" (Wolff, 1892) that this dynamic adaptive process, termed bone remodeling, occurs in bone mass and architecture due to stimuli obtained from its mechanical environment (Ahn & Grodzinsky, 2009; Duncan & Turner, 1995). Bones can receive stimuli in the form of mechanical loading resulting from various intensities in physical activities and sports. Ground reaction forces, which generate stresses and strains on our weight-bearing bones, are determinant factors of bone remodeling. They are greater when we move faster and/or

more intensively, hence vary according to the type of physical activities (Vainionpää et al., 2006). Low impact sports such as swimming, can produce lower ground reaction forces than high impact sports such as gymnastics or cross-country running (Mathey et al., 2002; Swissa-Sivan et al., 1989). A regular and sufficient amount of impact loading can prove to be very effective for bones at all ages (Warner, Shea, Miller, & Shaw, 2006).

Well-controlled and physiologic mechanical loading models are essential to successfully define and identify the anabolic and catabolic mechanisms involved in bone remodeling. To date, many loading models have been implemented in different animal studies, ranging from whole body rodent vibration, exercise models, and *in vivo* bone loading models such as tibial bending, ulnar and tibial axial loading (Lee, Maxwell, & Lanyon, 2002; Notomi et al., 2001; Prisby, Lafage-Proust, Malaval, Belli, & Vico, 2008; C. Turner, Akhter, Raab, Kimmel, & Recker, 1991; Wallace et al., 2007). Compared to other models, the tibial compression model has the potential to generate cortical and trabecular bone adaptation under applied mechanical load (De Souza et al., 2005; Fritton, Myers, Wright, & Van der Meulen, 2005). Axial loading in mouse tibia has been used for several years to investigate the effects of loading as a function of age (Main, Lynch, & van der Meulen, 2014; Razi et al., 2015), sex (Lynch et al., 2010), disease (Lynch et al., 2013) and strain level (Fritton et al., 2005). However, still, there is a lack of data on the loading mechanism and effects of non-invasive loading in bone formation for the rat tibial axial compression model.

Adolescence is a dynamic period for bone growth and development (Weaver, 2002). In this period, regular impact loading in sufficient amount can ensure a proper bone accrual and also contribute to building up a strong skeleton (Sievänen, 2012). It has been reported that (Deere, Sayers, Rittweger, & Tobias, 2012) performing a high impact physical activity, such as jumping, can effectively contribute to improving the hip bone strength in adolescents (Kannus et al., 1994). There are a few clinical and animal studies investigating the effects of impact loading on adolescent growth, but results are inconsistent. In some published clinical studies (Caine, Lewis, O'Connor, Howe, & Bass, 2001; Theintz, Howald, Weiss, & Sizonenko, 1993), researchers have not provided a clear, distinct separation between the nutritional and mechanical factors. The studies expressed the physical activities in hours per week whereas the intensity of the activity (repetitions, peak load, and frequency) have not been considered. As a result, it becomes challenging to infer about the isolated effect of impact loading on the growing bones from these studies. In animal studies, the effects of exercise on long bone growth are also inconsistent, resulting in either no change

(Niehoff, Kersting, Zaucke, Morlock, & Brüggemann, 2004), minimal change (Snyder, Zierath, Hawley, Sleeper, & Craig, 1992), or significant reduction (Bourrin, Genty, Palle, Gharib, & Alexandre, 1994; Forwood & Parker, 1987) in growth, measured as changes in long bone length. Hence, if any loading induced changes occur during the adolescence and whether they modify the bone microstructure are clinically relevant questions which remain still unresolved. This study aimed to use an animal model (rat tibia) to investigate the effects of well controlled *in vivo* low, medium and high impact loadings applied during puberty on bone growth, morphometry and biomechanics.

6.4 Results

6.4.1 Body Weight and Food Intake

The control and sham groups gained body weight whereas the HI group lost 13-16% of body weight compared to the shams at the end of the loading period (Figure 6.1A). Food intake was depressed by about 17-20% (Figure 6.1B) in HI group at the end of the study compared to the shams. However, no significant difference in the mean body weights and food consumption were found among the three impact groups during the loading period. A time effect (weight gain and increase in caloric consumption) was observed in rats as they were in their growing phase. A group effect was also noticed, but no effects of group/time interaction were found (Figure 6.1A, 6.1B). Also, no evidence of swelling or limb-use impairment, and no loss of hair was noticed in the animals throughout the experiment.

6.4.2 Bone Growth Rate and Tibial Length

Both HI and MI groups exhibited a reduction in proximal tibial growth rate (Figure 6.2B), resulting in 8.7% and 5.6% decrease for HI and MI groups, respectively, compared to shams (Figure 6.2B). Relative gross tibial length (value for control rats minus rats from other groups) exhibited significant differences for HI and MI groups (Figure 6.2C). No significant difference was observed between control and sham groups for both growth rates (Figure 6.2B) and relative tibial lengths (Figure 6.2C).
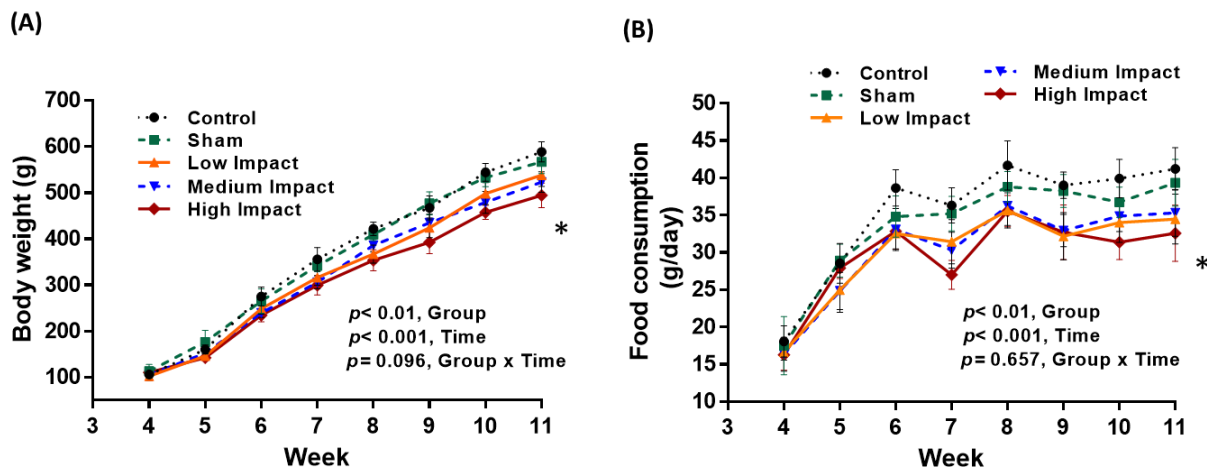
Figure 6.1 Rat body weight (g) and food consumption (g/day) during experimental period. (A) ANOVA test (general linear model) was performed to determine time effects, group effects, and their interaction on body weight. (B) ANOVA test (general linear model) was performed to determine time effects, group effects, and their interaction on food consumption

*N = 6 rats per group (mean value ± SD). *p < 0.05: significant compared to shams*

6.4.3 Growth Plate Histomorphometry

Hypertrophic (HZ) and proliferative (PZ) zone thicknesses (Figure 6.3A), as well as the number of proliferative cells per column and hypertrophic cells height (Figure 6.3B), have been evaluated for all the experimental groups. MI and HI group exhibited significantly thicker (13% and 17%, respectively) HZ thickness compared to the sham group (Figure 6.3C-I). Moreover, PZ thickness also increased in HI groups (12%) compared to shams (Figure 6.3C-II). Hypertrophic cell heights were also increased by 12% in HI group compared to the shams (Figure 6.3C-III). The number of proliferative chondrocytes per column was similar for all groups (Figure 6.3C-IV). Control vs. sham groups showed no significant difference in growth plate histomorphometric parameters (Figure 6.3C).
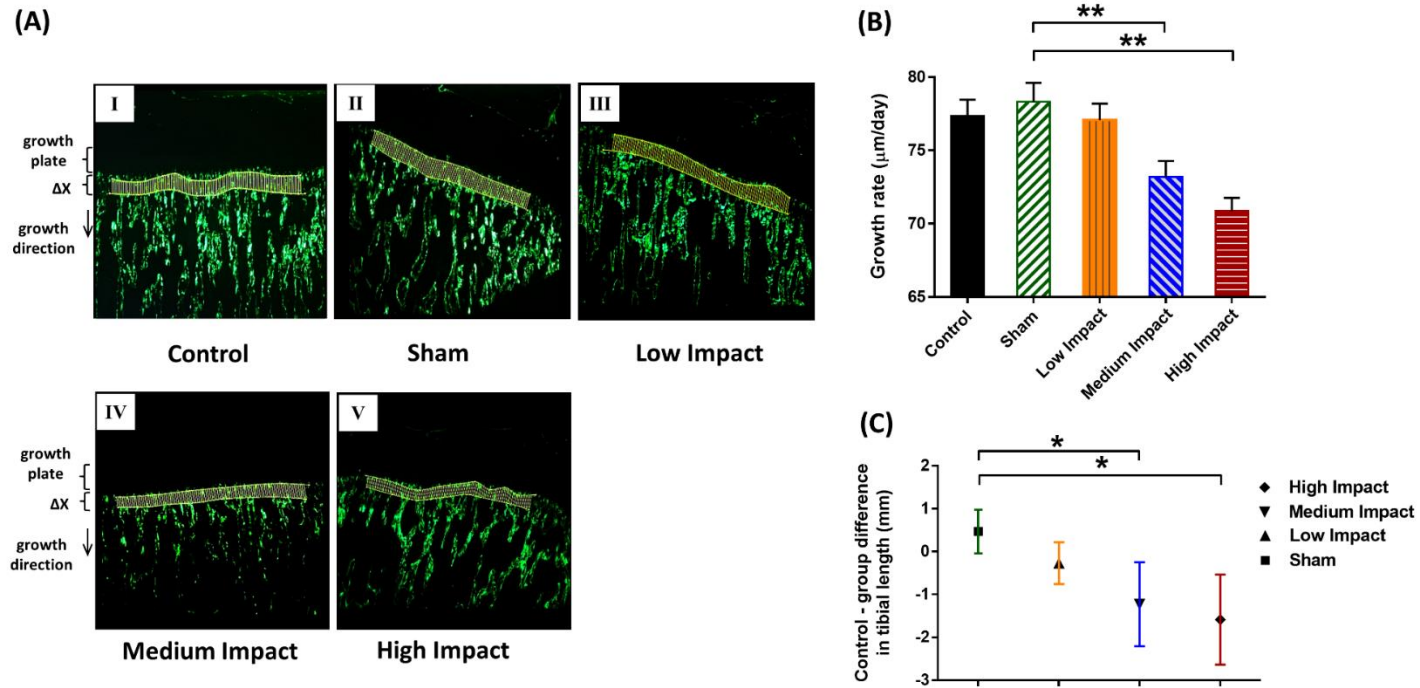
Figure 6.2 Bone growth rates (µm/day) and longitudinal tibial lengths (mm). (A) 2.5x magnified microscopic images of the tibial metaphysis labeled twice with calcein and representative images of tibiae for control, sham, LI, MI and HI groups (I-V). Bone growth (ΔX, µm) measured as the mean distance between the two calcein lines, which were modeled as splines and divided by the time interval (3 days) between the two applied injections. (B) Bone growth rates (µm/day) of rat proximal tibiae for control, sham, LI, MI and HI groups. (C) Relative (control minus individual group) gross tibial length (mm) of the tibiae. MI and HI groups exhibited approximately three and four times reduction in tibial length difference

N = 6 rats per group (mean value ± SD). *p < 0.05 and **p < 0.01: significant compared to shams
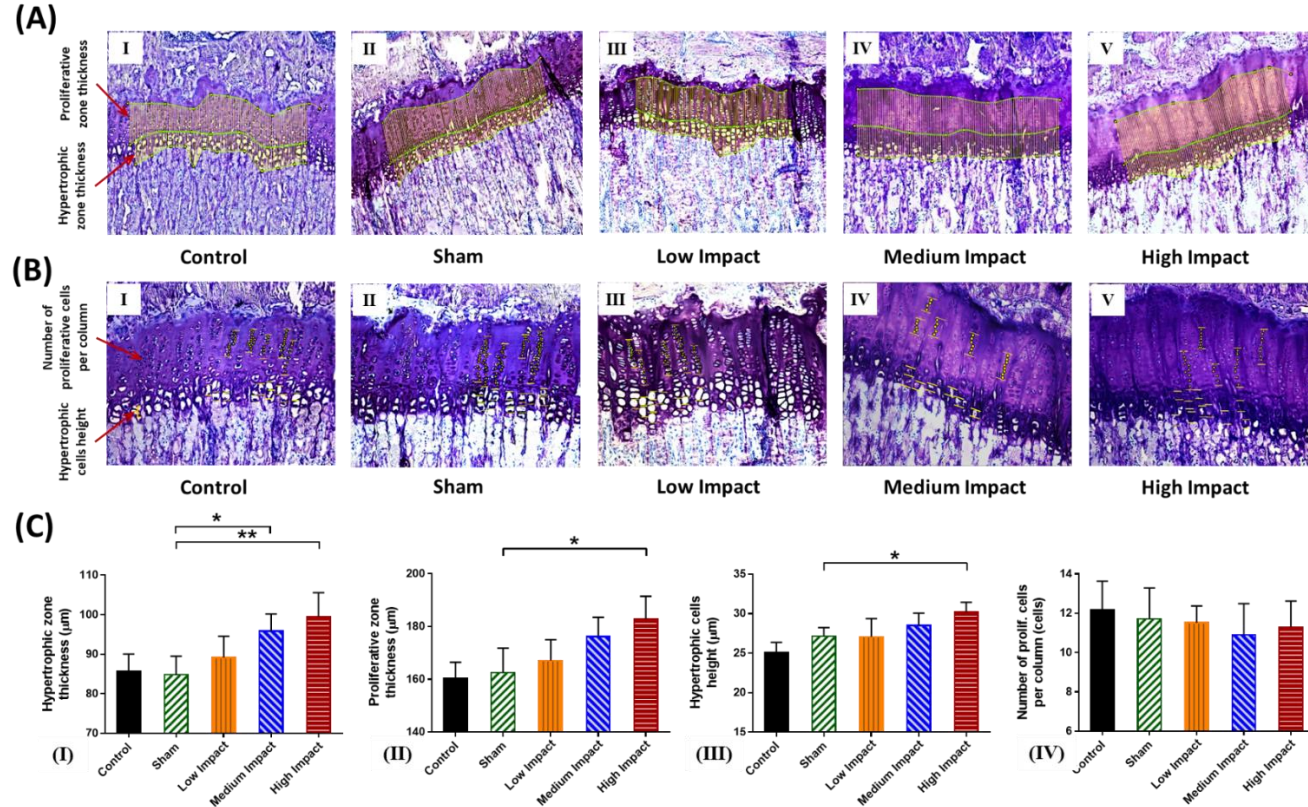
Figure 6.3 Growth plate histomorphometric parameters for control, sham, LI, MI and HI tibiae. (A) Growth plate section embedded in MMA and stained with toluidine blue (10x). Evaluation of the hypertrophic and proliferative zonal thicknesses (µm) for control, sham, LI, MI and HI groups (I-V). (B) Growth plate section embedded in MMA and stained with toluidine blue (20x). Evaluation of the hypertrophic cell height (µm) and number of proliferative cells per column (cells) for control, sham, LI, MI and HI groups (I-V). (C) Growth plate histomorphometry measurements of rat proximal tibiae for control, sham, LI, MI and HI groups (I-V)

*N = 6 rats per group (mean value ± SD). *p < 0.05 and **p < 0.01: significant compared to sham*

6.4.4 Trabecular and Cortical Bone Architecture

The effects of impact loading exercise on bone microstructure were assessed by comparing the impact groups with the shams after 4 and 8 weeks of repeated loading regime. For trabecular bone, the HI group showed an increase in BV/TV and a decrease in Tb.Sp (Table 6.1) after 4 weeks of loading. For cortical bone, Ct.Ar was increased in HI group at this time point (Table 6.2). After 8 weeks of loading, a significant increase was found in BMD and Tb.Th for both HI and MI groups (Table 6.1). However, only HI group showed a significant increment in BV/TV and a significant decrement in Tb.Sp at this time point (Table 6.1). For the cortical bone architecture, both HI and MI exhibited an increased Ps.Pm and Ct.Ar and a decreased Ec.Pm (Table 6.2) after 8 weeks. However, only HI group showed an increased Tt.Ar and Ct.Th and a decreased Ma.Ar at this time point (Table 6.2).

6.4.5 Tibial Mechanical Properties

From three-point bending tests, significant differences were found among the groups for some structural and intrinsic mechanical properties (Table 6.3). The mean ultimate load, as well as the mean ultimate stress were found higher in the MI and HI groups compared to the sham animals (Table 6.3). Energy to failure load and stiffness were also increased in MI and HI groups compared to shams (Table 6.3). Finally, failure stress was found to be significantly lower in the MI and HI groups compared to the sham group (Table 6.3).

Table 6.1 ANOVA test with Tukey's multiple comparisons for the trabecular microarchitecture of the right proximal tibial metaphysis in control, sham, LI, MI and HI groups of rats after 4 weeks and 8 weeks of loading regime.

Parameters/Groups	Control	Sham	L.I.	M.I.	H.I.
4 weeks of loading					
BMD (g.cm^{-3})	0.19 ± 0.01	0.18 ± 0.01	0.19 ± 0.02	0.19 ± 0.02	0.22 ± 0.02
BV/TV (%) *	21.7 ± 3.11	21.2 ± 1.13	22.1 ± 2.83	22.8 ± 2.19	**23.9 ± 1.26^{α}**
Tb.Th (mm)	0.08 ± 0.01	0.08 ± 0.02	0.09 ± 0.01	0.09 ± 0.02	0.09 ± 0.01
Tb.N (mm^{-1})	2.37 ± 0.11	2.32 ± 0.12	2.56 ± 0.12	2.44 ± 0.09	2.43 ± 0.09
Tb.Sp (mm) *	0.79 ± 0.09	0.77 ± 0.13	0.75 ± 0.13	0.76 ± 0.12	**0.71 ± 0.11^{α}**
Conn.Dn (mm^{-3})	174 ± 30.1	169 ± 33.1	175 ± 33.2	170 ± 36.3	162 ± 36.3
8 weeks of loading					
BMD (g.cm^{-3}) *	0.22 ± 0.01	0.23 ± 0.01	0.24 ± 0.01	**0.25 ± 0.01^{α}**	**0.27 ± 0.01^{α}**
BV/TV (%) *	23.7 ± 2.79	23.3 ± 3.12	24.3 ± 1.75	26.9 ± 1.69	**28.7 ± 2.55^{α}**
Tb.Th (mm) *	0.09 ± 0.01	0.09 ± 0.01	0.10 ± 0.02	**0.11 ± 0.01^{α}**	**0.11 ± 0.02^{α}**
Tb.N (mm^{-1})	2.92 ± 0.15	2.81 ± 0.15	3.15 ± 0.17	3.05 ± 0.09	2.98 ± 0.08
Tb.Sp (mm) *	0.78 ± 0.07	0.77 ± 0.06	0.66 ± 0.07	0.69 ± 0.07	**0.59 ± 0.05^{α}**
Conn.Dn (mm^{-3})	157 ± 22.3	161 ± 22.1	159 ± 25.9	156 ± 27.3	149 ± 28.3

Values are expressed as Mean ± SD, N = 6/group. In the parameter column, * indicates a significant effect ($p < 0.05$) from a one-way ANOVA with Tukey's multiple comparisons test. When there was a significant effect, Tukey's post-hoc pairwise comparisons evaluated whether the sham group was significantly different compared to the other groups [a bold value and 'α' indicate a significant difference versus sham group]. Abbreviations: BMD, bone mineral density; BV/TV, bone volume fraction; Tb.Th, trabecular thickness; Tb.N, trabecular number; Tb.Sp, trabecular spacing; Conn.Dn, connectivity density.

Table 6.2 ANOVA test with Tukey's multiple comparisons for the cortical microarchitecture of the right tibial mid-diaphysis in control, sham, LI, MI and HI groups of rats after 4 weeks and 8 weeks of loading regime.

Parameters/Groups	Control	Sham	L.I.	M.I.	H.I.
4 weeks of loading					
TMD (gm.cm^{-3})	0.87 ± 0.06	0.96 ± 0.06	0.91 ± 0.05	1.05 ± 0.08	1.08 ± 0.08
Tt.Ar (mm^2)	5.73 ± 0.97	5.84 ± 1.05	5.89 ± 0.88	6.12 ± 1.17	6.14 ± 0.98
Ct.Ar (mm^2) *	4.26 ± 0.61	4.12 ± 0.51	4.32 ± 0.59	4.89 ± 0.72	**5.41 ± 0.72$^\alpha$**
Ct.Th (mm)	0.51 ± 0.02	0.54 ± 0.02	0.54 ± 0.02	0.58 ± 0.02	0.62 ± 0.02
Ps.Pm (mm)	9.56 ± 0.37	9.12 ± 0.47	9.72 ± 0.71	9.94 ± 0.59	10.1 ± 0.51
Ec.Pm (mm)	4.73 ± 0.44	4.82 ± 0.33	4.93 ± 0.33	4.95 ± 0.47	4.75 ± 0.22
Ma.Ar (mm^2)	1.62 ± 0.05	1.73 ± 0.06	1.62 ± 0.06	1.71 ± 0.08	1.69 ± 0.07
Ecc	0.63 ± 0.03	0.63 ± 0.03	0.61 ± 0.06	0.64 ± 0.05	0.63 ± 0.04
8 weeks of loading					
TMD (gm.cm^{-3})	1.08 ± 0.08	1.04 ± 0.09	1.09 ± 0.07	1.15 ± 0.09	1.18 ± 0.09
Tt.Ar (mm^2) *	8.17 ± 1.11	7.92 ± 0.93	8.33 ± 1.03	8.89 ± 0.94	**9.24 ± 1.03$^\alpha$**
Ct.Ar (mm^2) *	6.12 ± 0.83	6.33 ± 0.88	6.23 ± 0.72	**7.38 ± 0.79$^\alpha$**	**7.83 ± 0.82$^\alpha$**
Ct.Th (mm) *	0.66 ± 0.02	0.62 ± 0.03	0.63 ± 0.02	0.67 ± 0.02	**0.69 ± 0.02$^\alpha$**
Ps.Pm (mm) *	13.5 ± 0.47	13.8 ± 0.62	13.2 ± 0.57	**14.9 ± 0.61$^\alpha$**	**15.5 ± 0.67$^\alpha$**
Ec.Pm (mm) *	6.43 ± 0.49	6.72 ± 0.48	6.34 ± 0.43	**5.94 ± 0.42$^\alpha$**	**5.83 ± 0.42$^\alpha$**
Ma.Ar (mm^2) *	1.92 ± 0.07	1.85 ± 0.08	1.83 ± 0.07	1.78 ± 0.09	**1.73 ± 0.09$^\alpha$**
Ecc	0.78 ± 0.02	0.79 ± 0.04	0.79 ± 0.04	0.81 ± 0.04	0.78 ± 0.05

Values are expressed as Mean ± SD, N = 6/group. In the parameter column, * indicates a significant effect ($p < 0.05$) from a one-way ANOVA with Tukey's multiple comparisons test. When there was a significant effect, Tukey's post-hoc pairwise comparisons evaluated whether the sham group was significantly different compared to the other groups [a bold value and 'α' indicate a significant difference versus sham group]. Abbreviations: TMD, tissue mineral density; Tt.Ar, cross-sectional area inside the periosteal envelope; Ct.Ar, cortical bone area; Ct.Th, cortical thickness; Ps.Pm, periosteum perimeter; Ec.Pm, endocortical perimeter; Ma.Ar, medullary area; Ecc, mean eccentricity.

Table 6.3 ANOVA test with Tukey's multiple comparisons for structural and intrinsic mechanical properties of the right tibiae from control, sham, LI, MI and HI groups of rats derived from three-point bending tests of the mid-diaphysis.

Parameters/Groups	Control	Sham	L.I.	M.I.	H.I.
Structural mechanical properties					
Ultimate load, F_{ult} (N) *	84.9 ± 13.3	80.1 ± 11.2	89.4 ± 9.22	**93.5 ± 7.43$^{\alpha}$**	**97.0 ± 8.16$^{\alpha}$**
Failure load, F_{fail} (N)	73.8 ± 11.6	67.3 ± 10.3	65.3 ± 10.6	63.4 ± 9.44	64.6 ± 9.82
Stiffness, k (N/mm) *	123 ± 18.7	113 ± 16.8	124 ± 15.8	**135 ± 17.6$^{\alpha}$**	**142 ± 15.8$^{\alpha}$**
Energy to ultimate load (mJ)	39.3 ± 5.7	35.3 ± 6.11	41.4 ± 6.82	42.2 ± 7.03	44.5 ± 7.26
Energy to failure load (mJ) *	55.2 ± 17.3	63.5 ± 15.2	77.6 ± 18.4	**81.7 ± 14.8$^{\alpha}$**	**79.8 ± 18.9$^{\alpha}$**
Intrinsic mechanical properties					
Ultimate stress, σ_{ult} (MPa) *	294 ± 44.5	286 ± 37.2	308 ± 52.1	**319 ± 49.2$^{\alpha}$**	**316 ± 38.2$^{\alpha}$**
Failure stress, σ_{fail} (MPa) *	223 ± 36.2	216 ± 21.2	187 ± 30.3	**184 ± 26.2$^{\alpha}$**	**186 ± 22.4$^{\alpha}$**
Young's modulus, E (GPa)	10.9 ± 1.22	10.5 ± 1.46	11.2 ± 1.31	11.8 ± 1.01	12.3 ± 1.06
Energy to ultimate stress (mJ/mm^3)	3.46 ± 1.11	2.71 ± 0.82	2.56 ± 0.96	2.89 ± 1.21	2.95 ± 0.85
Energy to failure stress (mJ/mm^3)	8.37 ± 3.46	11.4 ± 4.17	11.7 ± 4.61	12.2 ± 3.19	11.9 ± 4.89

Values are expressed as Mean ± SD, N = 6/group. In the parameter column, * indicates a significant effect ($p < 0.05$) from a one-way ANOVA with Tukey's multiple comparisons test. When there was a significant effect, Tukey's post-hoc pairwise comparisons evaluated whether the sham group was significantly different compared to the other groups [a bold value and 'α' indicate a significant difference versus sham group].

6.5 Discussion

In this study, the effects of eight weeks controlled impact loading during the adolescence on bone growth, quality and mechanics have been investigated using a rat tibial compression loading model. Our findings could be used as a basis for future investigation on the impact loading effects during the adolescence for finding a suitable loading protocol which would be beneficial for the overall bone microstructure during the growing period.

6.5.1 High impact loading triggers decreased body weight coupled with a reduced caloric consumption

Body weight was maximum for the control group followed by the shams and other impact groups at the end of the loading period (Figure 6.1A). The body weight in HI group was decreased significantly compared to shams after 8 weeks of loading regime (Figure 6.1A). Interestingly, food consumption was simultaneously reduced for the same group (HI) at the end of the study (Figure 6.1B). The food consumption is generally dependent on the energy expenditure and so is the change in body weight (T. Huang et al., 2003). Our findings showed that the HI group has less body weight and reduced food intake despite receiving the maximum intensity of the exercise regime. Part of this weight loss could be ascribed to the decreased appetite of the impact groups (Pitts & Bull, 1977), which was evidenced by a significantly lower caloric intake for the HI group (Figure 6.1B). Another intriguing fact was the transitory fatigue of the exercised rats. We observed reduced activity limited to less than seven minutes after the forced loading regime. The rats continued their regular cage activity shortly after this phenomenon. It is suggested that the forced exercise can influence the levels of stress hormones and behavior of the animals which may lead to a reduction in caloric intake in the rats (Rosenbaum, Hirsch, Murphy, & Leibel, 2000; Russek & Pina, 1962).

Our findings are supportive of other studies on adult animal models. Reduced body weight has been reported in trained animals by Jones et al. (Jones et al., 1964) and Huang et al. (T. Huang et al., 2003), after 15 and 8 weeks of exercise period in adult rats, respectively. Moreover, simultaneously reduced body weight and reduced caloric consumption have been reported for adult running rats by Crew et al. (Crews 3rd, Fuge, Oscai, Holloszy, & Shank, 1969), and treadmill exercised in post pubertal rats by Tisuji et al. (TSUJI, KATAYAMA, & KOISHI, 1975) and by Pitts and Bull (Pitts & Bull, 1977).

6.5.2 Medium and high impact loadings decrease longitudinal bone growth despite developing thicker HZ and PZ heights

Both MI and HI groups showed reduced bone growth rates at the proximal metaphysis compared to shams after 8 weeks of loading (Figure 6.2B). This phenomenon eventually resulted in significant longitudinal growth retardation for the same two groups (Figure 6.2C). Some noticeable histomorphometric changes were also concomitant along with this growth retardation. These changes include increased hypertrophic and proliferative zone thicknesses and hypertrophic cell heights (Figure 6.3C).

The relationship between applied compression and longitudinal bone growth rate proposed by Hueter-Volkmann law states that increased compression reduces bone growth rate whereas reduced compression increases it (Cancel, Grimard, Thuillard-Crisinel, Moldovan, & Villemure, 2009; Stokes, 2002). Moreover, large compressive loads can lead to retardation of bone growth or even cease completely the bone growth (Cancel et al., 2009; Ménard et al., 2014; Valteau, Grimard, Londono, Moldovan, & Villemure, 2011; Villemure & Stokes, 2009). Our findings are also consistent with other studies (Mosley, March, Lynch, & Lanyon, 1997; Ohashi, Robling, Burr, & Turner, 2002; Robling, Duijvelaar, Geevers, Ohashi, & Turner, 2001), where rat ulna longitudinal growth was decreased by compressive loading in adolescence.

Bone growth rate is generally correlated to the overall growth plate thickness (Swissa-Sivan et al., 1989; Walker & Kember, 1972). Moreover, it is considered to be linearly correlated with the PZ (T. Huang et al., 2003; Swissa-Sivan et al., 1989) and HZ (Kember & Walker, 1971; Niehoff et al., 2004) thickness. Hence, the thicker HZ and PZ heights of the MI and HI group were expected to result in elongated bone length. Conversely, bone growth in MI and HI group was depressed even after thickening of growth plates. Previous studies have also reported thicker growth plates under excessive loadings. However, these studies related this phenomenon with dyschondroplasia (osteochondrosis) (Duff, 1986; Robling et al., 2001). Osteochondroses are considered to be disorders of primary and secondary growth centers, or lesions at the apophyseal or epiphyseal growth areas of bones (Orava & Virtanen, 1982). Active young athletes are prone to osteochondroses (Orava & Virtanen, 1982), although it is not considered to be a permanent disability for diagnosed patients (Jürgensen, Bachmann, Haas, & Schleicher, 1998). In most cases, conservative treatment for such symptoms includes sufficiently long rest (Orava & Virtanen,

1982). In one form of such condition known as Scheuermann's disease (Bürge, Dolanc, Jenny, & Morscher, 1980), regular physical exercises are even recommended. In our study, the rats have been sacrificed immediately after the repeated loading regime. So, it remains unclear whether a sufficient amount of unloading period would affect the growth plate thickness and change it accordingly or not.

Moreover, the contradictory findings between bone growth rate and growth plate thickness can also be explained from the effect of loading on bone metabolism process. Bone metabolism in growing bones occurs through the processes of endochondral and intramembranous ossification (Shahi, Peymani, & Sahmani, 2017). It is possible that MI and HI loadings triggered an accelerated calcification in the primary spongiosa compared to chondrocyte activity rates, which are responsible for bone growth (Farnum & Wilsman, 2001; Hasan et al., 2018). Our overall findings indicate that the generalized claim of the linear relationship between bone growth and growth plate height (Krember, 1972; Swissa-Sivan et al., 1989) might not always be implemented. However, our findings are supportive of other studies (Ohashi et al., 2002; Robling et al., 2001; Swissa-Sivan et al., 1989), where a contrary relationship between the growth rate and height of the growth plate was also observed.

6.5.3 Changes in trabecular bone microstructure are time as well as impact level dependent

Compared to the MI group, the HI group showed load adaptive changes in trabecular microstructure at an earlier (after 4 weeks) period and affecting more structural parameters (Table 6.1). BMD was significantly increased in both MI and HI groups (Table 6.1) at the end of loading period. For healthy bone structure, bone mineral content shows an increasing trend during the adolescent period (Banu, Wang, & Kalu, 2002). Also, higher loading intensity is generally associated with an increased BMD (Chilibeck, Sale, & Webber, 1995). In fact, BMD in athletes is elevated under high impact training conditions (Slemenda & Johnston, 1993). The increase of BMD in our study could be related to hormones triggering mechanisms. Indeed, an increased BMD is controlled by a decreased parathyroid hormone response coupled with an increased calcitonin response (Bouassida et al., 2006; Drinkwater et al., 1984), both of which take time to react under favorable loading conditions. Hence, this could explain the significant increment of BMD assessed after 8 weeks instead of 4 weeks of loading. In similar studies, where adult rats have been tested

for repetitive jumping exercise (Ooi, Tavafzadeh, Hung, Hung, & He, 2014) or treadmill running exercise (Hagihara et al., 2005), an increased BMD was observed in the loaded limbs.

The BV/TV was also found to significantly increase in the exercised tibiae both after 4 and 8 weeks of loading in the HI group. For a healthy growing bone, an elevated BV/TV is generally correlated with an increased BMD (Jiang, Jiang, & Dai, 2007), as found in this study. The significant BV/TV in HI group after 8 weeks of loading can be explained with the increased BMD for the same group (Table 6.1). However, the significant increase after 4 weeks of exercise (without simultaneous BMD increase) could be related to triggering of bone metabolism under high impact loading (Slemenda & Johnston, 1993). Indeed, it has been reported that under controlled loading scenarios, the trabecular structure responds positively through diffusion and active transport of metabolites within the entire microstructure (Banu et al., 2002). So, it could be possible that HI loading has accelerated the diffusion and transportation process of the metabolites at an earlier stage and thus elevated the BV/TV in the exercised limb accordingly. Other studies support our findings in growing rats, where swimming exercise was found to significantly increase BV/TV (Kang, Kim, & Kim, 2017; Oh, Tanaka, Naka, & Igawa, 2016). Also, another study reported a greater BV/TV in the growing rat tibiae after 8-weeks of free fall exercise routine (Welch, Turner, Devareddy, Arjmandi, & Weaver, 2008). The observed increment in Tb.Th during the loading period is a part of normal bone development (Lu, Cui, Zuo, Lin, & Wu, 2015). However, a significant increment in the loaded limbs (compared to shams) indicated an additional improvement in trabecular structure under impact loading conditions. The significant reduction in Tb.Sp is often considered as the concomitant increase with BV/TV and Tb.Th (Kirmani et al., 2009). The significant reduction in Tb.Sp indicates the occurrence of a loading induced bone gain through increased connectivity and gradual thickening of the trabecular structure (Peng et al., 2014). The significant change in Tb.Sp in HI group at an earlier stage can be associated with the significant increase in BV/TV from the same group (Table 6.1). Our data are supportive of previous findings where an increased Tb.Th was reported in the loaded tibiae of 10-week old adult mice (Berman, Clauser, Wunderlin, Hammond, & Wallace, 2015), as well as with a decreased Tb.Sp reported in loaded tibiae of both growing and adult mice (De Souza et al., 2005).

6.5.4 Medium and high impact loadings benefit the cortical bone morphometry in the diaphysis, leading to significantly improved structural- and tissue-level bending mechanical properties

MI and HI loadings significantly affected tibial diaphysis, modifying both its cortical microstructure and its mechanical properties (Tables 6.2 and 6.3). Indeed, stiffness was significantly increased in these groups compared to the sham group (Table 6.3). This improved stiffness eventually triggered the bones to reach a significantly higher ultimate load (Table 6.3). Interestingly, MI and HI groups exhibited significantly increased cortical area, simultaneously coupled with periosteal perimeter expansion and endocortical perimeter reduction (Table 6.2) after 8 weeks of loading regime. The medullary area (Ma.Ar) in the HI group also decreased significantly (Table 6.2). Cortical bone area at the mid-diaphysis and the corresponding ultimate load (F_{ult}) are highly correlated to each other (Stürmer et al., 2006; X. Yang, Chan, Muthukumaran, & Lee, 2010). Hence, the increased ultimate loads for MI and HI groups can be justified from their significantly increased cortical area. Our findings agree with other studies on adult rodents, where an increased ultimate strength have been associated with exercised tibiae in 15 and 10 week old rats (T. Huang et al., 2003) and mice (Berman et al., 2015), respectively. Bone stiffness can be related to its morphology and cross-sectional geometry in growing rats (Main, Lynch, & van der Meulen, 2010). More specifically, stiffness can be associated with the increase or decrease in cortical thickness (Ct.Th), total area (Tt.Ar) and cortical area (Ct.Ar) (Schlecht, Bigelow, & Jepsen, 2014; Voide, van Lenthe, & Müller, 2008). Ct.Ar has been increased significantly for both MI and HI groups (Table 6.2). Also, Ct.Th and Tt.Ar significantly increased for the HI group (Table 6.2). Hence, a strengthened diaphysis associated with an increased stiffness can be justifiable for the MI and HI groups. Increased ultimate load and stiffness was also observed in a study (T. Huang et al., 2003) of 15-week old swimming and running rat groups along with an increased cortical area in the swimming groups. Another study with 10 week old mice reported an increased cortical thickness and stiffness, along with the cortical and total area increment in the loaded limbs (Berman et al., 2015).

No effects were found on Young's modulus when comparing LI, MI and HI loadings to shams (Table 6.3). Young's modulus or bone rigidity is an intrinsic mechanical property of the bone (Mustafy, Arnoux, et al., 2018). With the greater structural strength found in the MI and HI groups

(Table 6.3), an increase was also expected in the Young's modulus. In a bending test, the evaluation of rigidity depends linearly on stiffness and cubicly on the span length of the tibiae (Equation 2) (Schriefer et al., 2005). In the MI and HI groups, tibial lengths decreased by 4% and 5%, respectively. Even though their stiffnesses increased, the decreased span lengths in the cubic form might have counteracted this change, yielding unchanged Young's moduli. Another study also reported non-significant changes in Young's modulus in growing mice limbs (Berman et al., 2015) undergoing 2 weeks of axial loading regime generating a maximum 2400 $\mu\varepsilon$ at the mid-diaphysis of the tibiae.

Energy to failure load increased significantly for the MI and HI groups (Table 6.3). Greater energy to failure loads implies that the MI and HI tibiae sustained more deformation or strain before failure. Strengthening of bone tissue in the MI and HI groups is associated with its adaptation in response to the applied loading regime. During the loading period, compositional alterations might have occurred within the newly forming and pre-existing bone cellular matrix (Morris & Mandair, 2011), possibly involving type I collagen, which is known to affect the post-yield behavior of the bone (Burr, 2002; Viguet-Carrin, Garnero, & Delmas, 2006). Biochemical changes might have also interfered with collagen fibers orientation within the bone matrix and thus altered the toughening-mechanism in the bone microstructure (Wang, Shen, Li, & Agrawal, 2002). Ultimate stress (σ_{ult}) and failure stress (σ_{fail}) are significantly increased and decreased respectively in both MI and HI groups (Table 6.3). The ultimate/failure load is the controlling factor in the corresponding ultimate/failure stress for the same group of tibiae (Equation 3) (T. Huang et al., 2003; Mustafy, Londono, & Villemure, 2018). The respective significant increase and decrease in F_{ult} and F_{fail} for the MI and HI groups can explain the significant change in σ_{ult} and σ_{fail} for the same groups. Our results agree with other studies, where 15-week old rats exhibited increased stress and failure loads in the trained limbs (T.-H. Huang et al., 2010; T. Huang et al., 2003). Moreover, studies using 8-week old mice also observed increased ultimate stress in the loaded limbs after 2 weeks of axial loading regime (Berman et al., 2015).

6.5.5 Limitations

The current study has limitations involving some methodological aspects. For the trabecular VOI, only the proximal metaphysis was analyzed. It was chosen over the distal section because of the large amount of trabeculae in this region. Also, it has been reported that the proximal tibia has

greater bone volume compared to the distal tibia (Saers, Cazorla-Bak, Shaw, Stock, & Ryan, 2016) and has also been used more often in bone remodeling studies (Berman et al., 2015; Fritton et al., 2005; Lynch et al., 2010). As for bone growth rate, it was only measured at the proximal site. This choice was justified as proximal metaphysis is responsible for blood supply and vascular stasis in growing bone and the contribution of the proximal tibial growth plate in the total longitudinal growth was found to reach approximately 80% in adolescents (Pritchett, 1992). So, any loading effects on proximal bony region could presumably be considered as to have the main effects between the proximal and distal parts as well. Also, the biological effects of bone remodeling were not investigated as part of this study. A future study could investigate bio-markers to infer on bone formation and resorption for better understanding of bone growth mechanism involved in impact loading regimes. Moreover, rats were sacrificed immediately after the last *in vivo* loading regime at 81 days old. A detraining period before the sacrifice, which might have modified the growth plate histomorphometry (Ohashi et al., 2002; Spengler, Morey, Carter, Turner, & Baylink, 1983), was not evaluated as our primary objective was to investigate the bone growth rate and histomorphometry while the growth plate was still active (Hansson, Menander-Sellman, Stenström, & Thorngren, 1972; Mustafy, Benoit, Londono, Moldovan, & Villemure, 2018).

6.6 Conclusion

A significant decrease in body weight associated with a reduction in food intake was found for the high impact group. A thicker growth plate was observed for medium and high impact group despite having a significant longitudinal growth retardation. Also, the medium and high impact groups benefitted the trabecular and cortical microstructure and led to significant changes in structural- and tissue-level mechanical behavior in the diaphysis. The low impact group also altered bone structure, by exhibiting an increasing or decreasing trend in certain bone microstructural properties, but these changes were not statistically significant. In summary, a brief (10 min) daily exercise of medium (850 µε) and high (1250 µε) impact physical activity during adolescence can influence bone growth, and improve the quality and mechanics of bone microstructure at the end of the growing period. This loading model provides the scope to fully understand the role of controlled mechanical loading during the adolescent period and will be used in future for the design of non-invasive loading models to modify the bone microstructure and mechanical strength for building

up a healthy and robust skeleton. Future work will investigate whether these impact loads applied during puberty are determinant factors for bone quality and strength in adult life.

6.7 Materials and methods

6.7.1 Animals

Animals (n=30, male, Sprague-Dawley rats) were obtained from Charles River Laboratories (Montreal, Canada) at approximately 3 weeks of age and allowed to acclimate for one week before the start of *in vivo* loading. Animal care and use conformed to the guidelines of the Canadian Council on Animal Care (CCAC), and the Institutional Animal Care Committee approved the experimental protocol at the Sainte-Justine University Hospital, Montreal, Canada. Rats were housed two per cage at 25°C with a 12-h light/dark cycle. Standard laboratory diet and water ad libitum were provided. Three days prior to the beginning of loading, rats were randomly divided into five groups (n=6/group): control, sham, low impact (LI), medium impact (MI), and high impact (HI). Body weights and food intakes were monitored weekly from the beginning (4th week) of *in vivo* loading until the end (11th week) to monitor overall health.

6.7.2 *In vivo* Axial Tibial Loading

While the rats of the LI, MI, and HI groups were kept anesthetized (2% isoflurane, 1.0 L/min O_2), the cyclic impact loading was applied to the right tibia with a custom-built impact loading device (Figure 6.4A). The device was controlled using a Mach-1 V500C (Biomomentum Inc., Montreal, Canada). Haversine waveform displacements (Mustafy, Londono, & Villemure, 2019) (derived from the calibration experiment) were applied at 2Hz and characterized by symmetric active loading/unloading with a 0.10 sec of rest insertion between load cycles (Cullen, Smith, & Akhter, 2001; Mosley et al., 1997) (Figure 6.4B). The frequency of 2Hz was selected as it matches with the stride frequency range observed in rat normal locomotion (Mosley et al., 1997). A compressive preload of 0.5 N was applied to keep the tibia in position. Loadings were repeated for 1200 cycles, yielding a daily (5 days/week) loading period of 10 min (Fritton et al., 2005) (Figure 6.4B). Sham rats received the same experimental setup conditions without any load application. Controls were kept in the cages without any manipulation. Regular cage activity was allowed between loading sessions.
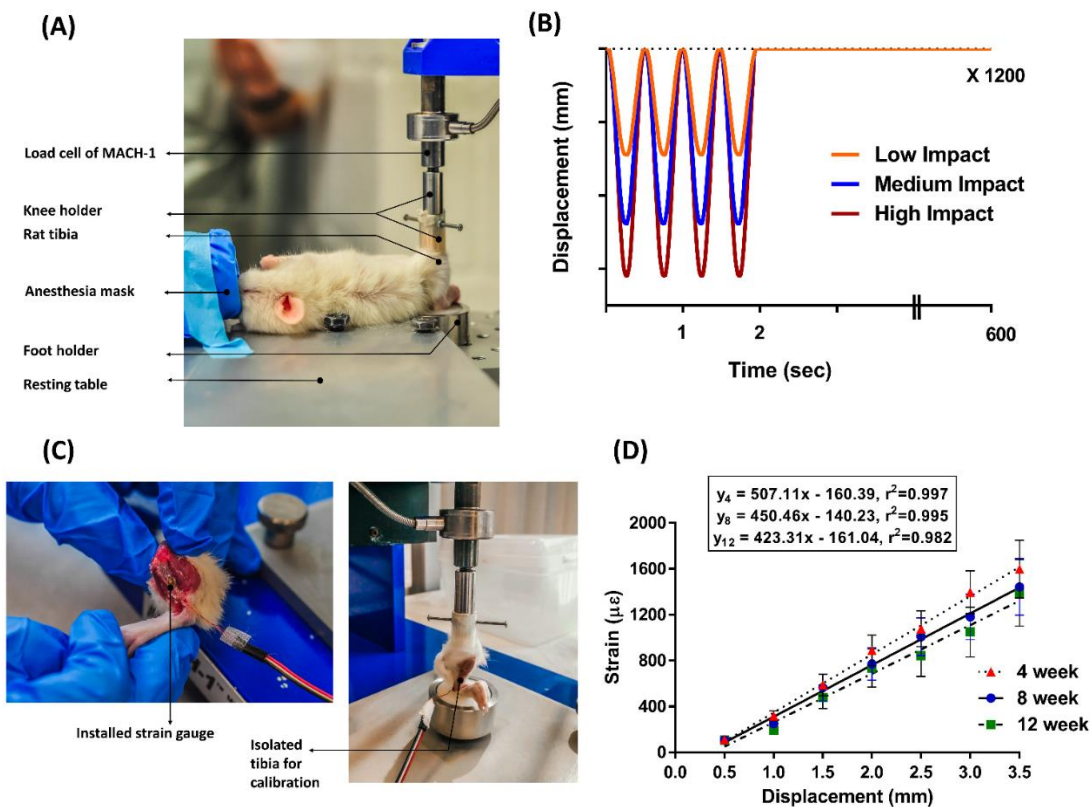
Figure 6.4 Impact loading setup and strain gauge calibration. (A) With the rats under anesthesia, the right tibiae from LI, MI and HI groups were loaded using a waveform generating 450, 850, and 1250 με at the medio-proximal tibial surface from the 4 to 11 week period. (B) The loading profile consisted of haversine waveform displacements at 2Hz and characterized by symmetric loading/unloading with a 0.10 sec of rest insertion between loading cycles. Loadings were repeated for 1200 cycles, yielding a daily (5 days/week) loading period of 10 minutes. (C) Strain gauge positioned at the medio-proximal surface of the tibia for allowing strain assessment for 0.5 mm to 3.5 mm of displacement. (D) Linear relationship between applied displacement and resulting strain at the medio-proximal surface of 4, 8 and 12 week old rat tibiae (mean value ± SD) (N = 6 rats/group)

6.7.3 Strain Calibrated Impact Loading

Prior to implementing the loading experiments, impact parameters were strain calibrated. The relationship between applied displacement and bone tissue deformation for the right tibia was

established in an *in vivo* compression-strain calibration experiment (Mustafy et al., 2019) for the 4, 8 and 12-week old rats. This relationship was adapted for determining the required displacement to generate 450, 850, and 1250 µε at the medio proximal surface of the rat tibia (Burr et al., 1996; Lanyon, Hampson, Goodship, & Shah, 1975; Milgrom et al., 2002; P. Yang, Bruggemann, & Rittweger, 2011). These strain magnitudes were chosen to correspond to peak strain values in the human tibia during unrestricted walking (450 µε), zig-zag uphill running (850 µε), and vertical jumping (1250 µε) conditions (Burr et al., 1996; Lanyon et al., 1975; Milgrom et al., 2002; P. Yang et al., 2011). Animals (n=18, male, Sprague-Dawley rats) were obtained from Charles River Laboratories (Montreal, Canada) at approximately 3, 7 and 11 weeks of age (n=6/age group) and allowed to acclimate for one week before the strain calibration experiment. After CO_2 asphyxiation, followed by decapitation, right tibiae were collected for each age group of rats. Tibiae were isolated from the middle of the femur to the toes. After tibial collection, an incision was made near the medio proximal surface of the tibia. Overlying skin and muscles were retracted to expose the bonding surface, polished with an abrasive paper and cleaned with ethanol solution. A single element strain gauge (C2A-06–015LW-120; dimensions: 0.86mm × 1.32mm, Micro-Measurements Group, Raleigh, NC, USA) was bonded with cyanoacrylate (M-Bond 200; Micro-Measurements Group) at 35% of the tibial length (L) (Figure 6.4C). A compressive preload of 0.5 N was applied to keep the tibia in position (Figure 6.4C). Haversine waveform displacements were applied at 2Hz with a 0.10-sec rest insertion between displacement cycles. Displacements ranging from 0.5 mm to 3.5 mm were applied with a 0.50 mm increment. The strain data were recorded simultaneously at 2.5 kHz with a PC via Labview software (Labview 8.6, NI) through the quarter-bridge completion and analog input modules. Applied displacement and resulting strain were also recorded simultaneously. Displacement versus strain curves was plotted for three age groups, and a linear fit was applied to obtain the compression-strain relationships (Figure 6.4D). Using these calibration curves, the amount of axial displacements were determined for producing the target tensile strain (450, 850, and 1250 µε) in LI, MI, and HI group of rat tibiae, respectively. The axial displacement values for the week's in-between the chosen calibration studies were adjusted by linear interpolation using the two known displacement values and the weekly-age of rats.

6.7.4 Micro Computed Tomography (micro-CT)

6.7.4.1 Weekly scanning regime

A micro-CT scanner was used to perform eight weekly CT scans of the right tibia of the rats, from 4 to 11 weeks of age. The imaging system was a Skyscan 1176 *in-vivo* micro-CT (Skyscan, N.V., Belgium) scanner with rotatable X-ray source and detector. Following the weekly loading regime, rats were anesthetized (2% isoflurane, 1.0 L/min O_2), positioned on the carbon fiber half-tube bed of the Skyscan 1176, and maintained on anesthetic gasses for the duration of the scanning process (5–12 min). A cylindrical shape Styrofoam holder was used to position the right tibia to ensure the placement of the tibia along the scanner midline. All scans were performed with 18 μm voxel resolution, 65 kV, 384 μA, 350 ms exposure time, 0.65° rotation step, and a 1-mm Al filter (Mustafy, Benoit, et al., 2018). A Phantom calibration was performed for each scanning day, prior to bone imaging using two cylindrical hydroxyapatite phantoms (0.25 and 0.75 g/cm^3 CaHA). Images were reconstructed using NRecon software (v.1.6.10, Bruker-microCT, Belgium) (Mustafy, Benoit, et al., 2018).

6.7.4.2 Trabecular bone morphometry

The volume of interest (VOI) for trabecular bone was selected as a percentage of the entire tibial length (L) (Figure 6.5A). The VOI started at ~0.35 mm distal to the growth plate, excluding the primary spongiosa, and extended for 12% of the total tibial length (L) (Lynch et al., 2010; Mustafy, Benoit, et al., 2018) (Figure 6.5A). The volumes of interest, including only trabecular bone, were semi-automatically segmented using an in-house algorithm (Mustafy, Benoit, et al., 2018). For all analyses, a global gray threshold value of 65 corresponding to an equivalent density of 0.413 g/cm^3 of calcium hydroxyapatite (CaHA) was applied (Lynch et al., 2010; Mustafy, Benoit, et al., 2018). CTAn software v.1.16 was used for performing morphometric analysis for the selected VOIs of trabecular bone and allowed evaluating the following parameters: bone mineral density (BMD), bone volume fraction (BV/TV), trabecular thickness (Tb.Th), trabecular number (Tb.N), trabecular spacing (Tb.Sp), and connectivity density (Conn.Dn) (Bouxsein et al., 2010) (Figure 6.5A).
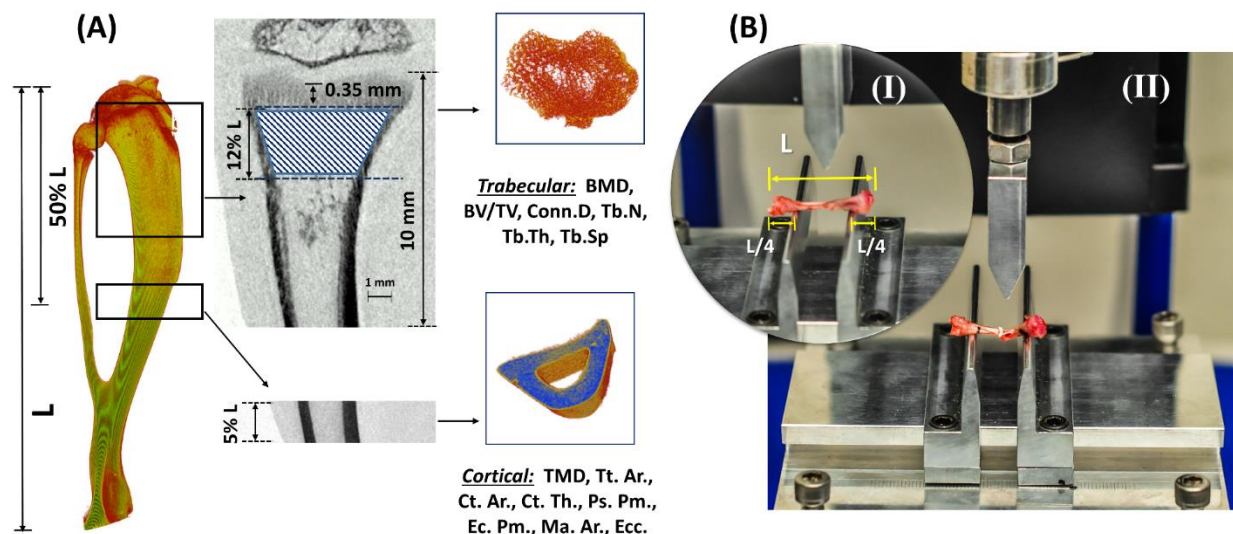
Figure 6.5 Trabecular and cortical volume of interests and experimental setup for three-point bending tests. (A) Representative 3D reconstructed tibia showing the total tibial length (L). The trabecular VOI started at ~0.35 mm distal to the growth plate and extended for 12% of the overall bone length (L). The VOI for cortical bone was centered at the tibial mid-diaphysis and extended proximally and distally for 5% of the tibial length (L). Volumes of interest including only trabecular and cortical bone were semi-automatically segmented using an in-house algorithm. (B) *I*-Experimental setup for the three-point bending tests. A distance of 50% of the total tibial length was fixed between the supports, while the remaining 50% was distributed equally between the external sides of the supports. *II*- Representative image of the fractured tibia after the bending test

6.7.4.3 Cortical bone morphometry

The VOI for cortical bone was chosen from the tibial mid-diaphysis and extended proximal-distally for a total of 5% of the tibial length (Figure 6.5A). The volumes of interest, including only cortical bone, were semi-automatically segmented using an in-house algorithm (Mustafy, Benoit, et al., 2018). A global gray threshold value of 65 was set for all analyses (Lynch et al., 2010; Mustafy, Benoit, et al., 2018). Cortical microarchitectural measurements, including tissue mineral density (TMD), cortical bone area (Ct.Ar), total area (Tt.Ar), medullary area (Ma.Ar), cortical thickness (Ct.Th), endocortical perimeter (Ec.Pm), periosteum perimeter (Ps.Pm), and mean eccentricity (Ecc) were evaluated from the cortical bone VOIs (Bouxsein et al., 2010) (Figure 6.5A).

6.7.5 Mechanical Testing

Following the last micro-CT scan (11th week), rats were sacrificed using CO_2 asphyxiation, followed by decapitation. Right tibiae (n=30) from all groups of rats were cleaned of soft tissues and tested to failure in three-point bending under displacement control at 0.20 mm/sec using a Mach-1 V500C (Biomomentum Inc, Montreal, Canada). A custom made bending setup was used to place the rat tibiae horizontally with the anterior surface upwards and centered between the supports (Figure 6.5B). A distance of 50% of the total tibial length was set between the supports, while the remaining 50% was distributed equally between the external sides of the supports (Figure 6.5B). The structural properties of the tibial samples, including the ultimate load (N), failure load (N), energy to ultimate load (mJ), energy to failure load (mJ), and linear stiffness (N/mm) were determined using force-deformation curves. Energies to ultimate load and failure load were computed as the areas under the force-deformation curves. Stiffness was calculated as the slope of the linear portion of the force-deformation curve. To calculate the intrinsic cortical mechanical properties, cross-sectional parameters were measured using the micro-CT images at the tibial mid-diaphysis (Mustafy, Londono, et al., 2018). Assuming the tibial cross sections were elliptically shaped (C. H. Turner, Akhter, & Heaney, 1992), the moment of inertia was evaluated using the following equation:

$$I = \frac{\pi\left[ab^3 - (a-2t)(b-2t)^3\right]}{64} \quad (1)$$

where I is the moment of inertia (mm^4), a is the width of the bone cross-section in the mediolateral direction (mm), b is the width of the bone cross-section in the anteroposterior direction (mm), and t is the average of the cortical thickness (mm) (T. Huang et al., 2003). Assuming linear elastic bone material (Mustafy, Moglo, Adeeb, & El-Rich, 2014; Schriefer et al., 2005) and using the beam bending theory, Young's modulus and ultimate stress were determined by the following equations:

$$E = \frac{kL^3}{48I} \quad (2)$$

$$\sigma_{ult} = \frac{F_{ult}Lc}{4I} \quad (3)$$

where, E is the Young's modulus (GPa), and σ_{ult} is the ultimate stress (MPa), k is the stiffness (N.mm^{-1}), L is the span length (mm), F_{ult} is the ultimate load (N), and c is the distance from the cross-section centroid to outermost point on the cross-section (mm), which was approximated as bone width/2 (Mustafy, Londono, et al., 2018). Moreover, energies to ultimate stress (mJ/mm^3) and failure stress (mJ/mm^3) were assessed by calculating the respective areas under the stress-strain curve.

6.7.6 Bone growth rate assessment

6.7.6.1 Calcein Injections

Calcein was used to mark the newly formed bone line on the proximal tibial surface to enable longitudinal bone growth rate measurement. Injections of calcein (Sigma-Aldrich, St. Louis, MO, USA) were made intraperitoneally at a dosage of 15 mg/Kg (Valteau et al., 2011) at 5 and 2 days prior to euthanasia.

6.7.6.2 Tissue processing

Proximal sections (~10 mm) from each tibia were fixed for 48h using the formalin solution (Anachemia, Montreal, QC, Canada). For dehydration and clarification, graded alcohol solutions and xylene were used respectively. Embedding process was performed using methylmethacrylate (MMA) (Fisher Scientific Canada, Nepean, ON, Canada) (Ménard et al., 2014). After polymerization, tibial blocks were cut in 6 µm sections using a microtome (Leica SM2500). The longitudinal bone axis was used to cut the tibiae for 36 slides, six series of six slides, containing two sections per slide. For each tibia, the first slide of each series was set aside from light for growth rate measurements, for a total of 6 slides (i.e., 12 sections total). Microscopic observations were performed with a microscope (Leica DMR with Retina Qimaging Camera) using 2.5x magnification.

6.7.6.3 Growth rate calculation

Bone growth rate was calculated as the distance between two calcein labels divided by the time interval (3 days) between injections (Hunziker & Schenk, 1989) (Figure 6.2A). Measurements were performed using a custom-made Matlab program, where both calcein lines were modeled as splines, and the distance between the labels was automatically calculated as the mean value of 100

segments parallel to the longitudinal growth direction (Ménard et al., 2014; Valteau et al., 2011) (Figure 6.2A).

6.7.7 Growth Plate Histomorphometry

Growth plate histomorphometric parameters were assessed to infer on the effects of impact loadings, similar to previous studies on bone growth mechanobiology (Cancel et al., 2009; Ménard et al., 2014). These parameters included the PZ and HZ heights, hypertrophic cell height, as well as the number of proliferative cells per column (Ménard et al., 2014; Valteau et al., 2011) (Figure 6.3A, 6.3B). Zone heights and hypertrophic cell height were measured by implementing a 10x and 20x magnified image sets, respectively, following a similar approach to bone growth rate measurement. Average zonal height values were calculated from 100 individual segmental measurements (Figure 6.3A). Also, 20x magnified image sets were used for measuring the number of proliferative chondrocytes per column (Figure 6.3B). For each proximal tibial segment, histomorphometric parameters were measured by averaging 72 values, 6 values per section, and 12 values per microscope slide with a six series repetition.

6.7.8 Statistical Analysis

SPSS Statistics (v. 23, IBM) was used to perform statistical analyses. To determine time effects, loading effects, and their interaction on body weight and food consumption during the experimental period, a repeated ANOVA test (general linear model) was performed. The sham and control groups were compared to isolate any handling and manipulation effects, whereas, the impact groups were compared with the sham group to infer on the impact loading effects. For assessing any significant differences in average bone growth rates and histomorphometric parameters measured at the 11th week for all tibiae, a paired Student's t-test was implemented. Moreover, the structural properties of trabecular and cortical bone microstructure from all rat groups were statistically analyzed after 4 and 8 weeks of experimental period. Mechanical properties extracted from the three-point bending tests were also statistically analyzed. A one-way ANOVA with Tukey's multiple comparisons was performed to assess the significant group difference and pairwise comparisons. Data are presented as means ± s.d. Statistical significance was fixed at $p<0.05$.

6.8 Acknowledgements

6.9 References

Ahn, A. C., & Grodzinsky, A. J. (2009). Relevance of collagen piezoelectricity to "Wolff's Law": A critical review. *Medical engineering & physics, 31*(7), 733-741.

Banu, J., Wang, L., & Kalu, D. (2002). Age-related changes in bone mineral content and density in intact male F344 rats. *Bone, 30*(1), 125-130.

Berman, A. G., Clauser, C. A., Wunderlin, C., Hammond, M. A., & Wallace, J. M. (2015). Structural and mechanical improvements to bone are strain dependent with axial compression of the tibia in female C57BL/6 mice. *PLOS ONE, 10*(6), e0130504.

Bouassida, A., Latiri, I., Bouassida, S., Zalleg, D., Zaouali, M., Feki, Y., . . . Tabka, Z. (2006). Parathyroid hormone and physical exercise: a brief review. *Journal of sports science & medicine, 5*(3), 367.

Bourrin, S., Genty, C., Palle, S., Gharib, C., & Alexandre, C. (1994). Adverse effects of strenuous exercise: a densitometric and histomorphometric study in the rat. *Journal of applied physiology, 76*(5), 1999-2005.

Bouxsein, M. L., Boyd, S. K., Christiansen, B. A., Guldberg, R. E., Jepsen, K. J., & Müller, R. (2010). Guidelines for assessment of bone microstructure in rodents using micro–computed tomography. *Journal of Bone and Mineral Research, 25*(7), 1468-1486.

Bürge, M., Dolanc, B., Jenny, H., & Morscher, E. (1980). Behandlung und Ergebnisse bei Osteochondritis dissecans des Kniegelenkes. *Orthopäde, 9*, 320-326.

Burr, D. (2002). The contribution of the organic matrix to bone's material properties. *Bone, 31*(1), 8-11.

Burr, D., Milgrom, C., Fyhrie, D., Forwood, M., Nyska, M., Finestone, A., . . . Simkin, A. (1996). In vivo measurement of human tibial strains during vigorous activity. *Bone, 18*(5), 405-410.

Caine, D., Lewis, R., O'Connor, P., Howe, W., & Bass, S. (2001). Does gymnastics training inhibit growth of females? *Clinical journal of sport medicine, 11*(4), 260-270.

Cancel, M., Grimard, G., Thuillard-Crisinel, D., Moldovan, F., & Villemure, I. (2009). Effects of in vivo static compressive loading on aggrecan and type II and X collagens in the rat growth plate extracellular matrix. *Bone, 44*(2), 306-315.

Chilibeck, P. D., Sale, D. G., & Webber, C. E. (1995). Exercise and bone mineral density. *Sports Medicine, 19*(2), 103-122.

Crews 3rd, E., Fuge, K. W., Oscai, L., Holloszy, J., & Shank, R. (1969). Weight, food intake, and body composition: effects of exercise and of protein deficiency. *American Journal of Physiology-Legacy Content, 216*(2), 359-363.

Cullen, D., Smith, R., & Akhter, M. (2001). Bone-loading response varies with strain magnitude and cycle number. *Journal of applied physiology, 91*(5), 1971-1976.

De Souza, R. L., Matsuura, M., Eckstein, F., Rawlinson, S. C., Lanyon, L. E., & Pitsillides, A. A. (2005). Non-invasive axial loading of mouse tibiae increases cortical bone formation and modifies trabecular organization: a new model to study cortical and cancellous compartments in a single loaded element. *Bone, 37*(6), 810-818.

Deere, K., Sayers, A., Rittweger, J., & Tobias, J. H. (2012). Habitual levels of high, but not moderate or low, impact activity are positively related to hip BMD and geometry: Results from a population-based study of adolescents. *Journal of bone and mineral research, 27*(9), 1887-1895.

Drinkwater, B. L., Nilson, K., Chesnut III, C. H., Bremner, W. J., Shainholtz, S., & Southworth, M. B. (1984). Bone mineral content of amenorrheic and eumenorrheic athletes. *New England Journal of Medicine, 311*(5), 277-281.

Duff, S. (1986). Histopathology of growth plate changes in induced abnormal bone growth in lambs. *Journal of comparative pathology, 96*(1), 15-24.

Duncan, R., & Turner, C. (1995). Mechanotransduction and the functional response of bone to mechanical strain. *Calcified tissue international, 57*(5), 344-358.

Farnum, C. E., & Wilsman, N. J. (2001). Converting a differentiation cascade into longitudinal growth: stereology and analysis of transgenic animals as tools for understanding growth plate function. *Current Opinion in Orthopaedics, 12*(5), 428-433.

Forwood, M. R., & Parker, A. W. (1987). Effects of exercise on bone growth mechanical and physical properties studied in the rat. *Clinical Biomechanics, 2*(4), 185-190.

Fritton, J., Myers, E., Wright, T., & Van der Meulen, M. (2005). Loading induces site-specific increases in mineral content assessed by microcomputed tomography of the mouse tibia. *Bone, 36*(6), 1030-1038.

Hagihara, Y., Fukuda, S., Goto, S., Iida, H., Yamazaki, M., & Moriya, H. (2005). How many days per week should rats undergo running exercise to increase BMD? *Journal of bone and mineral metabolism, 23*(4), 289-294.

Hansson, L., Menander-Sellman, K., Stenström, A., & Thorngren, K.-G. (1972). Rate of normal longitudinal bone growth in the rat. *Calcified tissue research, 10*(1), 238-251.

Hasan, A., Byambaa, B., Morshed, M., Cheikh, M. I., Shakoor, R. A., Mustafy, T., & Marei, H. (2018). Advances in osteobiologic materials for bone substitutes. *Journal of Tissue Engineering and Regenerative Medicine*.

Huang, T.-H., Hsieh, S. S., Liu, S.-H., Chang, F.-L., Lin, S.-C., & Yang, R.-S. (2010). Swimming training increases the post-yield energy of bone in young male rats. *Calcified tissue international, 86*(2), 142-153.

Huang, T., Lin, S., Chang, F., Hsieh, S., Liu, S., & Yang, R. (2003). Effects of different exercise modes on mineralization, structure, and biomechanical properties of growing bone. *Journal of applied physiology, 95*(1), 300-307.

Hunziker, E., & Schenk, R. (1989). Physiological mechanisms adopted by chondrocytes in regulating longitudinal bone growth in rats. *The Journal of physiology, 414*(1), 55-71.

Jiang, S.-D., Jiang, L.-S., & Dai, L.-Y. (2007). Changes in bone mass, bone structure, bone biomechanical properties, and bone metabolism after spinal cord injury: a 6-month longitudinal study in growing rats. *Calcified tissue international, 80*(3), 167-175.

Jones, E. M., Montoye, H. J., Johnson, P. B., John Martin Martin, S. M., Van Huss, W. D., & Cederquist, D. (1964). Effects of exercise and food restriction on serum cholesterol and liver lipids. *American Journal of Physiology-Legacy Content, 207*(2), 460-466.

Jürgensen, I., Bachmann, G., Haas, H., & Schleicher, I. (1998). Einfluß der arthroskopischen Therapie auf den Verlauf der Osteochondrosis dissecans des Knie-und oberen Sprunggelenks. *Arthroskopie, 11*(4), 193-199.

Kang, Y.-S., Kim, S.-H., & Kim, J.-C. (2017). Effects of swimming exercise on high-fat diet-induced low bone mineral density and trabecular bone microstructure in rats. *Journal of exercise nutrition & biochemistry, 21*(2), 48.

Kannus, P., Sievänen, H., Järvinen, T. L., Järvinen, M., Kvist, M., Oja, P., . . . Jozsa, L. (1994). Effects of free mobilization and low-to high-intensity treadmill running on the immobilization-induced bone loss in rats. *Journal of Bone and Mineral Research, 9*(10), 1613-1619.

Karlsson, M. K. (2004). Physical activity, skeletal health and fractures in a long term perspective. *Journal of Musculoskeletal and Neuronal Interactions, 4*(1), 12.

Kember, N., & Walker, K. (1971). Control of bone growth in rats. *Nature, 229*(5284), 428.

Kirmani, S., Christen, D., Van Lenthe, G. H., Fischer, P. R., Bouxsein, M. L., McCready, L. K., . . . Müller, R. (2009). Bone structure at the distal radius during adolescent growth. *Journal of Bone and Mineral Research, 24*(6), 1033-1042.

Krember, N. (1972). Comparative patterns of cell division in epiphyseal cartilage plates in the rat. *Journal of Anatomy, 111*(Pt 1), 137.

Lanyon, L., Hampson, W., Goodship, A., & Shah, J. (1975). Bone deformation recorded in vivo from strain gauges attached to the human tibial shaft. *Acta Orthopaedica, 46*(2), 256-268.

Lee, K., Maxwell, A., & Lanyon, L. (2002). Validation of a technique for studying functional adaptation of the mouse ulna in response to mechanical loading. *Bone, 31*(3), 407-412.

Lu, H., Cui, L., Zuo, C., Lin, S., & Wu, T. (2015). Evaluation of morphological parameters of bone formation in Sprague–Dawley rats of different ages by in vivo fluorochrome labeling. *Italian Journal of Zoology, 82*(1), 33-40.

Lynch, M. E., Brooks, D., Mohanan, S., Lee, M. J., Polamraju, P., Dent, K., . . . Fischbach, C. (2013). In vivo tibial compression decreases osteolysis and tumor formation in a human metastatic breast cancer model. *Journal of Bone and Mineral Research, 28*(11), 2357-2367.

Lynch, M. E., Main, R. P., Xu, Q., Walsh, D. J., Schaffler, M. B., Wright, T. M., & van der Meulen, M. C. (2010). Cancellous bone adaptation to tibial compression is not sex dependent in growing mice. *Journal of applied physiology, 109*(3), 685-691.

Main, R. P., Lynch, M. E., & van der Meulen, M. C. (2010). In vivo tibial stiffness is maintained by whole bone morphology and cross-sectional geometry in growing female mice. *Journal of biomechanics, 43*(14), 2689-2694.

Main, R. P., Lynch, M. E., & van der Meulen, M. C. (2014). Load-induced changes in bone stiffness and cancellous and cortical bone mass following tibial compression diminish with age in female mice. *Journal of Experimental Biology, 217*(10), 1775-1783.

Mathey, J., Horcajada-Molteni, M.-N., Chanteranne, B., Picherit, C., Puel, C., Lebecque, P., . . . Barlet, J.-P. (2002). Bone mass in obese diabetic Zucker rats: influence of treadmill running. *Calcified tissue international, 70*(4), 305-311.

Ménard, A. L., Grimard, G., Valteau, B., Londono, I., Moldovan, F., & Villemure, I. (2014). In vivo dynamic loading reduces bone growth without histomorphometric changes of the growth plate. *Journal of Orthopaedic Research, 32*(9), 1129-1136.

Milgrom, C., Finestone, A., Sharkey, N., Hamel, A., Mandes, V., Burr, D., . . . Ekenman, I. (2002). Metatarsal strains are sufficient to cause fatigue fracture during cyclic overloading. *Foot & ankle international, 23*(3), 230-235.

Morris, M. D., & Mandair, G. S. (2011). Raman assessment of bone quality. *Clinical Orthopaedics and Related Research®, 469*(8), 2160-2169.

Mosley, J., March, B., Lynch, J., & Lanyon, L. (1997). Strain magnitude related changes in whole bone architecture in growing rats. *Bone, 20*(3), 191-198.

Mustafy, T., Arnoux, P.-J., Benoit, A., Bianco, R.-J., Aubin, C.-E., & Villemure, I. (2018). Load-sharing biomechanics at the thoracolumbar junction under dynamic loadings are modified by anatomical features in adolescent and pediatric vs adult functional spinal units. *Journal of the Mechanical Behavior of Biomedical Materials, 88*, 78.

Mustafy, T., Benoit, A., Londono, I., Moldovan, F., & Villemure, I. (2018). Can repeated in vivo micro-CT irradiation during adolescence alter bone microstructure, histomorphometry and longitudinal growth in a rodent model? *PLOS ONE, 13*(11), e0207323. doi: 10.1371/journal.pone.0207323

Mustafy, T., Londono, I., & Villemure, I. (2018). Can the contralateral limb be used as a control during the growing period in a rodent model? *Medical engineering & physics, 58*, 31-40. doi: https://doi.org/10.1016/j.medengphy.2018.04.013

Mustafy, T., Londono, I., & Villemure, I. (2019). Experimental and finite element analyses of bone strains in the growing rat tibia induced by in vivo axial compression. *Journal of the Mechanical Behavior of Biomedical Materials, 94*, 176.

Mustafy, T., Moglo, K., Adeeb, S., & El-Rich, M. (2014). *Investigation of Upper Cervical Spine Injury due to Frontal and Rear Impact Loading Using Finite Element Analysis.* Paper presented at the ASME 2014 International Mechanical Engineering Congress and Exposition.

Niehoff, A., Kersting, U. G., Zaucke, F., Morlock, M. M., & Brüggemann, G.-P. (2004). Adaptation of mechanical, morphological, and biochemical properties of the rat growth plate to dose-dependent voluntary exercise. *Bone, 35*(4), 899-908.

Notomi, T., Okimoto, N., Okazaki, Y., Tanaka, Y., Nakamura, T., & Suzuki, M. (2001). Effects of tower climbing exercise on bone mass, strength, and turnover in growing rats. *Journal of Bone and Mineral Research, 16*(1), 166-174.

Oh, T., Tanaka, S., Naka, T., & Igawa, S. (2016). Effects of high-intensity swimming training on the bones of ovariectomized rats. *Journal of exercise nutrition & biochemistry, 20*(3), 39.

Ohashi, N., Robling, A. G., Burr, D. B., & Turner, C. H. (2002). The effects of dynamic axial loading on the rat growth plate. *Journal of Bone and Mineral Research, 17*(2), 284-292.

Ooi, F. K., Tavafzadeh, S. S., Hung, L., Hung, W., & He, Y. (2014). Tibial Bone Mineral Density, Geometry, and Mechanical Properties in Response to High-Impact Exercise and Honey Supplementation in Rats. *Asian Journal of Exercise & Sports Science, 11*(2).

Orava, S., & Virtanen, K. (1982). Osteochondroses in athletes. *British journal of sports medicine, 16*(3), 161-168.

Peng, J., Zhou, Y., Min, L., Zhang, W., Luo, Y., Zhang, X., . . . Tu, C. (2014). Analysis of correlation between trabecular microstructure and clinical imaging parameters in fracture region of osteoporotic hip. *Zhongguo xiu fu chong jian wai ke za zhi= Zhongguo xiufu chongjian waike zazhi= Chinese journal of reparative and reconstructive surgery, 28*(5), 576-580.

Pitts, G., & Bull, L. (1977). Exercise, dietary obesity, and growth in the rat. *American Journal of Physiology-Regulatory, Integrative and Comparative Physiology, 232*(1), R38-R44.

Prisby, R. D., Lafage-Proust, M.-H., Malaval, L., Belli, A., & Vico, L. (2008). Effects of whole body vibration on the skeleton and other organ systems in man and animal models: what we know and what we need to know. *Ageing research reviews, 7*(4), 319-329.

Pritchett, J. W. (1992). Longitudinal growth and growth-plate activity in the lower extremity. *Clinical orthopaedics and related research*(275), 274-279.

Razi, H., Birkhold, A. I., Zaslansky, P., Weinkamer, R., Duda, G. N., Willie, B. M., & Checa, S. (2015). Skeletal maturity leads to a reduction in the strain magnitudes induced within the bone: a murine tibia study. *Acta biomaterialia, 13*, 301-310.

Robling, A., Duijvelaar, K., Geevers, J., Ohashi, N., & Turner, C. (2001). Modulation of appositional and longitudinal bone growth in the rat ulna by applied static and dynamic force. *Bone, 29*(2), 105-113.

Rosenbaum, M., Hirsch, J., Murphy, E., & Leibel, R. L. (2000). Effects of changes in body weight on carbohydrate metabolism, catecholamine excretion, and thyroid function–. *The American journal of clinical nutrition, 71*(6), 1421-1432.

Russek, M., & Pina, S. (1962). Conditioning of adrenalin anorexia. *Nature, 193*(4822), 1296.

Saers, J. P., Cazorla-Bak, Y., Shaw, C. N., Stock, J. T., & Ryan, T. M. (2016). Trabecular bone structural variation throughout the human lower limb. *Journal of human evolution, 97*, 97-108.

Schlecht, S. H., Bigelow, E. M., & Jepsen, K. J. (2014). Mapping the natural variation in whole bone stiffness and strength across skeletal sites. *Bone, 67*, 15-22.

Schriefer, J. L., Robling, A. G., Warden, S. J., Fournier, A. J., Mason, J. J., & Turner, C. H. (2005). A comparison of mechanical properties derived from multiple skeletal sites in mice. *Journal of biomechanics, 38*(3), 467-475.

Shahi, M., Peymani, A., & Sahmani, M. (2017). Regulation of bone metabolism. *Reports of biochemistry & molecular biology, 5*(2), 73.

Sievänen, H. (2012). Bone: Impact loading—nature's way to strengthen bone. *Nature Reviews Endocrinology, 8*(7), 391-393.

Slemenda, C. W., & Johnston, C. C. (1993). High intensity activities in young women: site specific bone mass effects among female figure skaters. *Bone and mineral, 20*(2), 125-132.

Snyder, A., Zierath, J., Hawley, J., Sleeper, M., & Craig, B. (1992). The effects of exercise mode, swimming vs. running, upon bone growth in the rapidly growing female rat. *Mechanisms of ageing and development, 66*(1), 59-69.

Spengler, D. M., Morey, E. R., Carter, D. R., Turner, R. T., & Baylink, D. J. (1983). Effects of spaceflight on structural and material strength of growing bone. *Proceedings of the Society for Experimental Biology and Medicine, 174*(2), 224-228.

Stokes, I. (2002). Mechanical effects on skeletal growth. *Journal of Musculoskeletal and Neuronal Interactions, 2*(3), 277-280.

Stürmer, E. K., Seidlová-Wuttke, D., Sehmisch, S., Rack, T., Wille, J., Frosch, K. H., . . . Stürmer, K. M. (2006). Standardized bending and breaking test for the normal and osteoporotic metaphyseal tibias of the rat: effect of estradiol, testosterone, and raloxifene. *Journal of Bone and Mineral Research, 21*(1), 89-96.

Swissa-Sivan, A., Simkin, A., Leichter, I., Nyska, A., Nyska, M., Statter, M., . . . Samueloff, S. (1989). Effect of swimming on bone growth and development in young rats. *Bone and mineral, 7*(2), 91-105.

Theintz, G. E., Howald, H., Weiss, U., & Sizonenko, P. (1993). Evidence for a reduction of growth potential in adolescent female gymnasts. *The Journal of pediatrics, 122*(2), 306-313.

TSUJI, K., KATAYAMA, Y., & KOISHI, H. (1975). Effects of dietary protein level on the energy metabolism of rats during exercise. *Journal of nutritional science and vitaminology, 21*(6), 437-449.

Turner, C., Akhter, M., Raab, D., Kimmel, D., & Recker, R. (1991). A noninvasive, in vivo model for studying strain adaptive bone modeling. *Bone, 12*(2), 73-79.

Turner, C. H., Akhter, M., & Heaney, R. P. (1992). The effects of fluoridated water on bone strength. *Journal of Orthopaedic Research, 10*(4), 581-587.

Vainionpää, A., Korpelainen, R., Vihriälä, E., Rinta–Paavola, A., Leppäluoto, J., & Jämsä, T. (2006). Intensity of exercise is associated with bone density change in premenopausal women. *Osteoporosis International, 17*(3), 455-463.

Valteau, B., Grimard, G., Londono, I., Moldovan, F., & Villemure, I. (2011). In vivo dynamic bone growth modulation is less detrimental but as effective as static growth modulation. *Bone, 49*(5), 996-1004.

Viguet-Carrin, S., Garnero, P., & Delmas, P. (2006). The role of collagen in bone strength. *Osteoporosis international, 17*(3), 319-336.

Villemure, I., & Stokes, I. A. (2009). Growth plate mechanics and mechanobiology. A survey of present understanding. *Journal of biomechanics, 42*(12), 1793-1803.

Voide, R., van Lenthe, G. H., & Müller, R. (2008). Bone morphometry strongly predicts cortical bone stiffness and strength, but not toughness, in inbred mouse models of high and low bone mass. *Journal of Bone and Mineral Research, 23*(8), 1194-1203.

Walker, K., & Kember, N. (1972). CELL KINETICS OF GROWTH CARTILAGE IN THE RAT TIBIA II. MEASUREMENTS DURING AGEING. *Cell Proliferation, 5*(5), 409-419.

Wallace, J. M., Rajachar, R. M., Allen, M. R., Bloomfield, S. A., Robey, P. G., Young, M. F., & Kohn, D. H. (2007). Exercise-induced changes in the cortical bone of growing mice are bone-and gender-specific. *Bone, 40*(4), 1120-1127.

Wang, X., Shen, X., Li, X., & Agrawal, C. M. (2002). Age-related changes in the collagen network and toughness of bone. *Bone, 31*(1), 1-7.

Warden, S. J., Fuchs, R., Castillo, A., & Turner, C. (2005). Does exercise during growth influence osteoporotic fracture risk later in life? *Journal of Musculoskeletal and Neuronal Interactions, 5*(4), 344.

Warner, S., Shea, J., Miller, S., & Shaw, J. (2006). Adaptations in cortical and trabecular bone in response to mechanical loading with and without weight bearing. *Calcified tissue international, 79*(6), 395-403.

Weaver, C. M. (2002). Adolescence. *Endocrine, 17*(1), 43-48. doi: 10.1385/endo:17:1:43

Welch, J., Turner, C., Devareddy, L., Arjmandi, B., & Weaver, C. (2008). High impact exercise is more beneficial than dietary calcium for building bone strength in the growing rat skeleton. *Bone, 42*(4), 660-668.

Wolff, J. (1892). Das gesetz der transformation der knochen. *A Hirshwald, 1*, 1-152.

Yang, P., Bruggemann, G., & Rittweger, J. (2011). What do we currently know from in vivo bone strain measurements in humans. *J Musculoskelet Neuronal Interact, 11*(1), 8-20.

Yang, X., Chan, Y. H., Muthukumaran, P., & Lee, T. (2010). Morphological and mechanical changes in ovariectomized rat tibia with treatments of ibandronate and parathyroid hormone. *Osteoporosis, 8*(3), 255-265.

CHAPTER 7 ARTICLE #4: IMPACT EXERCISE DURING ADOLESCENCE IMPROVES BONE MICROSTRUCTURE AND STRENGTH AT ADULTHOOD

This chapter introduces the fourth article written in the context of this thesis and responds to the third objective of this thesis as detailed in Chapter 3.

The manuscript of this article was submitted to Journal of Bone and Mineral Research © on 23rd May 2019.

The contribution of the first author in the preparation, obtaining the results, writing and literature review of this paper is estimated at 85%.

Contribution of all authors:

Tanvir Mustafy: Conceptualization, Data curation, Formal analysis, Investigation, Methodology, Project administration, Software, Visualization, Writing - original draft.

Irene Londono: Data curation, Resources.

Florina Moldovan: Methodology, Supervision.

Isabelle Villemure: Conceptualization, Funding acquisition, Methodology, Project administration, Resources, Supervision, Writing - review & editing.

7.1 Abstract

Bone is a unique living tissue, which responds to the mechanical stimuli regularly imposed on it. Adolescence facilitates a favorable condition for the skeleton which enables the exercise to positively influence bone architecture and overall strength. However, it is still dubious for how long the skeletal benefits gained in the adolescence preserved at adulthood. The current study aims to use a rat model to investigate the effects of *in vivo* low (LI), medium (MI) and high (HI) impact loadings applied during puberty on longitudinal bone development, morphometry and biomechanics during adolescence as well as at the adulthood. Forty-two young (4-week-old) male rats were randomized into control, sham, LI, MI, and HI groups. After a 5 days/week for 8 weeks impact loading regime applied on the right tibiae, loaded rats underwent a subsequent 41-week of detraining period. Right tibiae were removed at 52-week of age and a comprehensive assessment was performed using micro-computed tomography, mechanical testing, and finite element analysis. HI and MI groups exhibited reduced body weight and food intake at the end of the loading period compared to shams, but these effects disappeared afterwards. HI loading increased bone mineral density, bone volume fraction, trabecular thickness, trabecular number and decreased trabecular spacing after loading. All loading induced benefits, except bone mineral density, persisted until the end of detraining period. Moreover, HI loading induced enhanced bone area, periosteal perimeter and moment of inertia, which remained up to the 52nd week. After the detraining at adulthood, HI group showed an increased ultimate force and stress, stiffness, post-yield displacement and energy, and toughness compared to the sham group. Overall, our findings suggest that even though both trabecular and cortical bone drifted through age-related changes during aging, high impact exercise performed during adolescence can render lifelong benefits in bone microstructure and biomechanics.

7.2 Keywords

Mechanical loading, Biomechanics, Detraining, Growth and development, Bone adaptation

7.3 Introduction

Bone is a unique living tissue, which responds to mechanical stimuli regularly imposed on it (M. K. Karlsson, 2004; Warden, Fuchs, Castillo, Nelson, & Turner, 2007). Mechanical forces are

considered beneficial to the skeleton at an early age for promoting healthy bone growth by increasing bone mass and mineral content through bone modeling process (Warden et al., 2007; Warden, Roosa, et al., 2014). This concept has been established for ages by rigorous theories and hypotheses (Wolff, 1892), and relationships have been formulated to correlate bone geometric and structural developments with respect to undergoing bone mechanical stresses (Chamay & Tschantz, 1972). During the adolescent period, rapidly growing bones react sensitively to induced mechanical loadings (D. R. Carter & Orr, 1992). Adolescence offers a favorable condition for the skeletal response to mechanical loadings, where impact exercise positively influences bone architecture and overall strength (Sievänen, 2012; Weaver, 2002). Indeed, both positive and negative influence in skeletal development and bone geometry were observed due to daily mechanical loadings from physical activities (D. Carter, Van der Meulen, & Beaupre, 1996). Mechanical loadings can be induced by compression/tension, bending, shear, or torsion depending on the type of physical activities (Forwood, 2008). However, physical activities producing higher ground reaction forces (i.e., impact exercise such as running, jumping, hiking, etc.) were shown to be more effective for strengthening bone microstructure (Robling, Castillo, & Turner, 2006).

For loading-based bone modification induced during adolescence, it has been hypothesized that it could have an impact later in life if the effect persists at adulthood (Health & Services, 2004; Rizzoli, Bianchi, Garabédian, McKay, & Moreno, 2010). However, it is still not clear for how long skeletal benefits gained during adolescence could be preserved at adulthood. Animal and clinical studies have been conducted to investigate the effects of pubertal loading impact on the bony structures. Clinical studies have reported that different forms of physical activities performed during adolescence resulted in 10–15% greater bone mass in the participating children compared to the non-participating ones (Bailey, McKay, Mirwald, Crocker, & Faulkner, 1999; Deere, Sayers, Rittweger, & Tobias, 2012; Janz et al., 2006). Another study on baseball players reported that the effects of ball-throwing persisted throughout life in the form of additional bone strength (Warden, Roosa, et al., 2014). However, few studies concluded that pubertal loading could induce bone mass increase, which prevailed for a short period but diminished over time and disappeared in adulthood (Duckham et al., 2014; Gunter et al., 2008). Similar to clinical investigations, animal studies have also shown contradictory results. In different studies (Jun Iwamoto, Yeh, & Aloia, 2000; M. Karlsson et al., 2000; Warden et al., 2007), researchers observed that bone structural changes during puberty due to induced loading tend to last long into adulthood. However, contradictory

findings showed the absence of skeletal benefits and even bone loss phenomena at adulthood (Jun Iwamoto et al., 2000; Yeh & Aloia, 1990a). This discrepancy in the findings could be associated with animal ages or genders, study design, and used exercise protocols. Most of the experimental studies started the exercise and/or loading regime at the mid or end of the adolescent period (~1.5 months to 2 months old) (Goodrick, 1980; Holloszy, Smith, Vining, & Adams, 1985; Honda, Sogo, Nagasawa, Kato, & Umemura, 2008; Mosekilde, Danielsen, Søgaard, & Thorling, 1994; Søgaard, Danielsen, Thorling, & Mosekilde, 1994). So, these studies lack the data for the entire adolescent period, which is considered one of the most crucial periods for bone development in rats (Sievänen, 2012; Weaver, 2002). Moreover, these studies investigated bone mass and mineral content at limited time points rather than looking at the longitudinal data, which would give a better understanding about the bone modeling dynamics and the temporal nature of bone response to the applied mechanical stimuli. Two studies investigating adolescence exercise effects on rat limb found contrary results regarding persisting skeletal benefits gained during the pubertal period. One study reported decreasing positive effects in the femoral mid-shaft and femoral neck in 47-week old rats (Pajamäki et al., 2003) while the other reported enhanced bone strength in 97-week old rat tibiae (Warden et al., 2007). Moreover, none of these studies assessed these changes longitudinally on both trabecular and cortical bone microstructures.

Hence, it is still not clear whether a controlled impact loading regime during puberty longitudinally influences bone quantity, quality, and mechanics and if/how long these changes persist into adulthood. The current study aimed to investigate the effects of *in vivo* impact loadings (low, medium and high-intensity compression) applied during puberty on longitudinal bone development, morphometry and biomechanics at the end of adolescence as well as during adulthood using a rat tibial model. Rat tibiae were scanned from 4- to 52-week old to assess trabecular and cortical bone changes to loading using *in vivo* micro-CT and at sacrifice (52 w.o.), bone biomechanical properties were extracted from three-point bending tests; strains were also investigated based on simulations of axial compression using voxel-based finite element models.

7.4 Materials and methods

7.4.1 Animals

Forty-two male Sprague-Dawley rats (Charles River Laboratories, Montreal, Canada) were received at approximately 3 weeks of age. Rats were housed two per cage with ad libitum access to food and water and kept at 25°C with a 12-h light/dark cycle. All animal experiments were carried out according to the policies of the Canadian Council on Animal Care (CCAC) and procedures approved by the Institutional Animal Care Committee at the Sainte-Justine University Hospital, Montreal, Canada. After one week of acclimatization to the diet and new environment, rats were randomly divided into five groups: control, sham, low impact (LI), medium impact (MI) and high impact (HI). Control and sham groups consisted of six animals while each impact group consisted of ten animals. Both body weights and food intakes were monitored weekly during the adolescent loading period (until the end of the 11th week) and monthly during the detraining period (12th to 52nd week) to monitor overall health.

7.4.2 Tibial Impact Loading

Tibial impact loading for LI, MI, and HI groups began at 4 week of age using a custom built impact loading device (Figure 7.1A). Rats were anesthetized (2% isoflurane, 1.0 L/min O_2) during cyclic impact loading, which was controlled using a Mach-1 V500C (Biomomentum Inc., Montreal, Canada), to apply a 2-Hz haversine waveform for 1200 cycles/day, 5 days/week for 8 weeks. A compressive preload of 0.5 N was applied to keep the tibia in a steady position. The cyclic loading was characterized by symmetric active loading/unloading with a 0.10 sec of rest period between load cycles (Clarke, 1971; Cullen, Smith, & Akhter, 2001; Mosley, March, Lynch, & Lanyon, 1997; Rabkin, Szivek, Schonfeld, & Halloran, 2001) (Figure 7.1C). The relationship between applied displacements and peak strains at the medio proximal surface of the right tibia was established in preliminary compression-strain calibration experiments with 18 rats of 4, 8 and 12 week old (n = 6/age group) (Figure 7.1B). The axial displacement values generating 450, 850, and 1250 µε tensile strain at the medio proximal tibial surface were respectively used for LI, MI, and HI groups (Figure 7.2A). These strain magnitudes correspond to peak tensile strain values in the human tibia during unrestricted walking (450 µε), zig-zag uphill running (850 µε), and vertical jumping (1250 µε) conditions (Burr et al., 1996; Lanyon, Hampson, Goodship, & Shah, 1975;

Milgrom et al., 2002; P. Yang, Bruggemann, & Rittweger, 2011). Also, the lowest selected peak strain (450 με) has been reported to be sufficient to induce bone adaptation (Ciani, Sharma, Doty, & Fritton, 2014; Turner & Akhter, 1999). Linear interpolation was applied to extract displacement values for the weeks in-between the chosen calibration ages. Similar experimental manipulations were applied to the sham rats without any axial loading. Controls were kept in the cage without any manipulation. For all rats, normal cage activity was allowed between loading sessions.
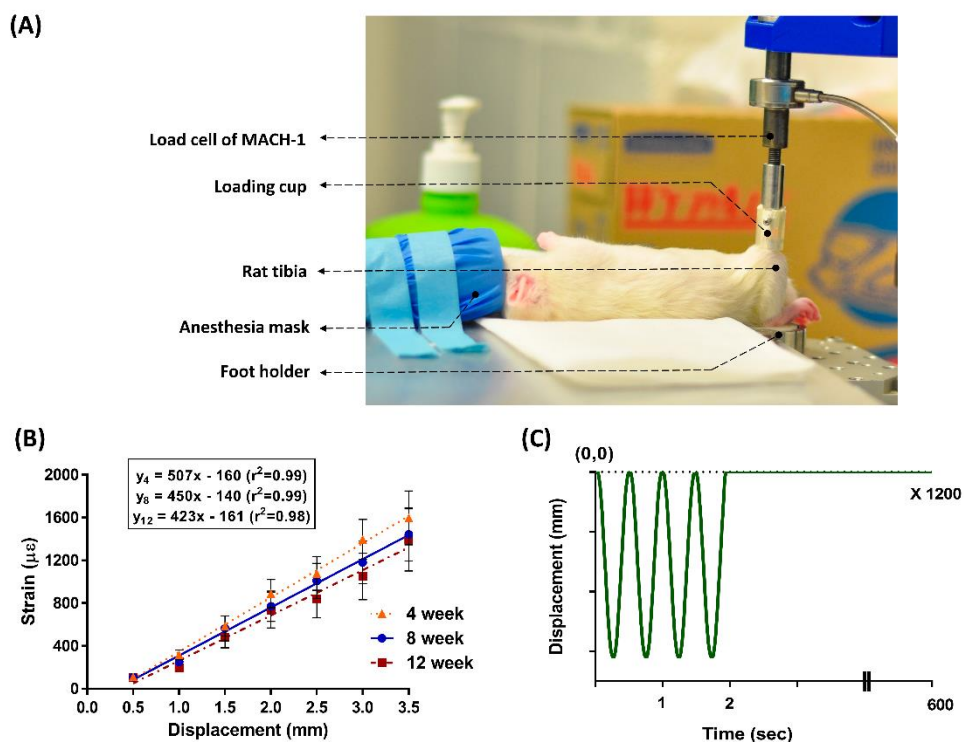
Figure 7.1 (A) *In vivo* loading of the right tibia of a 8 w.o. rat. (B) Strain gauge calibration curves at the medioproximal tibial surface for 4, 8 and 12 week old rats. Error bars represent standard deviations (n = 6 rats/age group). (C) Representative *in vivo* loading profile including 1200 repetitions over approximately 10 min/day. Peak-to-peak displacements were chosen based on the strain gauge calibration curves previously obtained for the three age groups
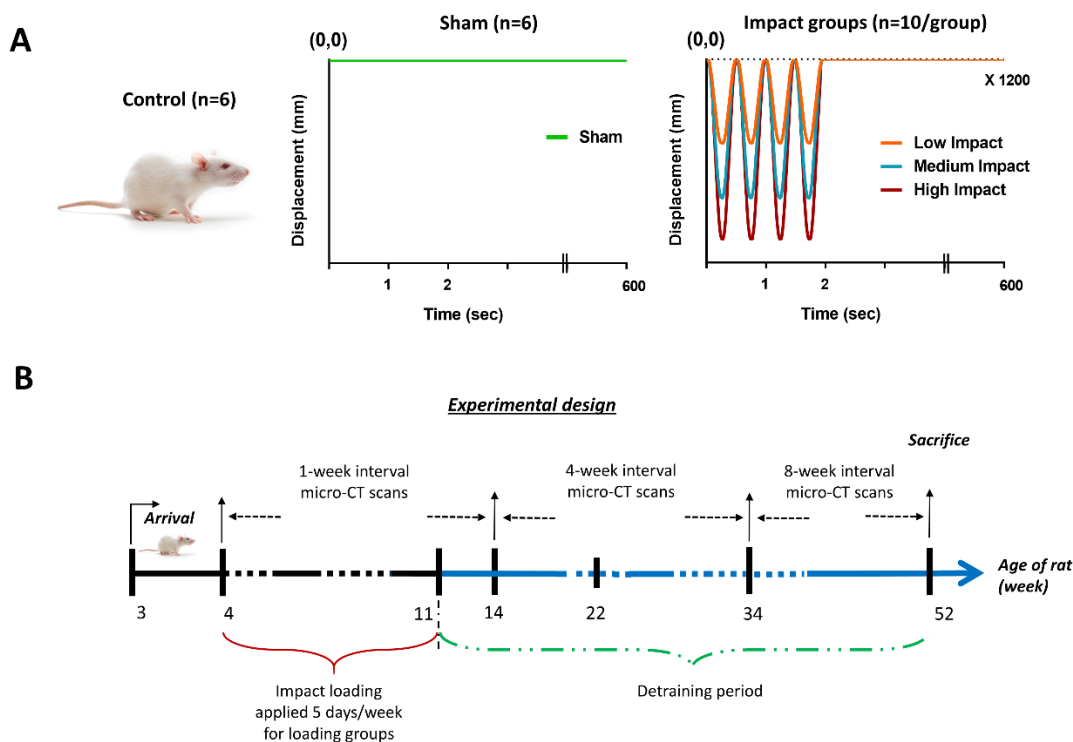
Figure 7.2 (A) Five rat groups (n=42 total) were used: control (C; n=6), sham (S; n=6), low impact (LI; n=10), medium impact (MI; n=10), and high impact (HI; n=10). The right tibia of each rat from LI, MI and HI groups were loaded using the waveform respectively triggering 450, 850, and 1250 με tensile strain at the medio-proximal tibial surface from 4 to 11 weeks of age, corresponding to rat adolescence. (B) Impact loadings were applied 5 days/week from 4 to 11 weeks of age. Rats were detrained from the 11th to 52nd week. At the end of the experiment (52 w.o.), rats were sacrificed, both structural and estimated tissue-level mechanical properties were obtained. Right tibiae were scanned during the entire experimental period, at different time intervals, for acquiring *in vivo* bone microstructural parameters

7.4.3 Micro-Computed Tomography (micro-CT)

7.4.3.1 Micro-CT scanning regime

An *in-vivo* micro-CT scanner (Skyscan 1176, N.V., Belgium) was used for the longitudinal assessment of the right tibial bone morphology using an isotropic voxel size of 18 μm, 65 kV, 384 μA, 350 ms exposure time, 0.65° rotation step, no frame averaging, and a 1-mm Al filter (Mustafy,

Benoit, Londono, Moldovan, & Villemure, 2018). The scans were performed at 1-week intervals from 4th to 14th week of age, at 4-week intervals for the next 22 weeks, and at 8-week intervals for the remaining detraining period of 17 weeks (total 52 week of age) (Figure 7.2B). Rats were positioned on the carbon fiber half-tube bed of the scanner and kept anesthetized (2% isoflurane, 1.0 L/min O_2) during the scanning procedure. The right tibia was positioned into a Styrofoam holder of cylindrical shape to ensure its placement in the midline of the scanner (Figure 7.3A.I). A Phantom calibration was performed on each scanning day using two cylindrical hydroxyapatite phantoms (0.25 and 0.75 g/cm^3 CaHA). Reconstructions of the scanned images were performed using NRecon software (v.1.6.10, Bruker-microCT, Belgium) (Mustafy, Benoit, et al., 2018).
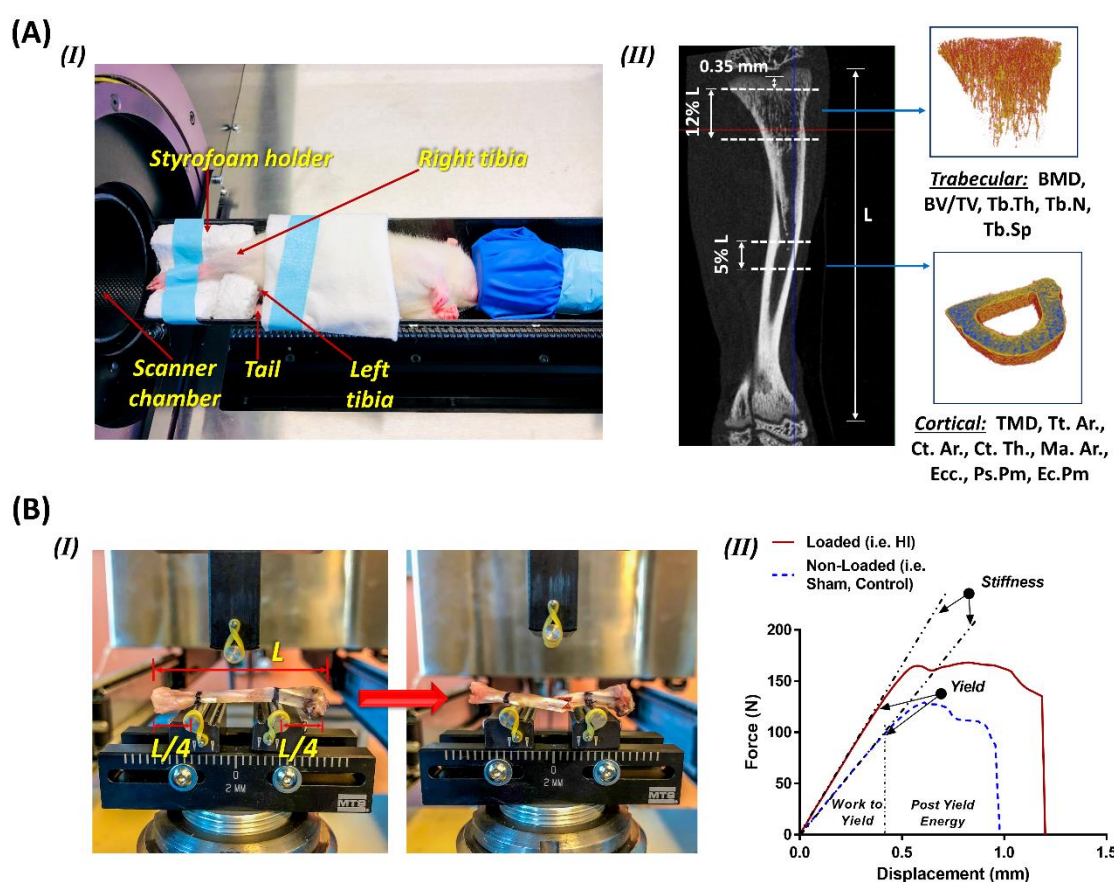
Figure 7.3 (A) (I) Rat positioning for the *in vivo* micro CT scanning. While anesthetized, the rat was placed sideways securing the right tibia into a Styrofoam holder and firmly held with medical adhesive tape. The left tibia was folded towards the animal's head and placed alongside with the tail. (II) Representative longitudinal section of a rat tibial CT scan showing the total tibial length (L). The trabecular VOI started at ~0.35 mm distal to the growth plate and extended for 12% L.

The cortical VOI was fixed at the tibial mid-diaphysis and equally spanned proximally and distally for a total of 5% L. Using a semi-automatic segmentation algorithm, trabecular and cortical sections were extracted to further evaluate bone morphometric parameters. (B) (I) Three-point bending test experimental setup, before and after bone fracture. Half of the total tibial length (L) was set between supports, with the remaining length equally distributed between the external sides of the supports. (II) Representative force vs. displacement curves for a HI tibia and sham tibia after detraining (52 week old)

7.4.3.2 *In vivo* assessment of trabecular bone morphometry

For each tibia, a trabecular bone volume of interest (VOI) was defined to include the secondary spongiosa in the proximal metaphysis, starting at ~0.35 mm distally to the growth plate and extending for 12% of the total tibial length (L) (Lynch et al., 2010; Mustafy, Benoit, et al., 2018) (Figure 7.3A.II). The trabecular bone VOI was semi-automatically segmented using an in-house algorithm to exclude the cortical shell. A global gray threshold of 65, corresponding to an equivalent density of 0.413 g/cm^3 of calcium hydroxyapatite (CaHA), was used for all analyses (CTAn software v.1.13) (Boyd, Davison, Müller, & Gasser, 2006; Lynch et al., 2010; Mustafy, Benoit, et al., 2018). Trabecular bone structural parameters included: bone mineral density (BMD), bone volume fraction (BV/TV), trabecular number (Tb.N), trabecular thickness (Tb.Th) and trabecular spacing (Tb.Sp) (Bouxsein et al., 2010).

7.4.3.3 *In vivo* assessment of cortical bone morphometry

The cortical VOI included the cortical part of the bone and the marrow cavity, centered at the midpoint of the tibial mid-diaphysis and equally extended proximally and distally for a total of 5% of the tibial length (L) (Figure 7.3A.II). A global gray threshold of 65 was also used for all analyses (Boyd et al., 2006; Lynch et al., 2010). Cortical bone structural parameters included: tissue mineral density (TMD), cross-sectional area inside the periosteal envelope (Tt.Ar), cortical bone area (Ct.Ar), cortical thickness (Ct.Th), periosteum perimeter (Ps.Pm), endocortical perimeter (Ec.Pm), medullary area (Ma.Ar), and mean eccentricity (Ecc) (Bouxsein et al., 2010). Polar moment of inertia (I_P, mm^4) was evaluated as the sum of I_{MIN} and I_{MAX}.

7.4.4 *Ex vivo* muscle weight measurements

After the last micro-CT imaging (52nd week), rats were sacrificed using CO_2 asphyxiation, followed by decapitation. The right tibiae and femur were then carefully dissected by trained professionals to isolate the gastrocnemius, tibialis anterior, quadriceps femoris, and soleus muscles with a scalpel. A precision electronic scale (Adam PW254 analytical balance, 0.1 mg precision) was used to evaluate the weight of the isolated muscles (Table 7.1).

7.4.5 Mechanical Testing

Right tibiae (n = 42) from all rat groups were cleaned of soft tissues and tested to failure in three-point bending under displacement control at 0.15 mm/sec using a MTS 793 servo-hydraulic testing system (MTS Systems Corporation, Eden Prairie, Minnesota USA). A load cell of 100 kN capacity combined to a MTS 3-point flexural mounting setup was used to rupture the tibias at their midshafts (Figure 7.3B.I). Support to support distance was set at 50% of the total tibial length while keeping the tibiae horizontally centered between the ends (Figure 7.3B.I). Force and displacement data were collected every 0.1 second to obtain force vs. displacement curves, from which were determined extrinsic biomechanical properties, including the ultimate force (N), yield force (N), work to yield (mJ), work to failure (mJ), and linear stiffness (N/mm). Intrinsic biomechanical properties were also calculated from the cross-sectional parameters measured from the micro-CT images at the tibial mid-diaphysis (Mustafy, Londono, & Villemure, 2018). Young's modulus E (GPa) was determined using the moment of inertia, stiffness, and span length (Schriefer et al., 2005). Yield stress, σ_y (MPa) and ultimate stress, σ_{ult} (MPa) were determined using yield and ultimate force, distance from the centroid of the cross-section to the outermost point on the cross-section, moment of inertia, and span length (Mustafy, Londono, et al., 2018; Schriefer et al., 2005). Assuming linear elastic bone material (Mustafy, Moglo, Adeeb, & El-Rich, 2014; Schriefer et al., 2005), resilience and toughness were determined by the following equations:

$$\text{Resilience} = \frac{\sigma_y^2}{2E} \quad (1)$$

$$\text{Toughness} = 0.75 * W * (\frac{b^2}{LI}) \quad (2)$$

where, σ_y is the Yield stress (MPa), E is the Young's modulus (GPa), and W is the work to failure (mJ), b is the width of the bone cross-section at the mid-diaphysis in the anteroposterior direction (mm), L is the span length (mm), and I is the cross-sectional moment of inertia (mm^4) (Mashiba et al., 2000; Mustafy, Londono, & Villemure, 2019).

7.4.6 Finite element (FE) analysis

Micro-CT images were used to develop specimen-specific finite element (FE) models of rat tibiae at sacrifice (52 w.o.) from all five groups. Average maximum and minimum principal strains were assessed for a proximal and a mid-diaphysis section of the tibia under a simulated 35N compressive force (Mustafy et al., 2019). This value of the applied compressive force was used in a previous study as a physiologic loading condition not causing any microdamage in the tibiae (Li, Jiang, Yan, Jiang, & Dai, 2011; Mustafy et al., 2019). The investigated VOIs for trabecular and cortical bones were similar to the ones used for the morphometric analyses. Micro-CT images of each tibia were processed using an in-house Matlab mesh generation program to generate a 3D voxel-based finite element model, where 8-noded brick elements were used to represent bone voxels (van Rietbergen, Weinans, Huiskes, & Odgaard, 1995). After a mesh convergence study, the models were created by combining 2x2x2 pixels in 18 μm resolution images to yield a single voxel with a side length of 36 μm. Linear elastic, isotropic but non-homogeneous material properties were assigned to the voxels with a Poisson's ratio of 0.3 (Mustafy, 2013). The elastic modulus was assigned to each voxel based on two calibration steps (Mustafy et al., 2019). Firstly, a calibration was performed to construct the grayscale-HU relationship as follows:

$$HU = 18.278 * grayscale - 1000 \quad (3)$$

Secondly, a phantom calibration (with Calcium Hydroxyapatite concentrations of 0.25 and 0.75 g.cm^{-3}) was performed to construct the following HU-density relationship:

$$\rho = 3.821 x 10^{-3} * HU - 0.062 \quad (4)$$

Finally, Young's modulus (E) was related to the bone density (ρ) of each voxel using the following equation (Chen, Wu, Liu, Yang, & Cui, 2015):

$$E = E_{max} * \left(\frac{\rho}{\rho_{max}} \right)^2 \quad (5)$$

where, $E_{max} = 28.6\ GPa$, which represented the maximum value of the Young's modulus for the cortical bone structure of 52 week old rat tibiae, and $\rho_{max} = 1.762\ g.cm^{-3}$, which represented the maximum value of density calculated from all the FE samples used in this study. The compressive force was applied at the proximal end of the tibia in the longitudinal (Z) direction. At the distal end, all nodes were constrained in the X and Y directions to prevent rigid-body motion. Strains were determined at the element centroids.

7.4.7 Statistical Analysis

Statistical analyses were performed using SPSS Statistics (v. 23, IBM). ANOVA test (general linear model) was performed on the body weight, food intake and food intake relative to body weight for the entire experimental period to assess the effects of loading, time and interaction between body weight and food intakes. To isolate the effects of impact loading, impact groups were compared among themselves and with respect to the sham group. In addition, the control and sham groups were compared to detect any handling and manipulation effects.

Bone structural properties of both trabecular and cortical microstructure from all rat groups were statistically analyzed at 11, 14, 22, 34, and 52 week of the experimental period. Biomechanical properties evaluated using three-point bending tests were also statistically analyzed. Muscle weights as well as strain results from the FE analyses were also statistically compared. In all cases, a one-way ANOVA with Tukey's multiple comparisons was performed to assess the significant group difference and pairwise comparisons. Data are presented as means ± s.d. Statistical significance was fixed at *p*<0.05.

7.5 Results

7.5.1 Animals

Four animals (9.5%) had to be sacrificed at earlier time points before the end of the study period due to the dryness in the paws (n=1), anesthesia complications (n=1), and unknown/natural causes (n=2). These animals were excluded from the study. The resulting group sizes for the 11, 14, 22, 34, and 52 week old period were then 42, 42, 40 (control/sham, n=6; LI, n=10; MI/HI, n=9), 39 (control/sham, n=6; LI/HI/MI, n=9), and 38 (control/sham, n=6; LI/HI, n=9; MI, n=8), respectively.
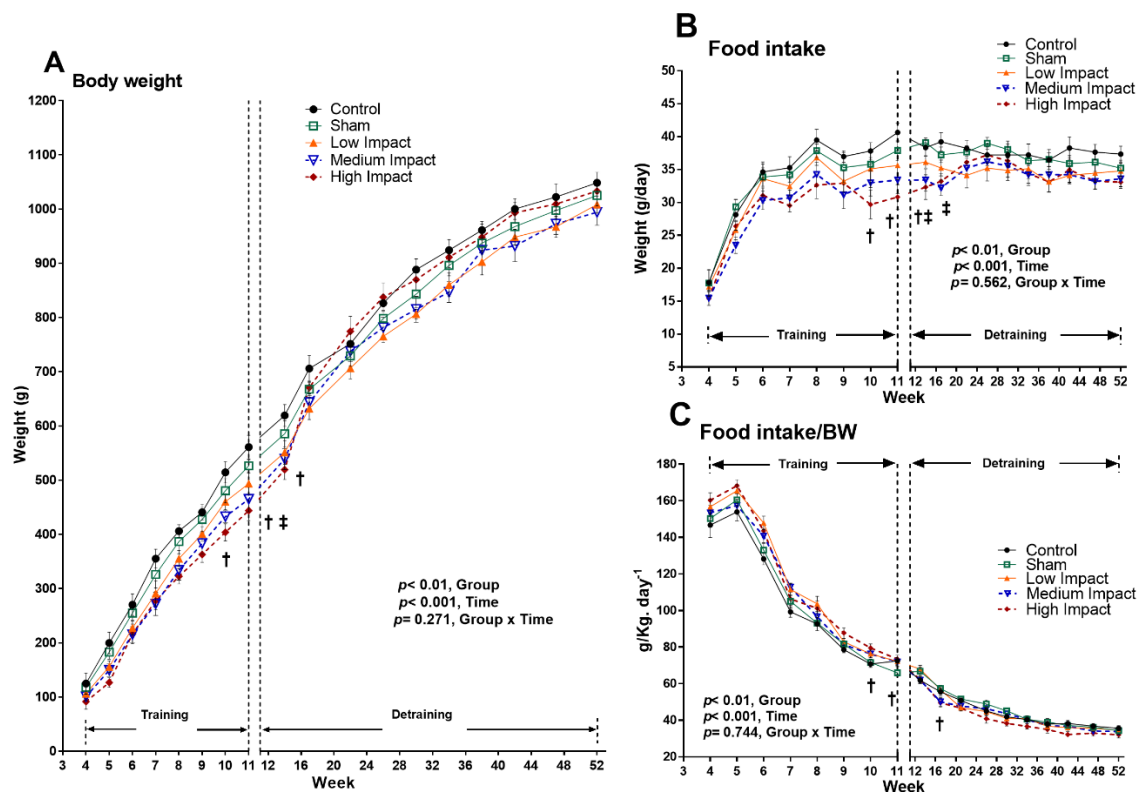
Figure 7.4 (A) Rat body weight (g). ANOVA test (general linear model) was performed to determine time effects, group effects, and their interactions on body weight. (B) Absolute daily food intake (g/day). ANOVA test (general linear model) was performed to determine time effects, group effects, and their interactions on food consumption. (C) Relative quantity of food intake per unit body weight (g/kg. day^{-1}). ANOVA test (general linear model) was performed to determine time effects, group effects, and their interactions on food intake per unit body weight

Graphs are plotted considering the values throughout the experimental period (4 to 52 week of age). Values are presented as means ± SDs; p < 0.05 ‡ medium impact vs. sham; † high impact vs. sham

7.5.2 Body Weight and Food Intake

During the impact loading regime, an increasing trend was noticed for control and sham groups compared to the loading groups (Figure 7.4A). HI group had significantly (p<0.05) less body weight compared to shams at the 10th, 11th and 14th week of age (17%, 15%, and 12%, respectively) (Figure 7.4A). MI group had significantly less body weight (13%) compared to shams at the 11th

week of age only (Figure 7.4A). Food intake was also reduced for the HI and MI groups during the study period. HI group showed reduced caloric intake compared to shams by 18%, 20%, and 17% for weeks 10, 11, and 14, respectively (Figure 7.4B). MI group had reduced caloric intake by 16% and 13% for weeks 14 and 17, respectively (Figure 7.4B). However, no significant differences were found among the three exercise groups in terms of body weight and food intake during the study period. A time effect (increase in weight gain and food consumption) was observed in rats (Figure 7.4A, 7.4B). A group effect was also noticed, but no effects of group/time interaction were found. Moreover, a significant difference in food intake relative to body weight was observed between HI and sham groups for weeks 10, 11, and 17 during the experiment (Figure 7.4C).

7.5.3 Long-Term Effects of Loading during Adolescence on Trabecular Bone Architecture

The long term effects of pubertal loading on trabecular bone architecture were assessed by evaluating the bone structural parameters at the end of the training period (week 11) and at four intermittent times during the detraining period (weeks 14, 22, 34, and 52). For each time point, HI loaded tibias showed significantly greater BV/TV, Tb.Th, Tb.N, and smaller Tb.Sp compared to the sham group (Figure 7.5). HI group also had higher BMD compared to sham but only until the 34th week of age (Figure 7.5). MI group showed significant differences with respect to shams for BV/TV, Tb.Th, and Tb.Sp at weeks 11 and 14 (Figure 7.5). There was also higher BMD for MI group observed at the 11th, 14th and 22nd weeks. Moreover, MI group resulted in higher Tb.N in weeks 11, 14, and 34 (Figure 7.5). No significant differences were found between control and sham groups and among the loading groups at any time points.
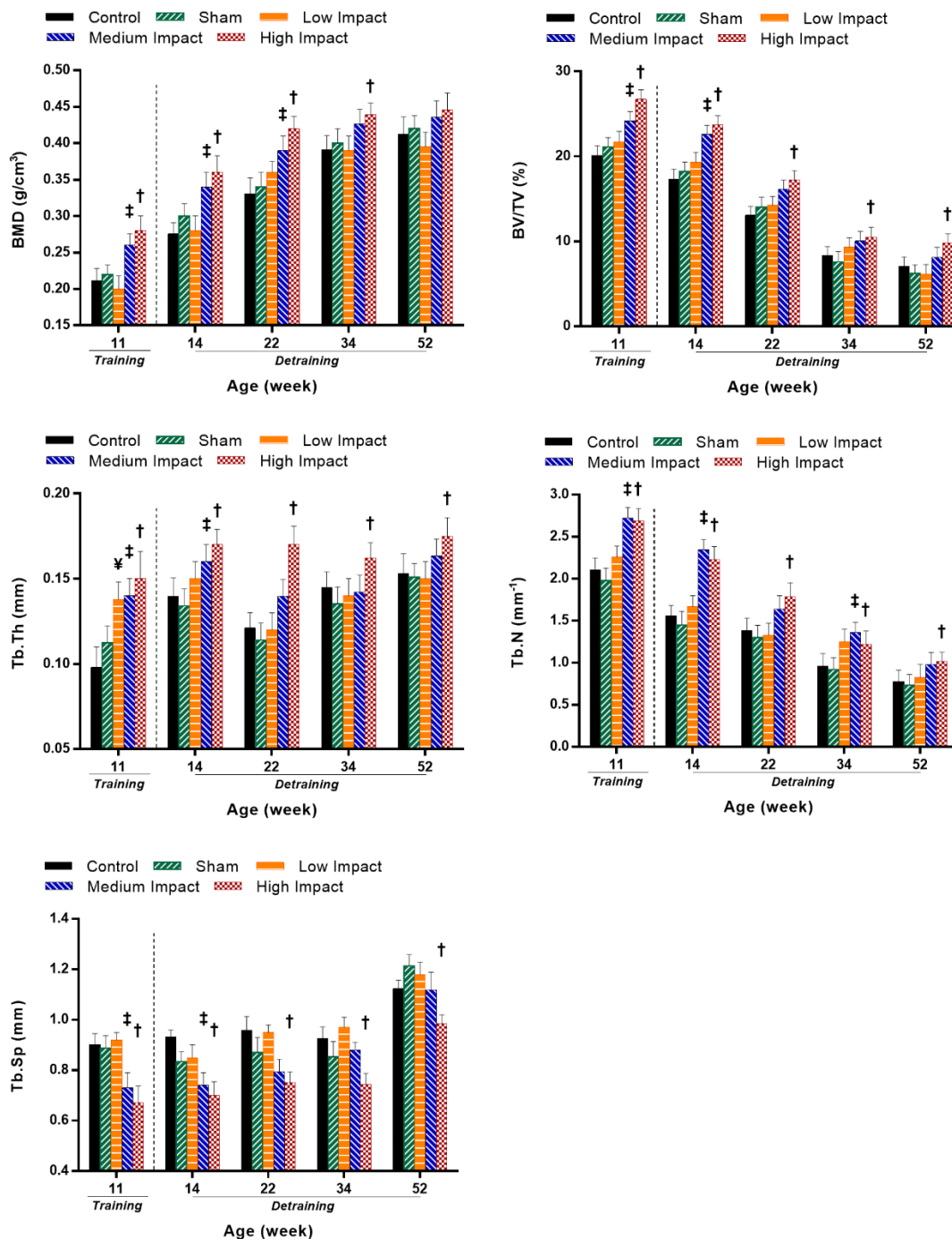
Figure 7.5 Trabecular bone morphometric parameters (means and standard deviations) for the five experimental groups at the end of training (11 week of age) and at selected detraining time points (14, 22, 34, and 52 week of age)

$p < 0.05$ ¥ low impact vs. sham; *‡ medium impact vs. sham; † high impact vs. sham*
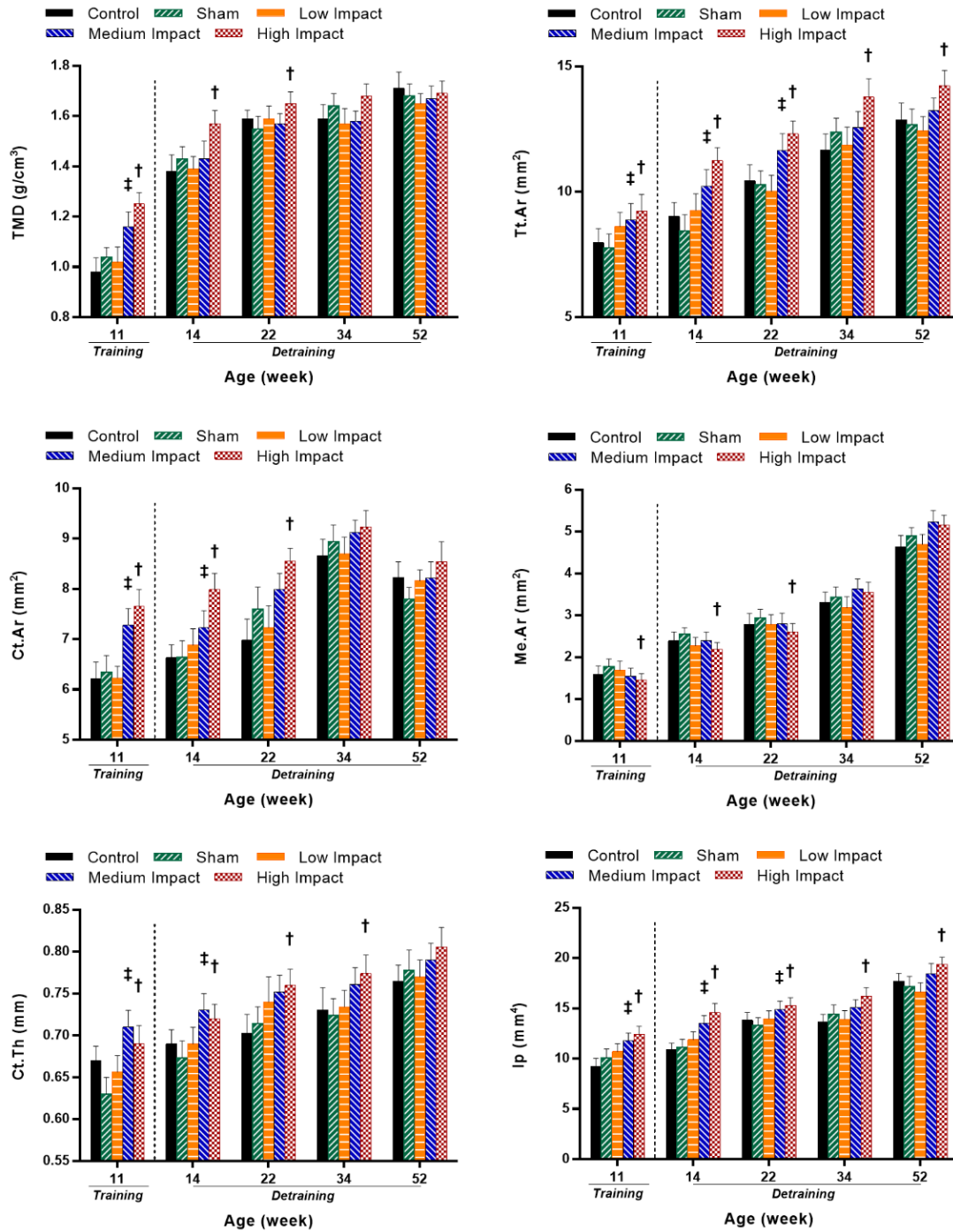
Figure 7.6 Cortical bone morphometric parameters (means and standard deviations) for the five experimental groups at the end of training (11 week of age) and at selected detraining time points (14, 22, 34, and 52 week of age)

p < 0.05 ‡ medium impact vs. sham; † high impact vs. sham

7.5.4 Long-Term Effects of Loading during Adolescence on Cortical Bone Architecture

Cortical bone structural parameters were evaluated for all rat groups at the end of the training period as well as during the detraining period to assess the effect of loading on cortical bone architecture. For each time point, loaded tibias in HI group showed significantly greater Tt.Ar and Ip compared to the sham group (Figure 7.6). HI group also resulted in higher TMD and Ct.Ar persisting until the 22nd week and a higher Ct.Th persisting until the 34th week compared to shams (Figure 7.6). Also, HI group had lower Me.Ar compared to sham persisting until week 22 (Figure 7.6). However, MI group showed a significant difference compared to shams for TMD only at the 11th week of age, for Ct.Ar and Ct.Th up to the 14th week of age, and for Tt.Ar and Ip up to the 22nd week of age (Figure 7.6). No significant differences were noticed among the loading groups or between the control and sham groups during the study period.

7.5.5 Muscle Weight

The effect of impact loading exercise on muscle weight is provided in Table 7.1, where weights of four different muscles associated with tibia were measured for all rat groups after sacrifice. Soleus muscle showed a significant weight increase in HI (27%) and MI (16%) groups compared to the sham group. Quadriceps muscle only showed significant weight increase in HI (12%) group compared to the sham group. However, no effect of impact loading exercise was observed on gastrocnemius and tibialis anterior muscles in the loaded rats (Table 7.1).

7.5.6 Mechanical Properties of Tibia

Structural and tissue-level mechanical properties obtained from the three-point bending tests are reported in Table 7.2. For structural mechanical properties, HI group showed greater ultimate force, stiffness, post-yield displacement, and post-yield energy compared to shams (Table 7.2). MI group showed significantly higher values for only ultimate force compared to shams (Table 7.2). For estimated intrinsic mechanical properties, HI group resulted in higher ultimate stress and toughness, whereas the MI group had only higher ultimate stress compared to the sham group (Table 7.2). No differences in structural or intrinsic mechanical properties were observed between the control and sham groups, and among the three loading groups for the applied loading regime.

Table 7.1 Muscle weights (g) for control, sham, LI, MI and HI groups evaluated at the end of experiment.

	Muscle weights (g)			
Groups	*Gastrocnemius*	*Tibialis Anterior*	*Soleus*	*Quadriceps*
Control	4.43 ± 0.39	1.08 ± 0.22	0.26 ± 0.02	4.83 ± 0.18
Sham	4.17 ± 1.19	1.23 ± 0.45	0.24 ± 0.04	5.03 ± 0.28
Low Impact (LI)	4.55 ± 0.75	1.02 ± 0.13	0.32 ± 0.04	4.93 ± 0.41
Medium Impact (MI) *	4.92 ± 0.60	1.13 ± 0.18	**0.34 ± 0.04**[α]	5.47 ± 0.29
High Impact (HI) *	4.82 ± 0.99	1.07 ± 0.22	**0.38 ± 0.07**[α]	**5.64 ± 0.24**[α]

Values are expressed as means ± SDs, N = 6/group for control and sham; N = 9/group for LI and HI; and N = 8 for MI. In the group column, * indicates a significant effect ($p < 0.05$) from a one-way ANOVA with Tukey's multiple comparisons. When there was a significant effect, Tukey's post-hoc pairwise comparisons evaluated whether the sham group was significantly different compared to the other groups. Significant differences are indicated in bold value with 'α'.

7.5.7 Finite Element Analysis of Tibia

Principal compressive and tensile strain distributions were evaluated for VOIs of the proximal tibia and mid-diaphysis. For the trabecular VOI (proximal region), average principal tensile strains ranged from 627 µε (±SD:283) for HI group to 774 µε (±SD: 216) for the sham group (Figure 7.7C), while average principal compressive strains varied from 842 µε (±SD: 210) for HI group to 971 µε (±SD: 311) for the control group (Figure 7.7C). Higher average strains were predicted in the cortical bone VOI (mid-diaphysis). Average principal tensile strains ranged from 959 µε (±SD: 194) for HI group to 1167 µε (±SD: 126) for the control group (Figure 7.7C) and average principal compressive strains varied between 1537 µε (±SD: 162) for HI group and 1835 µε (±SD: 183) for the sham group (Figure 7.7C). A significant difference was observed between the HI and sham groups (Figure 7.7C) for the average principal compressive strains at the cortical mid-diaphysis.
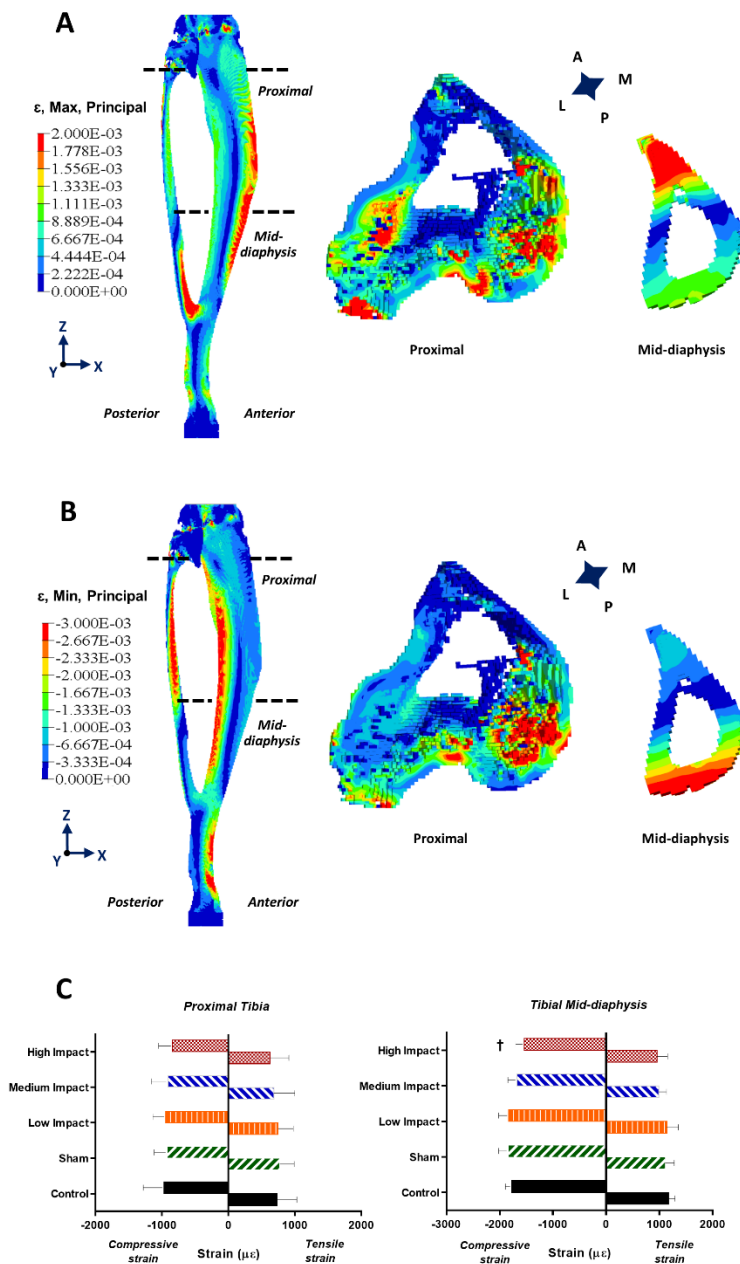
Figure 7.7 (A) Principal tensile strain distribution within a representative 52 w.o. rat tibia and within corresponding transverse sections of proximal trabecular and mid-diaphysis cortical bone VOIs. (B) Principal compressive strain distribution within a representative 52 w.o. rat tibia and within corresponding transverse sections of proximal trabecular and mid-diaphysis cortical bone VOIs. (C) Principal compressive and tensile strains within in the 52 w.o. rat tibial proximal trabecular VOIs and mid-diaphysis cortical VOIs for the five experimental groups

$p < 0.05$ † high impact vs. sham

Table 7.2 Structural and intrinsic mechanical properties of the right tibiae for control, sham, LI, MI and HI groups derived from three-point bending tests of the mid-diaphysis.

Values are expressed as Mean ± SD, N = 6/group for control and sham; N = 9/group for LI and HI; and N = 8 for MI. In the parameter column, *

Parameters/Groups	Control	Sham	LI	MI	HI
Structural Mechanical Properties					
Yield Force, F_y (N)	92.6 ± 13.8	96.3 ± 11.6	109 ± 12.7	103 ± 9.23	115 ± 12.5
Ultimate Force, F_{ult} (N) *	138 ± 10.5	135 ± 12.7	142 ± 15.5	**156 ± 12.5 $^\alpha$**	**164 ± 13.7 $^\alpha$**
Stiffness, k (N/mm) *	254 ± 19.2	263 ± 17.6	282 ± 25.8	290 ± 17.6	**320 ± 25.2 $^\alpha$**
Post Yield Displacement (µm) *	0.59 ± 0.15	0.52 ± 0.11	0.57 ± 0.17	0.61 ± 0.13	**0.73 ± 0.11 $^\alpha$**
Work to Yield (mJ)	19.7 ± 2.89	18.8 ± 2.61	18.2 ± 2.72	19.3 ± 2.69	20.9 ± 2.77
Post Yield Energy (mJ) *	82.2 ± 7.12	79.3 ± 8.24	85.2 ± 8.23	91.2 ± 9.23	**98.6 ± 7.82 $^\alpha$**
Work to Failure (mJ)	98.1 ± 10.3	106 ± 11.3	110 ± 12.6	101 ± 10.1	118 ± 9.45
Estimated Tissue-level Mechanical Properties					
Yield Stress, σ_y (MPa)	212 ± 25.4	222 ± 23.2	245 ± 26.1	232 ± 27.1	248 ± 24.1
Ultimate Stress, σ_{ult} (MPa) *	310 ± 23.7	297 ± 25.1	314 ± 19.3	**339 ± 20.2 $^\alpha$**	**352 ± 21.1 $^\alpha$**
Young's Modulus, E (GPa)	26.2 ± 3.56	25.2 ± 2.56	27.3 ± 3.55	25.1 ± 2.66	28.6 ± 3.41
Strain to Yield (µε)	8724 ± 1231	9014 ± 1244	8965 ± 989	9230 ± 1311	8655 ± 1277
Strain to Failure (µε)	10827 ± 1061	10566 ± 1237	10218 ± 1444	11302 ± 1023	11804 ± 1151
Resilience (MPa)	0.73 ± 0.19	0.82 ± 0.23	0.81 ± 0.17	0.78 ± 0.28	1.07 ± 0.35
Toughness (MPa) *	4.92 ± 1.07	4.63 ± 1.05	5.19 ± 1.55	5.73 ± 1.19	**7.34 ± 1.16 $^\alpha$**

indicates a significant effect ($p < 0.05$) from a one-way ANOVA with Tukey's multiple comparisons test. When there was a significant effect, Tukey's post-hoc pairwise comparisons evaluated whether the sham group was significantly different compared to the others [a bold value and 'α' indicate a significant difference versus sham group].

7.6 Discussion

Results of this study suggest that performing high impact exercise during adolescence results in a significant advantage in terms of both trabecular and cortical bone microstructural properties. Our findings demonstrate the importance of investigating impact loading effects during bone growth period to elucidate the long-term maintenance of loading-induced bone benefits using a rodent model.

7.6.1 Impact loading temporarily reduced body weight and food intake at the rat puberty/adult transition period

Loaded and non-loaded rats responded differently to pubertal impact loading of medium and high intensity with respect to body weights (BW) and food intakes (FI). However, the effects incurred through adolescence only sustained around the end of the adolescence and beginning of young adulthood phases but disappeared at adulthood. HI group had lower BW and reduced FI compared to shams at 10, 11 and 14 week of age (Figure 7.4A, 7.4B) while MI group showed lower BW only at 11 week of age (Figure 7.4A), and reduced FI at 14 and 17 week of age (Figure 7.4B), compared to shams. Exercise is generally correlated with an increase in FI in rats (Crews 3rd, Fuge, Oscai, Holloszy, & Shank, 1969; Nance, Bromley, Barnard, & Gorski, 1977). Our results for MI and HI groups showed the contrary, with a reduced BW coupled with a significant caloric reduction. The reduced BW could be related to the intensity of the applied tibial loading. The increased stress levels in MI and HI groups (Crews 3rd et al., 1969) might be associated with amplified hormone secretion (Russek & Pina, 1962; Vendsalu, 1960), which might have triggered the observed reduction in BW (Nikoletseas, 1980). The reduced BW can also be an indication of less body fat and of increased lean tissue in the exercised animals, where the exercised rats might have used their caloric intake into the synthesis of lean tissue, rather than storing them in adipose tissue (Widdowson & McCance, 1957). Moreover, previous studies have shown that male rats undergoing forced exercised regime do not tend to compensate for the excessive energy expenditure with increased FI, unlike their female counterparts (Nikoletseas, 1980). Our observations for the loading period are supported by previous studies, which have reported a decreased BW simultaneous with a reduced FI in adult rats after the end of forced swimming (Oscai, Mole, & Holloszy, 1971) and running regime (Crews 3rd et al., 1969).

During the detraining period, the effects from MI and HI groups on food intake disappeared after 17 and 14 weeks of age, respectively (Figure 7.4B). Hence, no effects remained in the long term. Moreover, when caloric intake was expressed relative to body weight, the FI of the HI group was significantly elevated at 10 and 11 week, and lowered at 17 week of age compared to shams. However, no significant effect was observed afterwards (Figure 7.4C). This is an interesting phenomenon as it shows different observations between absolute and relative measurements. The MI and HI groups exhibited a reduction in absolute measurements of BW and FI, but when the FI was expressed relative to the BW, the outcome was reversed (Figure 7.4C). However, increments in BW in HI and MI groups during late detraining can be considered as a natural phenomenon (Shindo, Matsuura, & Suzuki, 2014). It was indeed reported for both adult humans and rats that, once the exercise regime is withdrawn, the BW starts increasing to match the natural level (Leibel, 1990). Our study also demonstrated that even at 52 week of age (e.g., 41 week after the cessation of pubertal exercise), HI and MI rats had significantly higher soleus muscle weight compared to the sham group (Table 7.1). HI group also had higher quadriceps muscle weight compared to shams at this period (Table 7.1). So MI and HI loadings might have produced sustained adaptive physiological responses in skeletal muscle weight, which could result from increased energy metabolism and resting metabolic rate (RMR) (Shindo et al., 2014). Increased energy metabolism and RMR are reported to enhance the oxygen utilization capacity of skeletal muscles (Holloszy & Booth, 1976), which is further associated with increased catecholamines hormones (Bukowiecki et al., 1980; Holloszy & Booth, 1976) and lipoprotein lipase activity (Borensztajn, Rone, Babirak, McGarr, & Oscai, 1975), both regulators of fatty cells inside the body. All these changes might have reduced the energy available for fat storage. Therefore, the MI and HI groups gradually regained their BW to match the normal level after exercise. Our findings are supportive of other human and rat studies (MacLean et al., 2004; Weinsier et al., 1995; Yasari et al., 2006), where BW was reported to be suppressed during exercise period but started to re-increase after exercise cessation. Another study (Pajamäki et al., 2003) also reported similar findings stating that childhood running exercise for 14 weeks of age did not have any effect on the BW of the exercised rats after 40 weeks of detraining period.

7.6.2 High impact loading induced enhanced trabecular bone at the end of puberty, which was maintained during the adulthood detraining period

Both HI and MI groups exhibited pubertal loading induced changes in the trabecular bone structure even after the cessation of the exercise. HI loading of the rat tibiae for 8 weeks in the adolescent period resulted in trabecular microstructure with greater BMD, BV/TV, Tb.Th, Tb.N and less Tb.Sp compared to the sham group during the detraining period. For the HI group, all measured trabecular morphometric parameters, except BMD, maintained induced benefits during the entire detraining period up to 52 week of age (Figure 7.5). However, the enhanced BMD was discontinued after 34 week of age (Figure 7.5). For the MI group, the induced benefits disappeared at an earlier time point for most of the trabecular parameters. For the LI group, the only effect was observed immediately after the end of loading period (11 week) for Tb.Th, but disappeared afterwards (Figure 7.5).

BMD increment is a natural phenomenon during adolescence (Banu, Wang, & Kalu, 2002). In addition, it has been reported that strenuous activity during growth can significantly decrease the tartrate-resistant acid phosphatase (TRAP) levels in the blood serum, leading to a significant increase in BMD in trabecular metaphysis (Hagihara et al., 2005; Hagihara et al., 2009). Moreover, HI and MI loadings could have altered calciotropic hormones, which are responsible for promoting a positive calcium balance and lead to a significant increase in skeletal mass (Hagihara et al., 2009; Yeh & Aloia, 1990b). BMD increases after repeated exercise regime is confirmed from studies by Hagihara et al. (Hagihara et al., 2009), Iwamoto et al. (J Iwamoto, Yeh, & Aloia, 1999), and Joo, et al. (Joo, Sone, Fukunaga, Lim, & Onodera, 2003), after treadmill exercise regimes in growing rats. Discontinuation of BMD benefits in HI group after 34 week of age could be related to body weight and hormones (Epstein et al., 1986; Schapira, 1991). As rats grow older and body weight increases, a body weight burden can influence the bone mineral content in tibia (IIDA & FUKUDA, 2002; Wronski, Schenk, Cintron, & Walsh, 1987). Around 60% of the body weight is carried by the legs of rats in normal cage activities (IIDA & FUKUDA, 2002; Wronski et al., 1987). Hence, it could be possible that the increasing body weight has negatively influenced the BMD of tibiae in HI group at adulthood and thus the benefits gained up to 34 week of age eventually disappeared (Figure 7.5). The absence of benefits in BMD at adulthood observed in this study is supported by

others (Kiuchi, Arai, & Katsuta, 1998; Pajamäki et al., 2003), where the absence of load-induced benefits were also reported for bone mineral content in the long term period.

The significant BV/TV increase during adolescence can be associated with the increase in BMD (Jiang, Jiang, & Dai, 2007). In the detraining period, BV/TV gradually decreased for all rat groups. But the HI group maintained a greater BV/TV compared to the shams during the detraining period. HI loading may have triggered an effect on the osteoclasts of trabecular bone structure, which eventually led to the inhibition of bone resorption instead of the promotion of bone formation with aging (Ruimerman, van Rietbergen, Hilbers, & Huiskes, 2005). Indeed, it was shown that exercised animals have beneficial effects on BV/TV compared to the non-exercised ones (Hagihara et al., 2009; Warden, Galley, et al., 2014). A significant change in Tb.Th is an indication of loading induced positive effects on normal bone growing phenomena (Lu, Cui, Zuo, Lin, & Wu, 2015), and the change in Tb.N is directly associated with the change in BV/TV and Tb.Th (Kirmani et al., 2009). This explains why the MI group showed discontinued positive effects on Tb.N after 14 weeks of age, simultaneously with BV/TV and Tb.Th (Figure 7.5). Tb.Sp is measured by the diameter of the largest sphere that fits within the marrow space in between trabeculae. So, a significant decrease in Tb.Sp for HI group compared to sham can be associated with the induced bone gain (increasing BMD) and gradual thickening of trabeculae (increasing Tb.Th) (Figure 7.5) through increased connectivity as observed in our study. Our findings for BV/TV, Tb.Sp, Tb.Th, and Tb.N are in agreement with other studies (Buhl et al., 2001; Fujie et al., 2004; Lu et al., 2015; Saxon, Robling, Alam, & Turner, 2005; Warden, Galley, et al., 2014), where also similar patterns were observed for exercised and normal bone growing process for aged rats and mice bone structure.

7.6.3 High impact loading induced positive changes in cortical bone microstructure at the end of puberty, which partly remained during the adulthood detraining period

Our findings showed that HI loading positively affected cortical bone tissue in the long-term detraining period, and to some extent for MI loading group. HI group maintained the loading induced benefits with greater total bone area and moment of inertia at the mid-diaphysis compared to shams up to the end of the detraining period (Figure 7.6). Moreover, HI loading enhanced bone mechanical properties with increased tibial strength and toughness at 52nd week of age (Table 7.2).

Tissue mineral density (TMD) significantly increased for HI and MI groups at the end of loading period (Figure 7.6), until the 22nd week of age for the HI group, whereas the MI group lost this benefit after the training period. The loss of TMD benefits during detraining could be related to porous structural modification with rat aging process. Indeed, bone mineral density can be affected by the induction of new cortical pores and not simply enlarging the diameter of existing cortical pores with increasing age (Perrien et al., 2007; Raisz, 2005). These counteracting effects in cortical pore generation with age may be responsible for the observed reduced TMD in the HI group during the detraining period. Me.Ar, which represents the area enclosed by endocortical perimeter, showed an increasing pattern with age for all groups of rats (Figure 7.6). Ct.Ar represents the area between periosteal and endocortical surfaces. Hence, a significantly lower Me.Ar in HI group compared to shams might be correlated to the increased Ct.Ar for the HI group up to 22 week period (Figure 7.6). Increased Ct.Ar is also associated with the reduced strain distribution on the bone surface (Necas & Hlavácek, 2017). Hence, the reduced (19.3%) average principal compressive strain in HI group compared to the shams from our FE analyses can be justified (Figure 7.7C).

The continuous increase in radial growth (Ps.Pm) (Appendix B) for the HI group along with an increase in the Ct.Th eventually led to an increase in total bone area, which remained consistent during the entire detraining period. Our findings are supported by another study (Ooi, Singh, Singh, & Umemura, 2009), where impact loading (jumping) exercise was reported to increase cortical bone area primarily due to an increase in periosteal perimeter and with little changes in the endocortical perimeter or the medullary area. The exact reason why Ps.Pm remained significantly higher in HI group even after keeping both Ec.Pm (Appendix B) and Me.Ar (Figure 7.6) unchanged is not apparent. It might result from high impact influencing the bony structure by redistributing the bony materials from the endosteal region towards the periosteal region (Frost, 1997; Ooi et al., 2009). This phenomena also triggered a shift in the mass distribution with respect to the bone neutral axis, which significantly increased the polar area moment of inertia (Ip) (Buhl et al., 2002; Jast, 2011) in HI group (Figure 7.6).

HI group had greater ultimate force, stiffness, post-yield displacement, post-yield energy, ultimate stress, and toughness compared to the shams (Table 7.2) while MI group only exhibited significant increases in ultimate force and stress (Table 7.2). Having higher ultimate force and ultimate stress

indicate that the exercised tibiae in MI and HI groups at adulthood can sustain greater load before fracture compared to the LI and non-exercised tibiae. The total bone area is reported to be a key factor in determining the ultimate force (Stürmer et al., 2006; X. Yang, Chan, Muthukumaran, & Lee, 2010) and it was shown to increase in the HI group. Ultimate stress (σ_{ult}) can be directly correlated to the ultimate force (F_{ult}) experienced by the bony samples (Huang et al., 2003; Mustafy, Londono, et al., 2018), so a significant increase in both σ_{ult} and F_{ult} for MI and HI group can be explained (Table 7.2). Bone stiffness is associated with Tt.Ar, Ct.Th and Ct.Ar for any given samples (Schlecht, Bigelow, & Jepsen, 2014; Voide, van Lenthe, & Müller, 2008), and hence the increase in bone stiffness for the HI group can be explained (Table 7.2). Overall, the enhanced morphometric parameters for HI and MI groups during detraining period and at adulthood support the consequently improved mechanical properties. Post-yield displacement (PYD), which is a measure of ductility (Wolfram & Schwiedrzik, 2016), and post-yield energy significantly increased in HI group compared to shams. The greater PYD can be correlated to the higher stiffness and failure strength observed for the HI group (Jepsen, Silva, Vashishth, Guo, & van der Meulen, 2015; Schlecht et al., 2014; Voide et al., 2008). Bone toughness, which represents a measure of resistance to fracture, depends primarily on work to failure and bone width in the anteroposterior direction (Mori, Harruff, Ambrosius, & Burr, 1997). The enhanced toughness of the HI group at adulthood could hence partly result from the increased Ct.Th and Ps.Pm.

Our results disagree with some published studies, where increased bone mass and enhanced bone geometry were reported to disappear after 4 and 28 weeks of detraining period, respectively in growing rats experiencing treadmill running exercise for 8 weeks (Jun Iwamoto et al., 2000) and 14 weeks (Järvinen et al., 2003). Potential explanations for these dissimilarities might include the type of exercise used (tibial compression vs. treadmill running), site of investigation (tibial proximal metaphysis and mid-diaphysis vs. to femoral neck and midshaft), induced strain level (controlled calibrated strain vs. uncontrolled strain), and overall experimental study design (short detraining period vs. long detraining period). Also, the use of different imaging techniques with different scanner setup for bone morphological properties (micro computed tomography vs. peripheral quantitative computed tomography) might have contributed to the observed differences. However, the observed enhanced mechanical properties for MI and HI groups in this study agree with several previous findings. In a rodent study (Warden, Galley, et al., 2014), where 16 week old mice tibia were loaded for 4 weeks, improved bone morphology along with enhanced post-yield

properties have been reported after 52 weeks of detraining period. In separate human studies, enhanced bone properties were maintained in the primarily used arm after 5 years of detraining for female tennis players (Kontulainen et al., 2001) and for a lifetime period for professional baseball players (Warden & Roosa, 2014; Warden, Roosa, et al., 2014).

7.6.4 Strengths and limitations

The present study has some strengths over published studies, namely the refined longitudinal investigation of both trabecular and cortical morphometric properties. Changes in bone tissue properties were tracked after the exercise period (11 weeks of age) until rats reached one year old. This follow up period (up to 41 weeks) provided enough time to observe bone adaptation phenomena induced by pubertal loading regime and was refined enough to assess the time point at which bone morphological changes occurred or disappeared. The use of a sham group of rats also represents a strength of the completed study; it allowed truly isolating the effects of impact loading when comparing shams with LI, MI or HI rats, while the comparison of shams with controls isolated the effects of rat manipulation and handling. Also, our impact loading conditions were pre-calibrated with strain gauge measurements using rat tibiae of different age groups. These measurements were validated numerically using a finite element modeling tool in a previous study (Mustafy et al., 2019). This methodological approach allowed us to apply finely controlled loading with known resulting strain conditions in the tibiae.

The present study also includes some limitations. A relatively low number of rats were used for control and sham groups, although the samples size calculation was adapted from previous studies. Data from the literature showed that six rats per group is a minimum number while being sufficient to obtain statistically significant differences in bone morphological parameters among the groups (Stokes, 2007; Stokes, Aronsson, Dimock, Cortright, & Beck, 2006). Hence, our control and sham groups consisted of six animals, while each impact loading group consisted of ten animals. The use of a rat model for long term study has drawbacks. Rats have been reported to possess a limited ability for cortical bone resorption during detraining period due to a lack of secondary remodeling of Haversian canals (Jee & Li, 1990) and to continue their growth until relatively late in life. However, a previous study reported the existence of bone remodeling in cortical bone structure of adult rat in response to mechanical stimuli (Chambers, Evans, Gardner, Turner-Smith, & Chow,

1993). Hence, the use of rat models for investigating long term effects of mechanical stimuli on bone microstructure was considered adequate for the objectives of this study.

7.7 Conclusion

In summary, our data indicated that adolescent impact loading prompted a strong anabolic response in both trabecular and cortical bone microstructure at the end of growth and that it was maintained up to 52nd week of age in male rats. Body weights and food intakes in the medium and high impact groups were decreased during the transition period of adolescence and young adulthood phase, but these effects disappeared at adulthood. High impact loading allowed maintaining improved trabecular microstructure along with enhanced cortical bone size and improved strength at adulthood. Overall, our findings suggest that even though both trabecular and cortical bone drifted through age related changes during rat aging, high impact exercise performed during adolescence can preserve benefits in bone microstructure and strength for at least forty-one weeks following training period.

7.8 Acknowledgments

7.9 References

Bailey, D., McKay, H., Mirwald, R., Crocker, P., & Faulkner, R. (1999). A six-year longitudinal study of the relationship of physical activity to bone mineral accrual in growing children: the university of Saskatchewan bone mineral accrual study. *Journal of Bone and Mineral Research, 14*(10), 1672-1679.

Banu, J., Wang, L., & Kalu, D. (2002). Age-related changes in bone mineral content and density in intact male F344 rats. *Bone, 30*(1), 125-130.

Borensztajn, J., Rone, M., Babirak, S., McGarr, J. A., & Oscai, L. (1975). Effect of exercise on lipoprotein lipase activity in rat heart and skeletal muscle. *American Journal of Physiology-Legacy Content, 229*(2), 394-397.

Bouxsein, M. L., Boyd, S. K., Christiansen, B. A., Guldberg, R. E., Jepsen, K. J., & Müller, R. (2010). Guidelines for assessment of bone microstructure in rodents using micro–computed tomography. *Journal of Bone and Mineral Research, 25*(7), 1468-1486.

Boyd, S. K., Davison, P., Müller, R., & Gasser, J. A. (2006). Monitoring individual morphological changes over time in ovariectomized rats by in vivo micro-computed tomography. *Bone, 39*(4), 854-862.

Buhl, K. M., Jacobs, C. R., Turner, R. T., Evans, G. L., Farrell, P. A., & Donahue, H. J. (2001). Aged bone displays an increased responsiveness to low-intensity resistance exercise. *Journal of applied physiology, 90*(4), 1359-1364.

Buhl, K. M., Jacobs, C. R., Turner, R. T., Evans, G. L., Farrell, P. A., & Donahue, H. J. (2002). Parallel changes in extracellular matrix protein gene expression, bone formation and biomechanical properties in aging rat bone. *Journal of Musculoskeletal Research, 6*(03n04), 157-169.

Bukowiecki, L., Lupien, J., Follea, N., Paradis, A., Richard, D., & LeBlanc, J. (1980). Mechanism of enhanced lipolysis in adipose tissue of exercise-trained rats. *American Journal of Physiology-Endocrinology and Metabolism, 239*(6), E422-E429.

Burr, D., Milgrom, C., Fyhrie, D., Forwood, M., Nyska, M., Finestone, A., . . . Simkin, A. (1996). In vivo measurement of human tibial strains during vigorous activity. *Bone, 18*(5), 405-410.

Carter, D., Van der Meulen, M., & Beaupre, G. (1996). Mechanical factors in bone growth and development. *Bone, 18*(1), S5-S10.

Carter, D. R., & Orr, T. E. (1992). Skeletal development and bone functional adaptation. *Journal of bone and mineral research, 7*(S2), S389-S395.

Chamay, A., & Tschantz, P. (1972). Mechanical influences in bone remodeling. Experimental research on Wolff's law. *Journal of biomechanics, 5*(2), 173-180.

Chambers, T. J., Evans, M., Gardner, T. N., Turner-Smith, A., & Chow, J. W. (1993). Induction of bone formation in rat tail vertebrae by mechanical loading. *Bone and mineral, 20*(2), 167-178.

Chen, G., Wu, F., Liu, Z., Yang, K., & Cui, F. (2015). Comparisons of node-based and element-based approaches of assigning bone material properties onto subject-specific finite element models. *Medical engineering & physics, 37*(8), 808-812.

Ciani, C., Sharma, D., Doty, S. B., & Fritton, S. P. (2014). Ovariectomy enhances mechanical load-induced solute transport around osteocytes in rat cancellous bone. *Bone, 59*, 229-234.

Clarke, I. (1971). Surface characteristics of human articular cartilage--a scanning electron microscope study. *Journal of anatomy, 108*(Pt 1), 23.

Crews 3rd, E., Fuge, K. W., Oscai, L., Holloszy, J., & Shank, R. (1969). Weight, food intake, and body composition: effects of exercise and of protein deficiency. *American Journal of Physiology-Legacy Content, 216*(2), 359-363.

Cullen, D., Smith, R., & Akhter, M. (2001). Bone-loading response varies with strain magnitude and cycle number. *Journal of applied physiology, 91*(5), 1971-1976.

Deere, K., Sayers, A., Rittweger, J., & Tobias, J. H. (2012). Habitual levels of high, but not moderate or low, impact activity are positively related to hip BMD and geometry: Results from a population-based study of adolescents. *Journal of Bone and Mineral Research, 27*(9), 1887-1895.

Duckham, R. L., Baxter-Jones, A. D., Johnston, J. D., Vatanparast, H., Cooper, D., & Kontulainen, S. (2014). Does Physical Activity in Adolescence Have Site-Specific and Sex-Specific Benefits on Young Adult Bone Size, Content, and Estimated Strength? *Journal of Bone and Mineral Research, 29*(2), 479-486.

Epstein, S., Bryce, G., Hinman, J., Miller, O., Riggs, B., Hui, S., & Johnston Jr, C. (1986). The influence of age on bone mineral regulating hormones. *Bone, 7*(6), 421-425.

Forwood, M. R. (2008). Physical activity and bone development during childhood: insights from animal models. *Journal of applied physiology, 105*(1), 334-341.

Frost, H. M. (1997). On our age-related bone loss: insights from a new paradigm. *Journal of Bone and Mineral Research, 12*(10), 1539-1546.

Fujie, H., Miyagaki, J., Terrier, A., Rakotomanana, L., Leyvraz, P. F., & Hayashi, K. (2004). Detraining effects on the mechanical properties and morphology of rat tibiae. *Bio-medical materials and engineering, 14*(2), 219-233.

Goodrick, C. L. (1980). Effects of long-term voluntary wheel exercise on male and female Wistar rats. *Gerontology, 26*(1), 22-33.

Gunter, K., Baxter-Jones, A. D., Mirwald, R. L., Almstedt, H., Fuchs, R. K., Durski, S., & Snow, C. (2008). Impact exercise increases BMC during growth: an 8-year longitudinal study. *Journal of Bone and Mineral Research, 23*(7), 986-993.

Hagihara, Y., Fukuda, S., Goto, S., Iida, H., Yamazaki, M., & Moriya, H. (2005). How many days per week should rats undergo running exercise to increase BMD? *Journal of bone and mineral metabolism, 23*(4), 289-294.

Hagihara, Y., Nakajima, A., Fukuda, S., Goto, S., Iida, H., & Yamazaki, M. (2009). Running exercise for short duration increases bone mineral density of loaded long bones in young growing rats. *The Tohoku journal of experimental medicine, 219*(2), 139-143.

Health, U. D. o., & Services, H. (2004). Bone health and osteoporosis: a report of the Surgeon General: Rockville, MD: US Department of Health and Human Services, Office of the Surgeon General.

Holloszy, J. O., & Booth, F. W. (1976). Biochemical adaptations to endurance exercise in muscle. *Annual review of physiology, 38*(1), 273-291.

Holloszy, J. O., Smith, E., Vining, M., & Adams, S. (1985). Effect of voluntary exercise on longevity of rats. *Journal of applied physiology, 59*(3), 826-831.

Honda, A., Sogo, N., Nagasawa, S., Kato, T., & Umemura, Y. (2008). Bones benefits gained by jump training are preserved after detraining in young and adult rats. *Journal of applied physiology, 105*(3), 849-853.

Huang, T., Lin, S., Chang, F., Hsieh, S., Liu, S., & Yang, R. (2003). Effects of different exercise modes on mineralization, structure, and biomechanical properties of growing bone. *Journal of applied physiology, 95*(1), 300-307.

IIDA, H., & FUKUDA, S. (2002). Age-related changes in bone mineral density, cross-sectional area and strength at different skeletal sites in male rats. *Journal of Veterinary Medical Science, 64*(1), 29-34.

Iwamoto, J., Yeh, J., & Aloia, J. (1999). Differential effect of treadmill exercise on three cancellous bone sites in the young growing rat. *Bone, 24*(3), 163-169.

Iwamoto, J., Yeh, J. K., & Aloia, J. F. (2000). Effect of deconditioning on cortical and cancellous bone growth in the exercise trained young rats. *Journal of Bone and Mineral Research, 15*(9), 1842-1849.

Janz, K. F., Gilmore, J. M., Burns, T. L., Levy, S. M., Torner, J. C., Willing, M. C., & Marshall, T. A. (2006). Physical activity augments bone mineral accrual in young children: The Iowa Bone Development study. *The Journal of pediatrics, 148*(6), 793-799.

Järvinen, T. L., Pajamäki, I., Sievänen, H., Vuohelainen, T., Tuukkanen, J., Järvinen, M., & Kannus, P. (2003). Femoral neck response to exercise and subsequent deconditioning in young and adult rats. *Journal of Bone and Mineral Research, 18*(7), 1292-1299.

Jast, J. A. (2011). Investigation of ultrastructural and mechanical properties of rat cortical bone using micro-CT, three-point bending testing, and the reference point indentation technique.

Jee, W. S., & Li, X. J. (1990). Adaptation of cancellous bone to overloading in the adult rat: a single photon absorptiometry and histomorphometry study. *The Anatomical Record, 227*(4), 418-426.

Jepsen, K. J., Silva, M. J., Vashishth, D., Guo, X. E., & van der Meulen, M. C. (2015). Establishing biomechanical mechanisms in mouse models: practical guidelines for systematically evaluating phenotypic changes in the diaphyses of long bones. *Journal of Bone and Mineral Research, 30*(6), 951-966.

Jiang, S.-D., Jiang, L.-S., & Dai, L.-Y. (2007). Changes in bone mass, bone structure, bone biomechanical properties, and bone metabolism after spinal cord injury: a 6-month longitudinal study in growing rats. *Calcified tissue international, 80*(3), 167-175.

Joo, Y.-I., Sone, T., Fukunaga, M., Lim, S.-G., & Onodera, S. (2003). Effects of endurance exercise on three-dimensional trabecular bone microarchitecture in young growing rats. *Bone, 33*(4), 485-493.

Karlsson, M., Linden, C., Karlsson, C., Johnell, O., Obrant, K., & Seeman, E. (2000). Exercise during growth and bone mineral density and fractures in old age. *The lancet, 355*(9202), 469-470.

Karlsson, M. K. (2004). Physical activity, skeletal health and fractures in a long term perspective. *Journal of Musculoskeletal and Neuronal Interactions, 4*(1), 12.

Kirmani, S., Christen, D., Van Lenthe, G. H., Fischer, P. R., Bouxsein, M. L., McCready, L. K., . . . Müller, R. (2009). Bone structure at the distal radius during adolescent growth. *Journal of Bone and Mineral Research, 24*(6), 1033-1042.

Kiuchi, A., Arai, Y., & Katsuta, S. (1998). Detraining effects on bone mass in young male rats. *International journal of sports medicine, 19*(04), 245-249.

Kontulainen, S., Kannus, P., Haapasalo, H., Sievänen, H., Pasanen, M., Heinonen, A., . . . Vuori, I. (2001). Good maintenance of exercise-induced bone gain with decreased training of female tennis and squash players: a prospective 5-year follow-up study of young and old starters and controls. *Journal of Bone and Mineral Research, 16*(2), 195-201.

Lanyon, L., Hampson, W., Goodship, A., & Shah, J. (1975). Bone deformation recorded in vivo from strain gauges attached to the human tibial shaft. *Acta Orthopaedica, 46*(2), 256-268.

Leibel, R. (1990). Is obesity due to a heritable difference in'set point'for adiposity? *Western Journal of Medicine, 153*(4), 429.

Li, Z.-C., Jiang, S.-D., Yan, J., Jiang, L.-S., & Dai, L.-Y. (2011). Small-animal PET/CT assessment of bone microdamage in ovariectomized rats. *The Journal of Nuclear Medicine, 52*(5), 769.

Lu, H., Cui, L., Zuo, C., Lin, S., & Wu, T. (2015). Evaluation of morphological parameters of bone formation in Sprague–Dawley rats of different ages by in vivo fluorochrome labeling. *Italian Journal of Zoology, 82*(1), 33-40.

Lynch, M. E., Main, R. P., Xu, Q., Walsh, D. J., Schaffler, M. B., Wright, T. M., & van der Meulen, M. C. (2010). Cancellous bone adaptation to tibial compression is not sex dependent in growing mice. *Journal of applied physiology, 109*(3), 685-691.

MacLean, P. S., Higgins, J. A., Johnson, G. C., Fleming-Elder, B. K., Peters, J. C., & Hill, J. O. (2004). Metabolic adjustments with the development, treatment, and recurrence of obesity

in obesity-prone rats. *American Journal of Physiology-Regulatory, Integrative and Comparative Physiology*.

Mashiba, T., Hirano, T., Turner, C. H., Forwood, M. R., Johnston, C. C., & Burr, D. B. (2000). Suppressed bone turnover by bisphosphonates increases microdamage accumulation and reduces some biomechanical properties in dog rib. *Journal of Bone and Mineral Research, 15*(4), 613-620.

Milgrom, C., Finestone, A., Sharkey, N., Hamel, A., Mandes, V., Burr, D., . . . Ekenman, I. (2002). Metatarsal strains are sufficient to cause fatigue fracture during cyclic overloading. *Foot & ankle international, 23*(3), 230-235.

Mori, S., Harruff, R., Ambrosius, W., & Burr, D. (1997). Trabecular bone volume and microdamage accumulation in the femoral heads of women with and without femoral neck fractures. *Bone, 21*(6), 521-526.

Mosekilde, L., Danielsen, C., Søgaard, C., & Thorling, E. (1994). The effect of long-term exercise on vertebral and femoral bone mass, dimensions, and strength—assessed in a rat model. *Bone, 15*(3), 293-301.

Mosley, J., March, B., Lynch, J., & Lanyon, L. (1997). Strain magnitude related changes in whole bone architecture in growing rats. *Bone, 20*(3), 191-198.

Mustafy, T. (2013). *Prediction of Load-Sharing Mechanisms and Patterns of Human Cervical Spine Injuries Due to High-Velocity Impact Using Finite Element Method.* University of Alberta.

Mustafy, T., Benoit, A., Londono, I., Moldovan, F., & Villemure, I. (2018). Can repeated in vivo micro-CT irradiation during adolescence alter bone microstructure, histomorphometry and longitudinal growth in a rodent model? *PLOS ONE, 13*(11), e0207323. doi: 10.1371/journal.pone.0207323

Mustafy, T., Londono, I., & Villemure, I. (2018). Can the contralateral limb be used as a control during the growing period in a rodent model? *Medical engineering & physics, 58*, 31-40. doi: https://doi.org/10.1016/j.medengphy.2018.04.013

Mustafy, T., Londono, I., & Villemure, I. (2019). Experimental and finite element analyses of bone strains in the growing rat tibia induced by in vivo axial compression. *Journal of the Mechanical Behavior of Biomedical Materials, 94*, 176.

Mustafy, T., Moglo, K., Adeeb, S., & El-Rich, M. (2014). *Investigation of Upper Cervical Spine Injury due to Frontal and Rear Impact Loading Using Finite Element Analysis.* Paper presented at the ASME 2014 International Mechanical Engineering Congress and Exposition.

Nance, D. M., Bromley, B., Barnard, R. J., & Gorski, R. A. (1977). Sexually dimorphic effects of forced exercise on food intake and body weight in the rat. *Physiology & behavior, 19*(1), 155-158.

Necas, J., & Hlavácek, I. (2017). *Mathematical theory of elastic and elasto-plastic bodies: an introduction* (Vol. 3): Elsevier.

Nikoletseas, M. M. (1980). Food intake in the exercising rat: a brief review. *Neuroscience & Biobehavioral Reviews, 4*(2), 265-267.

Ooi, F., Singh, R., Singh, H., & Umemura, Y. (2009). Minimum level of jumping exercise required to maintain exercise-induced bone gains in female rats. *Osteoporosis international, 20*(6), 963-972.

Oscai, L., Mole, P., & Holloszy, J. (1971). Effects of exercise on cardiac weight and mitochondria in male and female rats. *American Journal of Physiology-Legacy Content, 220*(6), 1944-1948.

Pajamäki, I., Kannus, P., Vuohelainen, T., Sievänen, H., Tuukkanen, J., Järvinen, M., & Järvinen, T. L. (2003). The bone gain induced by exercise in puberty is not preserved through a virtually life-long deconditioning: a randomized controlled experimental study in male rats. *Journal of Bone and Mineral Research, 18*(3), 544-552.

Perrien, D. S., Akel, N. S., Dupont-Versteegden, E. E., Skinner, R. A., Siegel, E. R., Suva, L. J., & Gaddy, D. (2007). Aging alters the skeletal response to disuse in the rat. *American Journal of Physiology-Regulatory, Integrative and Comparative Physiology*.

Rabkin, B. A., Szivek, J. A., Schonfeld, J. E., & Halloran, B. P. (2001). Long-term measurement of bone strain in vivo: The rat tibia. *Journal of biomedical materials research, 58*(3), 277-281.

Raisz, L. G. (2005). Pathogenesis of osteoporosis: concepts, conflicts, and prospects. *The Journal of clinical investigation, 115*(12), 3318-3325.

Rizzoli, R., Bianchi, M. L., Garabédian, M., McKay, H. A., & Moreno, L. A. (2010). Maximizing bone mineral mass gain during growth for the prevention of fractures in the adolescents and the elderly. *Bone, 46*(2), 294-305.

Robling, A. G., Castillo, A. B., & Turner, C. H. (2006). Biomechanical and molecular regulation of bone remodeling. *Annu. Rev. Biomed. Eng., 8*, 455-498.

Ruimerman, R., van Rietbergen, B., Hilbers, P., & Huiskes, R. (2005). The Effects of Trabecular-Bone Loading Variables on the Surface Signaling Potential for Bone Remodeling and Adaptation. *Annals of biomedical engineering, 33*(1), 71-78. doi: 10.1007/s10439-005-8964-9

Russek, M., & Pina, S. (1962). Conditioning of adrenalin anorexia. *Nature, 193*(4822), 1296.

Saxon, L., Robling, A., Alam, I., & Turner, C. (2005). Mechanosensitivity of the rat skeleton decreases after a long period of loading, but is improved with time off. *Bone, 36*(3), 454-464.

Schapira, D. (1991). The rat as a model for studies of the aging skeleton. *Cells Mater.*, 181-188.

Schlecht, S. H., Bigelow, E. M., & Jepsen, K. J. (2014). Mapping the natural variation in whole bone stiffness and strength across skeletal sites. *Bone, 67*, 15-22.

Schriefer, J. L., Robling, A. G., Warden, S. J., Fournier, A. J., Mason, J. J., & Turner, C. H. (2005). A comparison of mechanical properties derived from multiple skeletal sites in mice. *Journal of biomechanics, 38*(3), 467-475.

Shindo, D., Matsuura, T., & Suzuki, M. (2014). Effects of prepubertal-onset exercise on body weight changes up to middle age in rats. *American Journal of Physiology-Heart and Circulatory Physiology*.

Sievänen, H. (2012). Bone: Impact loading—nature's way to strengthen bone. *Nature Reviews Endocrinology, 8*(7), 391-393.

Søgaard, C. H., Danielsen, C. C., Thorling, E. B., & Mosekilde, L. (1994). Long-term exercise of young and adult female rats: Effect on femoral neck biomechanical competence and bone structure. *Journal of Bone and Mineral Research, 9*(3), 409-416.

Stokes, I. A. (2007). Analysis and simulation of progressive adolescent scoliosis by biomechanical growth modulation. *European Spine Journal, 16*(10), 1621-1628.

Stokes, I. A., Aronsson, D. D., Dimock, A. N., Cortright, V., & Beck, S. (2006). Endochondral growth in growth plates of three species at two anatomical locations modulated by mechanical compression and tension. *Journal of Orthopaedic Research, 24*(6), 1327-1334.

Stürmer, E. K., Seidlová-Wuttke, D., Sehmisch, S., Rack, T., Wille, J., Frosch, K. H., . . . Stürmer, K. M. (2006). Standardized bending and breaking test for the normal and osteoporotic metaphyseal tibias of the rat: effect of estradiol, testosterone, and raloxifene. *Journal of Bone and Mineral Research, 21*(1), 89-96.

Turner, C. H., & Akhter, M. P. (1999). The mechanics of bone adaptation *Mechanical loading of bones and joints* (pp. 79-91): Springer.

van Rietbergen, B., Weinans, H., Huiskes, R., & Odgaard, A. (1995). A new method to determine trabecular bone elastic properties and loading using micromechanical finite-element models. *Journal of biomechanics, 28*(1), 69-81.

Vendsalu, A. (1960). Plasma concentrations of adrenaline and noradrenaline during muscular work. *Acta Physiol. Stand. Suppl, 173*, 37-69.

Voide, R., van Lenthe, G. H., & Müller, R. (2008). Bone morphometry strongly predicts cortical bone stiffness and strength, but not toughness, in inbred mouse models of high and low bone mass. *Journal of Bone and Mineral Research, 23*(8), 1194-1203.

Warden, S. J., Fuchs, R. K., Castillo, A. B., Nelson, I. R., & Turner, C. H. (2007). Exercise when young provides lifelong benefits to bone structure and strength. *Journal of Bone and Mineral Research, 22*(2), 251-259.

Warden, S. J., Galley, M. R., Hurd, A. L., Richard, J. S., George, L. A., Guildenbecher, E. A., . . . Fuchs, R. K. (2014). Cortical and trabecular bone benefits of mechanical loading are maintained long term in mice independent of ovariectomy. *Journal of Bone and Mineral Research, 29*(5), 1131-1140.

Warden, S. J., & Roosa, S. M. M. (2014). Physical activity completed when young has residual bone benefits at 94 years of age: a within-subject controlled case study. *Journal of musculoskeletal & neuronal interactions, 14*(2), 239.

Warden, S. J., Roosa, S. M. M., Kersh, M. E., Hurd, A. L., Fleisig, G. S., Pandy, M. G., & Fuchs, R. K. (2014). Physical activity when young provides lifelong benefits to cortical bone size and strength in men. *Proceedings of the National Academy of Sciences, 111*(14), 5337-5342.

Weaver, C. M. (2002). Adolescence. *Endocrine, 17*(1), 43-48. doi: 10.1385/endo:17:1:43

Weinsier, R. L., Nelson, K. M., Hensrud, D. D., Darnell, B. E., Hunter, G. R., & Schutz, Y. (1995). Metabolic predictors of obesity. Contribution of resting energy expenditure, thermic effect of food, and fuel utilization to four-year weight gain of post-obese and never-obese women. *The Journal of clinical investigation, 95*(3), 980-985.

Widdowson, E. M., & McCance, R. (1957). Effect of a low-protein diet on the chemical composition of the bodies and tissues of young rats. *British Journal of Nutrition, 11*(2), 198-206.

Wolff, J. (1892). Das gesetz der transformation der knochen. *A Hirshwald, 1*, 1-152.

Wolfram, U., & Schwiedrzik, J. (2016). Post-yield and failure properties of cortical bone. *BoneKEy reports, 5*.

Wronski, T., Schenk, P., Cintron, M., & Walsh, C. (1987). Effect of body weight on osteopenia in ovariectomized rats. *Calcified tissue international, 40*(3), 155-159.

Yang, P., Bruggemann, G., & Rittweger, J. (2011). What do we currently know from in vivo bone strain measurements in humans. *J Musculoskelet Neuronal Interact, 11*(1), 8-20.

Yang, X., Chan, Y. H., Muthukumaran, P., & Lee, T. (2010). Morphological and mechanical changes in ovariectomized rat tibia with treatments of ibandronate and parathyroid hormone. *Osteoporosis, 8*(3), 255-265.

Yasari, S., Paquette, A., Charbonneau, A., Gauthier, M.-S., Savard, R., & Lavoie, J.-M. (2006). Effects of ingesting a high-fat diet upon exercise-training cessation on fat accretion in the liver and adipose tissue of rats. *Applied physiology, nutrition, and metabolism, 31*(4), 367-375.

Yeh, J. K., & Aloia, J. F. (1990a). Deconditioning increases bone resorption and decreases bone formation in the rat. *Metabolism-Clinical and Experimental, 39*(6), 659-663.

Yeh, J. K., & Aloia, J. F. (1990b). Effect of physical activity on calciotropic hormones and calcium balance in rats. *American Journal of Physiology-Endocrinology and Metabolism, 258*(2), E263-E268.

CHAPTER 8   GENERAL DISCUSSION

This discussion takes up the key points of the methodology presented in each scientific paper and adds a complement to these points.

8.1   Cyclic axial compression (impact) loading

Impact loadings have been selected over the static loadings for this project due to the positive and rapid response of the skeletal system under dynamic loading regime. Also, several previous studies (Lance E Lanyon & Rubin, 1984; Liskova, 1971; Ohashi, Robling, Burr, & Turner, 2002; Robling, Burr, & Turner, 2001a, 2001b; Villemure & Stokes, 2009) have reported the greater effects on bone growth mechanisms under dynamic loading conditions. Moreover, studies reported that impact loading exercise during adolescence affected bone growth in young athletes (Caine et al., 2001; Lindholm et al., 1994; Tanghe et al., 1996). But, the studies haven't provided a distinct separation between the effects of nutritional and mechanical factors (Bernink et al., 1983; Caine et al., 2001; Haywood et al., 1986; Lindholm et al., 1994; Tanghe et al., 1996; Theintz et al., 1993). Experimental animal studies also reported contradictory results for the effects of impact loading during adolescence on bone growth (Duckham et al., 2014; Honda et al., 2008; Iwamoto et al., 2000; Kontulainen et al., 2001; Kontulainen et al., 2003; Nordström et al., 2005; Pajamäki et al., 2003; S. J. Warden et al., 2007; S. J. Warden et al., 2014). Hence, it is not well established whether a controlled impact loading during adolescence would affect bone development, quality, and mechanical strength at maturity or how long these effects would remain.

8.1.1   Cyclic axial compression loading parameters

In the second, third and fourth articles, similar cyclic axial compression protocols were used. The selection of strain level, required displacement, loading frequency, and cycle number have been selected to promote bone osteogenic activities. Strain levels for three cyclic axial compression groups were based on strains generated on human tibiae during three distinct types of physical activities performed in a physiologic condition. The low impact group received a cyclic axial compression corresponding to 450με in a human tibia undergoing a walking condition (D. Burr et al., 1996; L. Lanyon, Hampson, Goodship, & Shah, 1975). The medium impact group received an cyclic axial compression representing 850με on a human tibia undergoing zigzag uphill running in hillside condition (D. Burr et al., 1996; P. Yang, Bruggemann, & Rittweger, 2011). Finally, the

high impact group received the loading corresponding to 1250με on a human tibia under vertical jumping with two legs (Milgrom et al., 2002; P. Yang et al., 2011). A loading frequency of 2 Hz was chosen, as a very low frequency (<1 Hz) was reported to produce an insufficient response to trigger bone osteogenic activities (McBride & Silva, 2012). Bone formation can be increased with the use of higher frequency up to a maximum threshold of 10-20 Hz (Y.-F. Hsieh, Wang, & Turner, 1999; Y. F. Hsieh & Turner, 2001; Torrance, Mosley, Suswillo, & Lanyon, 1994). Beyond this frequency, bone formation stops reacting to the applied loading magnitude (S. Warden & Turner, 2004). However, for the studies involving rats, a commonly used frequency is the 2-4 Hz, as this frequency matches with the stride frequency range observed for normal locomotion in rats (Mosley, March, Lynch, & Lanyon, 1997). Furthermore, it has been reported in previous studies that bone growth activities and bone development process are more sensitive to the magnitude of the loading rather than the frequency at which the deformation takes place (Burger, 1993; D. Jones, Nolte, Scholübbers, Turner, & Veltel, 1991). Moreover, the use of 2 Hz loading frequency can be justified from the mechanical usage windows proposed by Turner and Akhter (Turner & Akhter, 1999), where it has been shown that with this frequency and 450 με peak strain condition, the loading is considered a physiologic loading regime, which can effectively trigger the mechanotransduction process. The number of loading cycles was fixed at 1200 cycles per day, based on data influencing the bone formation and initiating the cellular mechanotransduction process (Turner & Akhter, 1999). Moreover, according to the mechanical usage windows proposed by Turner and Akhter (Turner & Akhter, 1999), 1200 loading cycles coupled with the minimum strain magnitude of 450με ensures the mechanotransduction process at 2Hz of loading frequency.

8.1.2 Training and detraining periods

The adolescent period was selected in this project for cyclic axial compression because it is known for the rapid skeletal growth period when approximately 95% of the adult mass is accrued (Bailey, McKay, Mirwald, Crocker, & Faulkner, 1999; Weaver, 2002). Physical activity during this period results in increased bone length, bone mass, bone area and overall bone strength (S. J. Warden et al., 2014). Moreover, it has been reported that during this period, bones achieve 25–30% of the adult bone mineral content and that bone strength increased up to 50% depending on skeletal sites (Bailey et al., 1999; Bonjour, Theintz, Buchs, Slosman, & Rizzoli, 1991; Slemenda et al., 1994). For male Sprague Dawley rats, the adolescent time period is well documented, and ranges between

28 and 80 days old (Sengupta, 2013). In order to observe the loading effects at the adulthood period, the rats were further kept up to 1 year of age. This period was selected because a year time in rats life corresponds to the 35-40 years of adulthood period in humans life span (Sengupta, 2013). Hence, the detraining period used in this project could be related to the human life span to provide an insight of bone development at young human adulthood.

8.1.3 Radiation doses for *in vivo* scanning

The selection of the *in vivo* micro-CT radiation doses was critical for this project. As described in the third article, the rat tibiae were scanned *in vivo* on a weekly basis till the end of the growing period. Moreover, as described in the fourth article, the rat tibiae were scanned on a weekly basis during the growing period and then scanned less frequently for the detraining period up to 1 year of age. So, it was necessary to use a radiation doses which would provide high quality scanned images for investigation of the bone-morphometric properties and for the computation modeling purpose, but without interfering with the bone development process. Hence, three sets of radiation doses were investigated for repeated scanning of the right tibiae during the adolescent period in the first article (Mustafy, Benoit, Londono, Moldovan, & Villemure, 2018). The radiation doses (0.83, 1.65 and 2.47 Gy) were selected to produce high image quality for bone development investigation purpose. As it has been discussed in the first article, the 1.65 and 2.47 Gy radiation doses negatively affected the bone development process while under the 0.83 Gy doses radiation, bone growth remained unaffected during the scanning period (Mustafy, Benoit, et al., 2018). Accordingly, the 0.83 Gy radiation doses was selected for this project. The calculation of radiation doses of 0.83 Gy for the project is provided here for further clarification. The calculated radiation absorbed dose, and corresponding effective dose equivalent values were derived from the measured dose rates with several PMMA shielding depths, and extrapolated when necessary by exponential curve-fitting. For approximation of the mean dose rate at different tissue diameters, the tissue at all depth was assumed to be cylindrical, and the dose rate at all tissue cylinder diameters were averaged between the dose in the air (zero depth) and the dose at the cylinder center (half diameter). For the scanning settings of 65 kV, 384 μA x-ray - full power and 1mm Al filter, the local absorbed dose rate for *in vivo* rat tibial scanning is reported by Bruker to be 148.3 mGy/min [ref: SkyScan 1176 *in vivo* scanning: X-ray dosimetry]

$$\text{Scanning time} = 5 \min 34\ sec = \left\{5 + \left(\frac{34}{60}\right)\right\} \min = 5.567\ min$$

Radiation doses per scan $= Scanning\ time\ x\ dose\ rate$

$$= (5.567\ x\ 148.3)\ mGy = 825.59\ mGy = 0.83\ Gy$$

8.1.4 Right tibia for cyclic axial compression loading

All load applications and analyses performed in this project were done on right tibiae. As this project aimed to investigate bone growth and development process in the rat tibiae, so it was crucial to investigate any site dependence and symmetry between left and right tibiae in the rat. In a separate study, the symmetry of rat tibiae during the growing period was investigated (Mustafy, Londono, & Villemure, 2018). The study was performed on three groups of growing rats (4, 8, and 12 week old) and the degree of bilateral variability, 3D geometric similarity, bone morphology and mechanical properties between both tibiae was assessed. It was found that bone length and curvature along with overall geometry remained symmetric. Also, despite the significant changes of the morphometric and biomechanical properties in the growing tibiae, the contralateral pairs maintained bilateral symmetry throughput bone development. Hence, it was concluded that using the left or right tibia during the growing period would not affect the conclusion of the project. The right tibia was then chosen as the primary limb for the cyclic axial compression application.

8.1.5 Bone segmentation thresholds

For the evaluation of bone morphometric parameters, both the trabecular and cortical bone tissues needed to be segmented in this project. The threshold value used for the segmentation of these bony volumes of interests was not arbitrary. A global gray threshold value of 65 was used, as it corresponded to the equivalent density of 0.413 g/cm^3 of calcium hydroxyapatite (CaHA) (Hasan et al., 2018; Lynch et al., 2010). This threshold value was chosen based on the histogram plots of bone and non-bone peaks from the scanned images of the rat tibial micro-CT data during the growing period (Mustafy, Benoit, et al., 2018).

8.2 General limitations

In addition to the limitations described in the four scientific articles, the following general limitations can be stated as part of the presented project.

8.2.1 *In vivo* experimental protocol

In vivo experiments are subjected to intrinsic limitations for different reasons, namely daily handling, as well as manipulation during the loading procedure and micro-CT scanning protocols. First, forced loading conditions used in this project might have increased stress levels in the loaded rats. This could be associated with the observed decrease in body weight and food intake for the high impact group of rats (third and fourth articles). It would be interesting to include additional testing parameters in similar studies for the future to observe if such loading conditions affect the psychological behavioral pattern or not. Secondly, due to the increasing size and length of the rats with age, it became difficult to scan the tibia after eight months of age. The scanning chamber of the micro-CT scanner was not barely big enough to fit the matured rat body in place. Also, retaining the long tail without interfering with the tibial scan was proven to be quite challenging. In order to get a proper scan, the tibia needed to be stretched and extended during the entire scanning period. This manipulation might have left an effect on overall bone health. However, as the same manipulation was performed for all the rats once a month (during late detraining) and as the scanning time was short (less than 12 minutes), this effect was considered to be negligible. Finally, morphometric analyses provided in this project did not consider their spatial distribution within the proximal metaphysis. For example, changes in the mean trabecular spacing might have resulted from a few isolated trabecular thickening within the analyzed sample, while the rest of the structure remained unaffected or showed an opposite effect during that period. If the region consisting this isolated individual structure could have been identified through spatial distribution, more interesting and detailed insights about the load transmission throughout the metaphysis may have been achieved.

8.2.2 Rat tibial model

The rat tibial model is interesting and advantageous because it allows controlling external experimental conditions and further studying the biological responses of tissues (De Souza et al., 2005; Fritton, Myers, Wright, & Van der Meulen, 2005). Also, the rat tibial model has physiological similarity with humans. A major limitation in loading cases concerns its quadrupedy compared to bipedal humans, as well as the small size of this rodent model (Moran et al., 2016).

Rat studies are then often the first steps in validating or testing fundamental research hypotheses. Bigger animal models (goats, pigs, oxen, sheep, dogs) have been used by many researchers for assessing the different effects on sex (Lynch et al., 2010), disease (Hytönen & Lohi, 2016; Lynch et al., 2013; Vodicka et al., 2005) and age condition (Ali, Kumar, Bjornstad, & Duran, 1996; Main, Lynch, & van der Meulen, 2014; Razi et al., 2015). However, these animals are also four-legged and the loads applied must be adapted accordingly.

CHAPTER 9   CONTRIBUTIONS TO MECHANICAL ENGINEERING

This chapter presents the key contributions of this thesis to the advancement of knowledge in mechanical engineering from both methodological and research perspectives.

➢ A micro-CT based semi-automatic bone segmentation algorithm (both trabecular and cortical) has been developed; it can be used in other micro-CT scanning protocols.

➢ A non-invasive micro-CT based finite element modeling tool has been developed and validated for growing rats; it can be used with proper modification for other animal models.

➢ A detailed *in vivo* procedure has been developed for measuring strains (using strain gauges) in growing rat tibiae; it could be implemented in other bone sites or animal models.

➢ A four-point bending test setup has been devised to test various bone segments in rodents.

➢ A custom loading setup has been developed for cyclic axial loading of rat tibia in combination with the Mach-1 apparatus (Biomomentum Inc.).

➢ A loading protocol has been developed to apply *in vivo* cyclic axial compression on growing rat tibiae; it could be used for other animal models with proper adaptations.

➢ A strain vs. displacement calibration relationship has been established for growing rat tibiae to design different loading protocols for rodents.

➢ A safe scanning radiation dosage has been established for growing rats, namely in the rat tibiae, which could be used for other growing rodent models with proper protocol adaptations.

CHAPTER 10   CONCLUSION AND RECOMMENDATIONS

10.1 Conclusion

The main objective of this thesis was to investigate the effects of *in vivo* low, medium and high impact loadings applied as cyclic axial compression during the adolescence on bone growth, quality and mechanical strength at skeletal maturity as well as the effects of loadings on bone quality and mechanical strength at adulthood.

In order to determine the safe level of micro-CT radiation doses for acquiring high-quality images without affecting the bone growth, three different radiation doses were tested during the growing period of rats. Afterwards, displacement vs. strain relationships were developed for three different age groups of rat tibiae for inducing the target strain with cyclic axial compression conditions. A non-invasive micro-CT based finite element modeling tool was also developed and validated for growing rats. Then, the effects of cyclic axial compression during the growing period on bone growth, mechanics and strength were assessed for rat tibial model. Finally, the effects of cyclic axial compression using rat tibiae on bone quality and mechanical strength at adulthood were investigated.

Concerning the 1st research question of the project, the study on micro-CT radiation showed that a radiation dose of 0.83 Gy provided a reasonable high-quality image sets for trabecular and cortical bone microstructure without affecting bone growth and development. Results from this study could be useful for designing future similar *in vivo* studies, where repeated micro-CT radiation exposures are necessary for longitudinally investigating bone microstructures.

For the 2nd research question of the project, a study was performed to assess the pubertal cyclic axial compression effects up to the skeletal maturity. The high impact loading performed briefly on a daily basis in the pubertal period benefitted the bone quality at skeletal maturity. However, the bone growth process was negatively affected by the loading despite improving the cortical bone strength. It is now evident that a well-controlled loading protocol can positively influence the bone development process, but it comes at the cost of a moderately reduced longitudinal bone growth.

Regarding the 3rd research question of the project, a long-term study was performed to assess the pubertal cyclic axial compression effects up to the adulthood period. The study showed that bone quality and mechanical strength benefits gained through high impact loading applied during

puberty had lasting benefits, which persisted up to a yearlong detraining period at adulthood. Also, high impact loading was found to increase the toughness, suggesting a reduced bone fracture risk at adulthood.

Overall, this study investigated for the first time the effects of well-controlled cyclic axial compression during the entire pubertal period on bone growth, morphometry and biomechanics at skeletal maturity and at adulthood period using an *in vivo* approach. Obtained results could be relevant for designing non-invasive approaches to prevent bone loss with aging or due to diseases, by implementing high impact exercise training at the adolescent period. Moreover, they could be used for proposing recommendations for training programs prescribed to young adolescent athletes involved in high impact sports.

10.2 Recommendations for future studies

Recommendations for future studies could include the followings:

- Increasing sample size for different loading groups;

- Including both male and female study groups;

- Testing different loading frequencies and varying loading durations;

- Inserting a brief resting time between the loading cycles;

- Testing other types of caloric diet on bone health;

- Evaluating the effectiveness of the proposed loading protocol for animals with estrogen deficiency;

- Evaluating the effectiveness of the proposed loading protocol for animals with the osteoporotic condition;

- Evaluating the contribution of tibial metaphyses, which consist of both cortical and trabecular bony structures, to the overall strength of the bone;

- Confirming the obtained results with other animal models.

These points could be investigated in future studies for the advancement of the knowledge provided by this thesis. Moreover, it would help to explore new approaches for designing effective skeletal loading techniques with a view of helping the young adolescent athletes. Effective training regime can also be developed for patients with pathological conditions related to bone loss, without compromising their bone strength and health throughout life.

REFERENCES

Adams, J. E. (2009). Quantitative computed tomography. *European Journal of Radiology, 71*(3), 415-424. doi: https://doi.org/10.1016/j.ejrad.2009.04.074

Aghajanian, P., Hall, S., Wongworawat, M. D., & Mohan, S. (2015). The roles and mechanisms of actions of vitamin C in bone: new developments. *Journal of Bone and Mineral Research, 30*(11), 1945-1955.

Ahn, A. C., & Grodzinsky, A. J. (2009). Relevance of collagen piezoelectricity to "Wolff's Law": A critical review. *Medical engineering & physics, 31*(7), 733-741.

Ali, M., Kumar, S., Bjornstad, K., & Duran, C. (1996). The sheep as an animal model for heart valve research. *Cardiovascular Surgery, 4*(4), 543-549.

Aronsson, D. D., Stokes, I., Rosovsky, J., & Spence, H. (1999). Mechanical modulation of calf tail vertebral growth: implications for scoliosis progression. *Journal of spinal disorders, 12*(2), 141-146.

Bailey, D., McKay, H., Mirwald, R., Crocker, P., & Faulkner, R. (1999). A six-year longitudinal study of the relationship of physical activity to bone mineral accrual in growing children: the university of Saskatchewan bone mineral accrual study. *Journal of Bone and Mineral Research, 14*(10), 1672-1679.

Bankoff, A. D. P. (2007). *Morfologia e cinesiologia: aplicada ao movimento humano*: Guanabara Koogan.

Bankoff, A. D. P. (2012). Biomechanical characteristics of the bone *Human musculoskeletal biomechanics*: IntechOpen.

Bass, S., Pearce, G., Bradney, M., Hendrich, E., Delmas, P. D., Harding, A., & Seeman, E. (1998). Exercise Before Puberty May Confer Residual Benefits in Bone Density in Adulthood: Studies in Active Prepubertal and Retired Female Gymnasts. *Journal of Bone and Mineral Research, 13*(3), 500-507. doi: 10.1359/jbmr.1998.13.3.500

Beaupré, G., Orr, T., & Carter, D. (1990). An approach for time-dependent bone modeling and remodeling—application: A preliminary remodeling simulation. *Journal of Orthopaedic Research, 8*(5), 662-670.

Bernink, M., Erich, W., Peltenburg, A., Zonderland, M., & Huisveld, I. (1983). Height, body composition, biological maturation and training in relation to socio-economic status in girl gymnasts, swimmers, and controls. *Growth, 47*(1), 1-12.

Bessho, M., Ohnishi, I., Matsumoto, T., Ohashi, S., Matsuyama, J., Tobita, K., . . . Nakamura, K. (2009). Prediction of proximal femur strength using a CT-based nonlinear finite element method: differences in predicted fracture load and site with changing load and boundary conditions. *Bone, 45*(2), 226-231.

Bessho, M., Ohnishi, I., Matsuyama, J., Matsumoto, T., Imai, K., & Nakamura, K. (2007). Prediction of strength and strain of the proximal femur by a CT-based finite element method. *Journal of biomechanics, 40*(8), 1745-1753.

Biewener, A. A., & Bertram, J. E. (1993). Skeletal strain patterns in relation to exercise training during growth. *Journal of Experimental Biology, 185*(1), 51-69.

Bonewald, L. F., & Johnson, M. L. (2008). Osteocytes, mechanosensing and Wnt signaling. *Bone, 42*(4), 606-615. doi: https://doi.org/10.1016/j.bone.2007.12.224

Bonjour, J.-P., Theintz, G., Buchs, B., Slosman, D., & Rizzoli, R. (1991). Critical years and stages of puberty for spinal and femoral bone mass accumulation during adolescence. *The Journal of Clinical Endocrinology & Metabolism, 73*(3), 555-563.

Bourne, G. H. (2014). *The biochemistry and physiology of bone*: Elsevier.

Bourrin, S., Palle, S., Pupier, R., Vico, L., & Alexandre, C. (1995). Effects of physical training on bone adaptation in three zones of the rat tibia. *Journal of Bone and Mineral Research, 10*(11), 1745-1752.

Bouxsein, M. L., Boyd, S. K., Christiansen, B. A., Guldberg, R. E., Jepsen, K. J., & Müller, R. (2010). Guidelines for assessment of bone microstructure in rodents using micro–computed tomography. *Journal of Bone and Mineral Research, 25*(7), 1468-1486.

Bright, J. A., & Rayfield, E. J. (2011). Sensitivity and ex vivo validation of finite element models of the domestic pig cranium. *Journal of Anatomy, 219*(4), 456-471. doi: 10.1111/j.1469-7580.2011.01408.x

Brighton, C. T., & Hunt, R. M. (1991). Early histological and ultrastructural changes in medullary fracture callus. *JBJS, 73*(6), 832-847.

Burger, E. (1993). Influence of mechanical factors on bone formation, resorption and growth in vitro. *Bone, 7*, 37-56.

Burghardt, A. J., Kazakia, G. J., & Majumdar, S. (2007). A Local Adaptive Threshold Strategy for High Resolution Peripheral Quantitative Computed Tomography of Trabecular Bone. *Annals of biomedical engineering, 35*(10), 1678-1686. doi: 10.1007/s10439-007-9344-4

Burr, D., Milgrom, C., Fyhrie, D., Forwood, M., Nyska, M., Finestone, A., . . . Simkin, A. (1996). In vivo measurement of human tibial strains during vigorous activity. *Bone, 18*(5), 405-410.

Burr, D. B., & Allen, M. R. (2019). *Basic and applied bone biology*: Academic Press.

Caine, D., Lewis, R., O'Connor, P., Howe, W., & Bass, S. (2001). Does gymnastics training inhibit growth of females? *Clinical journal of sport medicine, 11*(4), 260-270.

Cancel, M., Grimard, G., Thuillard-Crisinel, D., Moldovan, F., & Villemure, I. (2009). Effects of in vivo static compressive loading on aggrecan and type II and X collagens in the rat growth plate extracellular matrix. *Bone, 44*(2), 306-315.

Cardoso, L., Herman, B. C., Verborgt, O., Laudier, D., Majeska, R. J., & Schaffler, M. B. (2009). Osteocyte Apoptosis Controls Activation of Intracortical Resorption in Response to Bone Fatigue. *Journal of Bone and Mineral Research, 24*(4), 597-605. doi: 10.1359/jbmr.081210

Cashman, K. D. (2007). Diet, nutrition, and bone health. *The Journal of nutrition, 137*(11), 2507S-2512S.

Chamay, A., & Tschantz, P. (1972). Mechanical influences in bone remodeling. Experimental research on Wolff's law. *Journal of biomechanics, 5*(2), 173-180.

Christen, D., Melton III, L. J., Zwahlen, A., Amin, S., Khosla, S., & Müller, R. (2013). Improved Fracture Risk Assessment Based on Nonlinear Micro-Finite Element Simulations From HRpQCT Images at the Distal Radius. *Journal of Bone and Mineral Research, 28*(12), 2601-2608. doi: 10.1002/jbmr.1996

Christen, D., Webster, D. J., & Müller, R. (2010). Multiscale modelling and nonlinear finite element analysis as clinical tools for the assessment of fracture risk. *Philosophical Transactions of the Royal Society A: Mathematical, Physical and Engineering Sciences, 368*(1920), 2653-2668.

Clarke, B. (2008). Normal bone anatomy and physiology. *Clinical journal of the American Society of Nephrology, 3*(Supplement 3), S131-S139.

Cockayne, E. A. (1933). *Inherited abnormalities of the skin and its appendages*: Oxford University Press, Humphrey Milford [Oxford, Printed by John Johnson ….

Courpron, P., Meunier, P., & Vignon, G. (1975). Dynamics of bone remodeling explained by Harold Frost. Theory of the BMU (basic multicellular unit). *La Nouvelle presse medicale, 4*(6), 421.

Crawford, R. P., Cann, C. E., & Keaveny, T. M. (2003). Finite element models predict in vitro vertebral body compressive strength better than quantitative computed tomography. *Bone, 33*(4), 744-750.

Crockett, J. C., Rogers, M. J., Coxon, F. P., Hocking, L. J., & Helfrich, M. H. (2011). Bone remodelling at a glance. *Journal of Cell Science, 124*(7), 991-998. doi: 10.1242/jcs.063032

Currey, J. D. (2014). *The mechanical adaptations of bones*: Princeton University Press.

De Souza, R. L., Matsuura, M., Eckstein, F., Rawlinson, S. C., Lanyon, L. E., & Pitsillides, A. A. (2005). Non-invasive axial loading of mouse tibiae increases cortical bone formation and modifies trabecular organization: a new model to study cortical and cancellous compartments in a single loaded element. *Bone, 37*(6), 810-818.

Dennis, S. C., Berkland, C. J., Bonewald, L. F., & Detamore, M. S. (2014). Endochondral ossification for enhancing bone regeneration: converging native extracellular matrix biomaterials and developmental engineering in vivo. *Tissue Engineering Part B: Reviews, 21*(3), 247-266.

Duckham, R. L., Baxter-Jones, A. D., Johnston, J. D., Vatanparast, H., Cooper, D., & Kontulainen, S. (2014). Does Physical Activity in Adolescence Have Site-Specific and Sex-Specific Benefits on Young Adult Bone Size, Content, and Estimated Strength? *Journal of Bone and Mineral Research, 29*(2), 479-486.

Duncan, R., & Turner, C. (1995). Mechanotransduction and the functional response of bone to mechanical strain. *Calcified tissue international, 57*(5), 344-358.

Eswaran, S. K., Gupta, A., & Keaveny, T. M. (2007). Locations of bone tissue at high risk of initial failure during compressive loading of the human vertebral body. *Bone, 41*(4), 733-739. doi: https://doi.org/10.1016/j.bone.2007.05.017

Evans, F. G., & Lebow, M. (1952). The strength of human compact bone as revealed by engineering technics. *The American Journal of Surgery, 83*(3), 326-331.

Faulkner, K. G., Cann, C. E., & Hasegawa, B. H. (1991). Effect of bone distribution on vertebral strength: assessment with patient-specific nonlinear finite element analysis. *Radiology, 179*(3), 669-674.

Follis Jr, R., Park, E., & Jackson, D. (1952). The prevalence of rickets at autopsy during the first two years of age. *Bulletin of the Johns Hopkins Hospital, 91*, 480-497.

Forwood, M. R., & Parker, A. W. (1987). Effects of exercise on bone growth mechanical and physical properties studied in the rat. *Clinical Biomechanics, 2*(4), 185-190.

Fritton, J., Myers, E., Wright, T., & Van der Meulen, M. (2005). Loading induces site-specific increases in mineral content assessed by microcomputed tomography of the mouse tibia. *Bone, 36*(6), 1030-1038.

Gardinier, J. D., Rostami, N., Juliano, L., & Zhang, C. (2018). Bone adaptation in response to treadmill exercise in young and adult mice. *8*(J. Clin. Endocrinol. Metab. 97 2012), 29-37. doi: 10.1016/j.bonr.2018.01.003

Genant, H. K., Engelke, K., & Prevrhal, S. (2008). Advanced CT bone imaging in osteoporosis. *Rheumatology, 47*(suppl_4), iv9-iv16. doi: 10.1093/rheumatology/ken180

Gerard, G. (1961). *Introduction to structural stability theory*: McGraw-Hill.

Green, E. L. (1948). Animal Genetics and Medicine. Hans Grüneberg. *The Quarterly Review of Biology, 23*(2), 148-149. doi: 10.1086/396277

Gunter, K., Baxter-Jones, A. D., Mirwald, R. L., Almstedt, H., Fuchs, R. K., Durski, S., & Snow, C. (2008). Impact exercise increases BMC during growth: an 8-year longitudinal study. *Journal of Bone and Mineral Research, 23*(7), 986-993.

Hadjidakis, D. J., & Androulakis, I. I. (2006). Bone Remodeling. *Annals of the New York Academy of Sciences, 1092*(1), 385-396. doi: 10.1196/annals.1365.035

Hart, N. H., Nimphius, S., Rantalainen, T., Ireland, A., Siafarikas, A., & Newton, R. U. (2017). Mechanical basis of bone strength: influence of bone material, bone structure and muscle action. *Journal of musculoskeletal & neuronal interactions, 17*(3), 114-139.

Hasan, A., Byambaa, B., Morshed, M., Cheikh, M. I., Shakoor, R. A., Mustafy, T., & Marei, H. (2018). Advances in osteobiologic materials for bone substitutes. *Journal of Tissue Engineering and Regenerative Medicine*.

Hay, E. D. (2013). *Cell biology of extracellular matrix*: Springer Science & Business Media.

Haywood, K. M., Clark, B. A., & Mayhew, J. L. (1986). Differential effects of age-group gymnastics and swimming on body composition, strength, and flexibility. *The Journal of sports medicine and physical fitness, 26*(4), 416-420.

Health, U. D. o., & Services, H. (2004). Bone health and osteoporosis: a report of the Surgeon General: Rockville, MD: US Department of Health and Human Services, Office of the Surgeon General.

Helgason, B., Perilli, E., Schileo, E., Taddei, F., Brynjólfsson, S., & Viceconti, M. (2008). Mathematical relationships between bone density and mechanical properties: A literature review. *Clinical Biomechanics, 23*(2), 135-146. doi: https://doi.org/10.1016/j.clinbiomech.2007.08.024

Hernandez, C., & Keaveny, T. (2006). A biomechanical perspective on bone quality. *Bone, 39*(6), 1173-1181.

Hert, J. (1969). Acceleration of the growth after decrease of load on epiphyseal plates by means of spring distractors. *Folia morphologica, 17*(2), 194.

Hert, J. (1971). Reaction of bone to mechanical stimuli, part 1: Continuous and intermittentloading of tibia in rabbit. *Folia Morphol (Praha), 19*, 290-300.

Hinwood, B. G. (1997). *A textbook of science for the health professions*: Nelson Thornes.

Holick, M. F. (1996). Vitamin D and bone health. *The Journal of nutrition, 126*(suppl_4), 1159S-1164S.

Hollister, S. J., Brennan, J., & Kikuchi, N. (1994). A homogenization sampling procedure for calculating trabecular bone effective stiffness and tissue level stress. *Journal of biomechanics, 27*(4), 433-444.

Hollister, S. J., & Riemer, B. A. (1993). *Digital-image-based finite element analysis for bone microstructure using conjugate gradient and Gaussian filter techniques* (Vol. 2035): SPIE.

Holtrop, M. (1975). The ultrastructure of bone. *Annals of Clinical & Laboratory Science, 5*(4), 264-271.

Homminga, J., Huiskes, R., Van Rietbergen, B., Rüegsegger, P., & Weinans, H. (2001). Introduction and evaluation of a gray-value voxel conversion technique. *Journal of biomechanics, 34*(4), 513-517. doi: https://doi.org/10.1016/S0021-9290(00)00227-X

Homminga, J., Van-Rietbergen, B., Lochmüller, E. M., Weinans, H., Eckstein, F., & Huiskes, R. (2004). The osteoporotic vertebral structure is well adapted to the loads of daily life, but not to infrequent "error" loads. *Bone, 34*(3), 510-516. doi: https://doi.org/10.1016/j.bone.2003.12.001

Honda, A., Sogo, N., Nagasawa, S., Kato, T., & Umemura, Y. (2008). Bones benefits gained by jump training are preserved after detraining in young and adult rats. *Journal of applied physiology, 105*(3), 849-853.

Hsieh, Y.-F., Wang, T., & Turner, C. (1999). Viscoelastic response of the rat loading model: implications for studies of strain-adaptive bone formation. *Bone, 25*(3), 379-382.

Hsieh, Y. F., & Turner, C. H. (2001). Effects of loading frequency on mechanically induced bone formation. *Journal of Bone and Mineral Research, 16*(5), 918-924.

Huesa, C., Helfrich, M. H., & Aspden, R. M. (2010). Parallel-plate fluid flow systems for bone cell stimulation. *Journal of biomechanics, 43*(6), 1182-1189. doi: https://doi.org/10.1016/j.jbiomech.2009.11.029

Hytönen, M. K., & Lohi, H. (2016). Canine models of human rare disorders. *Rare Diseases, 4*(1), e1006037.

Iannotti, J. P., & Parker, R. (2013). *The Netter Collection of Medical Illustrations: Musculoskeletal System, Volume 6, Part III-Musculoskeletal Biology and Systematic Musculoskeletal Disease* (Vol. 6): Elsevier Health Sciences.

Iwamoto, J., Yeh, J. K., & Aloia, J. F. (2000). Effect of deconditioning on cortical and cancellous bone growth in the exercise trained young rats. *Journal of Bone and Mineral Research, 15*(9), 1842-1849.

Jacobs, C. R., Temiyasathit, S., & Castillo, A. B. (2010). Osteocyte Mechanobiology and Pericellular Mechanics. *Annual Review of Biomedical Engineering, 12*(1), 369-400. doi: 10.1146/annurev-bioeng-070909-105302

Johnson, T., Socrate, S., & Boyce, M. (2010). A viscoelastic, viscoplastic model of cortical bone valid at low and high strain rates. *Acta biomaterialia, 6*(10), 4073-4080.

Jones, D., Nolte, H., Scholübbers, J., Turner, E., & Veltel, D. (1991). Biochemical signal transduction of mechanical strain in osteoblast-like cells. *Biomaterials, 12*(2), 101-110.

Jones, H. H., Priest, J. D., Hayes, W. C., Tichenor, C. C., & Nagel, D. A. (1977). Humeral hypertrophy in response to exercise. *J Bone Joint Surg Am, 59*(2), 204-208.

Kabel, J., van Rietbergen, B., Dalstra, M., Odgaard, A., & Huiskes, R. (1999). The role of an effective isotropic tissue modulus in the elastic properties of cancellous bone. *Journal of biomechanics, 32*(7), 673-680. doi: https://doi.org/10.1016/S0021-9290(99)00045-7

Karaplis, A. C. (2008). Embryonic development of bone and regulation of intramembranous and endochondral bone formation *Principles of bone biology* (pp. 53-84): Elsevier.

Karlsson, M., Linden, C., Karlsson, C., Johnell, O., Obrant, K., & Seeman, E. (2000). Exercise during growth and bone mineral density and fractures in old age. *The lancet, 355*(9202), 469-470.

Karlsson, M. K. (2004). Physical activity, skeletal health and fractures in a long term perspective. *Journal of Musculoskeletal and Neuronal Interactions, 4*(1), 12.

Karnofsky, D. A., Ridgway, L. P., & Patterson, P. A. (1951). Growth-inhibiting effect of cortisone acetate on the chick embryo. *Endocrinology, 48*(5), 596-616.

Kazakia, G. J., & Majumdar, S. (2006). New imaging technologies in the diagnosis of osteoporosis. *Reviews in Endocrine and Metabolic Disorders, 7*(1), 67-74. doi: 10.1007/s11154-006-9004-2

Kim, C. H., Takai, E., Zhou, H., Von Stechow, D., Müller, R., Dempster, D. W., & Guo, X. E. (2003). Trabecular bone response to mechanical and parathyroid hormone stimulation: the role of mechanical microenvironment. *Journal of bone and mineral research, 18*(12), 2116-2125.

Kontulainen, S., Kannus, P., Haapasalo, H., Sievänen, H., Pasanen, M., Heinonen, A., . . . Vuori, I. (2001). Good maintenance of exercise-induced bone gain with decreased training of female tennis and squash players: a prospective 5-year follow-up study of young and old starters and controls. *Journal of Bone and Mineral Research, 16*(2), 195-201.

Kontulainen, S., Sievänen, H., Kannus, P., Pasanen, M., & Vuori, I. (2003). Effect of Long-Term Impact-Loading on Mass, Size, and Estimated Strength of Humerus and Radius of Female Racquet-Sports Players: A Peripheral Quantitative Computed Tomography Study Between Young and Old Starters and Controls. *Journal of Bone and Mineral Research, 18*(2), 352-359. doi: 10.1359/jbmr.2003.18.2.352

Lanyon, L., Hampson, W., Goodship, A., & Shah, J. (1975). Bone deformation recorded in vivo from strain gauges attached to the human tibial shaft. *Acta Orthopaedica, 46*(2), 256-268.

Lanyon, L., & Smith, R. (1969). Measurements of bone strain in the walking animal. *Research in veterinary science, 10*(1), 93-94.

Lanyon, L. E. (1973). Analysis of surface bone strain in the calcaneus of sheep during normal locomotion: Strain analysis of the calcaneus. *Journal of biomechanics, 6*(1), 41-49. doi: https://doi.org/10.1016/0021-9290(73)90036-5

Lanyon, L. E., & Rubin, C. (1984). Static vs dynamic loads as an influence on bone remodelling. *Journal of biomechanics, 17*(12), 897-905.

Lee, K., Maxwell, A., & Lanyon, L. (2002). Validation of a technique for studying functional adaptation of the mouse ulna in response to mechanical loading. *Bone, 31*(3), 407-412.

Lindholm, C., And, K. H., & Ringertz, B.-M. (1994). Pubertal development in elite juvenile gymnasts: Effects of physical training. *Acta Obstetricia et Gynecologica Scandinavica, 73*(3), 269-273. doi: 10.3109/00016349409023452

Liskova, M. (1971). Reaction of bone to mechanical stimuli. Part 2. *Folia morphologica, 19*, 301-317.

Lynch, M. E., Brooks, D., Mohanan, S., Lee, M. J., Polamraju, P., Dent, K., . . . Fischbach, C. (2013). In vivo tibial compression decreases osteolysis and tumor formation in a human metastatic breast cancer model. *Journal of Bone and Mineral Research, 28*(11), 2357-2367.

Lynch, M. E., Main, R. P., Xu, Q., Walsh, D. J., Schaffler, M. B., Wright, T. M., & van der Meulen, M. C. (2010). Cancellous bone adaptation to tibial compression is not sex dependent in growing mice. *Journal of applied physiology, 109*(3), 685-691.

Mackie, E., Ahmed, Y., Tatarczuch, L., Chen, K.-S., & Mirams, M. (2008). Endochondral ossification: how cartilage is converted into bone in the developing skeleton. *The international journal of biochemistry & cell biology, 40*(1), 46-62.

MacNeil, J. A., & Boyd, S. K. (2007). Accuracy of high-resolution peripheral quantitative computed tomography for measurement of bone quality. *Medical engineering & physics, 29*(10), 1096-1105.

Main, R. P., Lynch, M. E., & van der Meulen, M. C. (2014). Load-induced changes in bone stiffness and cancellous and cortical bone mass following tibial compression diminish with age in female mice. *Journal of Experimental Biology, 217*(10), 1775-1783.

Marini, F., & Brandi, M. L. (2010). Genetic determinants of osteoporosis: common bases to cardiovascular diseases? *International journal of hypertension, 2010*.

Markings, B. (1995). The skeletal system.

Marks Jr, S. C., & Odgren, P. R. (2002). Structure and development of the skeleton *Principles of bone biology* (pp. 3-15): Elsevier.

McBride, S. H., & Silva, M. J. (2012). Adaptive and injury response of bone to mechanical loading. *BoneKEy reports, 1*.

Mente, P. L., Aronsson, D. D., Stokes, I. A. F., & Iatridis, J. C. (1999). Mechanical modulation of growth for the correction of vertebral wedge deformities. *Journal of Orthopaedic Research, 17*(4), 518-524. doi: 10.1002/jor.1100170409

Milgrom, C., Finestone, A., Sharkey, N., Hamel, A., Mandes, V., Burr, D., . . . Ekenman, I. (2002). Metatarsal strains are sufficient to cause fatigue fracture during cyclic overloading. *Foot & ankle international, 23*(3), 230-235.

Moran, C. J., Ramesh, A., Brama, P. A., O'Byrne, J. M., O'Brien, F. J., & Levingstone, T. J. (2016). The benefits and limitations of animal models for translational research in cartilage repair. *Journal of experimental orthopaedics, 3*(1), 1.

Mosley, J., March, B., Lynch, J., & Lanyon, L. (1997). Strain magnitude related changes in whole bone architecture in growing rats. *Bone, 20*(3), 191-198.

Müller, R. (2002). The Zürich experience: one decade of three-dimensional high-resolution computed tomography. *Topics in Magnetic Resonance Imaging, 13*(5), 307-322.

Müller, R., & Rüegsegger, P. (1995). Three-dimensional finite element modelling of non-invasively assessed trabecular bone structures. *Medical engineering & physics, 17*(2), 126-133. doi: https://doi.org/10.1016/1350-4533(95)91884-J

Munoz, F., Boutroy, S., Delmas, P. D., & Bouxsein, M. L. (2005). In Vivo Assessment of Trabecular Bone Microarchitecture by High-Resolution Peripheral Quantitative Computed Tomography. *The Journal of Clinical Endocrinology & Metabolism, 90*(12), 6508-6515. doi: 10.1210/jc.2005-1258

Mustafy, T., Benoit, A., Londono, I., Moldovan, F., & Villemure, I. (2018). Can repeated in vivo micro-CT irradiation during adolescence alter bone microstructure, histomorphometry and longitudinal growth in a rodent model? *PLOS ONE, 13*(11), e0207323.

Mustafy, T., Londono, I., & Villemure, I. (2018). Can the contralateral limb be used as a control during the growing period in a rodent model? *Medical engineering & physics, 58*, 31-40. doi: https://doi.org/10.1016/j.medengphy.2018.04.013

Mustafy, T., Londono, I., & Villemure, I. (2019). Experimental and finite element analyses of bone strains in the growing rat tibia induced by in vivo axial compression. *Journal of the Mechanical Behavior of Biomedical Materials, 94*, 176.

Myllyharju, J. (2014). Extracellular matrix and developing growth plate. *Current osteoporosis reports, 12*(4), 439-445.

Niehoff, A., Kersting, U. G., Zaucke, F., Morlock, M. M., & Brüggemann, G.-P. (2004). Adaptation of mechanical, morphological, and biochemical properties of the rat growth plate to dose-dependent voluntary exercise. *Bone, 35*(4), 899-908.

Nordström, A., Olsson, T., & Nordström, P. (2005). Bone gained from physical activity and lost through detraining: a longitudinal study in young males. *Osteoporosis international, 16*(7), 835-841. doi: 10.1007/s00198-004-1749-4

Norma, A. (2005). C39M. Standard Test Method for Compressive Strength of Cylindrical Concrete Specimens. *ASTM International*.

Norvell, S. M., Alvarez, M., Bidwell, J. P., & Pavalko, F. M. (2004). Fluid Shear Stress Induces β-Catenin Signaling in Osteoblasts. *Calcified tissue international, 75*(5), 396-404. doi: 10.1007/s00223-004-0213-y

Ohashi, N., Robling, A. G., Burr, D. B., & Turner, C. H. (2002). The effects of dynamic axial loading on the rat growth plate. *Journal of Bone and Mineral Research, 17*(2), 284-292.

Oksztulska-Kolanek, E., Znorko, B., Michałowska, M., & Pawlak, K. (2016). The biomechanical testing for the assessment of bone quality in an experimental model of chronic kidney disease. *Nephron, 132*(1), 51-58.

Owens, F. N., Dubeski, P., & Hanson, C. (1993). Factors that alter the growth and development of ruminants. *Journal of animal science, 71*(11), 3138-3150.

Pajamäki, I., Kannus, P., Vuohelainen, T., Sievänen, H., Tuukkanen, J., Järvinen, M., & Järvinen, T. L. (2003). The bone gain induced by exercise in puberty is not preserved through a virtually life-long deconditioning: a randomized controlled experimental study in male rats. *Journal of Bone and Mineral Research, 18*(3), 544-552.

Parfitt, A. M. (1982). The coupling of bone formation to bone resorption: A critical analysis of the concept and of its relevance to the pathogenesis of osteoporosis. *Metabolic Bone Disease and Related Research, 4*(1), 1-6. doi: https://doi.org/10.1016/0221-8747(82)90002-9

Peltz, S., Brewer, G., Bernstein, P., Hart, P., & Ross, J. (1991). Critical Reviews in Eukaryotic Gene Expression.

Pistoia, W., Van Rietbergen, B., Laib, A., & Ruegsegger, P. (2001). High-resolution three-dimensional-pQCT images can be an adequate basis for in-vivo µFE analysis of bone. *Journal of biomechanical engineering, 123*(2), 176-183.

Pistoia, W., van Rietbergen, B., Lochmüller, E. M., Lill, C. A., Eckstein, F., & Rüegsegger, P. (2002). Estimation of distal radius failure load with micro-finite element analysis models based on three-dimensional peripheral quantitative computed tomography images. *Bone, 30*(6), 842-848. doi: https://doi.org/10.1016/S8756-3282(02)00736-6

Raisz, L. G. (1999). Physiology and Pathophysiology of Bone Remodeling. *Clinical Chemistry, 45*(8), 1353-1358.

Razi, H., Birkhold, A. I., Zaslansky, P., Weinkamer, R., Duda, G. N., Willie, B. M., & Checa, S. (2015). Skeletal maturity leads to a reduction in the strain magnitudes induced within the bone: a murine tibia study. *Acta biomaterialia, 13*, 301-310.

Rizzoli, R., Bianchi, M. L., Garabédian, M., McKay, H. A., & Moreno, L. A. (2010). Maximizing bone mineral mass gain during growth for the prevention of fractures in the adolescents and the elderly. *Bone, 46*(2), 294-305.

Roark, R. J. (1954). Formulas for stress and strain.

Robling, A. G., Burr, D. B., & Turner, C. H. (2001a). Recovery periods restore mechanosensitivity to dynamically loaded bone. *Journal of Experimental Biology, 204*(19), 3389-3399.

Robling, A. G., Burr, D. B., & Turner, C. H. (2001b). Skeletal loading in animals.

Ross, M. H., Kaye, G. I., & Pawlina, W. (2003). *Histology: a text and atlas: with cell and molecular biology*: Lippincott Williams & Wilkins.

Roux, W. (1881). Der zuchtende Kampf der Teile, oder die "Teilauslese" im Organismus (Theorie der "funktionellen Anpassung"). *Leipzig: Wilhelm Engelmann.*

Rubin, C. T., & Lanyon, L. E. (1985). Regulation of bone mass by mechanical strain magnitude. *Calcified tissue international, 37*(4), 411-417.

Ruff, C., Holt, B., & Trinkaus, E. (2006). Who's afraid of the big bad Wolff?:"Wolff's law" and bone functional adaptation. *American Journal of Physical Anthropology: The Official Publication of the American Association of Physical Anthropologists, 129*(4), 484-498.

Ruffoni, D., & Van Lenthe, G. (2017). 3.10 Finite element analysis in bone research: a computational method relating structure to mechanical function. *Compr. Biomater. II, 3*, 169-196.

Santos, A., Bakker, A. D., Zandieh-Doulabi, B., de Blieck-Hogervorst, J. M. A., & Klein-Nulend, J. (2010). Early activation of the β-catenin pathway in osteocytes is mediated by nitric oxide, phosphatidyl inositol-3 kinase/Akt, and focal adhesion kinase. *Biochemical and Biophysical Research Communications, 391*(1), 364-369. doi: https://doi.org/10.1016/j.bbrc.2009.11.064

Schnitzler, C. M., Biddulph, S. L., Mesquita, J. M., & Gear, K. A. (1996). Bone structure and turnover in the distal radius and iliac crest: a histomorphometric study. *Journal of Bone and Mineral Research, 11*(11), 1761-1768.

Sengupta, P. (2013). The laboratory rat: relating its age with human's. *International journal of preventive medicine, 4*(6).

Siddiqui, J. A., & Partridge, N. C. (2016). Physiological Bone Remodeling: Systemic Regulation and Growth Factor Involvement. *Physiology, 31*(3), 233-245. doi: 10.1152/physiol.00061.2014

Sievänen, H. (2012). Bone: Impact loading—nature's way to strengthen bone. *Nature Reviews Endocrinology, 8*(7), 391-393.

Sissons, H., & Hadfield, G. (1955). The influence of cortisone on the structure and growth of bone. *Journal of Anatomy, 89*(Pt 1), 69.

Slemenda, C. W., Reister, T. K., Hui, S. L., Miller, J. Z., Christian, J. C., & Johnston Jr, C. C. (1994). Influences on skeletal mineralization in children and adolescents: evidence for varying effects of sexual maturation and physical activity. *The Journal of pediatrics, 125*(2), 201-207.

Smith, E. L. (1983). *Principles of biochemistry: general aspects* (Vol. 1): McGraw-Hill.

Snyder, A., Zierath, J., Hawley, J., Sleeper, M., & Craig, B. (1992). The effects of exercise mode, swimming vs. running, upon bone growth in the rapidly growing female rat. *Mechanisms of ageing and development, 66*(1), 59-69.

Spengler, D. M., Morey, E. R., Carter, D. R., Turner, R. T., & Baylink, D. J. (1983). Effects of spaceflight on structural and material strength of growing bone. *Proceedings of the Society for Experimental Biology and Medicine, 174*(2), 224-228.

Stokes, I. (2002). Mechanical effects on skeletal growth. *Journal of Musculoskeletal and Neuronal Interactions, 2*(3), 277-280.

Stokes, I. A., Aronsson, D. D., Dimock, A. N., Cortright, V., & Beck, S. (2006). Endochondral growth in growth plates of three species at two anatomical locations modulated by mechanical compression and tension. *Journal of Orthopaedic Research, 24*(6), 1327-1334.

Stokes, I. A., Gwadera, J., Dimock, A., Farnum, C. E., & Aronsson, D. D. (2005). Modulation of vertebral and tibial growth by compression loading: Diurnal versus full-time loading. *Journal of Orthopaedic Research, 23*(1), 188-195.

Su, P., Tian, Y., Yang, C., Ma, X., Wang, X., Pei, J., & Qian, A. (2018). Mesenchymal stem cell migration during bone formation and bone diseases therapy. *International journal of molecular sciences, 19*(8), 2343.

Takahashi, H. E., & Takahashi, H. (1999). *Mechanical loading of bones and joints*: Springer.

Tanghe, Y., Claessens, A., Beunen, G., Depraetere, S., Lefevre, J., Philippaerts, R., & Thomis, M. (1996). *Effect of gymnastic training on growth of bone length and bone width in girls.* Paper presented at the Book of Abstracts.

Theintz, G. E., Howald, H., Weiss, U., & Sizonenko, P. (1993). Evidence for a reduction of growth potential in adolescent female gymnasts. *The Journal of pediatrics, 122*(2), 306-313.

Torcasio, A., Zhang, X., Duyck, J., & van Lenthe, G. H. (2012). 3D characterization of bone strains in the rat tibia loading model. *Biomechanics and modeling in mechanobiology, 11*(3-4), 403-410.

Torrance, A., Mosley, J., Suswillo, R., & Lanyon, L. (1994). Noninvasive loading of the rat ulna in vivo induces a strain-related modeling response uncomplicated by trauma or periostal pressure. *Calcified tissue international, 54*(3), 241-247.

Tortora, G. J., & Derrickson, B. (2017). *Principles of anatomy & physiology*: John Wiley & Sons, Incorporated.

Trueta, J., & Morgan, J. (1960). The vascular contribution to osteogenesis. *J Bone Joint Surg Br, 42*, 97-109.

Turner, C. H., & Akhter, M. P. (1999). The mechanics of bone adaptation *Mechanical loading of bones and joints* (pp. 79-91): Springer.

Valteau, B., Grimard, G., Londono, I., Moldovan, F., & Villemure, I. (2011). In vivo dynamic bone growth modulation is less detrimental but as effective as static growth modulation. *Bone, 49*(5), 996-1004.

Van der Eerden, B., Karperien, M., & Wit, J. (2003). Systemic and local regulation of the growth plate. *Endocrine reviews, 24*(6), 782-801.

van Lenthe, G. H., & Müller, R. (2006). Prediction of failure load using micro-finite element analysis models: Toward in vivo strength assessment. *Drug Discovery Today: Technologies, 3*(2), 221-229. doi: https://doi.org/10.1016/j.ddtec.2006.06.001

Van Rietbergen, B., Huiskes, R., Eckstein, F., & Rüegsegger, P. (2003). Trabecular Bone Tissue Strains in the Healthy and Osteoporotic Human Femur. *Journal of Bone and Mineral Research, 18*(10), 1781-1788. doi: 10.1359/jbmr.2003.18.10.1781

van Rietbergen, B., Weinans, H., Huiskes, R., & Odgaard, A. (1995). A new method to determine trabecular bone elastic properties and loading using micromechanical finite-element models. *Journal of biomechanics, 28*(1), 69-81. doi: https://doi.org/10.1016/0021-9290(95)80008-5

Vico, L., Collet, P., Guignandon, A., Lafage-Proust, M.-H., Thomas, T., Rehailia, M., & Alexandre, C. (2000). Effects of long-term microgravity exposure on cancellous and cortical weight-bearing bones of cosmonauts. *The lancet, 355*(9215), 1607-1611. doi: https://doi.org/10.1016/S0140-6736(00)02217-0

Villemure, I. (2002). *Étude biomécanique du processus de croissance et de déformation du rachis scoliotique*.

Villemure, I., & Stokes, I. A. (2009). Growth plate mechanics and mechanobiology. A survey of present understanding. *Journal of biomechanics, 42*(12), 1793-1803.

Vodicka, P., SMETANA JR, K., DVOŘÁNKOVÁ, B., Emerick, T., Xu, Y. Z., Ourednik, J., . . . MotlÍk, J. (2005). The miniature pig as an animal model in biomedical research. *Annals of the New York Academy of Sciences, 1049*(1), 161-171.

Warden, S., & Turner, C. (2004). Mechanotransduction in the cortical bone is most efficient at loading frequencies of 5–10 Hz. *Bone, 34*(2), 261-270.

Warden, S. J., Fuchs, R., Castillo, A., & Turner, C. (2005). Does exercise during growth influence osteoporotic fracture risk later in life? *Journal of Musculoskeletal and Neuronal Interactions, 5*(4), 344.

Warden, S. J., Fuchs, R. K., Castillo, A. B., Nelson, I. R., & Turner, C. H. (2007). Exercise when young provides lifelong benefits to bone structure and strength. *Journal of Bone and Mineral Research, 22*(2), 251-259.

Warden, S. J., Roosa, S. M. M., Kersh, M. E., Hurd, A. L., Fleisig, G. S., Pandy, M. G., & Fuchs, R. K. (2014). Physical activity when young provides lifelong benefits to cortical bone size and strength in men. *Proceedings of the National Academy of Sciences, 111*(14), 5337-5342.

Weaver, C. M. (2002). Adolescence. *Endocrine, 17*(1), 43-48. doi: 10.1385/endo:17:1:43

Welch, J. M., Weaver, C. M., & Turner, C. H. (2004). Adaptations to free-fall impact are different in the shafts and bone ends of rat forelimbs. *Journal of applied physiology, 97*(5), 1859-1865. doi: 10.1152/japplphysiol.00438.2004

Winkelstein, B. A. (2012). *Orthopaedic biomechanics*: CRC Press.

Wojnar, R. (2010). Bone and cartilage–its structure and physical properties. *Biomechanics of hard tissues*, 1-75.

Wolbach, S. B. (1947). Vitamin-A deficiency and excess in relation to skeletal growth. *JBJS, 29*(1), 171-192.

Wolff, J. (1892). Das gesetz der transformation der knochen. *A Hirshwald, 1*, 1-152.

Yang, P., Bruggemann, G., & Rittweger, J. (2011). What do we currently know from in vivo bone strain measurements in humans. *J Musculoskelet Neuronal Interact, 11*(1), 8-20.

Yang, X., Willie, B. M., Beach, J. M., Wright, T. M., van der Meulen, M. C. H., & Bostrom, M. P. G. (2013). Trabecular bone adaptation to loading in a rabbit model is not magnitude-dependent. *Journal of Orthopaedic Research, 31*(6), 930-934. doi: 10.1002/jor.22316

Young, P. G., Raymont, D., Xuan, V. B., & Cotton, R. T. (2010). *New Tools for Image-Based Mesh Generation of 3D Imaging Data*, Berlin, Heidelberg.

Zysset, P. K., Dall'ara, E., Varga, P., & Pahr, D. H. (2013). Finite element analysis for prediction of bone strength. *BoneKEy reports, 2*, 386-386. doi: 10.1038/bonekey.2013.120

APPENDIX A   CALCULATION OF RADIATION DOSES

Radiation doses for the SkyScan 1176 has been calculated based on the "SkyScan 1176 *in vivo* scanning: X-ray dosimetry" report. A brief description of how the dose measurements have been performed and listed results from the report is provided here.

Method

The dose measurements were carried out using an UNFORS PS-2 patient skin dosimeter. Shielding was provided with acrylic plastic (PMMA) tubes of various wall thicknesses to simulate biological soft tissue.

Results

The calculated radiation absorbed dose and corresponding effective dose equivalent values are derived from the measured dose rates with several PMMA shielding depths, extrapolated where necessary by exponential curve-fitting. For approximation of the mean dose rate at different tissue diameters, the tissue at all depths is assumed to be a cylinder, and the dose rate at all tissue cylinder diameters averaged between the dose in air (zero depth) and the dose at the cylinder center (half diameter).

Scan doses for maximal image quality scan settings: For the scanning settings of 65 kV, 384 µA x-ray - full power and 1mm Al filter, the local absorbed dose rate for *in vivo* rat tibial scanning is reported by Bruker to be 148.3 mGy/min [ref: SkyScan 1176 *in vivo* scanning: X-ray dosimetry]

So, for our experiment, the doses per scan calculation is as follows:

Group 1: Scanning time $= 5 \min 34 \, sec = \left\{ 5 + \left(\frac{34}{60} \right) \right\} \min = 5.567 \, min$

So, the radiation doses per scan $= Scanning \; time \; x \; dose \; rate$

$$= (5.567 \; x \; 148.3) \; mGy = 825.59 \; mGy = \mathbf{0.83 \; Gy}$$

Group 2: Scanning time $= 11 \min 9 \, sec = \left\{ 11 + \left(\frac{9}{60} \right) \right\} \min = 11.15 \, min$

So, the radiation doses per scan $= Scanning \; time \; x \; dose \; rate$

$$= (11.15 \; x \; 148.3) \; mGy = 1653.55 \; mGy = \mathbf{1.65 \; Gy}$$

<u>Group 3:</u> Scanning time $= 16 \min 39 \, sec = \left\{16 + \left(\frac{39}{60}\right)\right\} \min = 16.65 \, min$

So, the radiation doses per scan $= Scanning \, time \, x \, dose \, rate$

$$= (16.65 \, x \, 148.3) \, mGy = 2469.19 \, mGy = \mathbf{2.47 \, Gy}$$

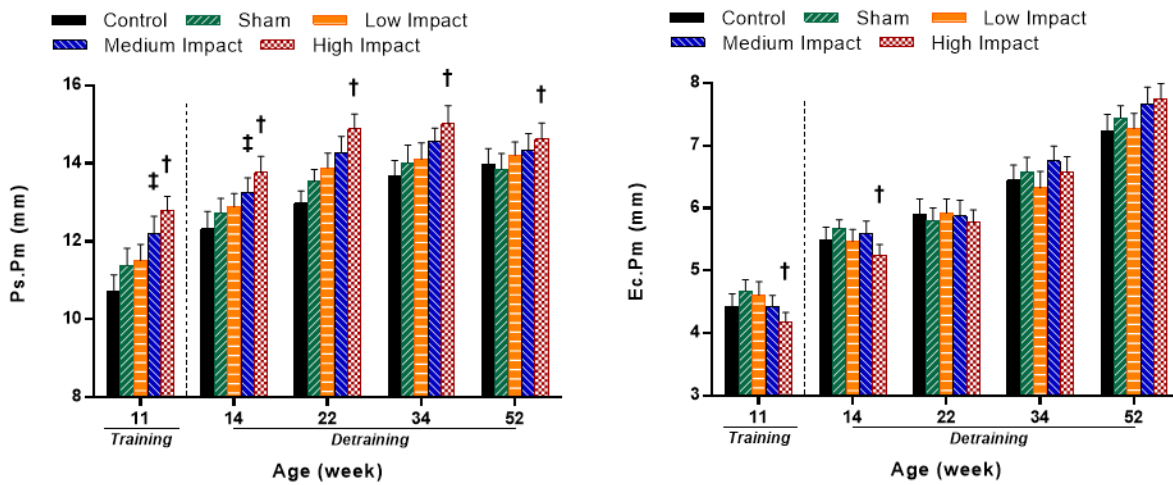# APPENDIX B   CORTICAL BONE MORPHOMETRY

Figure B.1 Mean values and standard deviations of the periosteal and endocortical perimeter for the five experimental groups at the end of training (11 week of age) and at selected detraining time points (14, 22, 34, and 52 week of age)

$p < 0.05$ ‡medium impact vs. sham; †high impact vs. sham